CIVIL ENGINEERING STUDIES
Illinois Center for Transportation Series No. 22-003
UILU-ENG-2022-2003
ISSN: 0197-9191

Performance Evaluation of Stabilized Support Layers for Concrete Pavements

Prepared By
John DeSantis, PhD
Jeffery Roesler, PhD, PE
University of Illinois Urbana-Champaign

Research Report No. FHWA-ICT-22-003

A report of the findings of

ICT PROJECT R27-193-6
Performance Evaluation of Stabilized Support Layers for Concrete Pavements

https://doi.org/10.36501/0197-9191/22-003

Illinois Center for Transportation

February 2022

TECHNICAL REPORT DOCUMENTATION PAGE

1. Report No.	2. Government Accession No.	3. Recipient's Catalog No.
FHWA-ICT-22-003	N/A	N/A

4. Title and Subtitle	5. Report Date
Performance Evaluation of Stabilized Support Layers for Concrete Pavements	February 2022
	6. Performing Organization Code N/A

7. Authors	8. Performing Organization Report No.
John DeSantis (https://orcid.org/0000-0002-3391-025X) Jeffery Roesler (https://orcid.org/0000-0001-6194-269X)	ICT-22-003 UILU-2022-2003

9. Performing Organization Name and Address	10. Work Unit No.
Illinois Center for Transportation Department of Civil and Environmental Engineering University of Illinois at Urbana-Champaign 205 North Mathews Avenue, MC-250 Urbana, IL 61801	N/A **11. Contract or Grant No.** R27-193-6

12. Sponsoring Agency Name and Address	13. Type of Report and Period Covered
Illinois Department of Transportation (SPR) Bureau of Research 126 East Ash Street Springfield, IL 62704	Final Report 10/16/19–2/28/22 **14. Sponsoring Agency Code**

15. Supplementary Notes

Conducted in cooperation with the U.S. Department of Transportation, Federal Highway Administration.
https://doi.org/10.36501/0197-9191/22-003

16. Abstract

A research investigation was conducted on the erosion potential of stabilized subbases under concrete pavements and asphalt layers supporting concrete overlays. Through field surveys and testing in Illinois, this project evaluated if existing concrete pavements with stabilized subbases and concrete overlays were exhibiting potential erosion of the underlying support layer. The field evaluation testing included falling weight deflectometer testing, distress surveys, coring, and ultrasonic tomography scanning. A laboratory performance test was also established using the Hamburg wheel-tracking device to assess the erodibility of the various stabilized subbase layers for new construction and existing asphalt layers available for a concrete overlay. The analyzed field test results were coupled together with the laboratory performance testing to provide recommendations for updating the Illinois Department of Transportation's "Bureau of Design and Environment Manual" guidance. No changes were recommended for hot-mix asphalt stabilized subbases, but testing using the Hamburg wheel-tracking device should be considered for Portland cement concrete stabilized support layers (e.g., CAM II) under concrete pavements. For testing of asphalt support layers for concrete pavement overlays, the Hamburg wheel-tracking device is recommended with performance criteria similar to flexible pavements for appropriate functional classes.

17. Key Words	18. Distribution Statement
Concrete Pavements, Jointed Plain Concrete Pavements, Falling Weight Deflectometer, MIRA, Hamburg Wheel-tracking Device	No restrictions. This document is available through the National Technical Information Service, Springfield, VA 22161.

19. Security Classif. (of this report)	20. Security Classif. (of this page)	21. No. of Pages	22. Price
Unclassified	Unclassified	48 + appendices	N/A

Form DOT F 1700.7 (8-72) **Reproduction of completed page authorized**

ACKNOWLEDGMENT, DISCLAIMER, MANUFACTURERS' NAMES

This publication is based on the results of **ICT-R27-193-6: Performance Evaluation of Stabilized Support Layers for Concrete Pavements**. ICT-R27-193-6 was conducted in cooperation with the Illinois Center for Transportation; the Illinois Department of Transportation; and the U.S. Department of Transportation, Federal Highway Administration.

Members of the Technical Review Panel (TRP) were the following:

- Charles Wienrank, Illinois Department of Transportation, TRP Chair
- Michael Ayers, Illinois Chapter—American Concrete Pavement Association
- Dennis Bachman, Federal Highway Administration
- Mike Brand, Illinois Department of Transportation
- James Krstulovich, Illinois Department of Transportation
- Tim Peters, Illinois Department of Transportation
- LaDonna Rowden, Illinois Department of Transportation
- John Senger, Illinois Department of Transportation
- Heather Shoup, Illinois Department of Transportation

The authors would like to acknowledge the Illinois Department of Transportation District's 1, 2, 4, 5, 6, and 7 for providing traffic control and coring operations as well as the Applied Pavement Technology field testing team for gathering the falling weight deflectometer test results.

EXECUTIVE SUMMARY

Concrete pavement performance is significantly related to the quality, uniformity, and stability of the underlying support layers. This research assessed the erosion potential of stabilized support layers under concrete pavements and concrete overlays in Illinois through laboratory testing and field investigations. Support layer erosion can lead to severe types of distress such as pumping, faulting, corner breaks, and longitudinal cracking. **Figure S1** illustrates an example of a longitudinal crack that spans multiple slabs and turns diagonally toward the lane-shoulder longitudinal joint as a result of erosion beneath the concrete pavement.

Figure S1. Photo. Loss of support beneath the concrete pavement on I-72 (92763).

The goal of this research was to recommend a performance test to measure the susceptibility of a hot-mix asphalt (HMA) or Portland cement concrete (PCC) stabilized subbase support layer to erosion mechanisms that could lead to premature distress in a concrete pavement. A literature review of existing erodibility test methods that assess stabilized subbases was conducted to identify and assess the suitability of different performance tests for Illinois. The Hamburg wheel-tracking device (HWTD) test was selected as the performance test for assessing the erodibility potential of HMA or PCC stabilized subbase support layers beneath rigid pavements and HMA pavement layers beneath concrete overlays. This test was performed on laboratory mixtures of the Illinois Department of Transportation's (IDOT's) Cement Aggregate Mixture II (CAM II) as well as cores obtained from the field of different subbases (HMA and CAM II) and existing HMA pavement beneath a bonded concrete overlay. The lab investigation of CAM II showed mixes with lower cement contents were more likely to experience erosion than mixes with higher cement contents.

A total of twelve IDOT concrete pavement sections were identified to perform falling weight deflectometer (FWD) testing, ultrasonic testing, distress surveys, and coring to assess the potential of erosion of different stabilized support layers (HMA and PCC). The FWD test data were used to backcalculate k-value, effective thickness, and slab-subbase interface friction of the in situ pavement structure. Nondestructive evaluation of the sections was completed using the MIRA ultrasonic tomography device, which determined the slab thickness, joint reinforcement details (dowel and tie bar depth and spacing), and contraction joint activation. Detailed distress surveys were performed in the tested regions to assess any distresses possibly caused by subbase erosion. Coring was also performed on four pavement sections (different structure type and subbases) to assess the erosion potential of the stabilized support layer and were evaluated using the established HWTD protocol.

Field survey results and analysis showed HMA stabilized subbases did not lead to poor performance of concrete pavements. One field site with a bonded concrete inlay of an existing composite pavement (HMA over PCC) was determined to be erosion susceptible and contributed to the severe failures of this section along with heavy truck traffic volume, inadequate slab thickness, and longitudinal joints in the outer wheel path. There was also evidence of erosion in poor drainage locations for pavements with a PCC stabilized subbase, but no faulting was observed at the transverse joints. Poor drainage locations were considered low elevation locations throughout a project section, such as underpasses or sag vertical curves.

The HWTD performance test was recommended to assess the potential of erosion in stabilized support materials underneath concrete pavements. Current IDOT requirements for applications of HMA and PCC stabilized subbase materials under rigid pavements in Chapter 54 of the *Bureau of Design and Environment (BDE) Manual* (54-4.01(h) Improved Subgrade and Subbase Type and Thickness and Figure 54-4.D Minimum Structural Design Requirements) should remain as is, as the field assessment revealed no significant distresses caused by stabilized subbase erosion throughout the state. The improved subgrade treatment options were not examined in this study nor were new traffic factor criterion for requiring stabilized support layers under PCC pavements. Additional criteria for HWTD testing of existing HMA stabilized support layers for concrete overlays were recommended for implementation into Section 53-4.02(b) Bonded Concrete Overlay on Asphalt (BCOA) and should follow Article 1030.05(d) of IDOT's *Standard Specifications for Road and Bridge Construction* for HWTD. Failure criteria for HWTD testing of PCC stabilized support layers of 0.08 in. (2 mm) rut depth at 10,000 cycles was also established for CAM II mixtures and recommended for implementation.

Table of Contents

CHAPTER 1: INTRODUCTION

The performance of new concrete pavements and concrete overlays is highly dependent on the support layers. Unstabilized base/subbase support layers are used for many new concrete pavements, but the criteria for moving from unstabilized to stabilized base/subbase layers varies with climate, traffic, drainage, site condition, and agency. In general, stabilized layers are specified directly beneath the slab once a certain truck traffic volume is reached. When used with concrete overlays, these stabilized layers beneath the slab must be erosion resistant. However, use of a stabilized layer does not guarantee that the support will have adequate long-term performance. The erodibility of the stabilized support layer must be measured to avoid premature pavement failure due to stripping of the binder and subsequent loss of the support materials. Current specifications and performance testing do not evaluate the potential for a cement stabilized support layer to erode under a new concrete pavement or a concrete overlay (bonded or unbonded). Although not directly evaluating erosion and stripping, Article 1030.05(d) of IDOT's *Standard Specifications for Road and Bridge Construction* (IDOT 2021) requires tensile strength, tensile strength ratio, and Hamburg wheel testing to be performed when designing and evaluating HMA stabilized subbase mixtures. Past performance studies have identified that the erosion of asphalt and cement stabilized support layers have resulted in premature failure of continuously reinforced concrete pavements (CRCP) and bonded concrete overlays of asphalt pavements (BCOA) in Illinois (Darter et al. 1979; Jung et al. 2009, 2012; King and Roesler 2014).

Subbase erosion is a function of the PCC and support layer interfacial bond, shear stresses along the interface, and cohesive strength of the stabilized layer (Jung et al. 2012). For erosion of a stabilized subbase to develop, first debonding must occur between the PCC slab and stabilized layer. This can initiate at the edges of the slab by curling of the PCC or water infiltration at this interface and repeated traffic loading. As this interface debonds, interfacial shear stresses develop with repeated traffic loading. These shear stresses can result in the abrasion of the stabilized subbase surface. As this degradation continues with traffic, water can expedite this process and also transport the eroded fine material. Further definition, discussion, and modeling of stabilized subbase erosion can be found in Jung et al. (2012).

Experimental data showed the shear stresses generated by the horizontal movement of the water at the bottom of the slabs can typically vary between 0.003 and 0.012 psi (Van Wijk 1985). Moving wheel loads generate pore water pressures beneath the slab that act to erode material along the slab-subbase interface. The magnitude of the slab deflections because of these wheel loads and the velocity of water displaced are a function of layer thicknesses, layer stiffnesses, layer material selection, traffic levels, and traffic velocity. This pumping action generated, leads to loss of support under the edge of the slab and near the transverse joints/cracks (see **Figure 1**).

To gain a better understanding of the potential pumping mechanism and generated water velocities, previous work by Phu and Ray (1979), Van Wijk (1985), and Caro et al. (2010) was examined. The initial stage of pumping can be caused by water infiltration into gaps or voids when separation between the PCC and stabilized support layer occur. Negative temperature differentials are one main

reason for slab-subbase separation near the slab edges. The water velocity generated beneath the slab can be calculated as follows based on hydrodynamics.

$$V_m = \frac{P h_{max}^2}{2\mu L I^2} \quad \text{Equation 1}$$

where V_m is the water velocity, *P* is the load of the vehicle, *L* is the length of the gap or void, h_{max} is the depth of the gap or void, *I* is the width of the gap or void, and μ is the dynamic viscosity. The velocities calculated based on this expression range between 0 and 10 ft/s. Although these speeds are not significantly high enough to likely erode stabilized materials, they can generate enough force to transport fines beneath the slab (across and out of the transverse joint). The shear stresses that develop at this interface increase with vehicle speed as long as the gap or void stays constant.

As the potential gap or void (separation between the PCC and stabilized layer) increases in size, the flow of water becomes transient. These water velocities can drastically change and result in an increase greater than those previously mentioned. As these velocities increase, the development of shear forces are present at the interface between the PCC and stabilized layer and can be critical to the development of erosion. However, as time and traffic increases, it is likely the gap or void will continue to develop and erosion and pumping is likely occurring. As these gaps or voids increase in size, the flow of water can result in laminar flow. Therefore, under these conditions, the water pressure directly underneath wheel loads depends mainly on the weight of the vehicle. As these gaps become larger than 40 mils (1 mm), water velocities can increase to between 13 and 26 ft/s. If the water is only expelled by the transverse joint, the velocity can be calculated by means of the following equation.

$$V_m = \frac{L V_z}{2(h_{max} - Z_{max})} \quad \text{Equation 2}$$

where V_z is the deflection velocity of the slab, h_{max} is the depth of the gap or void, and Z_{max} is the maximum deflection at the joint or slab edge under dynamic wheel loading conditions. If the water is expelled by the transverse joint and the longitudinal joint of the shoulder, the velocity can be calculated by means of the following equation.

$$V_m = \frac{L I V_z}{2(\frac{L}{Z_{max}} + 1)(h_{max} - Z_{max})} \quad \text{Equation 3}$$

As these gaps or voids increase over time with traffic, erosion or pumping will continue to develop and can result in the development of faulting or fatigue cracking because of insufficient support. This process can be observed in **Figure 1**.

The erosion development eventually leads to failure of the concrete slab, whether it be jointed plain concrete pavements (JPCP), CRCP, or BCOAs. **Figure 2** presents some of the distresses that can occur within these structures as a result of erosion of the stabilized support layer.

Current concrete (rigid) pavement design procedures used by IDOT assume that stabilized subbases are non-erodible and do not consider the direct impact of erosion in the design procedure and/or evaluation of the support layer materials. For the design of rigid pavements, an HMA or PCC stabilized layer is required in most cases, and an HMA interlayer is also what is typically supporting a concrete overlay. To prevent premature failure, the stabilized support layer must be assessed to determine if the material can withstand repeated loading in the presence of moisture in a confined space.

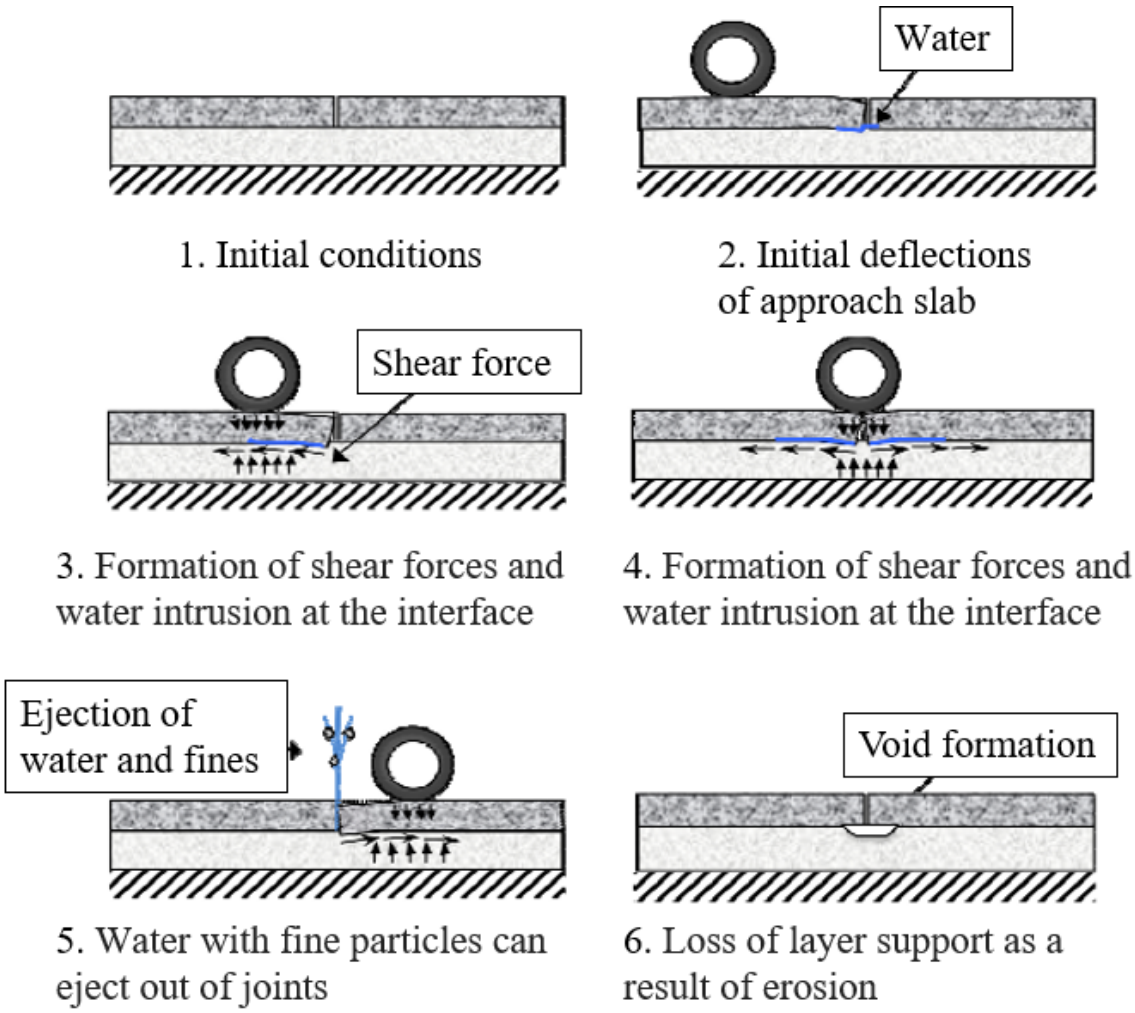

Figure 1. Schematic. Erosion development in stabilized subbase layers beneath concrete pavements (Caro et al. 2010).

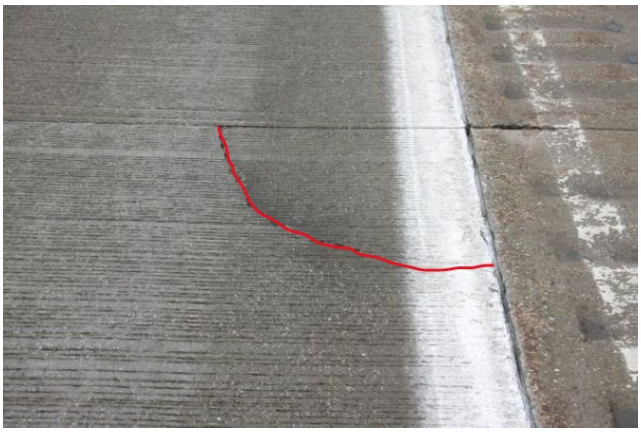

a) Corner breaks in JPCP (Hansen and Liu 2013)

b) Punchouts in CRCP (Ha et al. 2011)

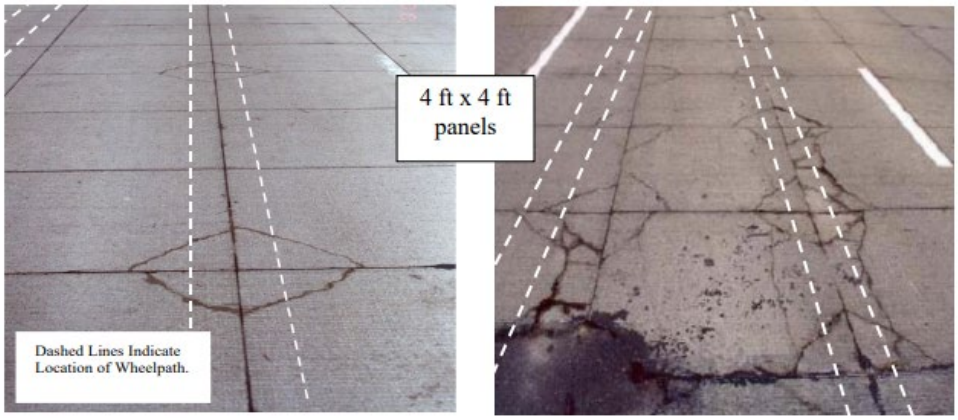

c) Corner breaks in BCOA (Barman et al. 2011)

Figure 2. Photos. Distresses from erosion of stabilized support layer.

Current concrete (rigid) pavement design procedures used by IDOT assume that stabilized subbases are non-erodible and do not consider the direct impact of erosion in the design procedure and/or evaluation of the support layer materials. For the design of rigid pavements, an HMA or PCC stabilized layer is required in most cases, and an HMA interlayer is also what is typically supporting a concrete overlay. To prevent premature failure, the stabilized support layer must be assessed to determine if the material can withstand repeated loading in the presence of moisture in a confined space.

RESEARCH OBJECTIVE

The objective of this research project is to provide IDOT with a performance test to quantify the susceptibility of a stabilized support layer under concrete pavements (JPCP, CRCP, or BCOA) to erode. The project evaluates the existing methods and then recommends a test method and criteria for assessing the erosion potential of HMA or PCC stabilized layers that support concrete pavement (new and overlays). The developed performance test and criteria will also assist pavement engineers in assessing whether a new concrete pavement or concrete overlay over a certain type of stabilized

support layer has the potential for premature erosion under repeated loading and presence of moisture.

RESEARCH TASKS

The overall research objective has been broken into the following four tasks and is explained in detail within the corresponding chapters.

1. Literature review of existing test methods that assess the erodibility of stabilized subbases (Chapter 2).

2. Laboratory and performance testing of HMA and PCC stabilized subbases in Illinois (Chapter 3).

3. Field testing of HMA and PCC stabilized subbases and HMA pavements under concrete overlays (FWD testing, ultrasonic testing, distress surveys, and coring) (Chapter 4).

4. Recommendations to IDOT for evaluating HMA and PCC stabilized subbases for concrete pavements and existing HMA pavements for concrete overlays (Chapter 5).

CHAPTER 2: REVIEW OF EXISTING EROSION TESTS FOR CONCRETE PAVEMENT SUBBASES

One key performance parameter of concrete pavements, such as JPCP, CRCP, and concrete overlays, is the resistance to erosion, uniformity, and stability of the support layers. There currently is not a standard method for measuring the resistance of erosion for HMA and PCC stabilized subbases under concrete pavements. The AASHTO T 135-17 standard assesses the "durability" of a soil-cement material by measuring the potential loss of stabilized material subjected to continuous wetting and drying cycles (AASHTO 2017). However, this method is not sufficient for accurately assessing HMA and PCC stabilized subbases under mechanisms of erosion. Therefore, different erosion tests have been developed using various testing devices, but none of these developed tests have been formally standardized. The following tests have previously been used to assess the erodibility of paving materials: rotational shear device for cohesive and stabilized materials (Van Wijk 1985), jetting test (Van Wijk 1985; Bhatti et al. 1996), linear and rotational brush tests (Phu and Ray 1979; Dempsey 1982; Van Wijk 1985), and the South African erosion test (De Beer 1990). More recent research by Dr. Zollinger at Texas A&M (Jung et al. 2009, 2010, 2012) for the Texas Department of Transportation (TxDOT) has provided several types of tests to evaluate field subbase conditions (FWD testing) as well as performance tests for subbases for concrete pavements through the Hamburg wheel-tracking device (HWTD) test. Recent work by the Portland Cement Association (PCA) of Argentina has employed this proposed HWTD test to evaluate a variety of stabilized materials under concrete pavement (Calo et al. 2019). Additionally, Caro et al. (2010) and Caicedo and Caro (2016) have studied stabilized subbase erosion potential under concrete pavements as a result of the premature failures observed in Bogota, Colombia, on the trans-millennium bus corridor project. They employed a dynamic cylinder test to simulate the movement of high velocity water across the stabilized material sample's surface as a way of performing an accelerated performance test. In addition to these erosion tests, compressive strengths of the supporting layers (tested accordingly with ASTM D1633) have been used to determine the erodibility instead of the stabilizer content because of the easy access to compressive strength results in comparison to mixture designs containing the stabilization content availability (Birmann 1998). This method is also applicable for assessing the resistance to erosion of HMA and PCC stabilized subbases (tested accordingly with AASHTO T 22). Stabilized layers must provide sufficient support, have minimal erosion potential, and not be overly stiff to cause cracking in the concrete surface layer.

ROTATIONAL SHEAR DEVICE AND JETTING DEVICE

Van Wijk (1985) developed two testing protocols: one for stabilized (cohesive) materials and the other for unstabilized (non-cohesive) materials. Stabilized (cohesive) materials are tested using a rotational shear device, while unstabilized (non-cohesive) materials are tested using a jetting device because they cannot be tested using the rotational shear device. Both methods consider only hydraulically induced shear in the erosion process. Weight loss is determined as a result of the test but it could be overestimated by the loss of aggregate-sized particles, which may not take place under field conditions. Stabilized test samples are eroded by the application of hydraulic shear stress using an annular water flow around a stationary test specimen (**Figure 3**). The exterior cylinder

rotates (rotation is imparted to the water) and transmits a shear to the surface of the test specimen. The weight of the eroded material is recorded as well as the torque required to hold the specimen stationary and used to determine the critical shear stress defined as the shear stress at which erosion of the particles abruptly accelerates (Wijk 1985). The critical shear stress of each material was recommended as an index of erosion resistance. For unstabilized materials, the jetting device test ejects pressurized water at an angle of approximately 20 degrees to the upper surface of the samples, generating weight loss over time. Critical shear stress on the surface are estimated based on the assumption of the stress being placed over a uniform area, even though the surface area and the distribution of pressure changes with time.

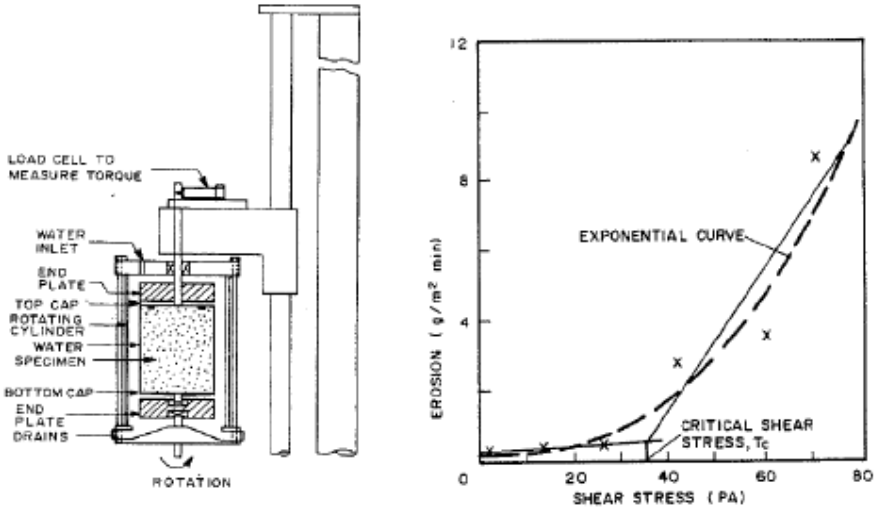

Rotational Shear Device

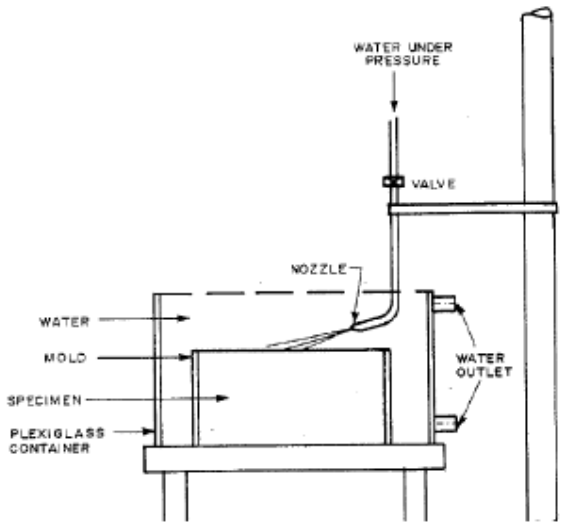

Jetting Device

Figure 3. Schematic. Rotational shear and jetting devices (Van Wijk, 1985).

BRUSH TEST DEVICE

French researchers, Phu and Ray (1979), developed brush devices to test various materials subjected to abrasion (shown in **Figure 4**). Van Wijk (1985) also performed a similar brush test. The major drawback of brush tests is that they can be time-consuming. Although a common issue with all erosion tests, subbase materials consisting of large-sized aggregates can loosen and dislodge during testing and exaggerate weight loss data. An erosion index or index of erosion (IE) is the outcome from this test and is defined as the ratio of the weight loss to that of a reference material. Lower IE means better erosion resistance. An IE of 0.2 to 0.4 is recommended for heavy traffic on undoweled rigid pavements, while an IE of 0.4 to 1.0 is recommended for doweled rigid pavements.

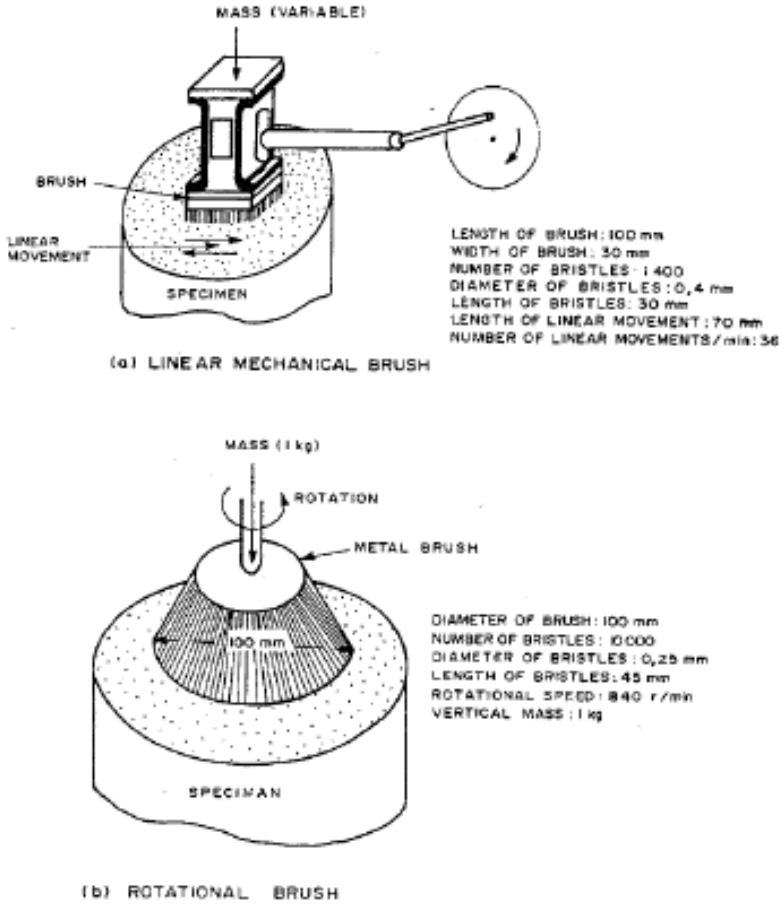

Figure 4. Schematic. Brush test devices (Phu and Ray 1979).

ROLLING WHEEL EROSION TEST DEVICE

Another testing device to assess the erosion potential of different subbase layers was developed by de Beer (1990). This procedure is also known as the South African erosion test, which uses a loaded wheel (40 lb) on a submerged specimen as seen in **Figure 5**. The wheel movement over a friction pad serves as the source of erosion of the test sample. Fines are produced on the surface of the test sample by direct contact between the friction pad (neoprene membrane) and the test sample.

Submerging the test sample during testing allows the specimen to undergo similar in situ conditions, where water accelerates base material washing out. The test specimens are subjected to 5,000 wheel load applications (back-and-forth motion) at an approximate loading frequency of 1 Hz. The average depth of wear on the tested specimen's surface is defined as the depth of erosion (erosion index). The average depth of erosion should be less than 0.04 in. (1 mm) after 5,000 wheel passes (de Beer 1990). The test method evaluates the erodibility based on the depth of erosion rather than the weight loss of the sample. It was determined to be more repeatable as a function of erosion depth versus weight loss.

This test attempts to simulate field conditions because it addresses mechanical abrasion and hydraulic erosion together. From this study, it was also determined the degree of compaction has a significant influence on the erodibility of the material. An increase in the degree of compaction results in an increase in strength (compression and bending) and erosion resistance. Specimens were compacted using a modified Proctor hammer with 56 blows per layer. To eliminate variability in compaction density, de Beer (1990) used a gyratory compactor for preparing specimens and samples to the same densities. This testing procedure was also carried out by Van Blerk and Scullion (1995) and later by Guthrie et al. (2001) at the Texas Transportation Institute utilizing the same procedure to characterize optimum cement contents for stabilizing base materials. These studies reported this device showed good potential for establishing the optimum stabilizer content for base materials. Erosion potential was more clearly defined for finer materials because coarse materials with low fines contents did not exhibit erosion. In addition, shrinkage and durability testing is recommended to be performed in conjunction with this testing.

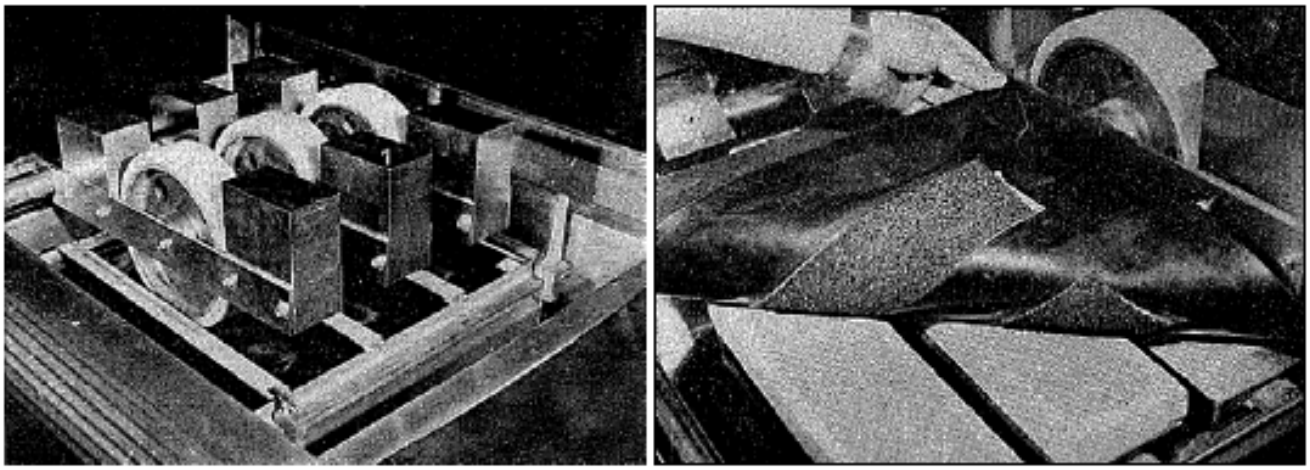

Figure 5. Photos. South African testing device with friction surface padding (de Beer 1990).

A more recent adaptation of the South African testing procedure uses the HWTD. Sebesta (2002) utilized the HWTD to assess the durability of asphalt-treated bases with different asphalt binder contents (2%, 4%, and 7%). This testing examined recycled soil or aggregate materials stabilized with an asphalt binder component. Sebesta found that given a material, as you increase the stabilizer content the number of passes of the wheel-load to failure increases. This testing was conducted to 20,000 load cycles or a failure depth of 0.5 in.

Another study at Texas A&M developed a performance test for subbases for concrete pavements using the HWTD test (Jung et al. 2009, 2010, 2012). Similar to the South African testing, this procedure simulates in situ conditions using the HWTD (**Figure 6a**). The cylindrical specimens for this testing procedure are composed of the concrete surface layer as well as the subbase layer, as compared to just the subbase material for all previous explained tests. The concrete layer has a formed joint to simulate a transverse joint in the field (**Figure 6b**). The depth of erosion after 5,000-wheel applications is used to assess the erodibility of a given subbase material. The subbase materials examined were unbound recycled soil or aggregate materials with a stabilizer. Three subbase materials were examined, reclaimed asphalt pavement (RAP), recycled crushed concrete, and a limestone base material with four levels of asphalt binder or cement content (0%, 2%, 4%, and 6%). All levels of the RAP, recycled crushed concrete with 2% cement or greater, and the cement-treated subbase with 2% cement or greater performed well with erosion depths less than 0.08 in. (2 mm) after 5,000 load applications, on average.

a) Hamburg wheel-tracking device

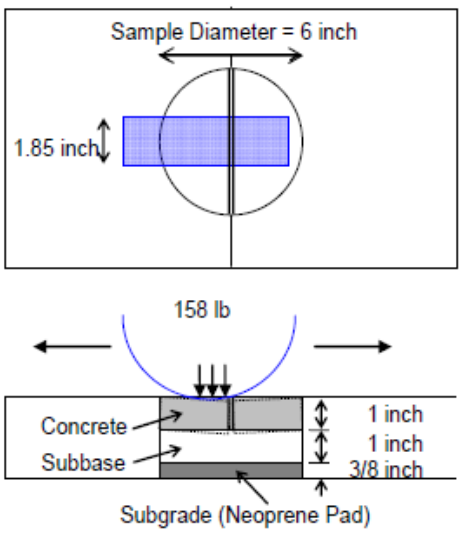

b) Hamburg wheel specimens

Figure 6. Photo and Schematic. Erosion test using the Hamburg wheel-tracking device test (Jung et al. 2010).

DYNAMIC CYLINDER TEST

Caro et al. (2010) and Caicedo and Caro (2016) have studied stabilized subbase erosion potential under concrete pavements as a result of the premature failures observed in Bogota, Colombia. They employed a dynamic cylinder test to simulate the movement of high velocity water across the stabilized material sample's surface as a way of performing an accelerated performance test. This work stemmed from previous work performed by Phu and Ray (1979), in which a laboratory investigation was performed using a vibrating table to mimic erosion mechanisms on a stabilized subbase specimen partially submerged in water (shown in **Figure 7**).

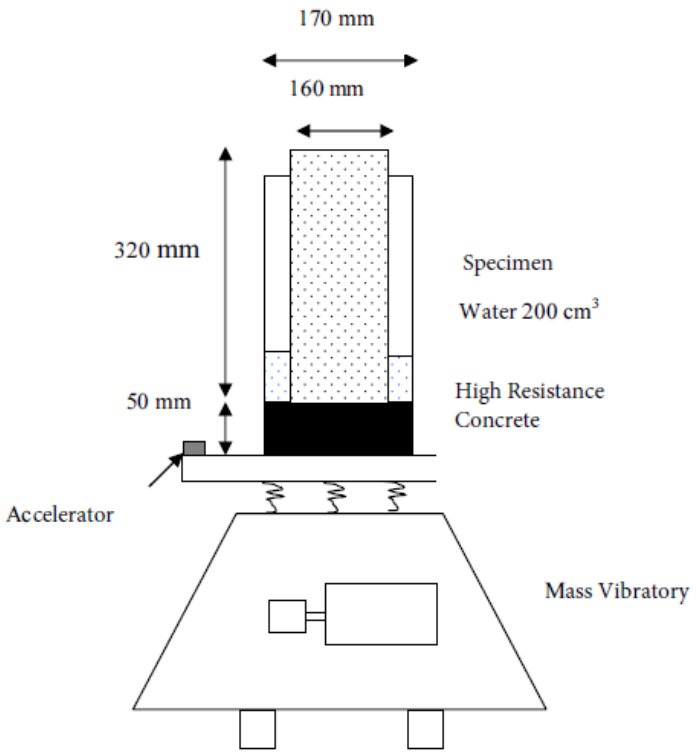

Figure 7. Schematic. Erosion test with vibrating table (Phu and Ray 1979).

The dynamic cylinder test (Caro et al. 2010) was developed to capture the effect of shear stresses that develop at the interface between the concrete and the stabilized subbase layers. These forces are a function of deflections and the velocity of water. A testing device was developed using an actuator, accelerometers, and water pressure sensors shown in **Figure 8**. The cylindrical specimen, composed of concrete bonded to subbase material, is placed into a steel mold containing 350 mL of water attached to the actuator. The actuator and container cycles vertically, which causes the specimen to move vertically. When the actuator returns to its initial position, the cylinder falls down into the steel mold and displaces the water. This water dispersion generates shear stresses along the exposed surface of the subbase specimen and can cause the material to erode depending on the material and level of stress. The specimen is tested at three loading frequencies (50, 80, and 100 Hz) for 200,000 cycles each. The eroded subbase material is removed and weighed after each of the 200,000 cycles. The different loading frequencies allow for three different horizontal water velocities to be generated that cause erosion that could be used to assess the different subbase layers for different road classifications. Hansen et al. (1991) reported that water velocities seen in the field range between 5–16 mph (2–7 m/s). The percent material loss versus water velocity is used to assess the performance of different subbase materials.

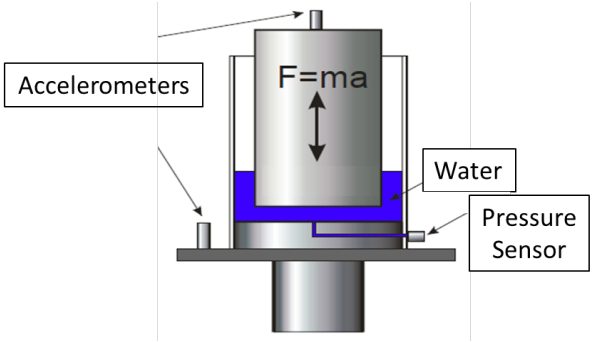

Figure 8. Schematic. Dynamic cylinder testing device (Caro et al. 2010).

EROSION TEST LITERATURE REVIEW SUMMARY

The majority of the examined performance tests were applied to testing the erosion potential of stabilized recycled material and not directly stabilized HMA or PCC subbases. The only test that evaluated stabilized HMA and PCC subbase materials was Caro et al. (2010). However, the other presented tests, except for the jetting device test, are applicable for testing the erosion potential of HMA and PCC stabilized subbases. The strengths, weaknesses, and the overall output for each of the examined performance tests are summarized in **Table 1**.

Table 1. Summary of Erosion Tests

Erosion Test	Strengths	Weaknesses	Output Criteria
Rotational shear device	Easy to control shear stress	Overestimation of weight loss due to coarse aggregates removal	Critical shear stress; Index of erosion resistance
Jetting device	Simple	Shear stress is not uniform (difficult to evaluate). Overestimation of weight loss because of coarse aggregates	Critical shear stress; Weight loss of material
Brush devices	Easy setup; considers durability under wet and dry conditions	Test times are long and weight losses are overestimated because of loss of coarse aggregates	Erosion Index based on weight loss of material
Rolling wheel erosion device	Simulation of field conditions for flexible pavement structures	Not developing pore water and jetting action	Erosion depth
Hamburg wheel-tracking device	Simulation of field conditions	Index test, specimen confinement, high contact pressure	Erosion depth; Erodibility index; Weight loss of material
Dynamic cylinder test	Simulation of field conditions	Overestimation of weight loss because of coarse aggregates removal	Erosion estimation using correlation between material loss and water velocity

CURRENT CRITERIA FOR SUBBASE DESIGN

The Illinois Department of Transportation's *Bureau of Design and Environment Manual* does not include an assessment method of the erodibility of the different stabilized subbase layers (IDOT 2021a). **Figure 9** presents the improved subgrade and subbase type and thickness requirements found in Chapter 54, Pavement Design. It provides the information regarding different layers to be used for the various traffic levels, when a subbase is required, and minimum layer thicknesses. Inherent in IDOT's requirements are to have an erosion-resistant subbase (HMA or PCC stabilized) for higher traffic volumes. Currently, there is no performance indicator test to assess the resistance to erosion of an HMA or PCC stabilized subbase. Although not directly evaluating erosion and stripping, Article 1030.05(d) of IDOT's *Standard Specifications for Road and Bridge Construction* (IDOT 2021b) requires HWTD testing to be performed when designing and evaluating HMA stabilized subbase mixtures.

Facility Type	Subbase ①		Improved Subgrade Type ② ③
	Type	Minimum Thickness (inches)	
Class I			
Interstate / Freeway	HMA or PCC Stabilized	4	ASI, GM, or MS
Other Marked Routes	HMA or PCC Stabilized	4	ASI, GM, or MS
Unmarked Routes (TF ≥ 2.0)	HMA or PCC Stabilized	4	ASI, GM, or MS
Unmarked Routes (0.7 < TF < 2.0)	Not required	n/a	ASI, GM ④
Unmarked Routes (TF ≤ 0.7)	Not required	n/a	ASI, GM, or MS
Class II			
Marked Routes	HMA or PCC Stabilized	4	ASI, GM, or MS
Unmarked Routes (TF ≥ 2.0)	HMA or PCC Stabilized	4	ASI, GM, or MS
Unmarked Routes (0.7 < TF < 2.0)	Not required	n/a	ASI, GM ④
Unmarked Routes (TF ≤ 0.7)	Not required	n/a	ASI, GM, or MS
Class III			
Marked Routes	HMA or PCC Stabilized	4	ASI, GM, or MS
Unmarked Routes (TF ≥ 2.0)	HMA or PCC Stabilized	4	ASI, GM, or MS
Unmarked Routes (0.7 < TF < 2.0)	Not required	n/a	ASI, GM ④
Unmarked Routes (TF ≤ 0.7)	Not required	n/a	ASI, GM, or MS
Class IV			
Marked Routes	HMA or PCC Stabilized	4	ASI, GM, or MS
Unmarked Routes (TF ≥ 2.0)	HMA or PCC Stabilized	4	ASI, GM, or MS
Unmarked Routes (0.7 < TF < 2.0)	Not required	n/a	ASI, GM ④
Unmarked Routes (TF ≤ 0.7)	Not required	n/a	ASI, GM, or MS

Notes:

① *For urban sections containing curb and gutter and a storm sewer system, the designer may omit the stabilized subbase when an ASI or GM improved subgrade is used, regardless of the traffic factor.*

② *Improved Subgrade Types include:*
ASI - Aggregate Subgrade Improvement (minimum of 12 in.)
GM – Granular over Modified Soil (4 in. CA 6 or CA 10 over 12 in. Modified Soil)
MS – Modified Soil (minimum of 12 in.)

③ *The minimum thickness of improved subgrade shall be according to Section 54-2.01(f).*

④ *Modified Soil may be used for the improved subgrade if a minimum 4-in. stabilized subbase is used.*

Figure 9. Chart. Minimum structural design requirements for subbases under concrete pavements (BDE Ch. 54: Figure 54-4.D [IDOT 2021a]).

Currently, the PCC stabilization material used is classified as cement aggregate mixture II (CAM II) in Section 312 of IDOT's *Standard Specifications for Road and Bridge Construction* (IDOT 2021b). CAM II mixture design is based upon trial mixtures and durability (freeze/thaw) testing. There is a minimum cement content of 200 lb/cy for this mixture, but there are no specific strength requirements (IDOT 2012). A desired compressive strength might be 750 to 1,500 psi.

A new HMA stabilized layer can be employed for construction under a JPCP, CRCP, or an unbonded concrete overlay (UBOL) of an existing concrete pavement. HMA stabilized subbases can incorporate recycled materials such as RAP. Before a rehabilitation of an existing asphalt or composite (HMA over PCC) pavement with new HMA, cores are extracted and can undergo tests such as maximum specific gravity test (AASHTO T 209), HWTD testing (AASHTO T 324), bulk specific gravity test, and split tensile test (AASHTO T 283 – Modified Lottman test) (IDOT 2021a). The results for the HWTD must not exceed a rut depth equal to or greater than 0.5 in. (12.5 mm) for a given volume of loading applications based upon different binder grades in **Table 2.**

Table 2. IDOT HMA Hamburg Wheel-Tracking Device Failure Criteria (IDOT 2021b)

Binder grade	Minimum number of passes at 0.5 in. rut depth
PG 58 or lower	5,000
PG 64	7,500
PG 70	15,000
PG 76 or higher	20,000

Note: It may be useful to run every test for 20,000 wheel passes to collect additional data on moisture sensitivity.

In addition to plant-mixed HMA and PCC subbase materials, a mix-in-place stabilization of the support layers can be completed. This mix-in-place technique includes full-depth reclamation (FDR) with cement or asphalt emulsion. Additionally, cold-in-place recycling (CIR) can be performed and act as the stabilized support layer for a concrete overlay. Note that these options are hypothetical and have not yet been used by IDOT on any projects.

Table 3 presents a summary of the different subbase design guides with their strengths and weaknesses. IDOT has a similar procedure as TxDOT (2008), which is selection of one of two stabilized subbase materials (HMA or PCC). IDOT requires that the stabilized subbase must be constructed of HMA for CRCP (BDE Manual Ch. 54-4.02(f) [2021a]).

Table 3. Summary of Subbase Design Guides (adapted from Jung et al. 2012)

Design Guide	Features	Strengths	Weaknesses
IDOT	Select either HMA or PCC stabilized subbase	Historical performance and erosion resistance	Higher cost designs may result
TxDOT	Select either asphalt or cement stabilized subbase; require minimum 7-day strength (cement stabilized)	Historical performance and erosion resistance	Higher cost designs may result
1993 AASHTO	Based on a composite modulus of subgrade reaction that is adjusted for the loss of support due to the foundation erosion	Accounting structural degradation of support due to erosion using the LS factor	k-value obtained from the chart is over estimated and LS is insensitive to various stabilized materials
PCA	Provide erosion factor as a function of the slab thickness, composite k-value, dowel, and shoulder type	Consider erosion analysis in design procedures as the most critical distress in rigid pavement performance	Require more detail discrimination for different stabilization levels
NCHRP 1-37A MEPDG	Classified erodibility of subbase materials for JPCP faulting prediction model as well as erosion under CRCP	Employed the erodibility class based on the type and level of stabilization along with compressive strength	Erodibility class is determined based on dry brush test results and strength even though erosion occurs mostly under saturated conditions

CHAPTER 3: LABORATORY AND PERFORMANCE TESTING OF HMA AND PCC STABILIZED SUBBASES IN ILLINOIS

From the background literature review, the HWTD test suggested by Jung et al. (2009, 2012) was a viable test for assessing the erosion potential of stabilized support layers beneath new concrete pavements and should be able to assess the stabilized HMA layers beneath concrete overlays. The dynamic cylinder test developed by Caicedo and Caro (2016) was also a candidate test but would have required a significant amount of equipment modification and fabrication and thus was not pursued at this time. The HWTD performance test is especially important with HMA and PCC stabilized subbase layers, which include recycled or by-product materials (crushed concrete, RAP, quarry fines) and in-place mixing and stabilization (e.g., FDR or CIR support layers). Additionally, this performance test could be used to evaluate the quality of an existing HMA material for serving as a support layer for a bonded or unbonded concrete overlay.

An evaluation of the standard HWTD test (AASHTO T 324) was conducted to assess the suitability of this method and also determine what needs to be enhanced to have a repeatable performance test. Laboratory specimens (HWTD specimens [2.44 in. thick × 5.91 in. diameter] and 4 × 8 in. cylinders) were cast using the material design methodology in the "PCC Level III Technician Course Manual: Appendix F" for CAM II mixtures following AASHTO R39 (IDOT 2012). These CAM II mixtures were then tested for compressive strengths at 14 days according to AASHTO T22 and tested in the HWTD test after 28 days. HWTD specimens were constructed with only 1 lift and rodded 25 times. Additionally, specimens were tested for split tensile strengths after HWTD testing or coring if dimensions were insufficient for HWTD testing. Testing was conducted according to ASTM C496 for CAM II specimens and ASTM D6931 for HMA specimens (ASTM 2017). Loading rates were adjusted accordingly based on specimen dimensions and each corresponding ASTM standard. Specimens were moist-cured prior to testing. In addition to the lab-made specimens, cores were obtained from four different pavements (different types and subbases) and were also tested using the HWTD test. Cores were obtained from the outer wheel path adjacent to the transverse joint and at the center of the panel not in the wheel path. For more information regarding coring see **Chapter 4**. Material was also obtained from a CIR project on IL 116 in Warren County. The testing protocol and full results are presented in **Appendix A**. **Table 4** provides the list of pavement sections that included coring and HWTD testing, as well as the number of mixtures constructed in the lab with their corresponding identification nomenclature. Additionally, the mixture designs for the corresponding lab mixes can be seen in **Table 5**.

Table 4. Cores or Lab Samples from Field Sections or Lab Molded

Section ID / IDOT Contract ID	County / Location	Pavement Type	HWTD
US 67 (92774)	Sangamon Co./D6	JPCP on CAM II	Y
US 30 (62277)	Cook Co./D1	JPCP on HMA	Y
I-72 EB (72G92)	Sangamon Co./D6	UBOL (asphalt)	Y[1]
IL 53 SB	Will Co./D1	BCOA (asphalt)	Y
IL 116	Warren Co./D4	CIR (asphalt)	Y
Mix 1 (402 and 625)	Lab	CAM II	Y
Mix 2 (409)	Lab	CAM II	Y
Mix 3 (416)	Lab	CAM II	Y
Mix 4 (629)	Lab	CAM II	Y
Mix 5 (701)	Lab	CAM II	Y

[1] HWTD testing was performed on HMA interlayer prior to construction. The mixture did not fail (failure criteria $\geq$ 0.5 in. rut depth) for the required 20,000 cycles.

Table 5. Lab Mix Design Matrix for CAM II Specimens

Trial Mixes	Cement Content, pcy (200-300)	Fly ash content, pcy (60-90)	% Cement (5-9%)	w/cm (0.6-1.6)
Mix 1 (402 and 625)	200	0	5	1.1
Mix 2 (409)	200	0	5.3	0.6
Mix 3 (416)	300	0	9	0.9
Mix 4 (629)	170	60	5	1.1
Mix 5 (701)	245	85	9	0.7

The coarse aggregate used for all lab mixtures was limestone and the gradation is shown in **Figure 10** (in accordance with ASTM C136). The gradation falls under IDOT classification CA-11. This gradation of coarse aggregate calls for a 50–50 percent volume ratio between coarse and fine aggregate within the mixture. The full mixture designs with fresh properties can be reviewed in **Appendix A**.

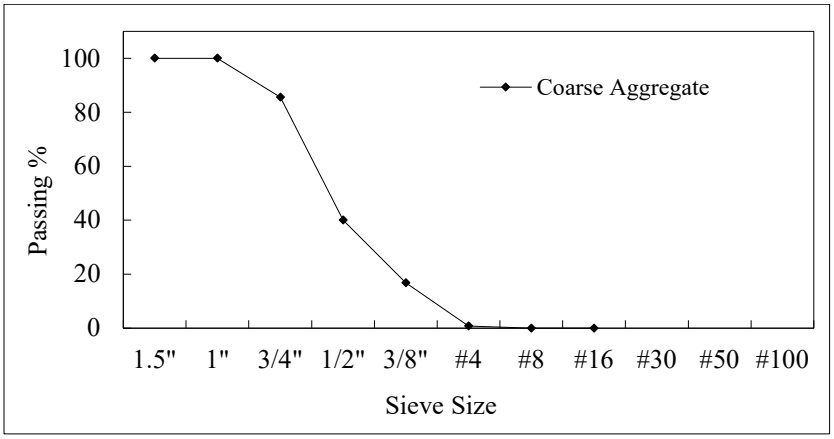

Figure 10. Graph. Coarse aggregate gradation for CAM II mixtures.

HAMBURG WHEEL-TRACKING DEVICE TEST SETUP

To test the erosion resistance potential of different stabilized materials, a fully submerged erosion test using the commercially available HWTD test device simulates conditions similar to in situ pavements. Fully submerged testing conditions help simulate in situ mechanical and hydraulic shear forces generated by varying surface deflections under hard-wheel traffic loading.

The HWTD test uses the same equipment and a similar testing procedure as in Illinois Modified AASHTO T 324. The test consists of using 2.44 in. thick specimens with a diameter of 5.91 in. Two specimens are able to be tested using a single wheel, and the testing frame is capable of testing up to four specimens at the same time. A schematic of the testing frame and setup with four specimens can be seen in **Figure 11a**. Specimens need to be cut appropriately for correct dimensions and for placing two specimens together. The finished surface of the laboratory compacted (HMA) and casted (PCC) specimens should not be tested. Testing the bottom of the compacted (HMA) or casted (PCC) surface allows for testing across a flush surface with negligible anomalies. The testing also allows for obtained cores from in-service pavements. Specimens are inserted into the appropriate molds and placed directly on a rubber pad, to avoid direct contact with the metal frame. Initial testing showed significant degradation at this interface. Additionally, a 158 lb wheel load is applied to the test samples at a 52 rpm load frequency up to 10,000 load repetitions or a maximum erosion depth of 0.5 in. under submerged conditions at a temperature of 122°F. Measurements consist of the depth of erosion at 11 locations versus the number of wheel load passes. In most cases, the maximum deflection occurs at the measuring points 5, 6, and 7, as these locations are the conjoining location between specimens (See **Figure 11b).**

a) HWTD with CAM II specimens

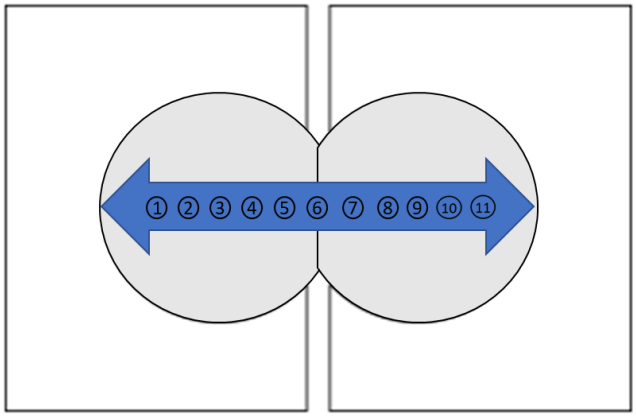

b) Depth measurement points

Figure 11. Photo and Schematic. Hamburg wheel-tracking device test with CAM II specimens prior to testing.

HAMBURG WHEEL-TRACKING DEVICE TESTING RESULTS

The overall results from the testing included both average depth of erosion across the specimen's surface and weight loss. The HWTD results can be presented as maximum erosion depth or the average depth of erosion across the HWTD test specimen. The testing typically ends after the

maximum erosion depth reaches 0.5 in. However, the average depth does not need to exceed this threshold. This study presents the average depth of erosion across the specimen's surface as it provides more information about the entire specimen (reduces the influence of potential voids or other flaws within specimen construction). An example of the average depth of erosion is presented in **Figure 12**, for CAM II Mix #2-409. In addition to the HWTD testing results, compressive strength testing and split tensile strength results are also presented. One component that was not assessed but can significantly contribute to HWTD performance was the density of specimens. From past literature, the denser the compaction levels for a specimen, the more resistant to erosion the specimen becomes (de Beer 1990).

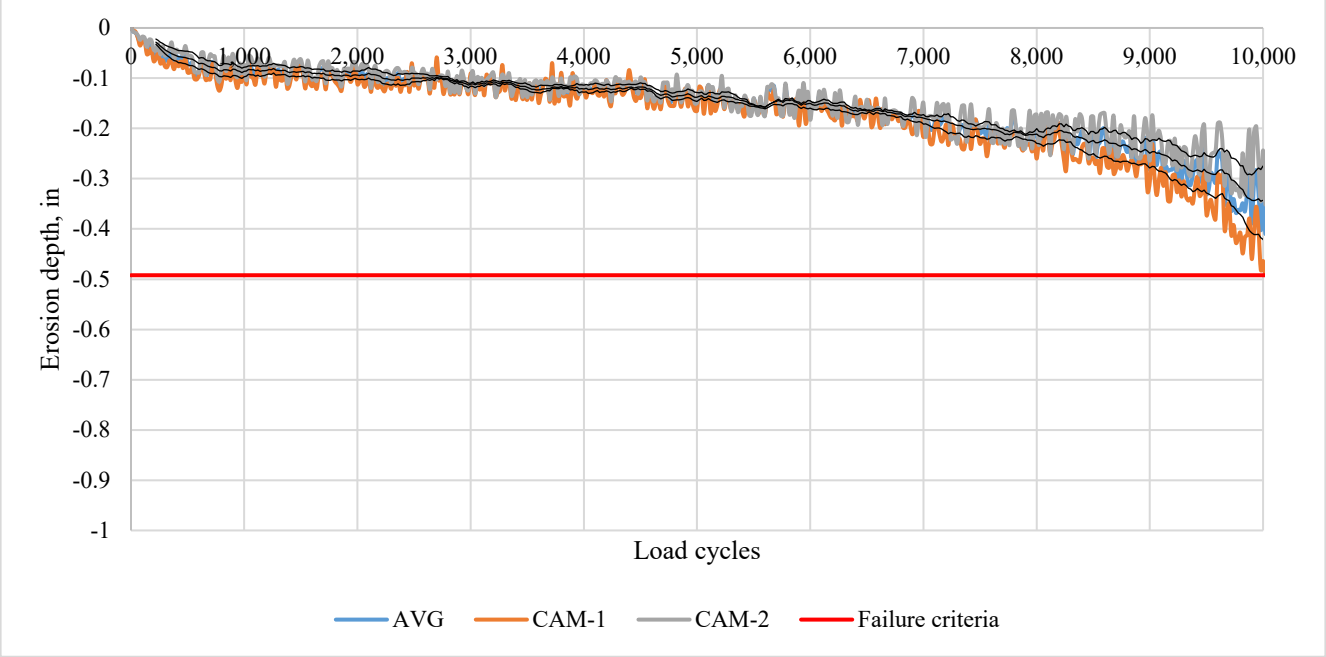

Figure 12. Graph. Hamburg wheel-tracking device test average depth of erosion for CAM II Mix #2-409.

The summary of average depth of erosion after HWTD testing for all specimens can be seen in **Table 6**. The weight loss summary after HWTD testing can be seen in **Table 7**. From this analysis, the greater the materials strength such as compression and tensile (**Table 8** and **Table 9**), the less abrasion, material deterioration, and subsequent erosion is likely. As the percentage of cement increased, the erosion depth decreased. As the upper bound of cement content for the CAM II mixture design guide (IDOT 2012) is reached (9% - Mix #3-416), the least erosion and material loss occurred. The results between Mix #3-416 and cores from US 67 (only in-service CAM II specimens acquired) tested very well in terms of erosion depth and weight loss, returning similar results. **Figure 13** presents the results from the HWTD comparing the average depth of erosion and weight loss.

Table 6. Hamburg Wheel-tracking Device Testing Average Depth of Erosion Analysis Results

	Average depth at 10,000 cycles, in.											
Specimen	Mix 1: 402[1]	Mix 2: 409	Mix 3: 416	Mix 1: 625	Mix 4: 629	Mix 5: 701	US 67	IL 53[2] Lift 1	IL 53[2] Lift 2	US 30 Lift 1	US 30 Lift 2	IL 116[3]
Material	CAM II	CAM II	CAM II	CAM II	CAM II	CAM II	CAM II	HMA	HMA	HMA	HMA	HMA
1	0.49	0.49	0.06	0.06	0.10	0.06	0.01	0.45	0.44	0.23	0.22	0.75
2	0.28	0.35	0.05	0.09	0.12	0.04	0.01	0.33	0.46	0.40	0.42	0.67
3	0.46	0.198	0.06	0.02	0.09	0.01	0.01	-	-	0.44	0.30	0.65
4	0.21	0.17	0.05	0.06	0.21	0.02	0.01	-	-	0.51	0.50	0.47
# of cycles to reach 0.5 in.	10k +	10k +	10k +	10k +	10k +	10k +	10k +	540	540	7.5k	3.5k	7.5k
Average depth at 10,000 cycles, in.	0.36	0.30	0.06	0.06	0.13	0.03	0.01	>0.5	>0.5	>0.5	>0.5	>0.5

[1] Mix 1: 402 was replicated with Mix 1: 625 because initial testing did not include a rubber pad beneath the specimens and resulted in excessive deterioration at the bottom interface. Weight loss was also not measured.

[2] IL 53 cores resulted in only four specimens with appropriate dimensions to be able to conduct HWTD testing.

[3] IL 116 weight loss was not measured before or after HWTD testing.

Table 7. Hamburg Wheel-tracking Device Testing Weight Loss Analysis Results

	Weight Loss, lb.									
Specimen	Mix 2: 409	Mix 3: 416	Mix 1: 625	Mix 4: 629	Mix 5: 701	US 67	IL 53[1] Lift 1	IL 53[1] Lift 2	US 30 Lift 1	US 30 Lift 2
Material	CAM II	CAM II	CAM II	CAM II	CAM II	CAM II	HMA	HMA	HMA	HMA
1	-	0.037	0.091	0.140	0.049	0.025	0.097	0.283	0.011	0.058
2	-	0.035	0.117	0.175	0.048	0.027	0.072	1.400	0.053	0.045
3	0.151	0.040	0.100	0.154	0.034	0.026	-	-	0.026	0.017
4	0.127	0.030	0.111	0.211	0.038	0.023	-	-	0.032	0.061
Average	0.139	0.035	0.105	0.170	0.042	0.025	0.085	0.842	0.031	0.045
Std. Dev.	0.012	0.003	0.010	0.027	0.006	0.002	0.012	0.559	0.015	0.017

[1] IL 53 cores resulted in only four specimens with appropriate dimensions to be able to conduct HWTD testing.

Note: Mix 1: 402 was not weighed due to excessive deterioration at bottom interface.

Note: IL 116 weight loss was not measured before or after HWTD testing.

Table 8. CAM II Compressive Strength Results

	Compressive Strength, psi					
Batching date	4/2/2021	4/9/2021	4/16/2021	6/23/2021	6/29/2021	7/1/2021
Mix ID	Mix 1: 402	Mix 2: 409	Mix 3: 416	Mix 1: 625	Mix 4: 629	Mix 5: 701
14-day testing date	4/16/2021	4/23/2021	4/30/2021	7/7/2021	7/13/2021	7/15/2021
Specimen 1	682	637	1337	830	381	852
Specimen 2	605	560	1305	820	312	816
Specimen 3	622	581	1316	734	351	969
Average f'c	636	593	1320	795	348	879
Std. Dev.	40.3	39.9	16.3	52.4	34.6	79.9

Table 9. Split Tensile Strength Results after Hamburg Wheel-tracking Device Testing

	Split Tensile Strength, psi										
Specimen	Mix 1: 402	Mix 2: 409	Mix 3: 416	Mix 1: 625	Mix 4: 629	Mix 5: 701	US 67	IL 53 Lift 1	IL 53 Lift 2	US 30 Lift 1	US 30 Lift 2[4]
Material	CAM II	CAM II	CAM II	CAM II	CAM II	CAM II	CAM II	HMA	HMA	HMA	HMA
1	153	–	318	143	85	252	437	47[2]	72.3	54.2[3]	–
2	182	–	320	117[1]	77	220	483	101	80.2	49.8[3]	22.5[3]
3	131	95.7	298	146	82	206	502	56[2]	–	70.4	54.6
4	–	121	343	161	75	213	440	–		83.2	73.5
Average	155	108	320	150	80	223	465	101	76	77	64
Std. Dev.	21.1	12.6	16.0	7.9	4.0	17.9	28.1	0.0	4.0	6.4	9.4

[1] Specimen had edge failures from HWTD prior to split tensile strength testing.

[2] User error, operator failed specimen when seating the load by applying max load instantaneously.

[3] Loading machine was not working properly and the loading rate did not reach the required range specified in ASTM D6931.

[4] Lift 2 was comprised of 1.5 in. of Lift 1 + 1 in. of a different mix.

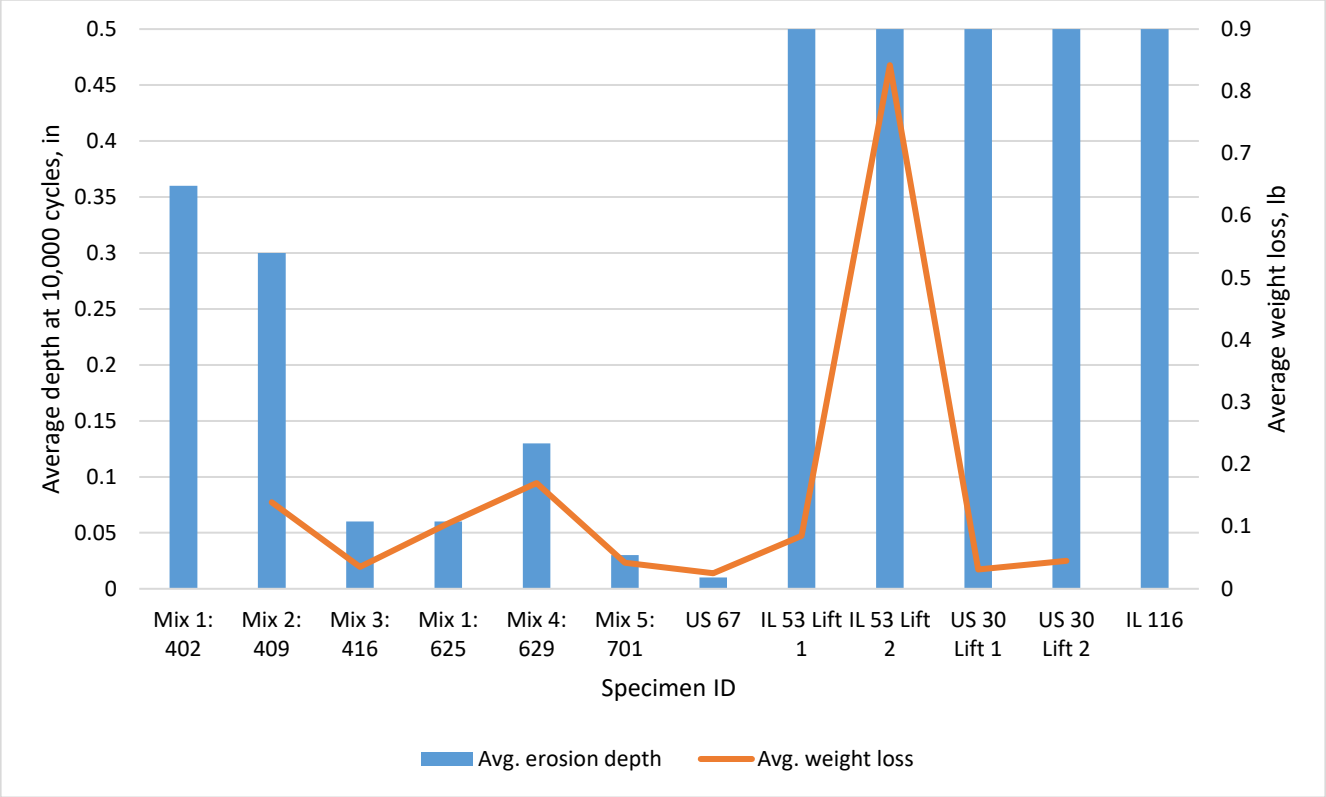

Figure 13. Graph. Hamburg wheel-tracking device results comparison between average erosion depth vs average weight loss. Note: weight loss was not recorded for Mix 1: 402 and IL 116 (CIR).

An example of specimens from a poor mixture design (Mix #2 – 409) that failed the HWTD test can be seen in **Figure 14**. All testing results can be seen in **Appendix A**. Some of the test results showed a fluctuation of erosion depth with the number of wheel passes, which is likely attributed to large aggregates being dislodged from the matrix. These testing conditions represent worst-case scenario moisture conditions, which is poor drainage, saturated moisture state, and repeated loading with high contact stress.

Figure 14. Photo. Hamburg wheel-tracking device test with Mix 2 – 409 CAM II specimens after testing.

The results also provided good indications of the level of rutting and erosion potential of existing HMA stabilized layers that are bonded concrete overlay of existing asphalt (BCOA) or unbonded concrete overlay (UBOL) of existing concrete or composite pavement candidates. The HWTD test results indicated the existing HMA for IL 53 was in poor condition and partially explains the significant distress experienced by this section (**Figure 15**). These results indicate the HWTD test, if performed, could have been informative on the poor condition of the existing HMA.

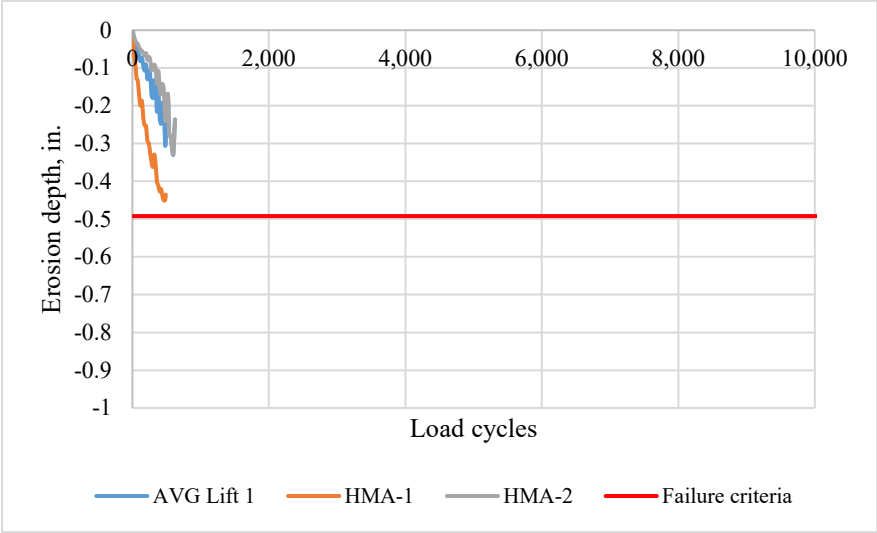

Figure 15. Graph. Hamburg wheel-tracking device test results for IL 53 BCOA.

CHAPTER 4: FIELD TESTING OF HMA AND PCC STABILIZED SUBBASES, EXISTING HMA, AND NEW HMA INTERLAYERS BENEATH CONCRETE PAVEMENTS

Multiple concrete pavement sections owned by IDOT that have different stabilized support layers (HMA and PCC) and service lives were identified in order to perform FWD testing to backcalculate the k-value, effective thickness (h_{eff}), and slab-subbase interface friction of the in situ pavement structure. The overwhelming majority of IDOT concrete pavements are constructed either directly on an aggregate layer (e.g., urban sections with curb and gutter) or on a HMA stabilized subbase. There are a limited number of JPCP with PCC stabilized subbase, e.g., U.S. 67 near Jacksonville.

Field testing consisted of FWD testing with concrete temperature profile measurements, ultrasonic tomography MIRA scanning, manual distress surveys, and coring. For the sections tested, MIRA testing was conducted to complement the FWD tests. MIRA can enable rapid estimation of the slab thickness, joint details (dowels and tie bars), and potentially the subbase layer thickness. Coring was also performed on each of the different stabilized support layers (four sections) for thickness and HWTD specimens. A compiled list of the twelve sections examined is presented in **Table 10** and the distribution of sections throughout the state of Illinois can be seen in **Figure 16**. In addition to the test sections outlined below, samples were also obtained from a CIR project in District 4 for laboratory performance testing. No FWD or MIRA testing was performed for this CIR section.

Table 10. Illinois Field Sections for Multiple Stabilized Base Layers Nondestructive Testing, Visual Survey, and Coring

Section ID/ IDOT Contract ID	County/ Location	Pavement Type	Field Testing			
			FWD	MIRA	Coring	Distress Survey
US 67 (92774)	Sangamon Co./D6	JPCP on CAM II	Y	Y	Y	Y
I-72 (92763)	Pike Co./D6	JPCP on CAM II	Y	Y	–	Y
US 20 (40455E & H)	Stephenson Co./D2	JPCP on CAM II	Y	Y	–	Y
US 30 (62277)	Cook Co./D1	JPCP on HMA	Y	Y	Y	Y
IL 64 (62410)	DuPage Co./D1	JPCP on HMA	Y	Y	–	Y
US 12/20/45 (60927/60748)	Cook Co./D1	JPCP on HMA	Y	Y	–	Y
I-72 EB/WB (72G92)	Sangamon Co./D6	Thin UBOL	Y	Y	Y	Y
I-70 (70044)	Clark Co./D7	CRCP UBOL	Y	Y	–	Y
IL 53 SB (60N05)	Will Co./D1	BCOA	Y	Y	Y	Y
IL 116 (CIR)	Warren Co./D4	CIR	–	–	Y	–
E-15 Parking Lot	Champaign Co./D5	BCOA	Y	Y	–	Y
McKinley Parking Lot	Champaign Co./D5	BCOA	Y	Y	–	Y

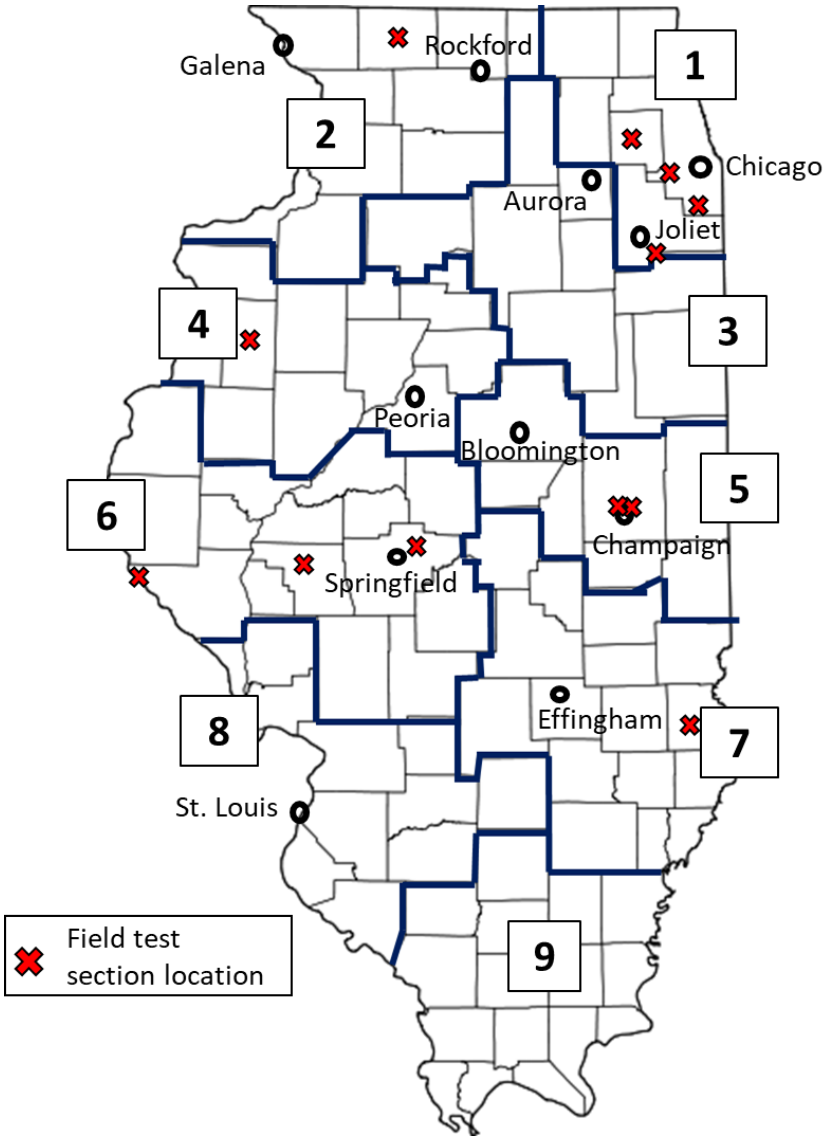

Figure 16. Photo. Map of all field testing sections for assessing stabilized support layers under concrete pavements.

FALLING WEIGHT DEFLECTOMETER ANALYSIS

FWD testing followed standard IDOT testing protocol but for this project, intensive testing was performed on five adjacent concrete panels at 10 distinct slab locations along the pavement section. This intensive testing can potentially show the variability within a 75 ft section versus testing at 100 to 250 ft intervals along the entire pavement section. The full testing protocol is described in **Appendix B**. Additionally, historical FWD testing was analyzed and compared with the testing performed for this study. A detailed FWD analysis for each section is presented in **Appendix C**.

Additional testing was conducted in May 2021 on two bonded concrete overlays of asphalt (BCOA) parking lots located on the University of Illinois Urbana-Champaign (UIUC) campus: E-15 and McKinley Health Center Lots. Fifteen adjacent slabs were tested on four sections for E-15 and three

sections in the McKinley lot. At each test location, target loads of 6, 9, and 12 kips were applied and the resulting slab deflections were measured with transducers located around the loading plate. This testing protocol followed historical testing conducted by Roesler et al. (2008) and King and Roesler (2014). As seen in **Figure 17**, the transducer spacings are: D0=0", D1=12", D2=24", D3=36", D4=12" Behind, D5=12"Right, D6=12"Left.

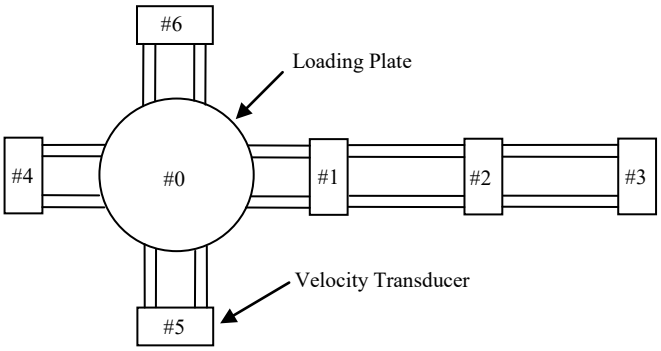

Figure 17. Schematic. Additional FWD testing sensor layout for parking lots.

Standard backcalculation procedures were applied for the majority of sections (JPCP with conventional joint spacing) based on an infinite slab assumption. However, for the concrete overlays with shorter joint spacing, the backcalculation procedure developed by King and Roesler (2014) was employed. Additionally, the method for backcalculation of CRCP developed by Zhang and Roesler (2018) and Zhang et al. (2020) was used and compared with existing methods.

FALLING WEIGHT DEFLECTOMETER RESULTS

The results and analysis of each section are presented in **Appendix C**. In general, all sections in **Table 10** are performing well and have exhibited negligible changes in deflections, joint load transfer efficiency (LTE), and the modulus of subgrade reaction (k-value). In summary, **Table 11** provides FWD highlights for each section from the most recent FWD testing in 2020 and 2021. The testing suggests that the stabilized subbases are performing as intended and are not leading to premature failure of the concrete pavements. However, the one BCOA section (IL 53 [60N05]) is showing significant levels of distress as this was a thin inlay and is experiencing a larger truck traffic volume than originally designed. In addition, the HWTD testing performed on the HMA showed significant deformation and did not pass the HWTD criteria by IDOT presented in **Table 2**.

Table 11. FWD Analysis Summary Results of Testing in 2020 and 2021 for 9 kip Normalized Deflections

	Average Results			
	D0* (mils)[1]	LTE (%)[2]	h_{eff} (in.)[3]	k-value (psi/in.)
US 67 (92774)	2.44	89.4	11.4	106
I-72 (92763)	2.80	91.7	9.84	105
US 20 (40455E)	2.88	90.4	8.20	168
US 20 (40455H)	5.30	80.5	7.23	73.8
US 30 (62277)	2.71	92.2	10.2	101
IL 64 (62410)	1.64	89.8	10.5	263
US 12/20/45 (60927)	1.77	88.9	9.62	274
US 12/20/45 (60748)	1.54	86.9	9.83	488
I-72 EB (72G92)	3.54	88.2	8.04	198
I-72 WB (72G92)	4.48	74.3	7.25	125
I-70 (70044)	1.15	89.9	10.5	1000+
IL 53 SB (60N05)	6.42	79.9	4.66	242
IL 116 (CIR)	–	–	–	–
E-15 Parking Lot	12.2	79.7	3.97	113
McKinley Parking Lot	13.1	76.7	3.64	121

[1]D0* is the normalized 9-kip maximum deflection at the center of the panel.

[2]LTE is the transverse joint load transfer efficiency.

[3]h_{eff} is the effective thickness of the PCC and stabilized support layer (subbase, existing HMA, or interlayer).

US 67 (92774) is performing well and FWD results are consistent with testing 4 years prior. I-72 (92763) is performing very well with slight decreases in deflections, which were likely a function of thermal effects. US 20 (40455) Section E is performing well and has exhibited no change since the last FWD testing in 2017. However, Section H appears to be experiencing wider joint widths causing a decrease in LTE and also exhibiting higher center slab deflections (5.3 mils) in comparison to testing performed in 2017 (3.13 mils). High thermal gradients present during testing could result in the center of the slab to be more unsupported. Section E was tested first thing in the morning when zero gradient was present. However, as testing began for Section H, a positive temperature differential of 7°F (11 AM) and 12°F (1:30 PM) was present with the surface temperature exceeding 100°F.

US 30 (62277) also experienced an increase in average normalized 9 kip center slab deflections (2 mils in 2017 and 3 mils in 2020). This is also likely related to environmental conditions as testing in 2017 was performed in November, whereas testing was performed in August of 2020. Although deflections show an increase, the LTE across the transverse joints remains very good (greater than 90% on average). IL 64 (62410) was tested in late Spring of 2018 and showed little change in terms of deflections and LTE in September 2020. Deflections on average are less than 2 mils and LTE is about 90%, indicating good performance. US 12/20/45 (60927 & 60748) was tested in October 2018 and showed little change in terms of deflections and LTE in September 2020. Deflections on average are less than 2 mils and LTE is approximately 90%, indicating good performance. I-70 (70044) did not have any historical performance data for comparison. This section is performing well with deflections less than 1.5 mils (as expected for a CRCP). The LTE of the lane shoulder joint in the eastbound direction is significantly lower than westbound (77% versus 90%, respectively). More punchouts

(patched and unpatched) were observed in the eastbound direction along this joint and is likely associated with one another. IL 53 southbound was exhibiting medium to high severity distress in the driving lane specifically the outer wheel path. The deflections at the middle of the panel between the center panels and right panels were 6.4 mils and 7.5 mils, respectively. Additionally, the LTE across the transverse joint was similar between the center panel and right panels (78% and 77%, respectively). However, the deflections across the transverse joint were 1.5 mils larger in the right panel (6.5 mils in the center panel and 8.1 mils in the right edge panel). It is likely the existing pavement was not the same width as the overlay, resulting in less structural support of the right edge panels in the overlay.

In general, the backcalculated k-values were very consistent between the different dates of testing. However, the effective thicknesses were not consistent, as these values are a function of different environmental conditions present during testing. As all testing in 2020 was performed in August or September, the temperatures were near the maximum values within the year in Illinois. Whereas testing performed in previous years was conducted either in the late fall or spring. Sections with an HMA stabilized layer will result in a greater fluctuation in effective thickness as a function of the stiffness of the HMA. Additionally, all sections resulted in low predicted friction between the concrete and stabilized support layer.

The specific case, I-72 eastbound (72G92), has developed a significant increase in deflections in all locations. This can be a function of the stiffness of the HMA interlayer. However, evidence of stripping and erosion of this interlayer could be the reason for the increase in deflections and decrease in LTE. Center deflections have increased from 2.4 mils in 2016 to 3.5 mils in 2020. I-72 westbound (72G92) has exhibited similar deflections as experienced shortly after construction. Although these deflections are larger in magnitude compared to eastbound (4.0 mils in 2016 and 4.5 mils in 2020), no cracking has been exhibited in westbound. Additionally, LTE values are consistent between the two dates of testing and are approximately 75%. Both eastbound and westbound sections are exhibiting some longitudinal faulting across the lane shoulder longitudinal joint (shoulder greater elevation than driving lane). The LTE across this joint is highly variable and on average is 45%. The macro-fibers present in the concrete and across the contraction joint are mostly sheared or pulled out and not contributing to LTE.

In addition to the testing conducted in 2021, previous testing results presented in Roesler et al. (2008) and King and Roesler (2014) were compared with the most recent testing for the UIUC parking lots. The corresponding testing locations within a given section between dates cannot be confirmed as the exact same slabs, but the general location is the same. The backcalculation averages for joint load transfer, k-value, effective thickness, and the temperature during the different dates of testing can be seen in **Appendix C**. The average transverse joint and longitudinal joint LTE did not appear to change very much over the years since the original construction dates. All joint LTE averages are above 70%. The effective thickness has significantly decreased, indicating a decrease in bond between the PCC and existing HMA, see **Table 12**. This would be expected especially for how thin these sections are and their expected service life. Overall, these parking lots are still in great shape and have been proven to be a great cost-effective option for rehabilitation with negligible to zero maintenance requirements.

Table 12. UIUC Parking Lots FWD Backcalculation Analysis Results of Average k-value and Effective Thickness

Project/Section		Date	Average Modulus of Subgrade Reaction, k (psi/in.)	Average Effective Slab Thickness (in.)	Thickness Standard Deviation (in.)	Design Thickness: PCC + AC = Total (in.)
McKinley Lot	Northeast	2008	197	5.06	0.475	3.5+4 = 7.5
		2012	241	5.52	0.938	
		2021	114	3.06	0.280	
	Northwest	2008	279	6.63	0.603	
		2012	291	7.23	1.30	
		2021	126	3.94	0.415	
	Southeast	2008	421	6.89	0.583	
		2012	324	7.45	2.35	
		2021	124	3.91	0.423	
E-15	Northeast (1)	2008	182	5.71	0.603	3.5+2.5=6
		2012	152	5.81	0.963	
		2021	97.5	4.18	0.953	
	East (2)	2008	241	6.20	0.617	
		2012	202	5.80	0.810	
		2021	129	4.13	0.555	
	Southeast (3)	2008	200	6.66	2.07	
		2012	186	6.62	1.46	
		2021	116	3.91	0.273	
	Northwest (4)	2012	202	5.94	0.666	
		2021	109	3.66	0.309	

FWD Example: US 67 (92774)

A summary of the FWD testing performed in 2016 and 2020 is provided. Additional analysis and plots are included for comparison in **Appendix C**.

Table 13. FWD Summary from Normalized Center Slab Deflection and Foundation Layer Stiffness for US 67 (92774)

	10/27/2016						9/9/2020					
Parameter	D0* (mils)		Area_36 (in.)		Eri		D0* (mils)		Area_36 (in.)		Eri	
Direction	NB	SB	NB	SB	NB	SB	NB	SB	NB	SB	NB	SB
Average	2.26	2.33	31.7	31.3	15.5	15.3	2.42	2.45	31.5	31.3	14.4	14.4
Std. Dev.	0.29	0.41	1.42	1.21	1.55	1.58	0.34	0.45	1.32	1.10	1.03	1.52
COV	12.8	17.6	4.5	3.9	10.0	10.3	14.1	18.5	4.18	3.51	7.19	10.6

Table 14. FWD Summary for Normalized Deflection (D0*) and Leave Joint LTE for US 67 (92774)

	10/27/2016				9/9/2020			
Parameter	D0* (mils)		LTE (%)		D0* (mils)		LTE (%)	
Direction	NB	SB	NB	SB	NB	SB	NB	SB
Average	4.8	4.7	86.4	87.7	3.51	3.33	89.6	89.2
Std. Dev.	1.05	1.02	6.76	5.85	0.58	0.50	5.90	7.03
COV	21.8	21.9	7.82	6.68	16.6	14.9	6.59	7.89

ULTRASONIC MIRA ANALYSIS

In addition to FWD testing, an ultrasonic evaluation of the pavement structure using MIRA was employed. MIRA is a portable commercial ultrasonic tomography device that contains a multi-phase array of 4 × 12 transducers. This arrangement can obtain tomographic information from a small section of the concrete pavement, about 12 in. in length (transducers are spaced approximately 1 in. on center). The equipment evaluates the small section of concrete pavement beneath the device, analyzes the ultrasonic response, and presents a tomographic image in under 5 seconds (Hoegh et al. 2011).

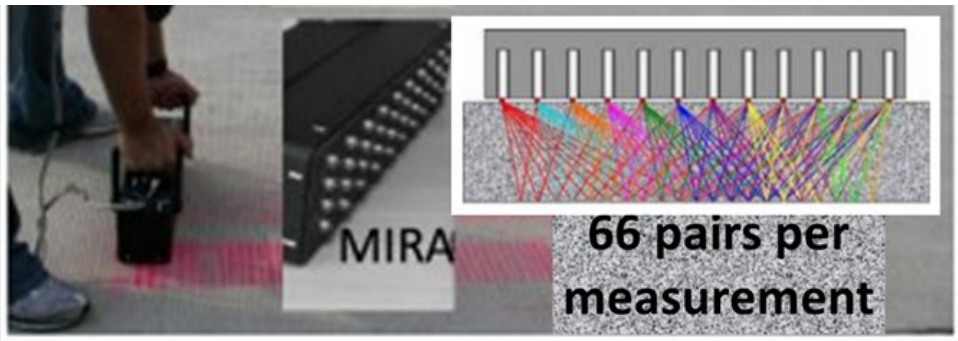

Figure 18. Photo. Ultrasonic tomography device (MIRA) used during field investigations.

This multi-array ultrasonic tomography device works by sending multiple ultrasonic shear waves through the concrete slab and recording the received direct, reflected, and diffracted signals. The received signals are interpreted as the distance from the surface to a change in the surveyed element, which includes voids, a different material, change in density, or any other component that reflects the ultrasound waves (Popovics et al. 2017). The recorded ultrasonic image can be used to detect slab thickness, dowel and tie bar placement (depth and spacing), and whether a contraction joint is activated. **Figure 19** shows an example of the tomographic image taken from a specific project and its interpretation.

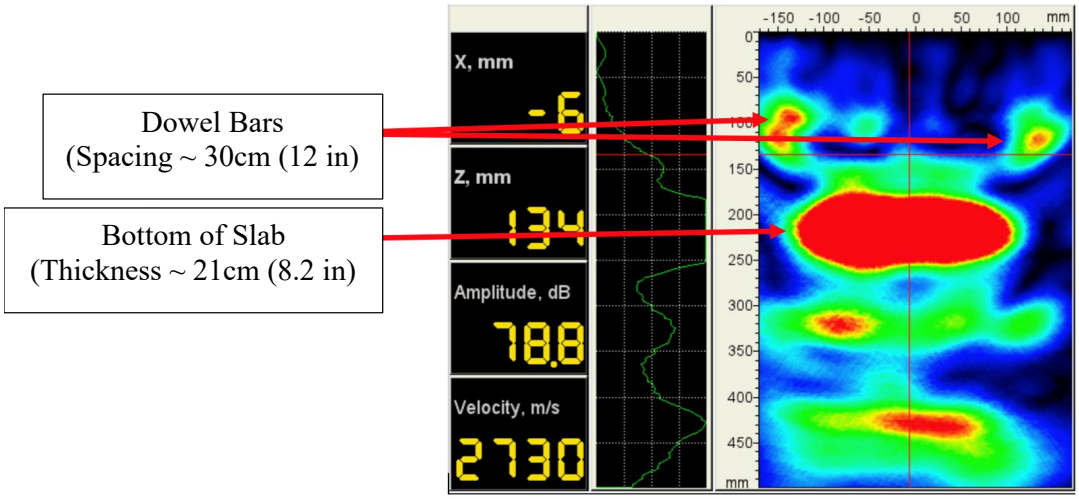

Figure 19. Photo. Ultrasonic tomographic image from example concrete pavement section.

The MIRA device was utilized in conjunction with the FWD testing. MIRA scanning was conducted for 3–4 subsections out of the 10 FWD intensive testing sections. MIRA scanning followed the intensive testing pattern of the FWD, consisting of five adjacent joints/panels with repeatability testing of 3–5 scans per location. The full testing protocol can be seen in **Appendix B** and the results for each section can be found in **Appendix D**. The objective of the intensive testing using the MIRA device was to determine the following:

- Surface layer thickness, presence and thickness of base, cracks/defects, or delamination;
- Joint details (presence of dowels and tie bars);
- Transverse joint activation; and
- Kissing bond or degree of interface bond between slab and stabilized support layer.

Surface Layer and Subbase Thickness

One of the main functions of MIRA is estimating the concrete layer thickness and possibly the stabilized subbase layer thickness. It is not always possible to determine the thickness of the stabilized layer beneath the concrete from the signal reconstruction. The depth could be too large, the transmission of wave energy across the interface could be low, or the material itself could be eroding. Thinner pavement sections, such as an unbonded overlay with an asphalt interlayer (e.g., I-72 eastbound) recorded and depicted the cross-sectional image from the device (B-scan). Additionally, if the material properties between the two different layers are similar (e.g., when an asphalt layer stiffness is similar to concrete), the wave velocities for penetration are the same and can result in prediction of one very thick layer. This can also indicate a fully bonded interface with similar layer material properties.

To assess the layer thicknesses, an evaluation of the MIRA B-scans conducted for each pavement section was performed. Each B-scan was analyzed to estimate the concrete layer thickness. When the stabilized subbase was depicted within the B-scan, the thickness was recorded. However, the thicknesses for this layer was not always apparent. Additional comments were provided if there were any anomalies within the B-scans that were indicative of potential poor consolidation (honeycombing) within the concrete, horizontal cracks or defects, delamination or potential debonding, and/or observations regarding reinforcement details.

Joint Activation

Joint activation early in the service life (after saw-cutting has been performed) is important to prevent premature cracking that develops from internal stresses exceeding the concrete strength. When a contraction joint does not activate, this causes an increase in the effective slab length and an increase in the load and environmental tensile stresses in the slab. As these tensile stress levels approach and exceed the concrete strength, a crack may develop away from the intended contraction joint location. Additionally, the increased effective slab lengths will generate wider joint openings at active joints as a function of temperature and moisture changes. These wider joint openings can result in increased friction stresses between the concrete pavement and the supporting layer, and potentially increase the susceptibility of erosion of the subbase layer.

To assess the joint activation in the field, Tran and Roesler (2020) developed an algorithm that uses the MIRA shear wave response across the theoretical plane of the contraction joint. The algorithm uses the received signal energy from specific transducer pairings and calculates a normalized transmission energy (NTE) quantity. From the energy analysis, sensor pairings 2–7 and 2–11 resulted in the best prediction of whether a joint was activated for concrete overlays. In addition to the optimal transducer pairings, a hyperplane model was defined that separates an activated joint with a crack (below the hyperplane) and a joint that has been sawed but is not activated (above the hyperplane). The MIRA sensor pairings and hyperplane equation are based primarily on NTE and observations from bonded concrete overlays of asphalt, where the concrete thickness was less than 6 in. and sawcut notch depth was 25% to 33% of the slab thickness.

Slab-Subbase Interfacial Bond Assessment

Significant effort was spent developing and testing potential algorithms to determine the interfacial conditions between the concrete surface layer and the stabilized subbase layer. The initial work included past research studies of flaw detection using nondestructive ultrasonic testing. Detecting flaws may be indicative of a delamination or horizontal crack and could provide overall interfacial friction conditions between two materials in contact.

The slab-subbase interface bond problem includes knowing the material properties of the different layers, thickness of each layer, and acoustic impedance. It is possible that if the pavement structure is too thick, the MIRA device is not large enough to be able to transmit and receive sufficient reflection waves. The following techniques from previous research studies were assessed for potential use and or expansion to determine the interfacial conditions using the ultrasonic tomography MIRA device. The different techniques are further explained in **Appendix D**.

1. Image analysis and color intensity
2. Normalized transmission energy (Tran and Roesler 2020)
3. Pearson's correlation coefficient
4. Hilbert Transform Indicator (HTI)
5. Snell's Law—Bonding Degree Index (BDI)

Although extensive data collection and analysis was performed, a final algorithm was not validated, and work continues by the researchers on a proposed methodology and algorithm.

MIRA Example US 67 SB

An example of the MIRA results for the PCC thickness of US 67 SB (92774) can be seen in **Figure 20.**

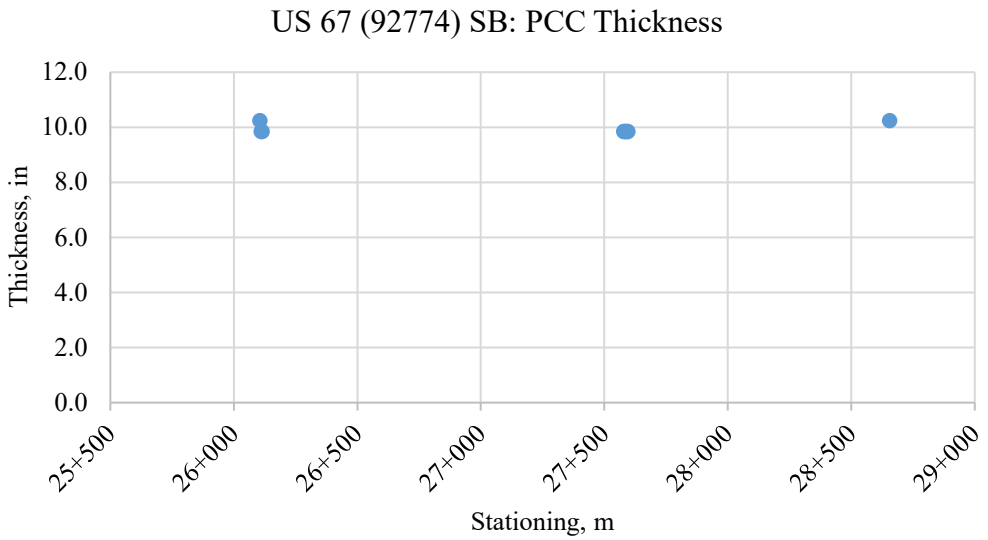

Figure 20**. Graph. US 67 SB PCC thickness results obtained from MIRA.**

CORING OBSERVATIONS AND ANALYSES

Coring was performed on four projects containing five different support layers. The four pavement projects with five support layers are summarized in **Table 15**. The objectives of coring these pavement sections were to determine layer thicknesses, compare MIRA estimated thickness with the cores, assess the interface between the concrete and the stabilized subbase (bonded, unbonded, partially bonded, erosion occurring, etc.), and finally, test the support layer using the HWTD device.

Table 15. Details of Project Sections Cored

Section ID	Date Cored	Pavement Type	Support Layer (Base Type)	Stationing for Coring
US 67 (92774)	5/13/2021	JPCP	CAM II	26+000 NB, 28+600 NB, 26+600 SB
US 30 (62277)	11/20/2020	JPCP	HMA Stabilized	8+00 EB, 95+00 EB, 56+00 WB
I-72 EB UBOL	12/10/2020	UBOL	HMA IL (new)	15+47 EB, 20+00 EB, 80+00 EB
I-72 EB UBOL[1]	6/10/2021	UBOL	HMA IL (new)	14+02 EB, 75+30 EB, 150+50 EB; 145+57 EB, 145+75 EB
I-72 WB UBOL	12/10/2020	UBOL	Fabric IL (new)	142+50 WB, 102+50 WB
IL 53 SB[2]	11/23/2020	BCOA	Existing HMA	5+70 SB, 61+10 SB, 101+50 SB

[1] Coring in 2021 was performed directly over the transverse joint in the wheel paths of the driving lane to assess longitudinal cracking at 14+02 EB, 75+30 EB, and 150+50 EB. Coring was performed over the longitudinal lane-shoulder joint to assess longitudinal faulting at 145+57 EB and 145+75 EB.

[2] No stationing: Assumed 0+00 at intersection of West Hoff Road and IL-53 and increased heading south to West Arsenal Road.

Coring was performed both in the outer wheel path on the leave slab near the transverse joint and near the center of the same slab of the driving lane. The leave joint in the outer wheel path was assumed to be where any erosion or pumping would be occurring or initial signs of distress. The center slab location was also extracted since it should be a position where susceptibility of erosion or pumping would be very low. The coring protocol and locations for each corresponding section can be found in **Appendix E**.

Additionally, a coring plan was developed to further characterize the distress occurring on I-72 (both eastbound and westbound). On I-72 eastbound (HMA interlayer), cores were obtained in the outer wheel path on the approach slab as well as on the leave slab away from the wheel path. These locations were selected to assess if permanent deformation was occurring in the HMA in the wheel path and causing longitudinal cracking to initiate in the concrete overlay at the transverse joint. Similarly, to identify the mechanisms causing the difference in elevation along the longitudinal joint between the driving lane and shoulder on I-72 westbound with a nonwoven geotextile fabric interlayer (shoulder elevation greater than the driving lane by approximately 0.16 in.), cores were taken in the shoulder, outer wheel path in the driving lane, and offset from the wheel path in the driving lane. Several mechanisms contributing to the faulting are the 0.125 in. thick fabric in the wheel path of the driving lane has partially collapsed causing this elevation difference between the driving lane and shoulder and there may be some erosion of the asphalt subbase layer in the shoulder.

Coring results indicated some signs of erosion occurring beneath one of the older JPCP sections without the development of any surface distresses. Cores obtained in the center of each panel from US 67 with the CAM II subbase were fully bonded with the stabilized layer for two out of three

locations; the third location was not bonded and showed signs of delamination within the coring hole, but no erosion was occurring to the CAM II surface. However, all cores obtained in the outer wheel path were debonded and core hole observations showed delamination at the interface. One location showed visible signs of erosion, as seen in **Figure 21**. Although debonding and surface erosion was present in the subbase layer, there were no visible surface distresses in these locations, particularly with the presence of dowels at the transverse joints.

The coring results for all sections are presented in **Table 16**, along with the design thicknesses. Detailed information and coring results regarding each section can be seen in **Appendix E**. All cores obtained from US 30 with the HMA subbase in the center of each panel and outer wheel path were fully bonded. All cores obtained from I-72 eastbound locations with the HMA interlayer were fully bonded to the concrete overlay and debonding of the core occurred between the interlayer and the original concrete pavement (CRCP). For the cores obtained from I-72 westbound with the fabric interlayer, the cement paste penetrated the fabric and adhered to the concrete overlay, and there was no bond between the fabric interlayer and existing concrete pavement, except for one location in the shoulder. The tack coat in this location was heavily applied and impregnated into the fabric. The fabric interlayer in the wheel path appeared to be more compressed than the shoulder and non-wheel path areas. However, the difference in compression between the wheel path and shoulder (approximately 0.02 in.) does not equate for the entire difference in elevation across the longitudinal joint (approximately 0.16 in.). Further coring over the longitudinal joint through the entire depth of the existing CRCP is recommended to determine the mechanism occurring.

In addition to the coring results from I-72 eastbound, a special project investigation resulted from the developing distress. DeSantis and Roesler (2022) investigated the cause of the longitudinal cracking occurring directly over the transverse joints and longitudinal joint faulting occurring along the lane-shoulder longitudinal joint (shoulder elevation on average was approximately 0.5 in. greater than the driving lane). This study included coring directly over the intersection of the longitudinal cracking in the wheel paths of the driving lane and the transverse joints. The coring showed significant stripping and erosion of the HMA interlayer, thus leading to the longitudinal cracking in the wheel paths. Additionally, coring directly over the longitudinal lane-shoulder joint showed stripping and erosion was also occurring along this joint and resulting in the shoulder elevation to be greater than the driving lane.

An additional section that showed evidence of erosion was IL 53. All concrete cores extracted from IL 53 with the existing HMA pavement in the center of each panel were fully bonded. One location at the beginning of the project was fully bonded at the PCC/HMA interface but debonded between HMA lifts. This interface was smooth without signs of erosion. This also occurred in two of the three locations along the leave joint. The third leave joint location was debonded at the PCC/HMA interface and exhibited features of erosion at this location.

a) US 67 SB 26+600 outer wheel path coring hole

b) US 67 SB 26+600 outer wheel path core (CAM II potentially eroded surface on left)

Figure 21. Photos. US 67 SB 26+600 outer wheel path core with erosion.

Table 16. Field Coring Summary

Section ID	Concrete			Subbase		
	Design Thickness, in.	Core Thickness, in.		Design Thickness, in.	Core Thickness, in.	
		Average	Std. Dev.		Average	Std. Dev.
US 67 SB & NB	10	10.1	0.09	4	4.04	0.42
US 30 EB & WB	9.75	10.2	0.38	4	6.40	1.02
I-72 EB[1]	6	6.43	0.28	1.25	1.46	0.08
I-72 WB	6	6.32	0.25	0.125	0.12	0.01
IL 53 SB	4	4.25	0.41	6-10	5.08	1.14

[1] I-72 EB coring results from 2020 coring.

DISTRESS SURVEY ANALYSIS

A detailed distress survey was performed for each pavement section. The detailed distress survey was conducted at each of the extensive FWD testing locations, which was approximately 100 to 200 ft. **Table 17** provides a summary of the presence and type of major distresses observed for each corresponding pavement section. In summary, sections with a PCC stabilized subbase layer exhibited signs of erosion, which seemed to be manifested in distresses at poor drainage locations. Sections with an HMA stabilized subbase layer resulted in minimal to no observed distress. Concrete inlays with existing HMA used as support layers (e.g., IL 53) appear to be developing stripping, debonding, and potential erosion related surface distresses.

Table 17. Distress Survey Summary

Section ID/ IDOT Contract ID	County/ District Location	Pavement Type	Year Constructed	Major Distress Present (Y/N)	Type of Major Distress Present	Erosion Related Distress (Y/N)
US 67 (92774)	Sangamon Co./D6	JPCP on CAM II	1999	Y	Joint deterioration (ASR)	N[1]
I-72 (92763)	Pike Co./D6	JPCP on CAM II	1999 and 2000	Y	Longitudinal cracking near poor drainage locations	Y
US 20 (40455E&H)	Stephenson Co./D2	JPCP on CAM II	1996	Y	Longitudinal cracking near poor drainage locations	Y
US 30 (62277)	Cook Co./D1	JPCP on HMA	2003	N	Minimal distress	N
IL 64 (62410)	DuPage Co./D1	JPCP on HMA	2012 and 2013	N	Minimal distress	N
US 12/20/45 (60927/60748)	Cook Co./D1	JPCP on HMA	2004	N	Minimal distress	N
I-72 EB (72G92)	Sangamon Co./D6	Thin UBOL	2015	Y	Longitudinal cracking in wheel path of driving lane; stripping and erosion of HMA	Y
I-72 WB (72G92)	Sangamon Co./D6	Thin UBOL	2015	Y	Longitudinal joint faulting along outside shoulder	N
I-70 (70044)	Clark Co./D7	CRCP UBOL	2002	Y	Punchouts	N
IL 53 SB (60N05)	Will Co./D1	BCOA	2012	Y	Corner breaks, faulting, shattered slabs	Y
IL 116	Warren Co./D4	CIR	2020	N	No distress - Newly constructed	N/A
UIUC E-15 Parking Lot	Champaign Co./D5	BCOA	2006 and 2012	N	Minimal distress	N
UIUC McKinley Parking Lot	Champaign Co./D5	BCOA	2006	Y	Joint raveling	N

[1] Joint deterioration was caused by ASR and unlikely caused by erosion of CAM II. Potential erosion is occurring, but no distress was observed related to erosion of CAM II.

Note: ASR = Alkali-Silica reaction, N/A = not applicable

The detailed distress surveys can be seen for all pavement sections in **Appendix F**. An example of the detailed distress survey of US 67 is presented next, which was the main conventional concrete pavement section with distress.

Distress Survey Example: US 67 SB

A total of 10 testing locations were evaluated on US 67, with five in the northbound and five in the southbound directions. All transverse and longitudinal joint reservoirs appear to be recently re-sealed with a hot-applied sealant. This maintenance was likely scheduled because of the high level of distress occurring along the transverse joints (See **Figure 22**). The major distress present was alkali-silica reaction (ASR), a material related distress and not caused by subbase erosion.

Figure 22. Photos. US 67 SB 23+839 distress at transverse joint.

The southbound lanes of US 67 do not appear to be performing as well as the northbound lanes with a large number of full-depth repairs over the transverse joints (new and old repairs observed) that are tied into the existing structure with tie bars and dowel bars. A significant part of the southbound lanes were also overlaid recently with HMA, and therefore not included in the testing. The weather at the time of testing was overcast with fog and a light mist throughout the morning, but conditions cleared up in the afternoon. This likely contributed to a small temperature difference between the top and bottom of the concrete pavement throughout testing (negligible to minimal slab curvature). The concrete temperature profile using three depths from the surface of the pavement can be seen in **Table 18**.

Table 18. US 67 (92774) Temperature Profile (9/09/2020)

	Temperature @ corresponding depths from surface (°F)				
Time of measurement	1.5 in. depth	5 in. depth	9 in. depth	Air	UV Index
9:00 a.m.	69	70	72	64	0
12:15 p.m.	75	75	76	70	1
2:45 p.m.[1]	80	79	77	70	1

[1]Temperature was recorded using the same temperature holes drilled at 9:00 a.m.

Test sections were 75 ft long with five consecutive panels and approximately 5,000 ft between sections. MIRA scanning was performed with 35 kHz testing frequency across transverse joints to assess joint activation. All other slab locations were tested using 50 kHz frequency setting on the MIRA. Transverse joint (reservoir) widths were 0.25 in. and longitudinal joint (reservoir) widths were 0.5 in. and sealed well. Detailed distress surveys were conducted of the driving lane at locations where FWD and MIRA testing were performed. The intensive test section stations and detailed distress survey for the southbound intensive sections can be seen in **Table 19** and **Table 20**. Common distresses present throughout US 67 (92774) southbound can be observed in **Figure 23**.

Table 19. US 67 (92774) Intensive Test Sections and Stationing

Intensive test sections	Time @ start of section	Stationing	
		Beginning of test section	End of test section
SB-1	11:45 a.m.	28+655	28+632
SB-2	12:20 p.m.	27+610	27+587
SB-3	12:50 p.m.	26+526	26+503
SB-4	1:15 p.m.	26+116	26+093
SB-5	1:40 p.m.	25+370	25+347

Table 20. US 67 (92774) Detailed Distress Survey Notes (Southbound)

Stationing	Detailed Distress Survey Notes: US 67 (28+650 to 21+537)[1]
Section SB-1 (28+655)	
28+660	New full-depth repair (FDR) performing well (6 ft length 12 ft wide; DL only); should have extended into PL due to corner failures
28+655	Temperature holes drilled and recorded at 12:15 pm (1.5 in., 5 in., and 9 in.)
28+655 to 28+632	Corner distress throughout section similar to NB (DL approach and leave along the DL/PL longitudinal joint); severe failures include HMA patches or spray injection patching
28+646	Reflector in PL has HMA patch over reflector
28+615	Old FDR joints are excessively wide and spalling (7.5 ft length spanning DL and PL); some HMA patching or spray injection patching has been done along the joints
28+632	End of Section SB-1 intensive FWD testing (No MIRA testing performed)
Section SB-2 (27+610)	
27+610 to 27+587	Corner distress throughout section (DL and PL approach and leave) with majority in PL; severe failures include HMA patches in corners and over damaged raised pavement markers
27+587	End of Section SB-2 intensive FWD testing and MIRA
Section SB-3 (26+526)	
26+526	Corner distress in DL along DL/PL longitudinal joint
26+498	Severe transverse crack spanning entire pavement width and shoulder; spalling and faulting occurring along crack (~0.12 in. [3 mm]); MIRA was conducted across both adjacent transverse joints and tested along the leave crack in three locations similar to MIRA testing protocol
26+503	End of Section SB-3 intensive FWD testing (No MIRA testing performed)
Section SB-4 (26+116)	
26+116 to 26+093	MIRA scans at center of slabs reporting first reflection at 16 in. (400 mm) for some locations and others resulting in 10 in. (250 mm); Suggested coring location to assess bonding conditions
26+056	Longitudinal joint spalling; D-cracking occurring parallel to transverse joint in approach and leave slabs
26+026	New FDR 6 ft x 12 ft in DL; PL also has D-cracking along the transverse joint
26+093	End of Section SB-4 intensive FWD testing and MIRA
Section SB-5 (25+370)	
25+370 to 25+347	Corner distress in DL along DL/PL longitudinal joint; severe locations include HMA patches or spray injection patching in corners and over damaged raised pavement markers
25+340	Corner distress in DL on approach and leave along DL/PL longitudinal joint
25+330	Spalling along transverse joint
25+347	End of Section SB-5 intensive FWD testing (No MIRA testing performed)

[1]US 67 SB was rehabilitated with an HMA overlay from ~25+000 to ~21+537.

a) New FDR performing well in DL; corner distress in PL along leave joint adjacent to repair (28+660 SB)

b) Old FDR with excessively wide joints and HMA or spray injection patching (28+615 SB)

c) Corner distress in DL and PL (27+590 SB)

d) Transverse crack with spalling and faulting (26+498 SB)

e) Longitudinal joint spalling and transverse joint deterioration (26+056 SB)

f) Corner distress in DL (25+340 SB)

Figure 23**. Photos. Distress photos within US 67 (92774) SB (FDR = full-depth repair).**

CHAPTER 5: RECOMMENDATIONS FOR EVALUATING HMA AND PCC STABILIZED SUBBASE MATERIALS FOR CONCRETE PAVEMENTS, EXISTING HMA PAVEMENT STRUCTURES FOR CONCRETE OVERLAYS, AND OTHER RECYCLED BASE MATERIALS

IDOT's requirements for applications of HMA and PCC stabilized subbase layers under rigid pavements in Chapter 54 of the BDE Manual (54-4.01(h) Improved Subgrade and Subbase Type and Thickness and Figure 54-4.D Minimum Structural Design Requirements) were assessed in this study (IDOT 2021a). However, the improved subgrade treatments were not examined in this study or traffic factor criterion for changing from unstabilized to stabilized subbase layers beneath PCC pavements. It was found that no immediate changes to Figure 54-4.D Minimum Structural Design Requirements (shown in **Figure 9** of this report) are required, as negligible distress occurred in all of the sections designed and constructed with a new HMA or PCC stabilized subbase. A performance test and accompanying specification are recommended to minimize the potential of erosion in HMA and PCC stabilized support materials underneath concrete pavements and unbonded concrete overlays. Performance testing to minimize the potential of base/subbase erosion of materials or constituents is also recommended for materials that have not historically been specified beneath concrete pavements, e.g., FDR with cement or CIR. Likewise, criteria for evaluating existing support layers for bonded concrete overlays will be recommended for inclusion in Section 53-4.02(b) Bonded Concrete Overlay on Asphalt (BCOA) and should follow Article 1030.05(d) of IDOT's *Standard Specifications for Road and Bridge Construction* for HWTD (IDOT 2021b).

The recommendation of conducting the HWTD performance test for PCC stabilized subbase erosion susceptibility should be included in Section 54-4.01(h) *Improved Subgrade and Subbase Type and Thickness*. This test should not replace any existing material test, such as durability, but verify subbase material or constituent erosion resistance. The proposed performance testing protocol for the erosion testing procedure using the HWTD testing device can be seen in **Appendix G**. The HWTD testing for new HMA stabilized mixtures to be used beneath a new concrete pavement should continue to be performed as specified in Article 1030.05(d) of IDOT's *Standard Specifications for Road and Bridge Construction* for HWTD Testing (IDOT 2021b).

The failure criteria for CAM II specimens is a function of the mixture design, material constituents, and final material properties of a given mixture. The CAM II mix first needs to pass the Illinois Modified AASHTO T 161-08 "Standard Method of Test for Resistance of CAM II Mixes to Rapid Freezing and Thawing, Procedure B." The CAM II mixture shall meet the test requirements in Article 312.26 of IDOT's *Standard Specifications for Road and Bridge Construction* for relative durability (freeze/thaw resistance), air entrainment, and slump. The mix design with the lowest cement content (or cement and fly ash contents) that meets the requirements will be initially selected. HWTD testing shall be performed next to assess if the amount of cement stabilization is adequate to resist material degradation and subsequent potential erosion. Higher traffic volumes and speeds likely need a higher level of stabilization because of the increase in pore water pressure build-up beneath the slab. Ideally, good performing CAM II mixtures should result in average HWTD erosion depths ≤ 0.08 in.

(2 mm) after 10,000 load cycles. Two factors to consider in assessing the allowable erosion depth are presence of subsurface drainage and the level of precipitation. Joint sealant can also reduce moisture infiltration and dowels reduce differential slab deflections, which lead to high water velocity, hydraulic pressure, pumping, and potential erosion.

The failure criteria for HMA specimens should follow the current criteria outlined in Article 1030.05(d) of IDOT's *Standard Specifications for Road and Bridge Construction* for HWTD testing and presented in **Table 2** (IDOT 2021b). This testing should continue to be performed on new HMA stabilized mixtures to be used beneath a new concrete pavement. The HWTD performance testing has indicated that the current HMA stabilized mix designs appear to be sufficient as negligible field distress was observed for sections containing HMA stabilized subbase layers.

HWTD testing should be conducted on existing HMA pavements that are candidates for concrete overlays (bonded or unbonded). The HWTD test can be a good indicator of the suitability of an existing HMA layer to accept a concrete overlay and be erosion resistant. Reference to this testing should be recommended and implemented into Section 53-4.02(b) Bonded Concrete Overlay on Asphalt (BCOA). If milling will be completed on the existing HMA layer, the HWTD test should be run on the layer of HMA material that will interface with the new concrete overlay. The failure criteria previously established by IDOT should be followed, shown in **Table 2** (IDOT 2021a).

CHAPTER 6: SUMMARY AND CONCLUSIONS

The performance of new concrete pavements and concrete overlays is highly dependent on the uniformity, durability, and erosion resistance of the support layers. Unstabilized base and subbase foundation layers are applied to many new concrete pavements but the criteria for upgrading to a stabilized subbase layer from an unstabilized layer varies with climate, traffic, drainage, site condition, and agency guidance. Generally, stabilized layers are specified directly beneath the concrete slab once a certain truck traffic volume is reached. Additionally, concrete overlays assume that the stabilized support layer, typically HMA, is going to be resistant to stripping and erosion. Given the variety of HMA and PCC stabilized subbase support layers that can be used beneath a concrete pavement, its potential for erosion should be quantified to avoid premature failures that result from stripping or material breakdown and subsequent loss of support. Current specifications and performance testing do not evaluate the potential for a PCC stabilized support layer to erode under a new concrete pavement or an existing HMA pavement prior to a concrete overlay (bonded or unbonded). The research evaluated and measured, through a performance test, the erosion potential of IDOT specified stabilized support layers (HMA and PCC) under a concrete pavement or concrete overlay.

A literature review was conducted to identify previous performance tests for assessment of stabilized subbase erodibility under concrete pavements. Some of the performance tests were the rotational shear and jetting device, a brush testing device, HWTD, and the dynamic cylinder test. The suitability of these performance tests were evaluated based on their ability to assess erodibility accurately, repeatedly, and rapidly with stabilized materials and available equipment in IDOT labs.

The HWTD test was selected to be the most viable performance test for assessing the potential erodibility of HMA and PCC stabilized subbase support layers beneath concrete pavements and HMA pavement layers under concrete overlays. This device is also commonly used and available in IDOT labs to conduct HWTD testing on HMA and HMA stabilized subbases (Article 1030.05(d) of IDOT's *Standard Specifications for Road and Bridge Construction* for HWTD testing). This test was performed on laboratory designed mixtures of CAM II as well as various field cores obtained from different stabilized subbases such as new HMA, CAM II, and existing HMA beneath a bonded concrete overlay. The laboratory investigation of the CAM II showed that mixtures with a lower cement content are more likely to experience erosion beneath the concrete as compared to those with a higher cement content and subsequent strength. With the large range of potential mixtures allowed, the HWTD test is a proposed method to evaluate the erosion potential of an HMA or PCC stabilized subbase mixture in addition to the existing testing procedures needed for strength and freeze-thaw durability.

A total of twelve IDOT concrete pavement sections were selected with different stabilized support layers (HMA or PCC) and service lives to evaluate subbase support through FWD testing and subsequent backcalculation of the k-value, effective thickness, and slab-subbase interface friction. Several of these sections had FWD data spanning multiple years. From the FWD analysis, some sections showed an increase in deflections over time, which were likely a combination of factors such as erosion, existing slab curvature (temperature gradients), and/or decrease in LTE (loss in aggregate interlock, dowel looseness). The MIRA ultrasonic tomography device was also used on these field

sections to determine the slab thickness, joint reinforcement details (dowel and tie bar depth and spacing), contraction joint activation, and interface bond condition. MIRA showed evidence of missing dowels along one section, although no distress resulted from this error. Visual distress surveys were performed to link any distresses or FWD and MIRA results with potential of support erosion. The FWD and MIRA results reinforced that the as-built sections are consistent overall with the design expectations (slab thickness, dowel bars, and tie bars).

Coring was performed on four distinct concrete pavement sections with different types of subbase support, which showed some asphalt stripping on a BCOA project and surface erosion on a CAM II. Overall, the field survey results and coring showed HMA stabilized subbases are performing very well under JPCP and CRCP. For one BCOA , the existing asphalt layer was not erosion resistant, which contributed to higher distresses on the section. The longitudinal joint of the BCOA was directly in the outer wheel path, and a high volume of heavy trucks, along with the presence of water, lead to water pressure build-up and erosion at the PCC-HMA interface. Additional coring on an UBOL with an HMA interlayer showed evidence of stripping and erosion directly beneath the transverse joints, causing longitudinal cracking to develop in the wheel paths. By conducting the HWTD performance test on candidate asphalt support layers, asphalt layers with a high risk for potential erosion can be identified and avoided or removed prior to placing the concrete overlay. Finally, there was some evidence of erosion in poor drainage locations for US 67 with the CAM II subbase, but no faulting was observed at the transverse joints because of the presence of dowel bars. Joint deterioration was present in the form of cracks at the surface because of repeated loading and materials-related distress (ASR) in the concrete.

The HWTD performance test is recommended for evaluating the erosion potential of new HMA and PCC stabilized subbase support layers under concrete pavements and existing or new support layers under concrete overlays. The criterion for the HWTD for a new concrete pavement with an HMA stabilized subbase is 0.5 in. (12.5 mm) at a set number of passes depending on the PG binder grade of the asphalt. Similarly for concrete overlays, the existing HMA support layer should be tested to determine if it can be left in place or if it needs to be removed and replaced with new material. For a PCC stabilized subbase, the recommended criteria for the HWTD is less than 0.08 in. (2 mm) after 10,000 repetitions. Recommendations were made for keeping IDOT's requirements for applications of HMA and PCC stabilized subbase support layers under rigid pavements unchanged in Chapter 54 of the *BDE Manual* (54-4.01(h) Improved Subgrade and Subbase Type and Thickness and Figure 54-4.D Minimum Structural Design Requirements). Additional criteria for testing of support layers for bonded concrete overlays is recommended for inclusion in Section 53-4.02(b) Bonded Concrete Overlay on Asphalt (BCOA) and should follow Article 1030.05(d) of IDOT's *Standard Specifications for Road and Bridge Construction* for HWTD test.

REFERENCES

Alland, K., J. Vandenbossche, S. Sachs, J. W. DeSantis, and T. Burnham (2016). Failure Modes in Unbonded Concrete Overlays. Proceeding's 11th International Conference on Concrete Pavements, San Antonio, TX, pp. 1–18.

American Association of State Highway and Transportation Officials. (1993). AASHTO Guide for Design of Pavement Structures. Washington, D.C.

American Association of State and Highway Transportation Officials. (2017). AASHTO T 135-13: Standard Method of Test for Wetting-and-Drying Test of Compacted Soil-Cement Mixtures.

American Standard Testing Methods (2013). ASTM C642 – 13: Standard Test Method for Density, Absorption, and Voids in Hardened Concrete.

American Standard Testing Methods (2017). ASTM C496/ C496M-17: Standard Test Method for Splitting Tensile Strength of Cylindrical Concrete Specimens.

American Standard Testing Methods (2017). ASTM D1633 – 17: Standard Test Methods for Compressive Strength of Molded Soil-Cement Cylinders.

American Standard Testing Methods (2017). ASTM D6931-17: Standard Test Method for Indirect Tensile (IDT) Strength of Asphalt Mixtures.

American Standard Testing Methods (2019). ASTM C136 / C136M – 19: Standard Test Method for Sieve Analysis of Fine and Coarse Aggregates.

Barman, M., Mu, F., and Vandenbossche, J.M. (2011). Development of a Rational Mechanistic-Empirical Based Design Guide for Thin and Ultra-Thin Whitetopping. Task 1 Report. Minneapolis, MN: University of Pittsburgh, Federal Highway Administration Pooled Fund study, TPF 5–165.

Bhatti, M.A., J.A. Barlow, and J.W. Stoner. (1996). *Modeling Damage to Rigid Pavements Caused by Subgrade Pumping*. ASCE, Journal of Transportation Engineering, Vol. 122, No. 1, Jan-Feb 1996, pp. 12-21.

Birmman, D. (1998). "Erosion of Cement Treated Subbases Below Concrete Pavements." Eighth International Symposium on Concrete Roads. Theme III, Pavement Performance and Evaluation. Lisbon, Portugal.

Calo, D. (2019). Personal conversation.

Caro, S. et al. (2010). Estudio de la Resistencia a la Erosión De Materiales Empleados como Bases en Pavimentos de Concreto Hidráulico, Universidad de Los Andes.

Caicedo, B., and Caro, S. (2016), Estudio de la Resistencia a la Erosión de materiales empleados como Bases en Pavimentos de Concreto Hidráulico, Fase II, Universidad de Los Andes.

Darter, M.I., LaCoursiere, S.A., and Smiley, S.A. (1979). Structural distress mechanisms in continuously reinforced concrete pavement. Transportation Research Record 715, pp. 1-7.

De Beer, M. *Erodibility of Cementitious Subbase Layers in Flexible and Rigid Pavements*. Second International Workshop on the Theoretical Design of Concrete Pavements, Siguenza, Spain, 1990.

Dempsey, B.J. Laboratory and Field Studies of Channeling and Pumping. Transportation Research Board, Transportation Research Record 849, 1982, pp. 1-12.

DeSantis, J.W. and Roesler, J.R. (2022). *Longitudinal Cracking Investigation on I-72 Experimental Unbonded Concrete Overlay*. (Report No. ICT-22-002) Illinois Center for Transportation. https://doi.org/10.36501/0197-9191/22-002

Dwight, C., Khazanovich, L., and Salles, L. (2016). Linear Array Ultrasonic Test Results from Alkali-Silica Reaction (ASR) Specimens. Report No ORNL/TM-2016/159. Oak Ridge National Laboratory. Electrical and Electronics Systems Research Division. US Department of Energy, Washington, D.C.

Freeseman, K., Hoegh, K., and Khazanovich, L. (2015). Characterization of Concrete at Various Freeze-Thaw Damage Conditions Using SH-Waves. Proceedings of the 42nd Review of Progress in Quantitative Nondestructive Evaluation (QNDE), Minneapolis, MN.

Guthrie, W.S., Sebesta, S., and Scullion, T. (2002). "Selecting Optimum Cement Contents for Stabilized Aggregate Base Materials." Report 4920-2. Texas Transportation Institute, The Texas A&M University System, College Station, Texas.

Ha, S., Yeon, J., Choi, B., Jung, Y., Zollinger, D.G., Wimsatt, A., Won, M.C. (2011). Develop Mechanistic-Empirical Design for CRCP. Texas Department of Transportation and Federal Highway Administration Report 0-5832-1.

Hansen, E. C., Johannesen, R. and Armaghani, J. M. (1991). "Field Effects of Water Pumping beneath Concrete Pavement Slabs". Journal of the Transportation Engineering (ASCE), 17(6): 679-696.

Hoegh, K., Khazanovich L., and Yu, H. T. (2011). Ultrasonic tomography technique for evaluation of concrete pavements. *Transportation Research Record: Journal of the Transportation Research Board*, *2232*, 85–94.

Hoegh, K. and Khazanovich, L. (2012). "Correlation Analysis of 2D Tomographic Images for Flaw Detection in Pavements." ASTM International. Journal of Testing and Evaluation. Volume 40. Issue 2.

Hoegh, K., Khazanovich, L., Maser, K., and Tran, N. (2012). Evaluation of an Ultrasonic Technique for Detecting Delamination in Asphalt Pavements. *Transportation Research Record: Journal of the Transportation Research Board.*

Hansen, W. and Liu, Z. (2013). Improved Performance of JPCP Overlays. Michigan Department of Transportation Report RC-1574.

IDOT. (2012). PCC Level III Technician Course Manual: Appendix F – Cement Aggregate Mixture (CAM) II. Published by Illinois Department of Transportation.

IDOT. (2018). Illinois Modified Test Procedure of AASHTO T 324-17: Standard Method of Test for Hamburg Wheel-Track Testing of Compacted Hot Mix Asphalt (HMA). Illinois Department of Transportation. Published June 2012, Revised December 2018.

IDOT. (2021a). Bureau of Design and Environment Manual. Prepared and Published by Illinois Department of Transportation, Bureau of Design and Environment, Springfield, Illinois, Published September 2010, Revised November 2021.

IDOT. (2021b). *Standard Specifications for Road and Bridge Construction*. Illinois Department of Transportation. Published July 2015, Revised April 2021.

Jung, Y., Zollinger D., Wimsatt A. (2010) "Test Method and Model Development of Subbase Erosion for Concrete Design." Transportation Research Record. 2154(1):22-31. https://doi.org/10.3141/2154-03.

Jung, Y., Zollinger, D. Won, M, Wimsatt, A. (2009) Subbase and Subgrade Performance Investigation for Concrete Pavement, TTI Report 0-6037-1, 112 pp.

Jung, Y., Zollinger, D., Cho, B., Won, M., Wimsatt, A. (2012), Subbase and Subgrade Performance Investigation and Design Guidelines for Concrete Pavement, Report 0-6037-2, 170 pp.

King, D. and Roesler, J. (2014), Structural Performance of Ultra-Thin Whitetopping on Illinois Roadways and Parking Lots, Illinois Center for Transportation Research Report ICT-14-018, UILU-ENG-2014-2022, University of Illinois, Urbana, IL, 136 pp.

Ma, Y., Elseifi, M.A., Dhakal, N., Bashar, M.Z., and Zhang, Z. (2021). Non-Destructive Detection of Asphalt Concrete Stripping Damage using Ground Penetrating Radar. Transportation Research Record. https://doi.org/10.1177/03611981211014199.

Phu, N.C., and M. Ray. The Erodibility of Concrete Pavement Subbase and Improved Subgrade Materials. Bulletin de Liaison des Laboratoires des Ponts et Chaussees, Special Issue 8, France, July 1979, pp. 32-45.

Pierce, L. et al. (2021). Evaluation of Bonded Concrete Overlays on Asphalt Pavements. NCHRP 01-61. (In review)

Popovics, J. S., Roesler, J. R., Bittner, J., Amirkhanian, A. N., Brand, A. S., Gupta, P., and Flowers, K. (2017). Ultrasonic imaging for concrete infrastructure condition assessment and quality assurance (Report No. FHWA-ICT-17-011). Rantoul, IL: Illinois Center for Transportation.

Roesler, J.R, A. Bordelon, A. Ioannides, M. Beyer, and D. Wang. (2008). Design and Concrete Material Requirements for Ultra-Thin Whitetopping. Report No. FHWA-ICT-08-016, Illinois Center for Transportation, University of Illinois at Urbana-Champaign.

Salles, L.S., Balbo, J.T., and Khazanovich, L. (2017). "Non-destructive ultrasonic tomography for concrete pavement evaluation: signal processing and image analysis of crucial parameters." Ibracon Structures and Materials Journal. Volume 10. Issue 6. Pp. 118-1191.

Schubert, F. and Kohler B. (2008). "Ten Lectures on Impact-Echo." Journal of Nondestructive Evaluation. Special Issue: Acoustic and Electromagnetic Nondestructive Evaluation of Concrete Structures. Volume 27, Pages 1-3, 5-21.

Sebasta, S. (2002). Investigation of Maintenance Base Repairs Over Expansive soils: Year 1 Report. Report 0-4395-1 Texas Department of Transportation. 122 pp.

Souder, N., J.W. DeSantis, J. Vandenbossche, and S. Sachs. Modeling the Development of Permanent Deformation in Asphalt Interlayers of Unbonded Concrete Overlays of Concrete Pavements. 2020. https://doi.org/10.1177/2F0361198120930013

TxDOT. (2008). "Pavement Design Guide Manual," https://ftp.txdot.gov/pub/txdot-

info/cst/pavement-manual-0516.pdf. Texas Department of Transportation. Updated: May 2016; accessed: October 1, 2021.

TxDOT. (2021). Test Procedure for Hamburg Wheel-Tracking Test: TxDOT Designation Tex-242-F. Texas Department of Transportation.

Tran, Q. and Roesler, J. R. (2020). Rapid detection of concrete joint activation using normalized shear wave transmission energy. *International Journal of Pavement Engineering*, https://doi.org/10.1080/10298436.2020.1785448

Van Blerk, P. and T. Scullion. (1995). Evaluation of Stabilized Base Durability Using a Modified South African Wheel Tracking Device. Report 2919-1 Texas Transportation Institute. 88 pp.

Van Wijk, A.J. Rigid Pavement Pumping: (1) Subbase Erosion and (2) Economic Modeling. Joint Highway Research Project File 5-10, School of Civil Engineering, Purdue University, West Lafayette, Indiana, May 16, 1985.

Zhang, Y. and Roesler, J.R. (2018). Improved Backcalculation Procedure for Continuously Reinforced Concrete Pavement. TRR. https://doi.org/10.1177/0361198118758010.

Zhang, Y., Roesler, J.R., and Huang, Z. (2020). A method for evaluating CRCP performance based on edge-loaded FWD test. Materials and Structures 53:46 https://doi.org/10.1617/s11527-020-01481-0.

APPENDIX A: LABORATORY TESTING

CEMENT AGGREGATE MIXTURE II (CAM II) DESIGNS

The cement aggregate mixtures II (CAM II) were designed using guidelines provided in Appendix F of the PCC Level III Technician Course Manual (IDOT 2012). Prior to designing the mixtures, material properties of the different materials (cement, fly ash, and aggregates) needed to be obtained including specific gravity, water absorption capacity, moisture content adjustments, and aggregate gradation. The aforementioned material properties are presented below.

Table 21. Specific Gravity and Water Absorption of Materials

	Specific Gravity	Water Absorption Capacity (%)	Water Content (%) Based OD	Surface Water (%)
Cement	3.15	n/a	n/a	n/a
Fly ash, Class C	2.65	n/a	n/a	n/a
Coarse aggregate	2.67	3.31	0.22	-3.09
Fine aggregate	2.65	2.21	0.17	-2.04

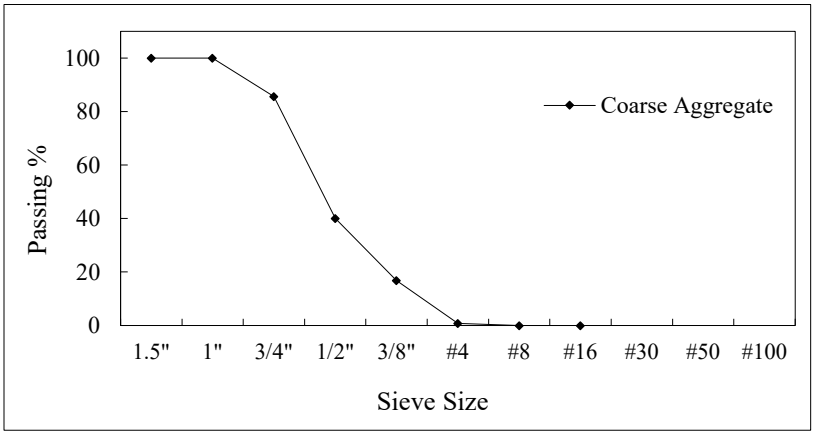

Figure 24. Graph. Coarse aggregate gradation (IDOT CA 11).

Based upon experience, the BDE Manual recommends using a 50-50 percent blend of coarse aggregate to fine aggregate when using coarse aggregate gradations of IDOT Class CA 7, CA 9, or CA 11 (IDOT 2017). The aggregate gradation resulted in a IDOT CA 11. Therefore, a 50-50 percent blend was selected for all mixture designs.

Table 22. CAM II Mixture Design Summary of Laboratory Mixtures

Date of casting	4/2/2021	4/9/2021	4/16/2021	6/23/2021	6/29/2021	7/1/2021
Mix ID #	Mix #1	Mix #2	Mix #3	Mix #1 (2)	Mix #4[1]	Mix #5[1]
Water/cementitious material (w/cm)	1.1	0.6	0.9	1.1	1.1	0.7
Cement content, pcy	200	200	300	200	170/60	245/85
CA, lbs	45.3	48.8	42.26	45.3	43.6	43.7
FA, lbs	45.3	49.0	42.43	45.3	43.7	43.7
Cement, lbs	5.56	5.56	8.33	5.56	4.72/1.67	6.81/2.36
Water, lbs	8.43	5.8	9.67	8.43	9.26	8.29
W+C time	10:30 AM	10:25 AM	10:55 AM	1:45 PM	10:00 AM	10:00 AM
Slump, in.	1.0	0.0	3.0	0.5	7.0	5.5
Slump time	10:45 AM	10:35 AM	11:05 AM	1:50 PM	10:20 AM	10:20 AM
Air content, %	7.5	8.5	9.0	10.5[2]	10.5[2]	10.5[2]
Air content time	10:50 AM	10:40 AM	11:10 AM	1:55 PM	10:25 AM	10:25 AM
Finished specimens time	11:15 AM	11:05 AM	11:55 AM	2:10 PM	10:45 AM	10:45 AM
14-day f'c date	4/16/2021	4/23/2021	4/30/2021	7/7/2021	7/13/2021	7/15/2021
28-day HWTD date	4/30/2021	5/7/2021	5/14/2021	7/21/2021	7/27/2021	7/29/2021

[1]Mix ID 4 and 5 contained Class C fly ash. Quantities reported for cement content and cement are listed as total Type I Portland cement/Class C fly ash.

[2]Air meter was not working properly, the seal was not fully maintained.

Table 23. Unit Weight Summary of Laboratory Mixtures

		Unit weight, pcf		
Specimen		**Mix #1 (2)**	**Mix #4**	**Mix #5**
4"x8" Cylinders	1	146	133	135
	2	147	138	135
	3	147	136	134
	Average	147	136	135
	Std. Dev.	0.63	2.52	0.51
HWTD Cylinders	1	147	133	138
	2	149	136	140
	3	152	141	141
	4	146	138	140
	Average	149	137	140
	Std. Dev.	2.65	3.43	1.43
Total	Average	148	136	137
	Std. Dev.	2.00	2.71	2.92

COMPRESSIVE STRENGTH RESULTS

Compressive strength testing was conducted after 14 days of moist curing of the laboratory prepared CAM II mixtures. Testing was performed following ASTM C 39. The summary of the results are presented below. Currently, no minimum strength is required, but typical 14-day strengths are between 750 and 1,500 psi.

Figure 25. Photo. Compressive strength testing using 4- by 8-in. cylinders (CAM II Mix #3 – 416).

Table 24. Compressive Strength Summary of Laboratory Mixtures

Batching date	4/2/2021	4/9/2021	4/16/2021	6/23/2021	6/29/2021	7/1/2021
Mix ID	Mix #1	Mix #2	Mix #3	Mix #1 (2)	Mix #4	Mix #5
14-day testing date	4/16/2021	4/23/2021	4/30/2021	7/7/2021	7/13/2021	7/15/2021
Specimen 1, psi	682	637	1337	830	381	852
Specimen 2, psi	605	560	1305	820	312	816
Specimen 3, psi	622	581	1316	734	351	969
Average f'c, psi	636	593	1320	795	348	879
Std. Dev.	40.3	39.9	16.3	52.4	34.6	79.9
COV	6.34	6.73	1.24	6.59	9.95	9.09

HAMBURG WHEEL-TRACKING DEVICE TESTING

All HWTD testing includes depths recorded at 11 locations across the combined specimen's surface, **Figure 11**. The maximum rut depth and failure is likely to occur at the interface between specimens (recorded depth locations 5, 6, and 7). The results presented within the appendices include the average rut depth of the individual specimens. Two specimens were tested per wheel and the HWTD includes two wheels (total of four specimens tested per trial). The results also include the average rut depth of both specimens. The final testing protocol included 10,000 load cycles or a maximum rut depth of 0.5 in. (12.5 mm).

CAM II Hamburg Wheel-Tracking Device Shakedown Testing

Preliminary testing was conducted to 20,000 load cycles or a maximum rut depth of 1 in. (25 mm). This was conducted to assess the testing protocol and performance testing capabilities. No weight loss was recorded for the shakedown testing as specimens crumbled after testing was completed and specimens were removed from the frame.

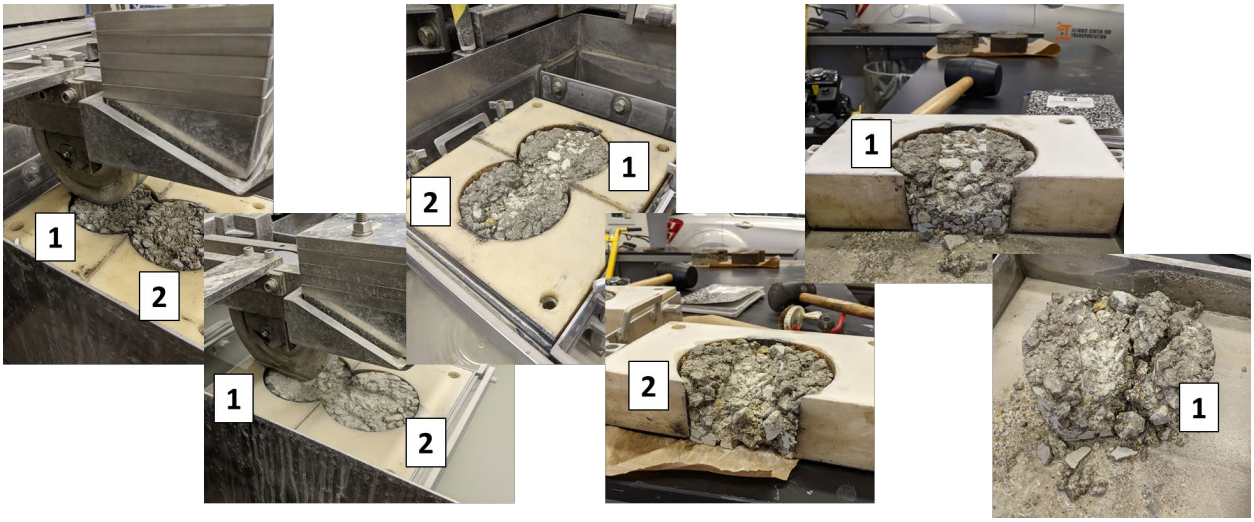

Figure 26. Photos. CAM II Hamburg wheel-tracking device (HWTD) testing shakedown specimens process during testing.

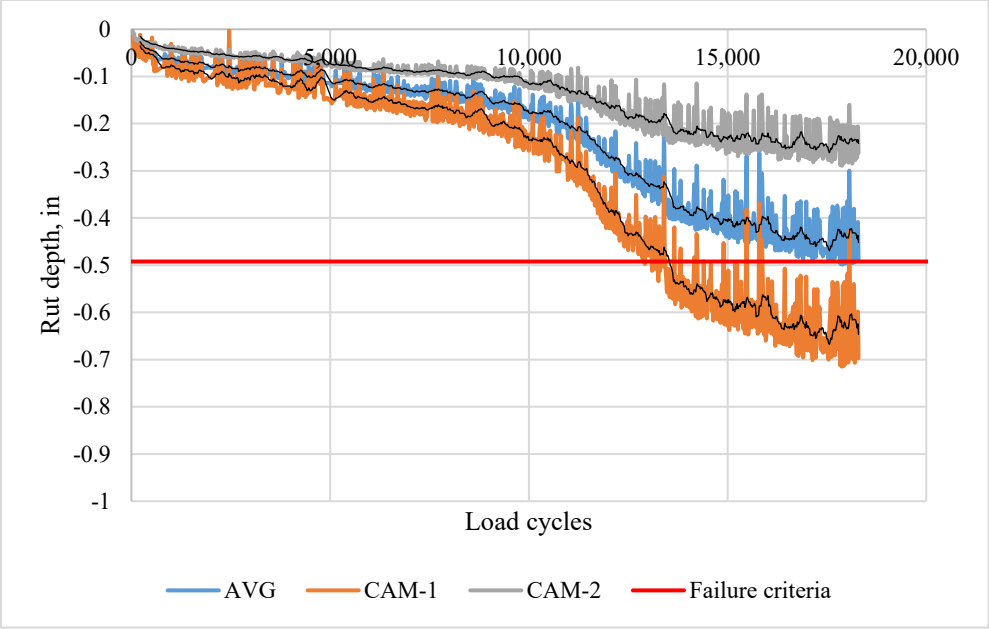

Figure 27. Graph. CAM II Hamburg wheel-tracking device (HWTD) shakedown results.

Cold In-Place Recycling IL 116

Six HWTD specimens were cured and compacted using the same method. The mixture sample was obtained from field construction prior to compaction and stored within a moisture seal-tight container for 14 days. The mixture was then dried at 230 °F (110 °C) for an hour (typically dried at 122 °F [50 °C] for 40 hours), then conditioned at compaction temperature (295 °F [146 °C]) for two hours before compacting to 2.5 in. (62 mm) height. The compacted specimens resulted in an air voids content of 5.9%. No weight loss measurements were recorded for IL 116 CIR.

a) Gyratory compacted specimens

b) Specimens in HWTD

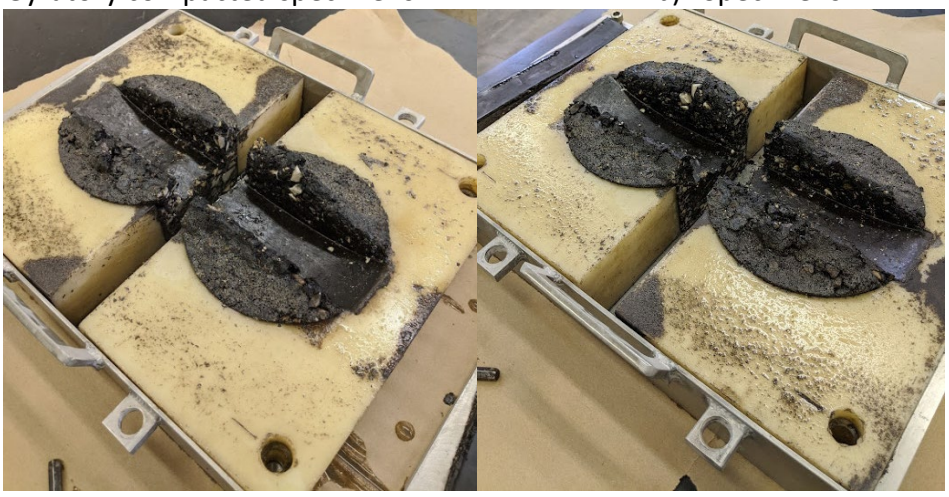

c) Specimens after HWTD completion

Figure 28. Photos. IL 116 Cold in-place recycling (CIR) Hamburg wheel-tracking device (HWTD) specimens.

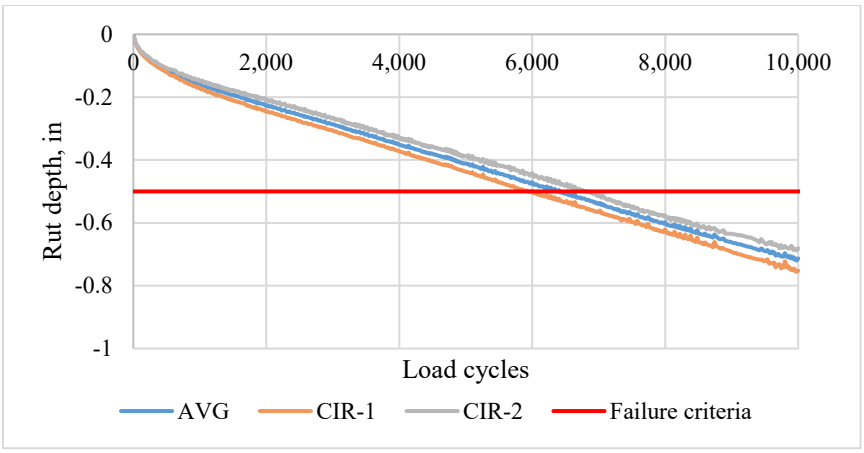

a) IL 116 CIR Specimens 1 and 2

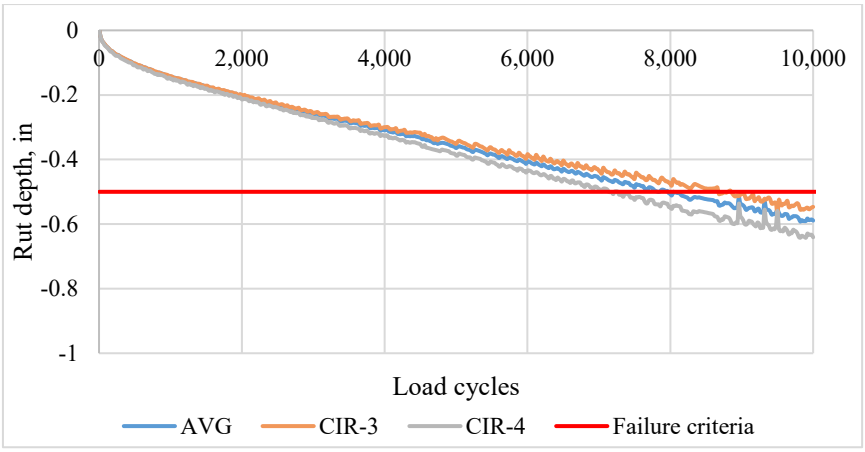

b) IL 116 CIR Specimens 3 and 4

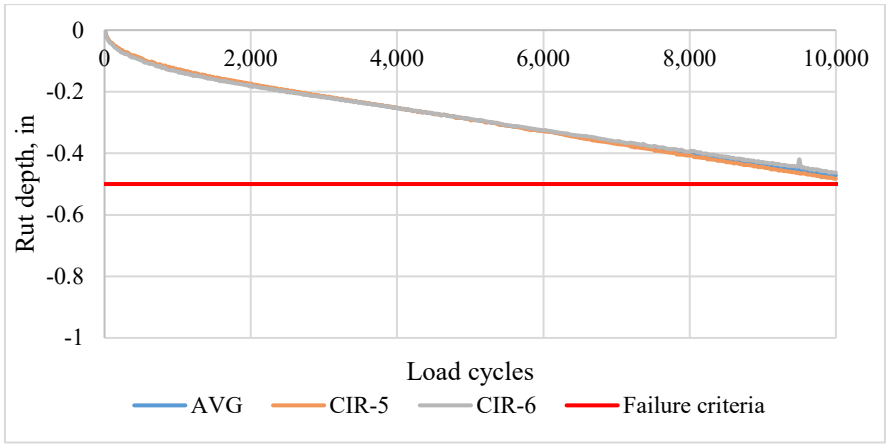

c) IL 116 CIR Specimens 5 and 6

Figure 29. Graphs. IL 116 Cold in-place recycling (CIR) Hamburg wheel-tracking device results.

CAM II Lab Mix #1

The initial testing performed on CAM II Mix #1 did not include a rubber pad beneath the specimens, causing deterioration to occur between the interface of the bottom of the specimen and the metal frame. This also influenced failures of the specimen and caused violent movements of the testing device. These violent movements influenced the decision to reduce the maximum loading to 10,000 cycles which allows testing to be completed within one day and an operator present throughout testing. To eliminate this undesirable affect, a rubber pad was placed beneath all future specimens within the HWTD frame. No weight loss measurements were recorded for CAM II Lab Mix #1. Testing of this mixture was repeated to examine the effects from the rubber pad and weight loss.

a) Specimens in HWTD

b) Specimens after HWTD

c) Specimens after HWTD completion

d) Bottom of specimens (deterioration from contact with metal frame)

Figure 30. Photos. CAM II Mix #1-402 Hamburg wheel-tracking device (HWTD) specimens.

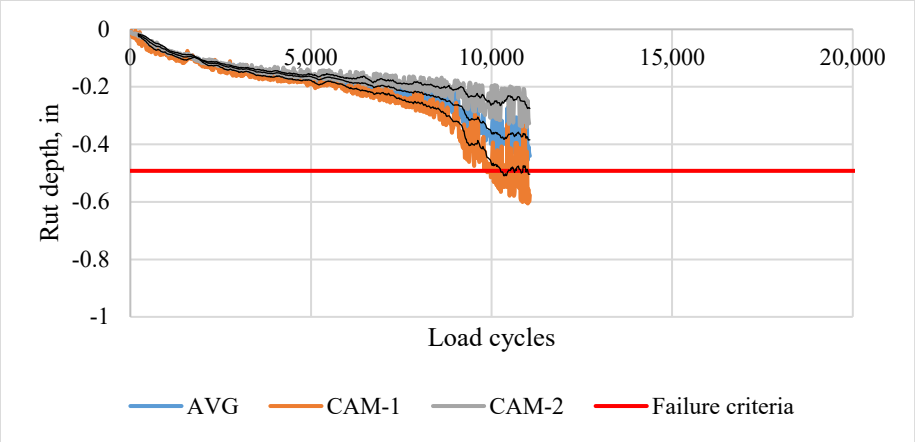

a) CAM II Mix #1-402 Specimens 1 and 2

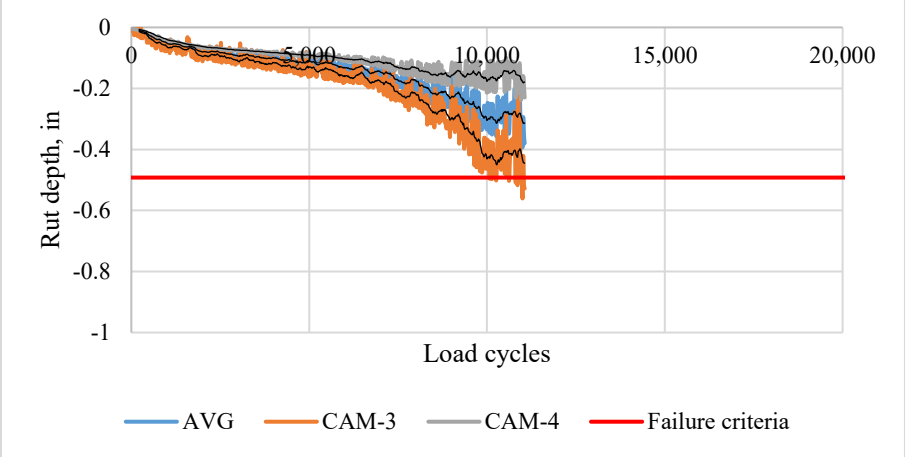

b) CAM II Mix #1-402 Specimens 3 and 4

Figure 31. Graphs. CAM II Mix #1-402 Hamburg wheel-tracking device (HWTD) results.

CAM II Lab Mix #2

a) Specimens in HWTD

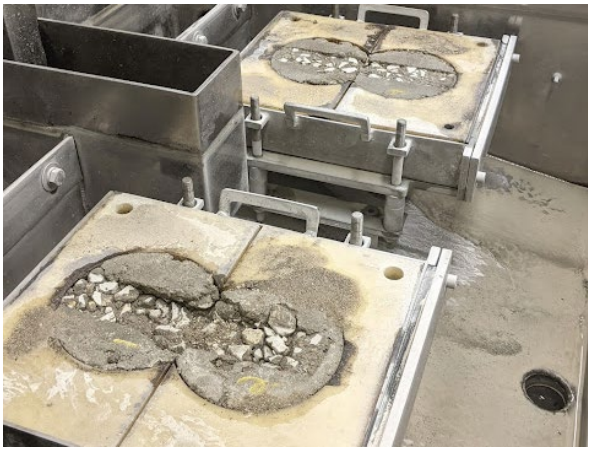

b) Specimens after HWTD completion with eroded material

Figure 32. Photos. CAM II Mix #2-409 Hamburg wheel-tracking device (HWTD) specimens.

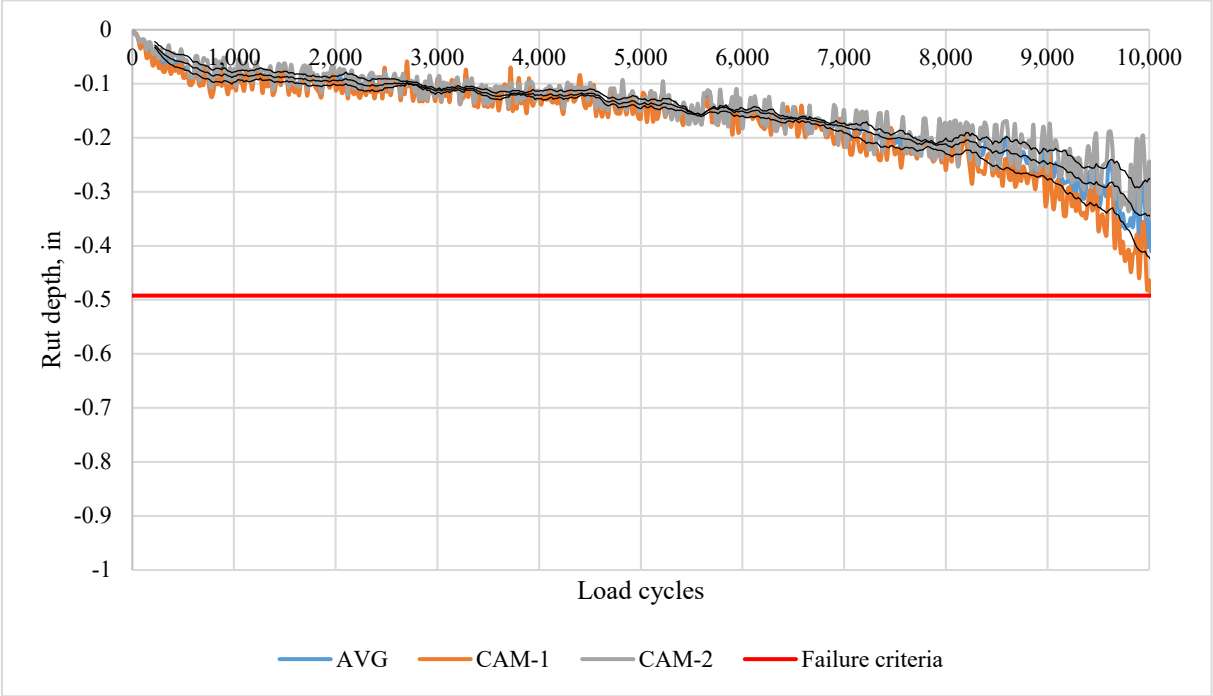

a) CAM II Mix #2-409 Specimens 1 and 2

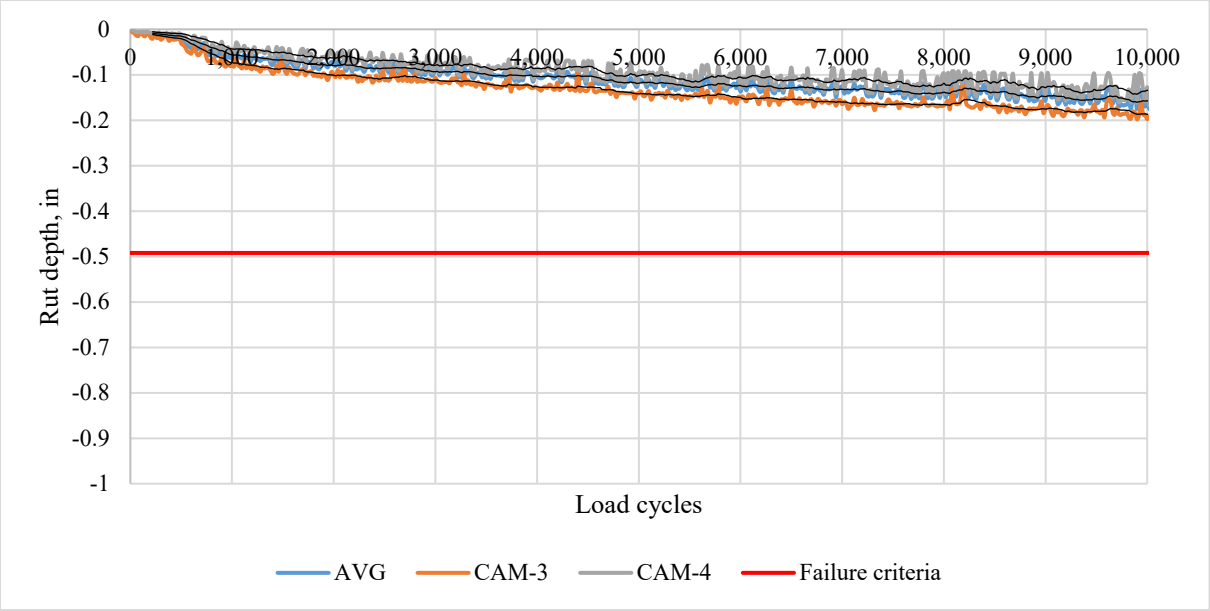

b) CAM II Mix #2-409 Specimens 3 and 4

Figure 33. Graphs. CAM II Mix #2-409 Hamburg wheel-tracking device (HWTD) results.

Table 25. CAM II Mix #2-409 Hamburg Wheel-tracking Device (HWTD) Weight Loss

	Weight Loss, lbs
Specimen	**Mix #2-409**
1	Crumbled
2	Crumbled
3	0.151
4	0.127
Average	0.139
Std. Dev.	0.012

CAM II Lab Mix #3

a) Specimens in HWTD

b) Specimens after HWTD completion with eroded material

c) Specimens after HWTD completion

Figure 34. Photos. CAM II Mix #3-416 Hamburg wheel-tracking device (HWTD) specimens.

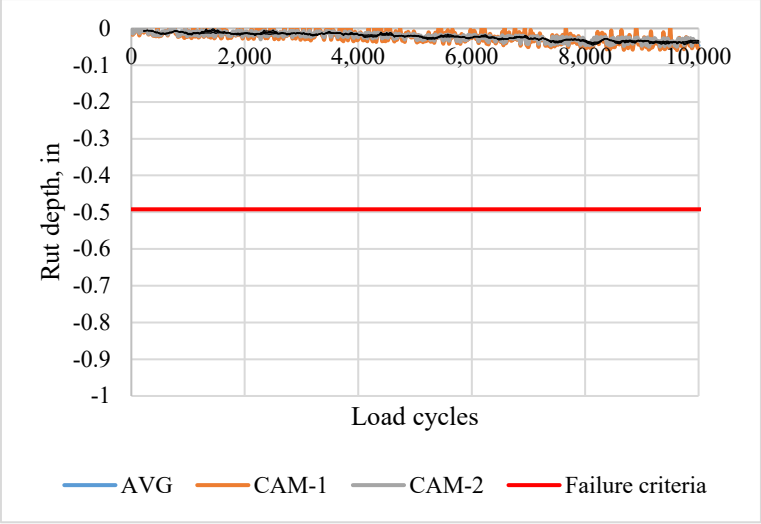

a) CAM II Mix #3-416 Specimens 1 and 2

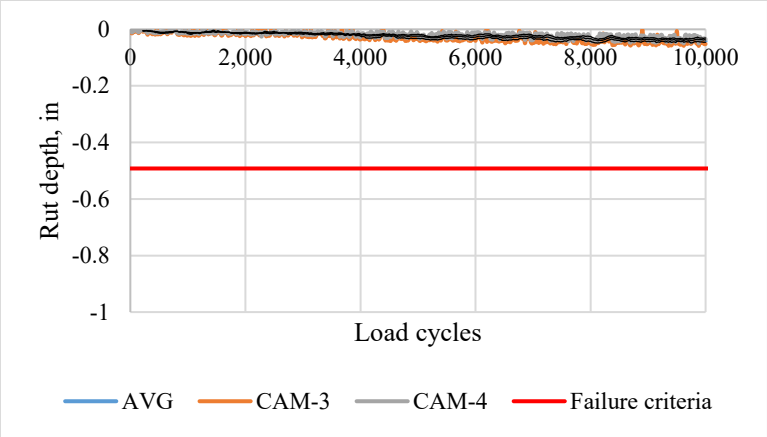

b) CAM II Mix #3-416 Specimens 3 and 4

Figure 35. Graphs. CAM II Mix #3-416 Hamburg wheel-tracking device (HWTD) results.

Table 26. CAM II Mix #3-416 Hamburg Wheel-tracking Device (HWTD) Weight Loss

	Weight Loss, lbs
Specimen	**Mix #3-416**
1	0.037
2	0.035
3	0.040
4	0.030
Average	0.035
Std. Dev.	0.003

CAM II Lab Mix #1 (2)

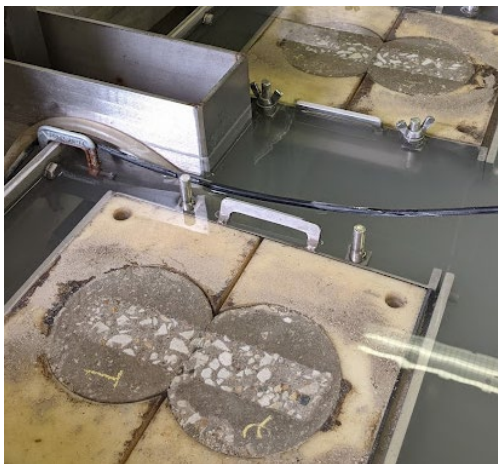

a) Specimens after HWTD completion with eroded material

b) Specimens after HWTD completion with eroded material

Figure 36. Photos. CAM II Mix #1 (2) – 625 Hamburg wheel-tracking device (HWTD) specimens.

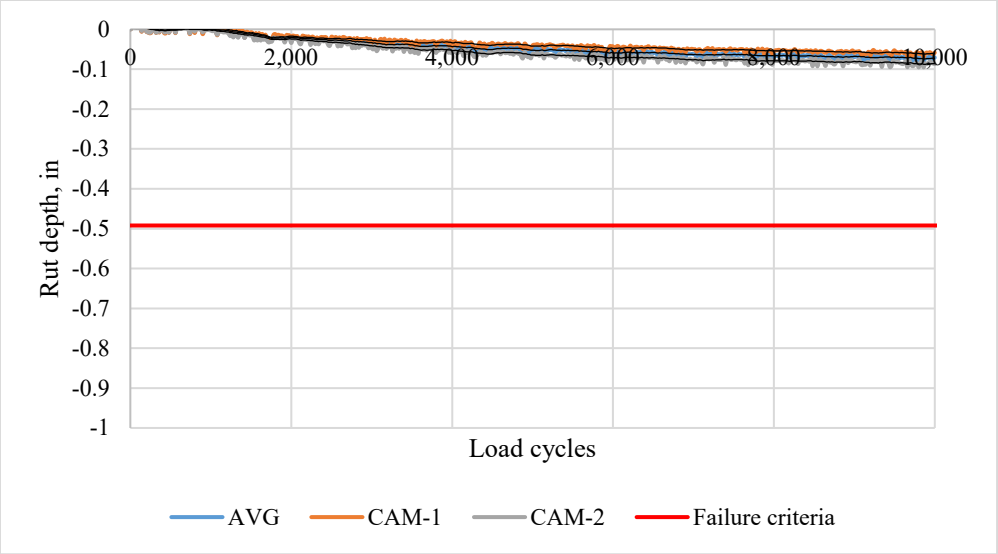

a) CAM II Mix #1 (2) - 625 Specimens 1 and 2

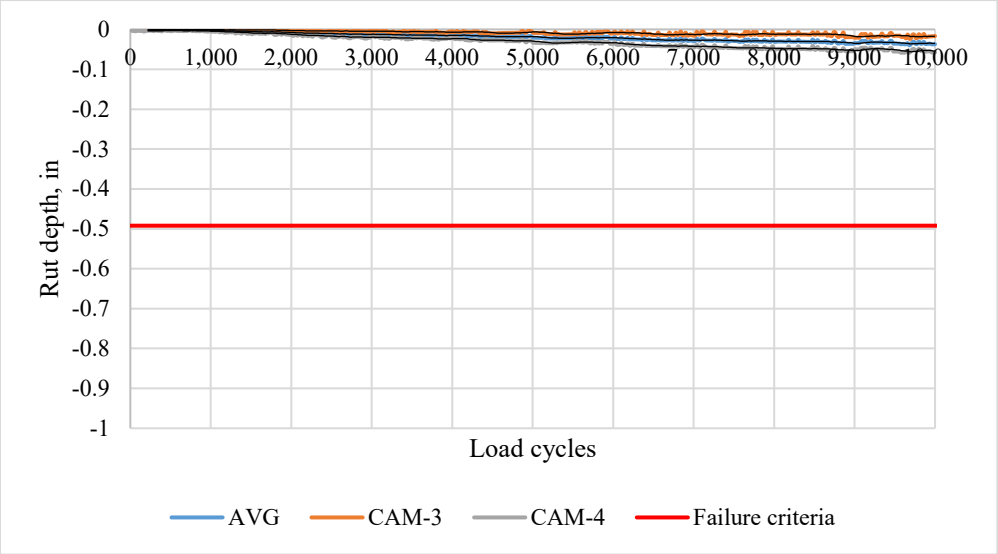

b) CAM II Mix #1 (2) - 625 Specimens 3 and 4

Figure 37. Graphs. CAM II Mix #1 (2) – 625 Hamburg wheel-tracking device (HWTD) results.

Table 27. CAM II Mix #1 (2) – 625 Hamburg Wheel-tracking Device (HWTD) Weight Loss

	Weight Loss, lbs
Specimen	**Mix #1 (2)-625**
1	0.091
2	0.117
3	0.100
4	0.111
Average	0.105
Std. Dev.	0.010

CAM II Lab Mix #4

a) Specimens in HWTD

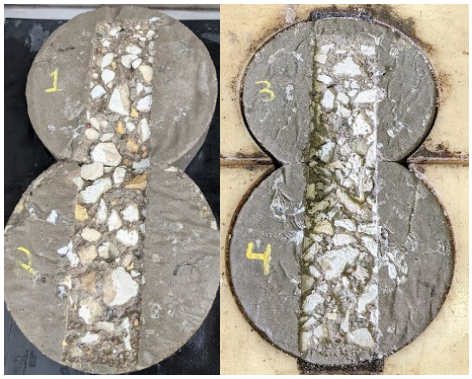

b) Specimens after HWTD completion with eroded material

Figure 38. Photos. CAM II Mix #4 – 629 Hamburg wheel-tracking device (HWTD) specimens.

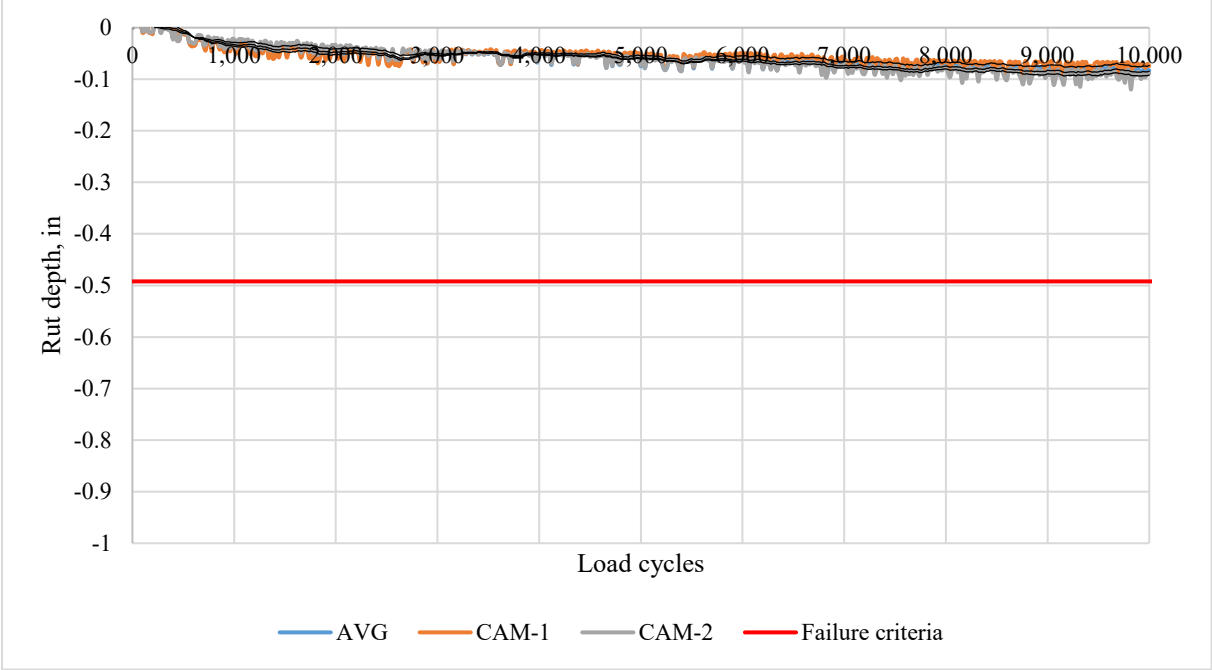

a) CAM II Mix #4-629 Specimens 1 and 2

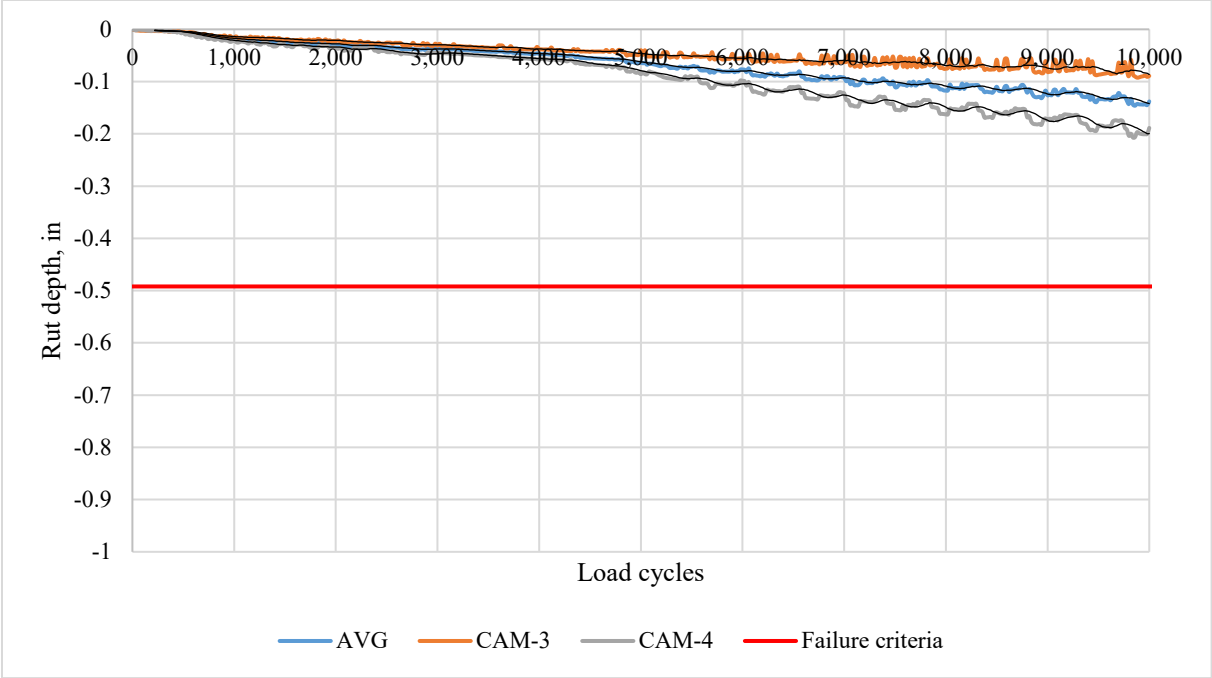

b) CAM II Mix #4-629 Specimens 3 and 4

Figure 39. Graphs. CAM II Mix #4 – 629 Hamburg wheel-tracking device (HWTD) results.

Table 28. CAM II Mix #4 – 629 Hamburg Wheel-tracking Device (HWTD) Weight Loss

	Weight Loss, lbs
Specimen	**Mix #4-629**
1	0.140
2	0.175
3	0.154
4	0.211
Average	0.170
Std. Dev.	0.027

CAM II Lab Mix #5

a) Specimens in HWTD

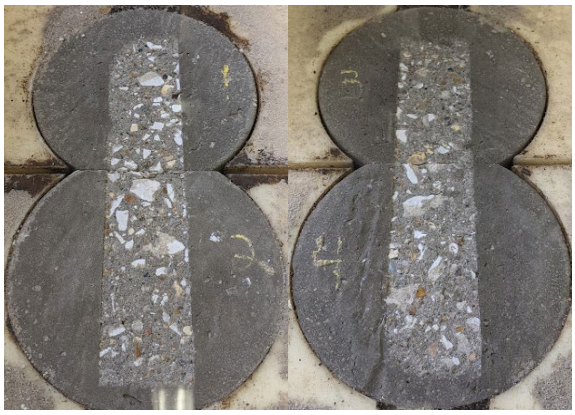

b) Specimens after HWTD completion with eroded material

Figure 40. Photos. CAM II Mix #5 – 701 Hamburg wheel-tracking device (HWTD) specimens.

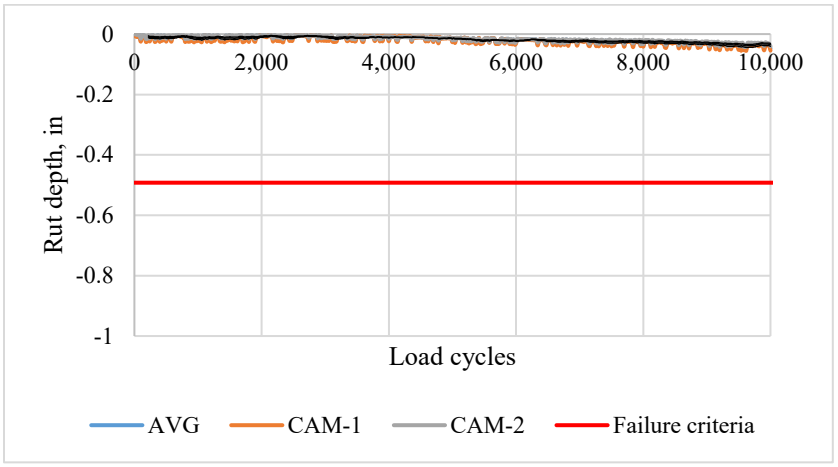

a) CAM II Mix #5-701 Specimens 1 and 2

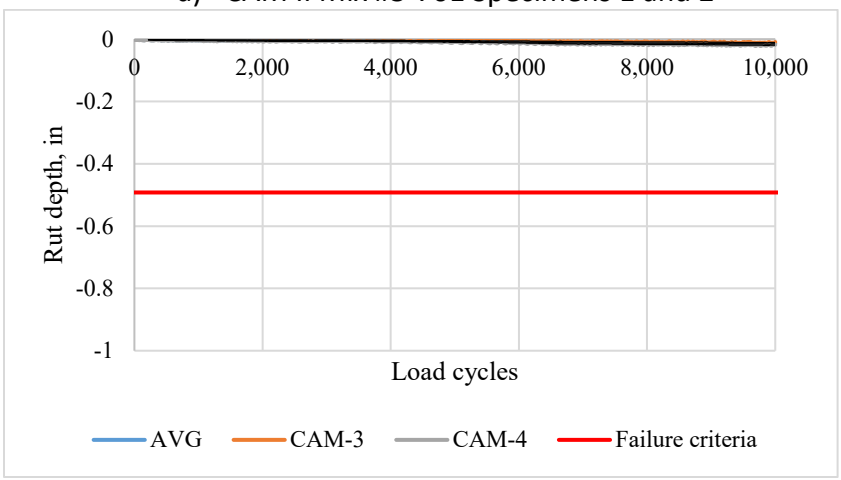

b) CAM II Mix #5-701 Specimens 3 and 4

Figure 41. Graphs. CAM II Mix #5 – 701 Hamburg wheel-tracking device (HWTD) results.

Table 29. CAM II Mix #5 – 701 Hamburg Wheel-tracking Device (HWTD) Weight Loss

	Weight Loss, lbs
Specimen	**Mix #5-701**
1	0.049
2	0.048
3	0.034
4	0.038
Average	0.042
Std. Dev.	0.006

US 67 CAM II Stabilized Base

Specimen 2 was obtained from the center of the slab panel in the driving lane at Station 26+000 NB (US 67 Core #2). Specimen 3 was obtained from outer wheel path at the transverse joint on the approach slab in the driving lane at Station 28+600 NB (US 67 Core #3). Specimen 4 was obtained from the center of the slab panel in the driving lane at Station 28+600 NB (US 67 Core #4). Specimen 6 was obtained from the center of the slab panel in the driving lane at Station 26+600 SB (US 67 Core #6). Specimens 2 and 4 were fully bonded to the JPCP and were cut at the interface to be able to test the CAM II. Specimens 3 and 6 were unbonded (no erosion occurring) and the top finished surface was tested.

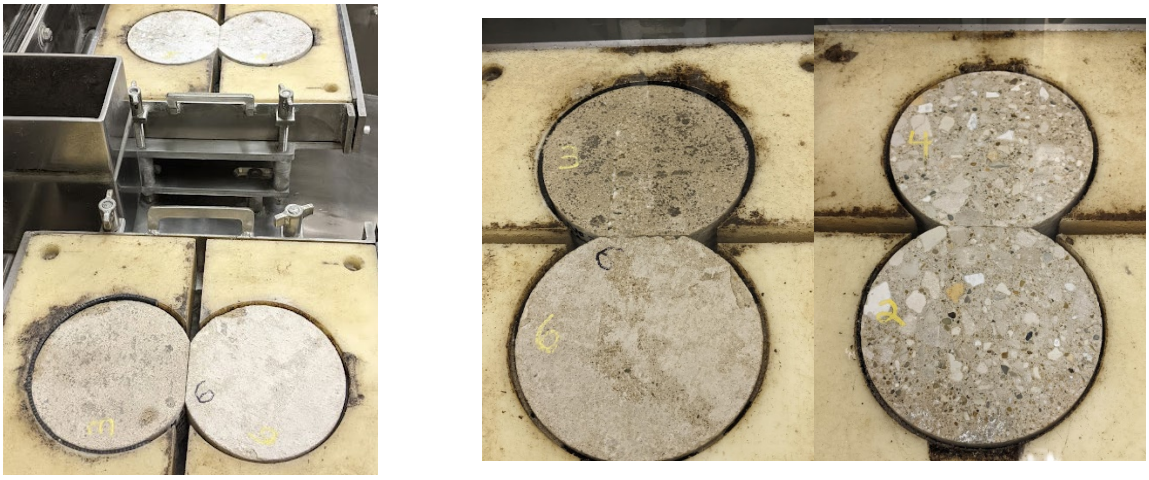

a) Specimens in HWTD b) Specimens after HWTD completion

Figure 42. Photos. US 67 CAM II - Hamburg wheel-tracking device (HWTD) specimens.

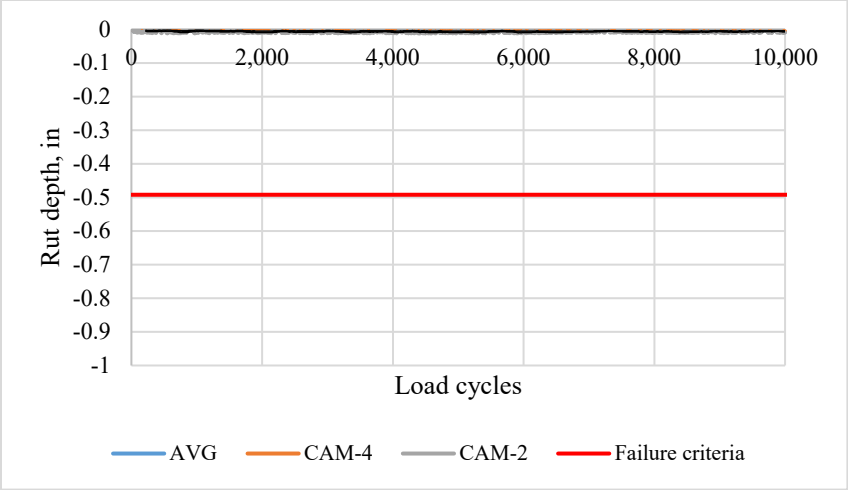

a) CAM II US 67 Specimens 4 and 2

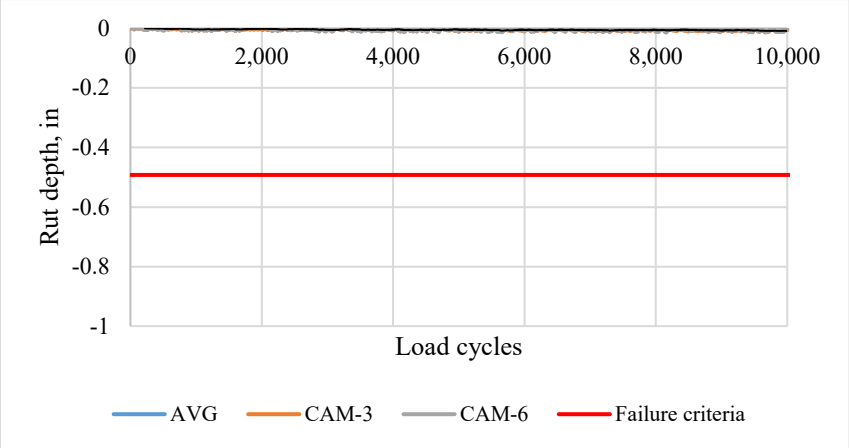

b) CAM II US 67 Specimens 3 and 6

Figure 43. Graphs. US 67 CAM II - Hamburg wheel-tracking device (HWTD) results.

Table 30. US 67 CAM II - Hamburg Wheel-tracking Device (HWTD) Weight Loss

	Weight Loss, lbs
Specimen	**US 67**
1 (CAM-6)	0.025
2 (CAM-3)	0.027
3 (CAM-2)	0.026
4 (CAM-4)	0.023
Average	0.025
Std. Dev.	0.002

IL 53 BCOA

Specimens 1 and 3 were obtained from the same location, center of panel at Station 61+10 SB (IL 53 Core #4). Specimens 2 and 4 were obtained from the same location, center of panel at Station 101+50 SB (IL 53 Core #6). Specimens 1 and 2 were the top lift of HMA (interface between PCC overlay),

whereas Specimens 3 and 4 were the second lift from the surface. The second lift from the surface failed drastically and can be observed in the following figures.

a) Specimens in HWTD (2&4 left, 1&3 right)

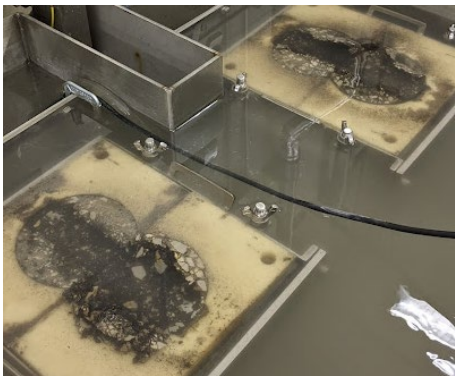

b) Specimens after HWTD completion

c) Specimens 2 and 4

d) Specimens 1 and 3

Figure 44. Photos. IL 53 BCOA Hamburg wheel-tracking device (HWTD) specimens.

The HWTD results are presented based on the different lifts. Therefore Specimens 1 and 2 (Lift 1) are presented and compared together, and Specimens 3 and 4 (Lift 2) are presented and compared together.

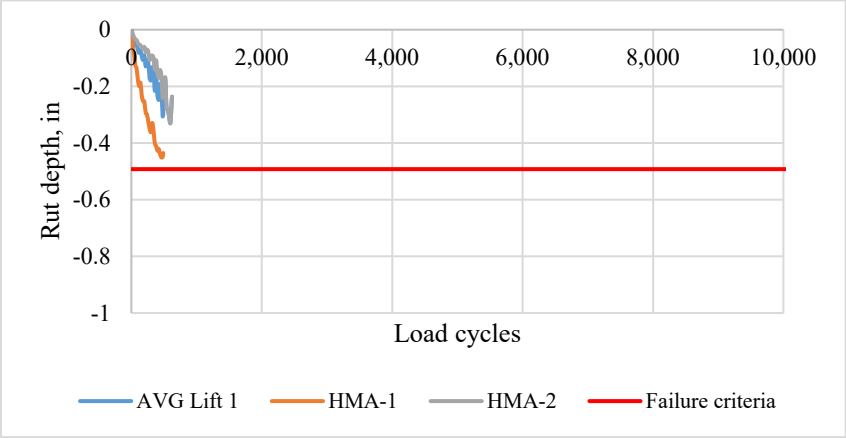

a) IL 53 BCOA Specimens 1 and 2 (Lift 1)

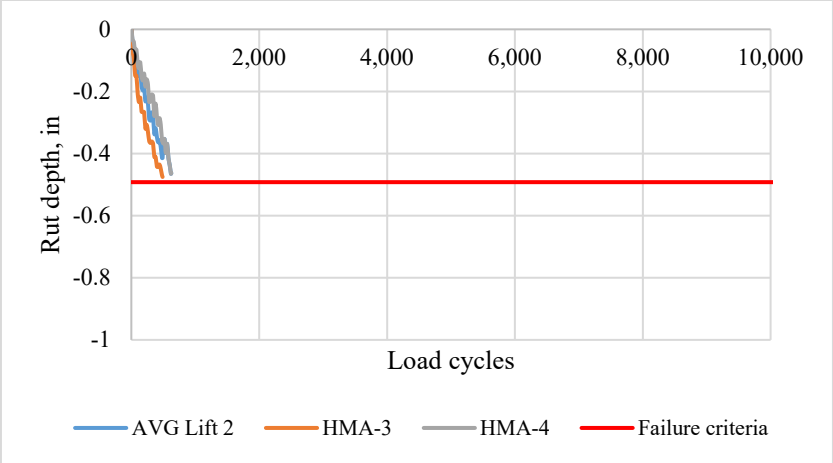

b) IL 53 BCOA Specimens 3 and 4 (Lift 2)

Figure 45. Graphs. IL 53 BCOA Hamburg wheel-tracking device (HWTD) results.

Table 31. IL 53 BCOA Hamburg Wheel-tracking Device (HWTD) Weight Loss

	Weight Loss, lbs	
Specimen	**IL 53 – Lift 1**	**IL 53 – Lift 2**
1	0.097	0.283
2	0.072	1.400
3	-	-
4	-	-
Average	0.085	0.842
Std. Dev.	0.012	0.559

US 30 HMA Stabilized Subbase

Specimens 1 and 3 were obtained from the same location, center of panel at Station 56+00 WB (US 30 Core #3). Specimens 2 and 4 were obtained from the same location, center of panel at Station 8+00 EB (US 30 Core #5). Specimens 1 and 2 were the top lift of HMA (interface between PCC), whereas Specimens 3 and 4 were comprised of the second lift from the surface or a different HMA mixture. This second lift HMA resulted in poor performance as compared to the HMA mixture at or close to the interface of the PCC.

This test was conducted to reach a maximum threshold of 10,000 cycles or a maximum rut-depth of 1 in. (25 mm) instead of the set protocol of 0.5 in. (12.5 mm) to assess the possible stripping index.

a) Specimens in HWTD (1&2 left, 3&4 right)

b) Specimens after HWTD completion

c) Specimens 1 and 2

d) Specimens 3 and 4

Figure 46. Photos. US 30 HMA subbase Hamburg wheel-tracking device (HWTD) specimens.

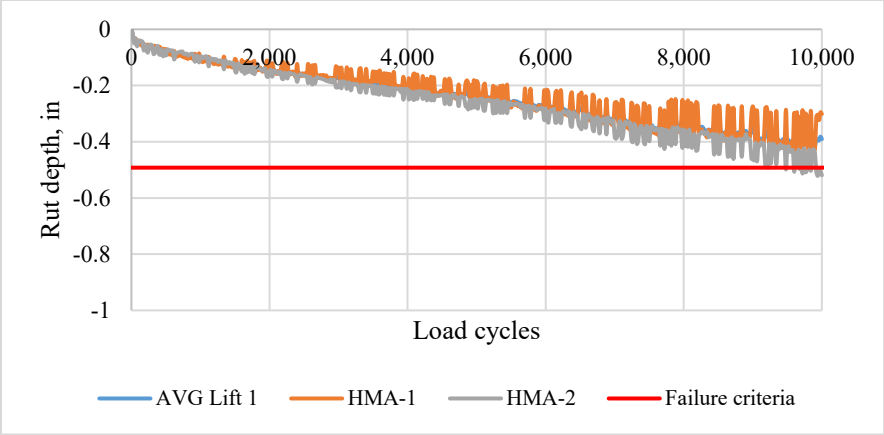

a) US 30 Specimens 1 and 2 (Lift 1)

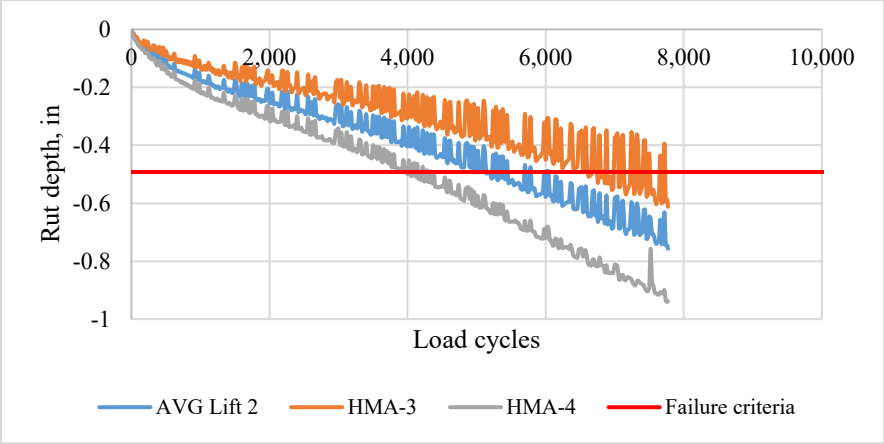

b) US 30 Specimens 3 and 4 (Lift 2)

Figure 47. Graphs. US 30 HMA subbase Hamburg wheel-tracking device (HWTD) results.

Table 32. US 30 HMA Subbase Hamburg Wheel-tracking Device (HWTD) Weight Loss

	Weight Loss, lbs	
Specimen	**US 30 – Lift 1**	**US 30 - Lift 2**
1 (US 30 Core #3)	0.011	-
2 (US 30 Core #5)	0.053	-
3 (US 30 Core #3)	-	0.058
4 (US 30 Core #5)	-	0.045
Average	0.032	0.052
Std. Dev.	0.021	0.006

Additional testing was performed on other cores obtained from US 30. Specimens 1 and 3 were obtained from the same location, outer wheel path on the leave slab at the transverse joint at Station 95+00 EB (US 30 Core #2). Specimens 2 and 4 were obtained from the same location, outer wheel path on the leave slab at the transverse joint at Station 8+00 EB (US 30 Core #4). Specimens 1 and 2 were the top lift of HMA (interface between PCC overlay), whereas Specimens 3 and 4 were the second lift from the surface. The bottom of Specimen 4 was very erodible prior to testing.

a) Specimens in HWTD (1&2 left, 3&4 right)

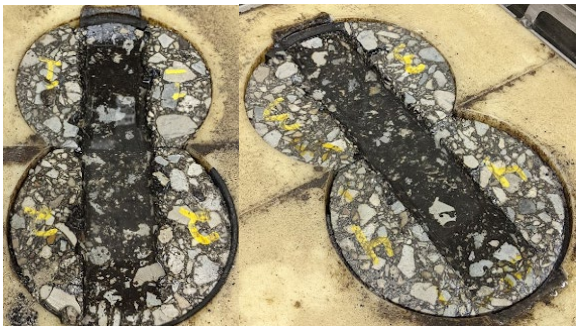

b) Specimens after HWTD completion

c) Specimens 1 and 2

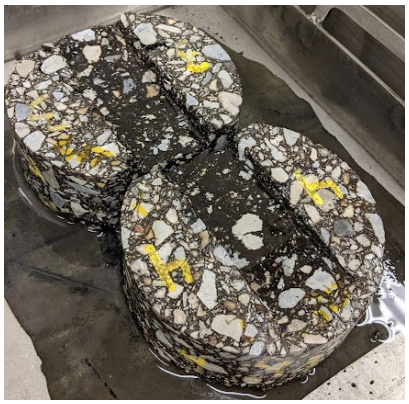

d) Specimens 3 and 4

Figure 48. Photos. US 30 HMA subbase Hamburg wheel-tracking device (HWTD) specimens.

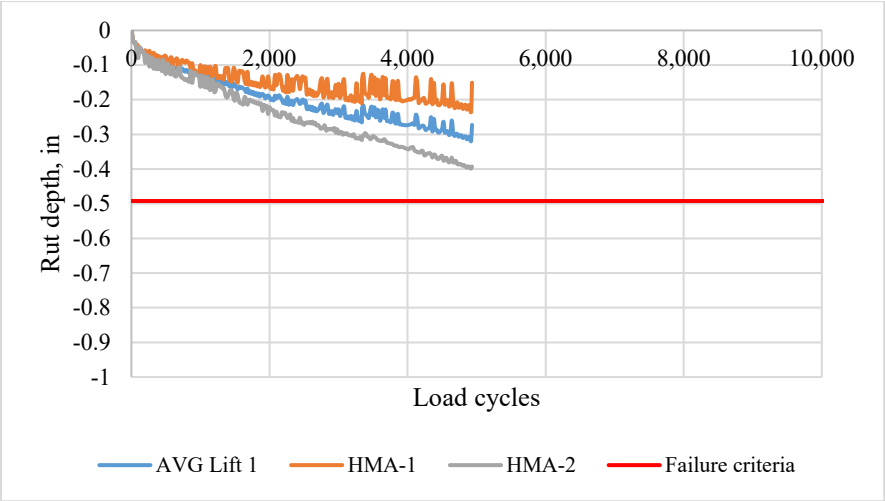

a) US 30 Specimens 1 and 2 (Lift 1)

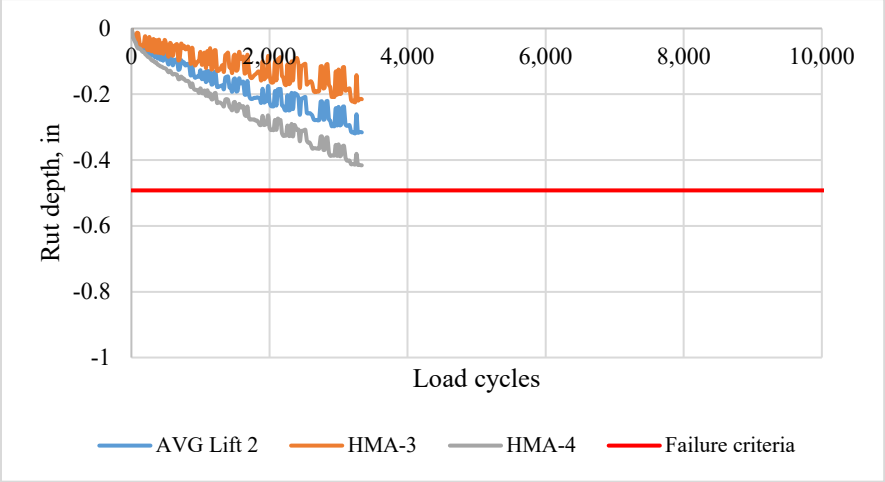

b) US 30 Specimens 3 and 4 (Lift 2)

Figure 49. Graphs. US 30 HMA subbase Hamburg wheel-tracking device (HWTD) results.

Table 33. US 30 HMA Subbase Hamburg Wheel-tracking Device (HWTD) Weight Loss

	Weight Loss, lbs	
Specimen	**US 30 – Lift 1**	**US 30 – Lift 2**
1 (US 30 Core #2)	0.026	-
2 (US 30 Core #4)	0.032	-
3 (US 30 Core #2)	-	0.017
4 (US 30 Core #4)	-	0.061
Average	0.029	0.039
Std. Dev.	0.003	0.022

SPLIT TENSILE RESULTS

Split tensile testing was conducted in accordance with ASTM C496 and ASTM D6931for CAM II and HMA specimens, respectively. Testing was performed on CAM II specimens after HWTD testing. The results are likely lower than true values due to the erosion at the surface of the specimens from the HWTD testing, but provide an estimate for correlation of results. The cored HMA specimens were too small in thickness to be able to conduct HWTD testing, and therefore were only tested using the split tensile test. The standard loading rate was adjusted as a function of the length and diameter of the specimens.

a) CAM II Mix #2 - 409

b) US 30 HMA

c) IL 53 BCOA

d) IL 53 BCOA

Figure 50. Photos. Split tensile strength testing.

Table 34. Split Tensile Strength Results

	Split Tensile Results, psi										
Specimen ID	Mix 1: 402	Mix 2: 409	Mix 3: 416	Mix 1: 625	Mix 4: 629	Mix 5: 701	US 67	IL 53 Lift 1	IL 53 Lift 2	US 30 Lift 1	US 30 Lift 2[4]
1	153	-	318	143	85	252	437	47[2]	72.3	54.2[3]	-
2	182	-	320	117[1]	77	220	483	101	80.2	49.8[3]	22.5[3]
3	131	95.7	298	146	82	206	502	56[2]	-	70.4	54.6
4	-	121	343	161	75	213	440	-		83.2	73.5
Average	155	108	320	150	80	223	465	101	76	77	64
Std. Dev.	21.1	12.6	16.0	7.9	4.0	17.9	28.1	0.0	4.0	6.4	9.4

[1]Specimen had edge failures from HWTD prior to split tensile strength testing.

[2]User error, operator failed specimen when seating the load by applying max load instantaneously.

[3]Loading machine was not working properly and the loading rate did not reach the required range specified in ASTM D6931.

[4]Lift 2 was comprised of 1.5 in. of Lift 1 + 1 in. of a different mix.

APPENDIX B: SUMMARY OF FIELD-TESTING PLAN

FIELD TESTING PLAN EVALULATING STABILIZED SUPPORT LAYERS UNDER CONCRETE PAVEMENTS

Testing consisted of FWD with concrete temperature profile measurements, MIRA scanning, and manual distress surveying. Coring was also performed on each of the different stabilized support layers (4 sections). The list of sections examined is presented in **Table 35**.

In addition to the test sections outlined below, samples were prepared from a CIR project within District 5 for laboratory testing.

Table 35. Field Sections Evaluated and Tested

Section ID	County/District Location	Pavement Type	Field Testing			
			FWD	MIRA	Coring	Distress Survey
US 67 (92774)	Sangamon Co./D6	JPCP on CAM II	Y	Y	Y	Y
I-72 (92763)	Pike Co./D6	JPCP on CAM II	Y	Y	-	Y
US 20 (40455E)	Stephenson Co./D2	JPCP on CAM II	Y	Y	-	Y
US 30 (62277)	Cook Co./D1	JPCP on HMA	Y	Y	Y	Y
IL 64 (62410)	DuPage Co./D1	JPCP on HMA	Y	Y	-	Y
US 12/20/45	Cook Co./D1	JPCP on HMA	Y	Y	-	Y
I-72 EB/WB	Sangamon Co./D6	Thin UBOL	Y	Y	Y	Y
I-70	Clark Co./D7	CRCP UBOL	Y	Y	-	Y
IL 53 SB	Will Co./D1	BCOA	Y	Y	Y	Y
CH 27[1]	Macon Co.	BCOA	-	-	-	-
UIUC E-15 Parking Lot	Champaign Co./D5	BCOA	Y	Y	-	Y
UIUC McKinley Parking Lot	Champaign Co./D5	BCOA	Y	Y	-	Y

Note: Y (yes) indicates field testing performed for the corresponding section.
[1]CH-27 not tested but assessed with historical performance data.

The following breaks down the individual tests that were conducted, as well as the protocol and the information gained from the specific testing. FWD testing, MIRA scanning, and manual distress surveying were conducted on the same day for each corresponding section. Coring was performed by the corresponding District on a separate date.

1. FWD
    - ❑ Protocol:
        1. Existing FWD drop location testing protocol from IDOT followed (See **Figure 51a**)
        2. Three drop/load sequence per location (6, 9, and 12 kips)
        3. Up to 10 distinct locations tested using the five-slab intensive testing protocol (**Figure 51b**). Distance between locations depend on project length.
        4. Surface temperature at each drop location measured and recorded
        5. Drilled three temperature holes at the beginning of testing, halfway through testing, and 30 minutes from end of testing
    - ❑ Outcome from backcalculation:
        1. Effective thickness (adhesion / composite action properties)
        2. Structural support conditions (k-value)
        3. Interfacial contact friction (Slab-subbase interface friction)
        4. Temperature with slab depth during testing (adjust backcalculation based on slab curvature)
2. MIRA
    - ❑ Protocol:
        1. Three to four subsections tested out of the 10 tested with FWD; consisted of five adjacent joints/panels with repeatability testing of three to five scans per location
        2. Specific protocol was based on different panel size (See **Figure 52**)
    - ❑ Outcome from scans:
        1. Surface layer thickness, presence and thickness of base, cracks/defects, or delamination
        2. Joint details (presence of dowels and tie bars)
        3. Transverse joint activation
        4. “Kissing bond” - degree of interfacial bond
3. Manual distress survey
    - ❑ Protocol:
        1. Recorded distresses where FWD, MIRA, and Coring were conducted
        2. FHWA distress surveying guidelines were followed
    - ❑ Outcome:
        1. Section cracking/distresses present and whether they are caused by erosion of stabilized support layers were determined
4. Coring
    - ❑ Protocol:
        1. Four to six cores per subbase type (dictated by time for each District)

2. Taken from good, fair, poor sections within the project stationing and based on visual distresses observed by surveyors
3. Five sections total
    - ❑ CAM II (US 67)
    - ❑ HMA
        - ❑ Stabilized HMA subbase (US 30)
        - ❑ HMA interlayer (I-72 EB)
        - ❑ Fabric interlayer (I-72 WB)
        - ❑ Existing HMA surface layer (IL-53)

❑ Outcome:

1. Layer thicknesses and interface condition
2. Task 2 lab testing – HWTD testing, if possible

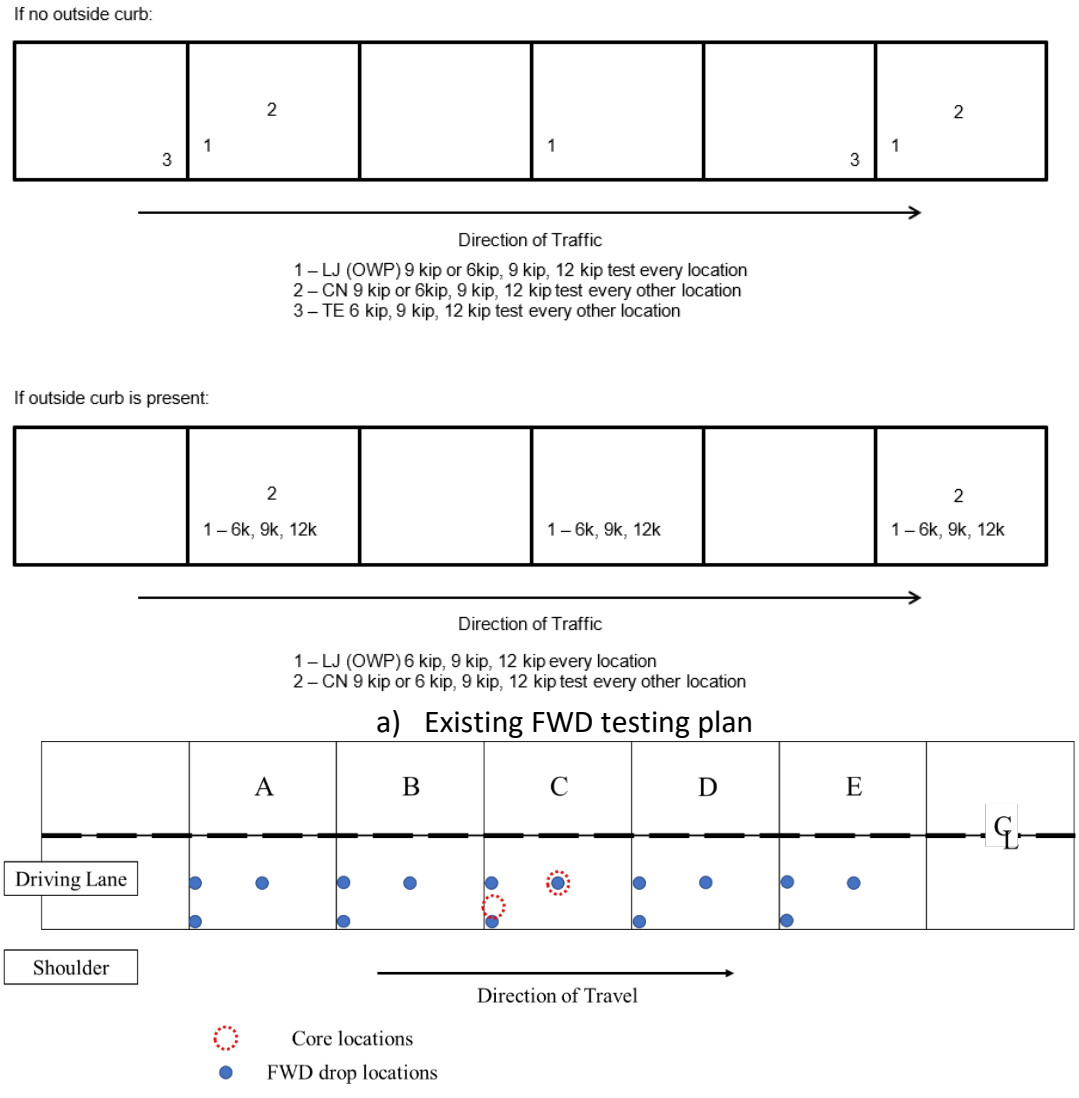

Figure 51. Schematics. FWD testing protocol proposed by a) IDOT and b) UIUC.

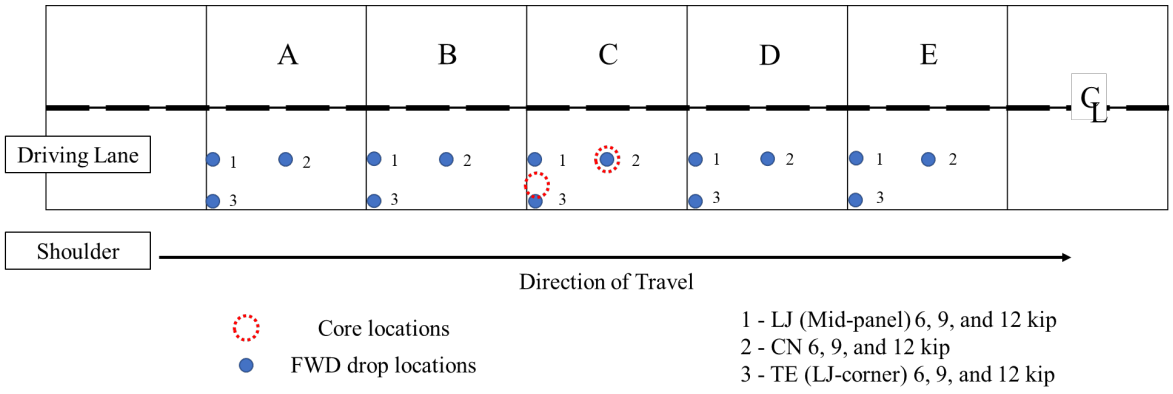

a) Full-lane width panels

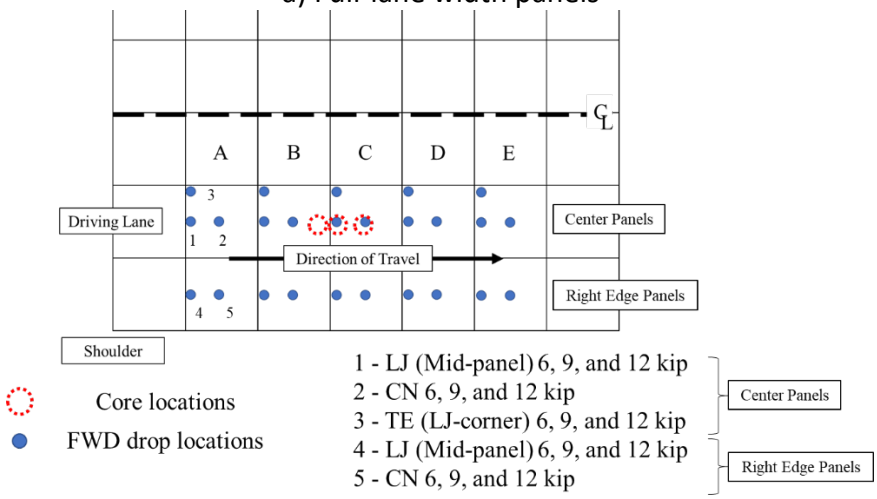

b) Partial-lane width panels (Only test six distinct locations)

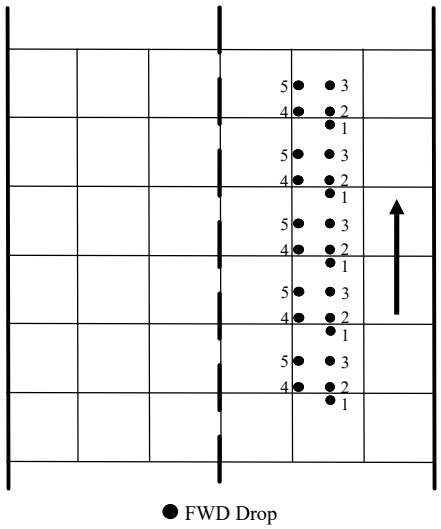

c) Partial-lane width panels: UIUC Parking Lots

Figure 52. Schematics. Final FWD testing protocol.

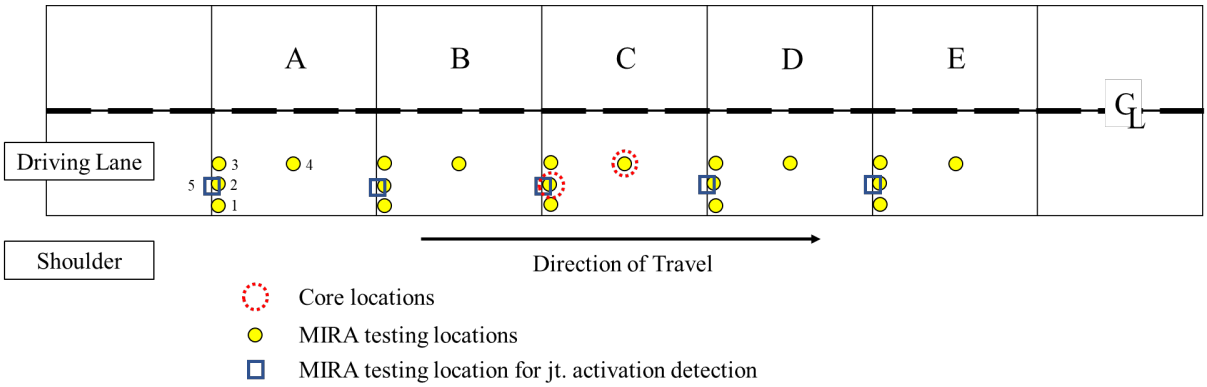

a) MIRA testing plan for full-lane width panels

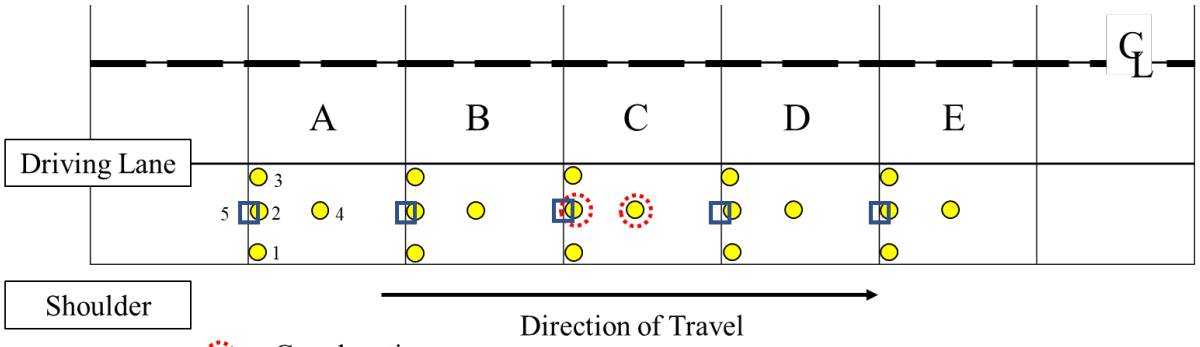

b) MIRA testing plan for half-lane width panels

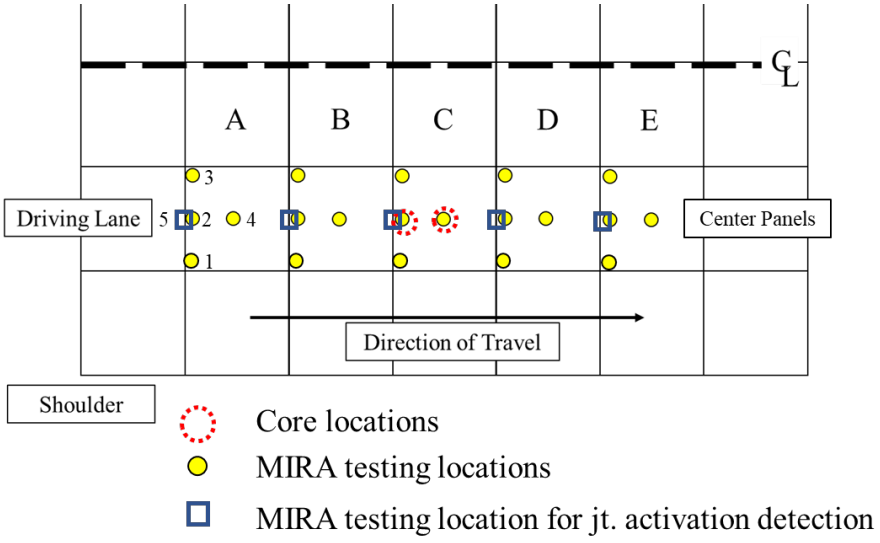

c) MIRA testing plan for small panels

Figure 53. Schematics. MIRA testing protocol.

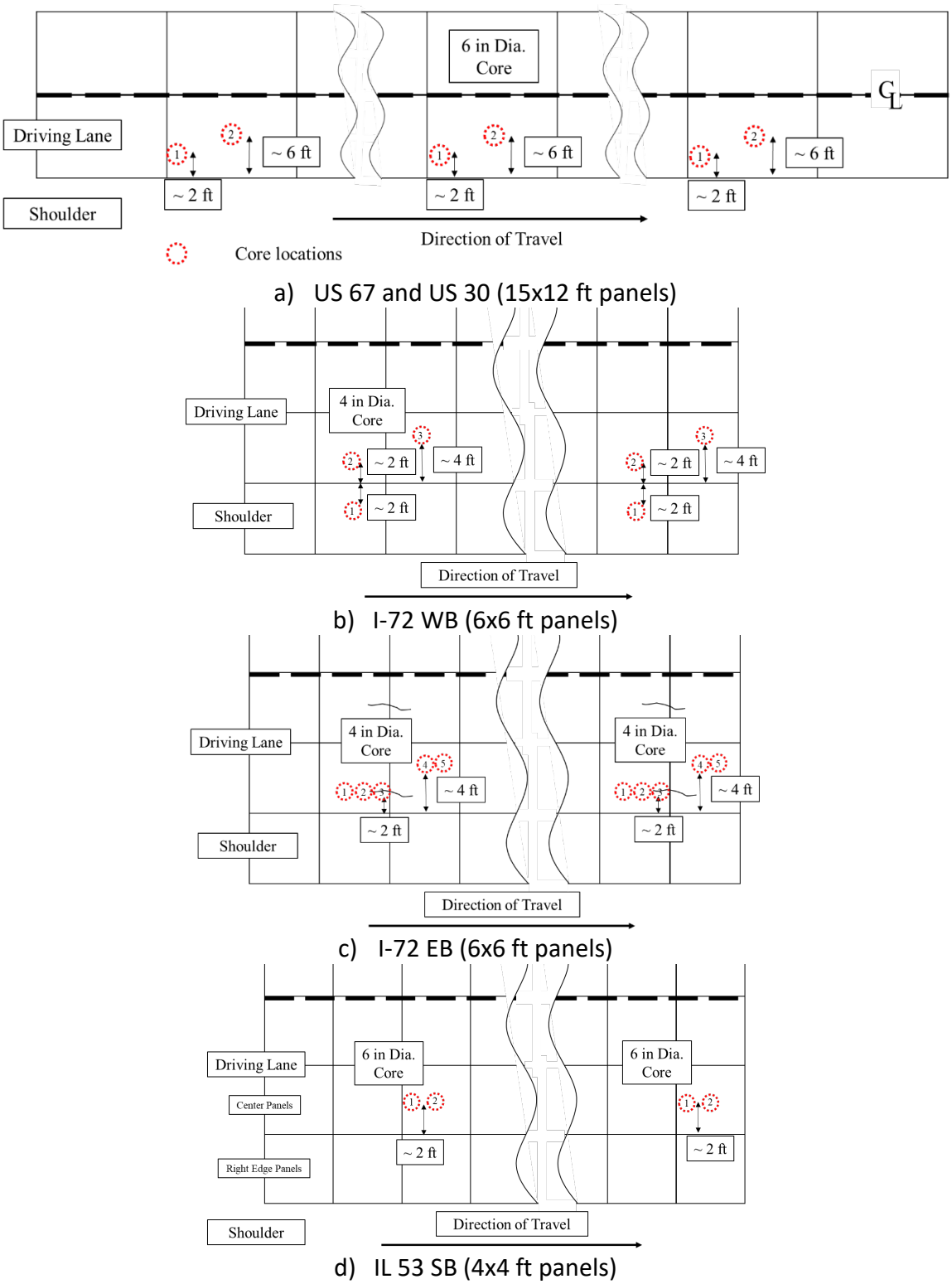

Figure 54. Schematics. Coring location protocol.

Additionally, temperature holes were used to measure the pavement temperature profile according to the LTPP testing protocol (Schmalzer 2006). The holes were drilled in the outer wheel path (OWP).

Three holes were drilled for each location. Depths were approximately 1 in. below the surface, mid-depth, and 1 in. from the bottom of the concrete. The bottom 0.5 in. of each hole was filled with mineral spirits to provide thermal conductivity between the concrete and the thermocouple.

APPENDIX C: FALLING WEIGHT DEFLECTOMETER RESULTS

Each section presents FWD testing results performed during the summer of 2020 and spring of 2021. Additionally, if any historical FWD testing was available, it is also presented for time-series comparisons. Information presented includes slab-base or slab-subbase interface friction, backcalculated effective thickness, and static k-value (modulus of subgrade reaction). It also includes the normalized deflection, D0* directly beneath the load normalized to 9-kip load level (half an ESAL), AREA, and Eri (for comparison with the modulus of subgrade reaction). Joint LTE is also examined across transverse joints and longitudinal joints (leave joint and corner of leave joint).

US 67 (92774)

A summary of the FWD testing performed in 2016 and 2020 is provided. Additionally, plots are included for comparison.

Table 36. FWD Summary from Center Slab Testing for US 67 (92774)

	10/27/2016						9/9/2020					
Parameter	D0* (mils)		Area_36		Eri		D0* (mils)		Area_36		Eri	
Direction	NB	SB	NB	SB	NB	SB	NB	SB	NB	SB	NB	SB
Average	2.26	2.33	31.7	31.3	15.5	15.3	2.42	2.45	31.5	31.3	14.4	14.4
Std. Dev.	0.29	0.41	1.42	1.21	1.55	1.58	0.34	0.45	1.32	1.10	1.03	1.52
COV	12.8	17.6	4.5	3.9	10.0	10.3	14.1	18.5	4.18	3.51	7.19	10.6

Table 37. FWD Summary from Leave Joint LTE Testing for US 67 (92774)

	10/27/2016				9/9/2020			
Parameter	D0* (mils)		LTE (%)		D0* (mils)		LTE (%)	
Direction	NB	SB	NB	SB	NB	SB	NB	SB
Average	4.8	4.7	86.4	87.7	3.51	3.33	89.6	89.2
Std. Dev.	1.05	1.02	6.76	5.85	0.58	0.50	5.90	7.03
COV	21.8	21.9	7.82	6.68	16.6	14.9	6.59	7.89

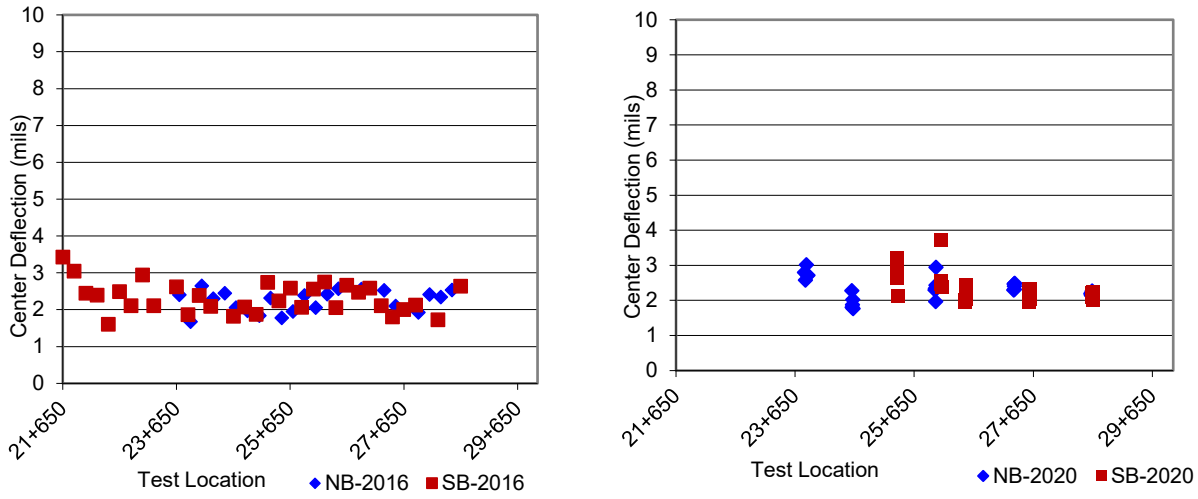

a) 10/27/2016 b) 9/9/2020

Figure 55. Graphs. Normalized 9-kip deflection, D0*, at center panel for US 67 (92774).

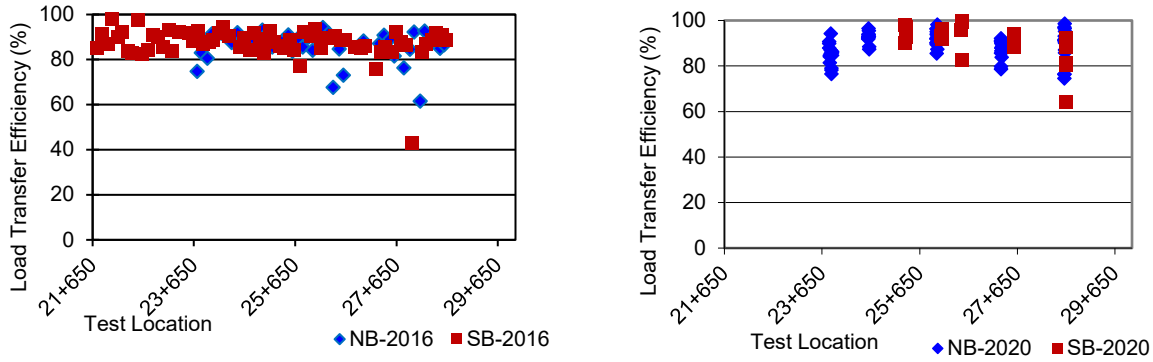

a) 10/27/2016 b) 9/9/2020

Figure 56. Graphs. Load transfer efficiency (LTE) for US 67 (92774).

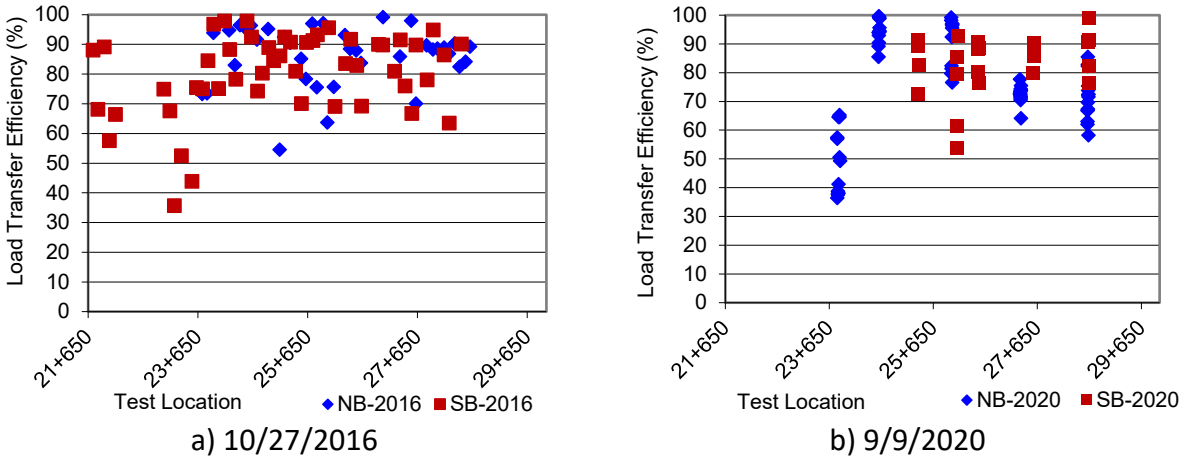

a) 10/27/2016 b) 9/9/2020

Figure 57. Graphs. Lane shoulder longitudinal joint load transfer efficiency (LTE) for US 67 (92774).

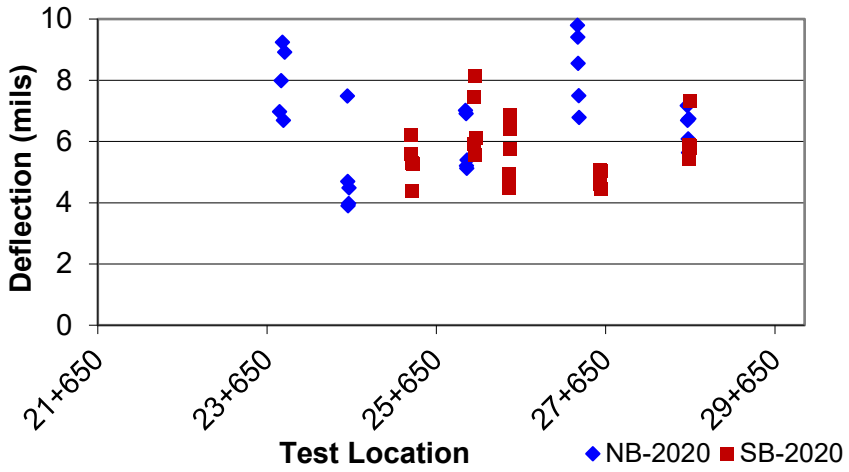

Figure 58. Graph. Normalized 9-kip deflection in the corner along the lane shoulder longitudinal joint for US 67 (92774).

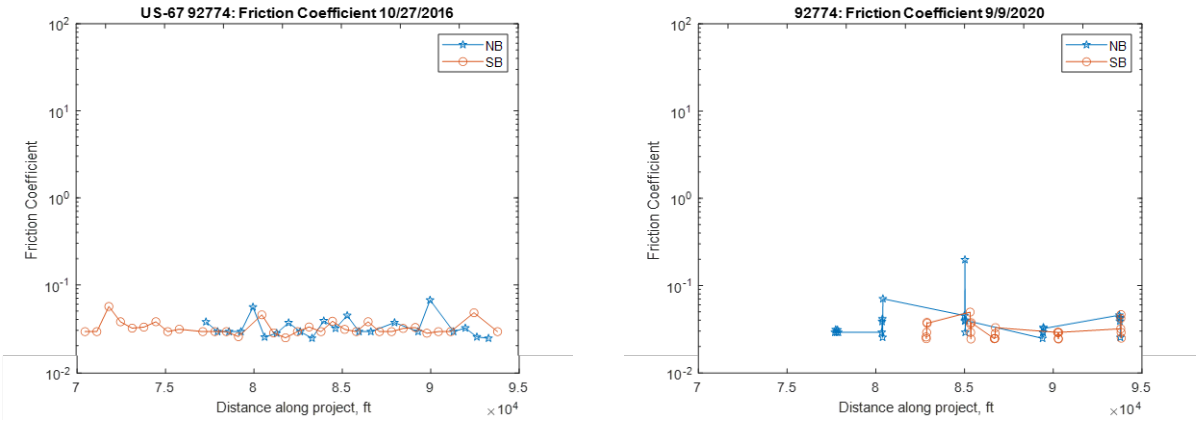

a) 10/27/2016 b) 9/9/2020

Figure 59. Graphs. Friction coefficient along US 67 (92774).

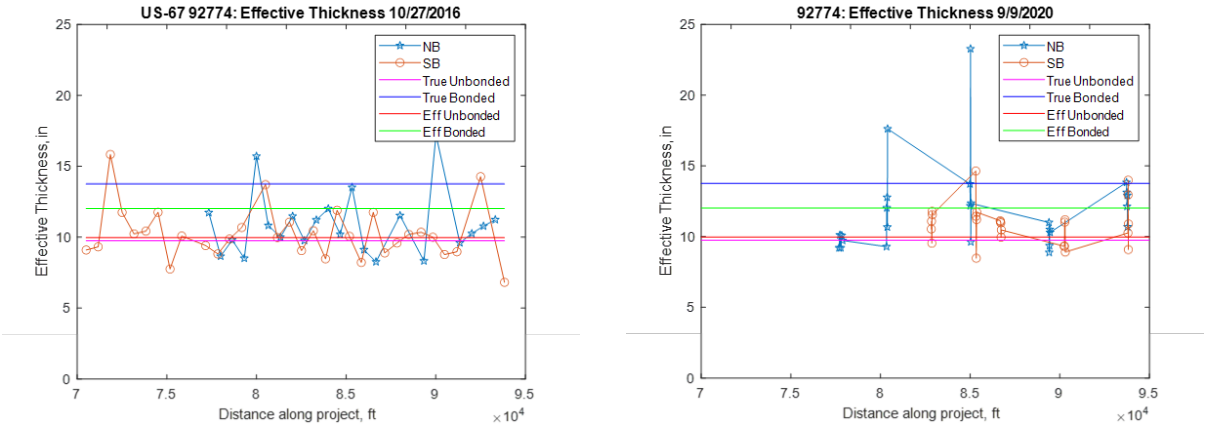

a) 10/27/2016 b) 9/9/2020

Figure 60. Graphs. Effective thickness along US 67 (92774).

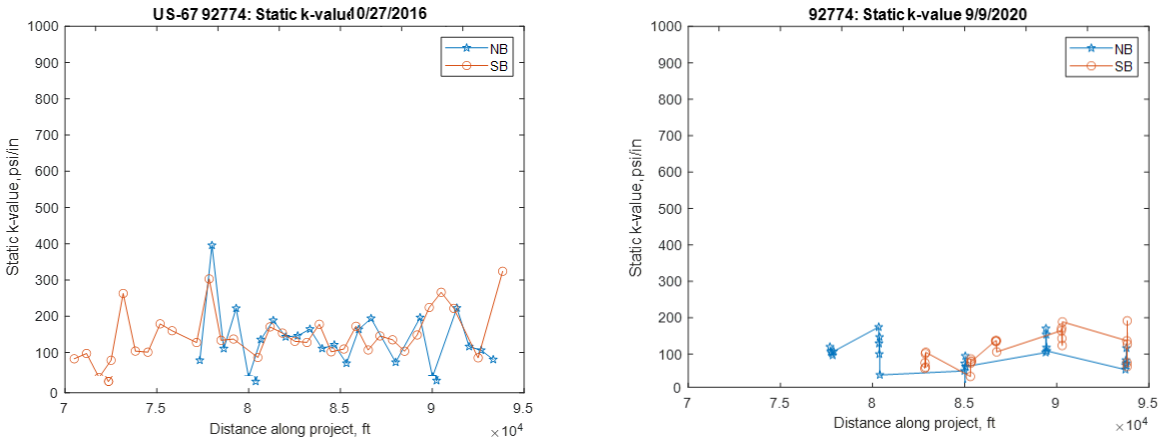

a) 10/27/2016 b) 9/9/2020

Figure 61. Graphs. Static k-value along US 67 (92774).

I-72 (92763)

A summary of the FWD testing performed in 2016 and 2020 is provided. Additionally, plots are included for comparison.

Table 38. FWD Summary from Center Slab Testing for I-72 (92763)

	11/16/2016						9/10/2020					
Parameter	D0* (mils)		Area_36		Eri		D0* (mils)		Area_36		Eri	
Direction	WB	EB	WB	EB	WB	EB	WB	EB	WB	EB	WB	EB
Average	3.07	2.89	32.4	32.1	11.7	12.8	2.77	2.88	31.6	31.0	13.1	13.1
Std. Dev.	0.90	0.37	2.93	1.50	3.08	1.54	0.35	0.38	0.71	0.95	1.41	1.28
COV	29.1	12.6	9.04	4.66	26.2	12.0	12.7	13.1	2.25	3.06	10.8	9.74

Table 39. FWD Summary from Leave Joint LTE Testing for I-72 (92763)

	11/16/2016				9/10/2020			
Parameter	D0* (mils)		LTE (%)		D0* (mils)		LTE (%)	
Direction	WB	EB	WB	EB	WB	EB	WB	EB
Average	5.13	4.24	88.5	85.0	4.87	4.23	88.9	94.4
Std. Dev.	1.48	1.46	6.23	16.3	1.10	0.51	16.2	4.81
COV	28.9	34.6	7.04	19.1	22.5	12.1	18.3	5.10

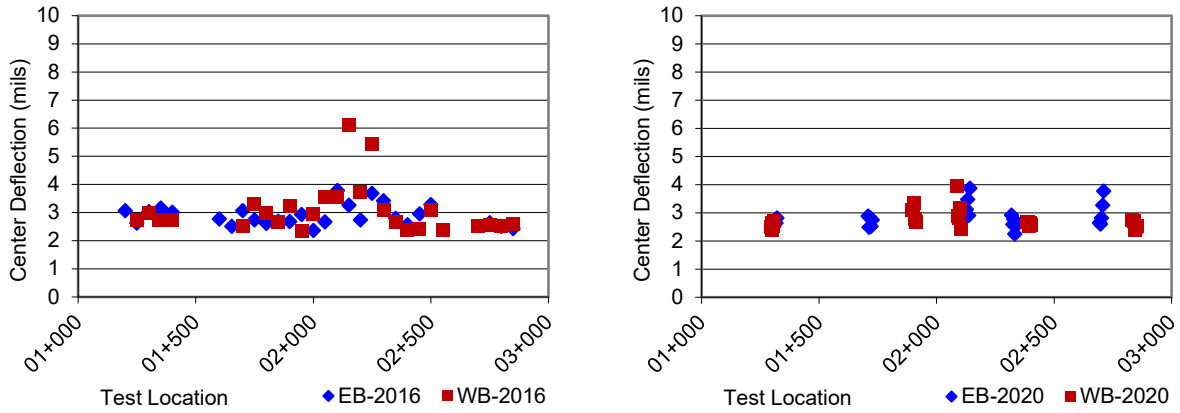

a) 11/16/2016 b) 9/10/2020

Figure 62. Graphs. Normalized 9-kip deflection, D0*, at center panel for I-72 (92763).

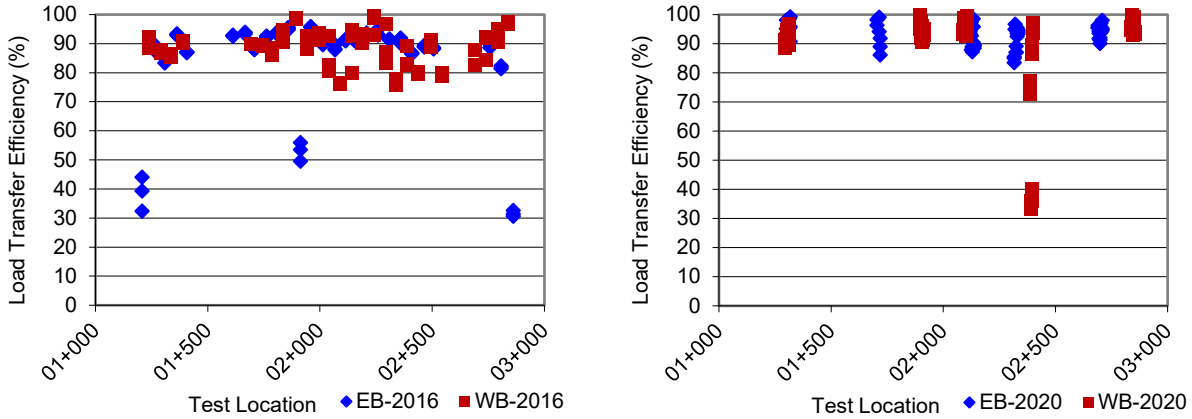

a) 11/16/2016 b) 9/10/2020

Figure 63. Graphs. Load transfer efficiency (LTE) for I-72 (92763).

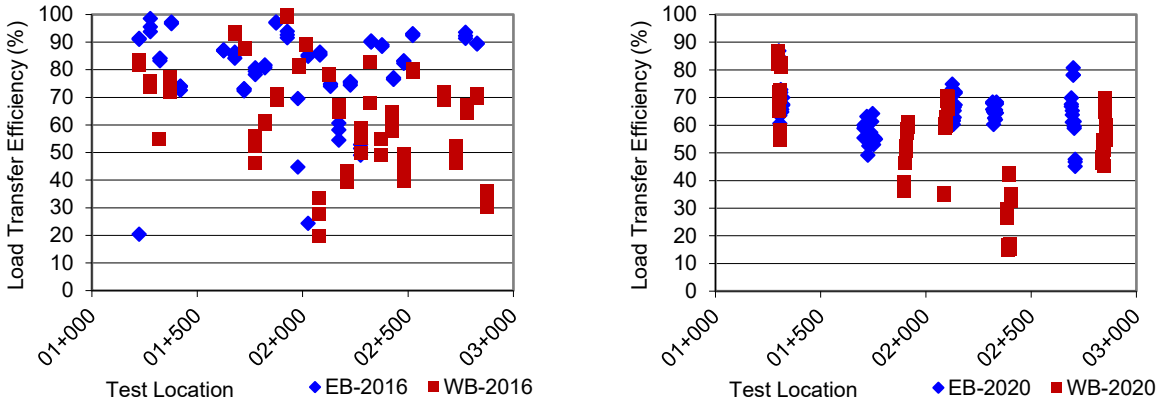

a) 11/16/2016 b) 9/10/2020

Figure 64. Graphs. Lane shoulder longitudinal joint load transfer efficiency (LTE) for I-72 (92763).

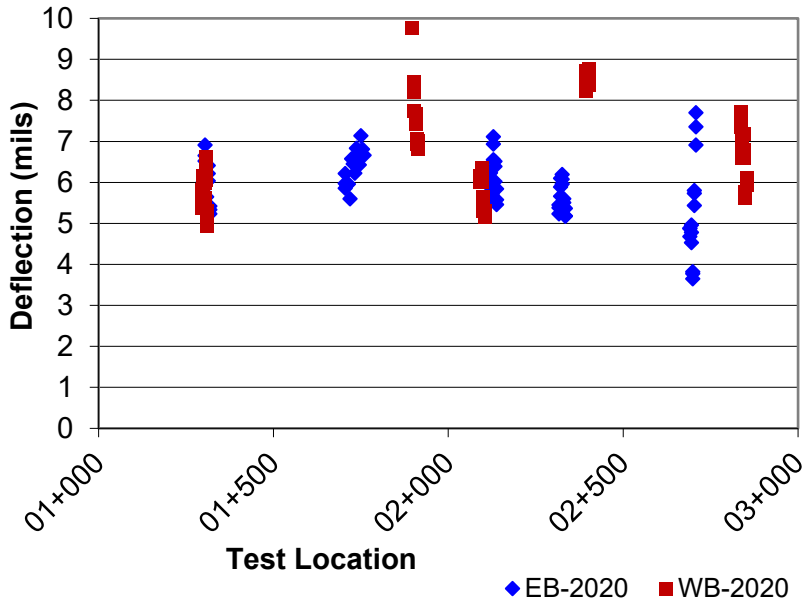

Figure 65. Graph. Normalized 9-kip deflection in the corner along the lane shoulder longitudinal joint for I-72 (92763).

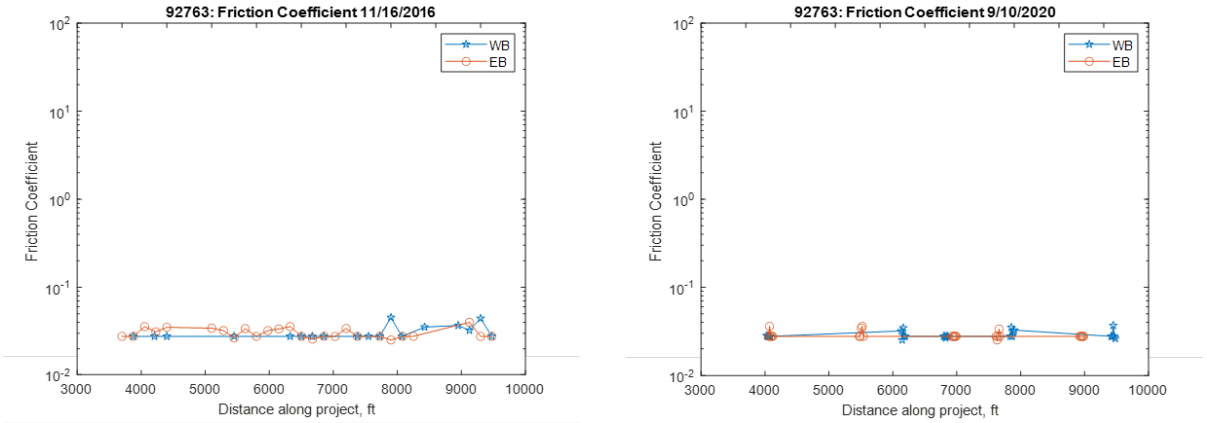

a) 11/16/2016 b) 9/10/2020

Figure 66. Graphs. Friction coefficient along I-72 (92763).

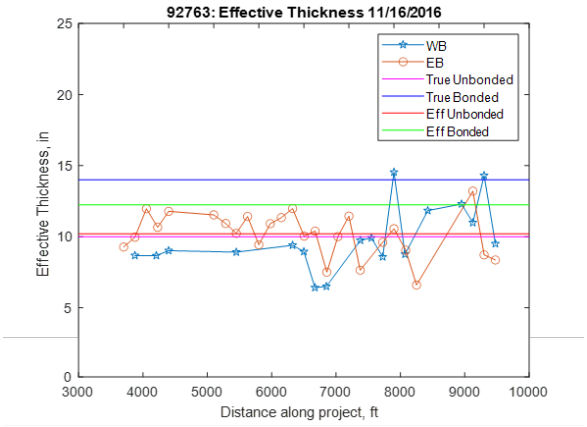

a) 11/16/2016

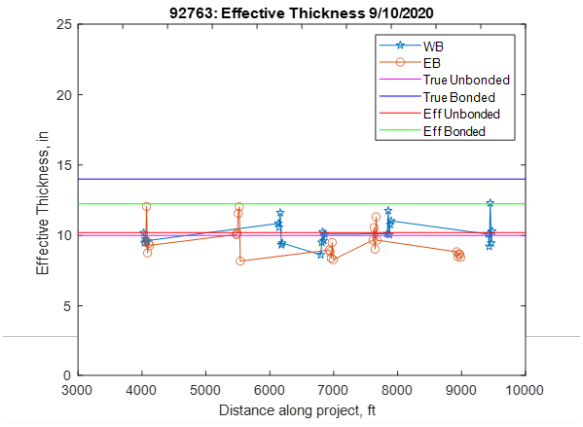

b) 9/10/2020

Figure 67. Graphs. Effective thickness along I-72 (92763).

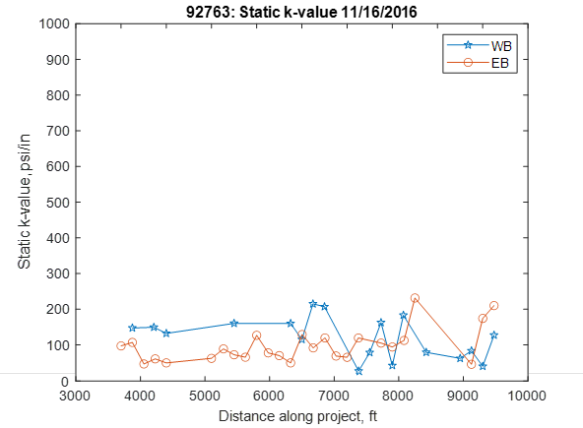

a) 11/16/2016

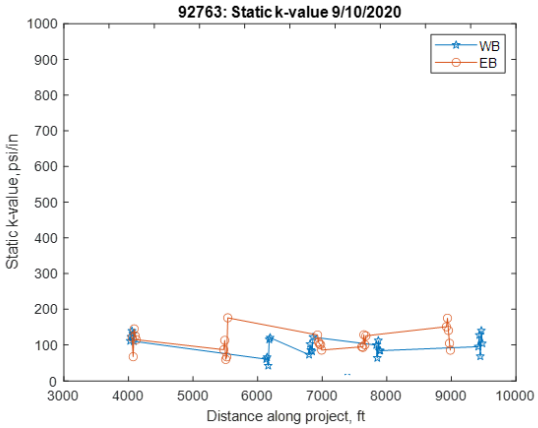

b) 9/10/2020

Figure 68. Graphs. Static k-value along I-72 (92763).

US 20 (40455)

Section E

A summary of the FWD testing performed in 2017 and 2020 is provided. Additionally, plots are included for comparison.

Table 40. FWD Summary from Center Slab Testing for US 20 (40455E & 40455H)

	10/31/2017						8/20/2020					
Parameter	D0* (mils)		Area_36		Eri		D0* (mils)		Area_36		Eri	
Direction	E-EB	H-EB	E-EB	H-EB	E-EB	H-EB	E-EB	H-EB	E-EB	H-EB	E-EB	H-EB
Average	2.89	3.13	31.1	31.8	14.9	13.1	2.90	5.30	30.0	31.1	14.1	6.70
Std Dev.	1.66	1.01	3.97	1.29	1.31	2.17	0.51	0.87	0.69	1.71	1.56	2.17
COV	57.5	32.1	12.8	4.05	8.80	16.6	17.4	16.5	2.31	5.49	11.1	32.4

Table 41. FWD Summary from Leave Joint LTE Testing for US 20 (40455E & 40455H)

	10/31/2017				8/20/2020			
Parameter	D0* (mils)		LTE (%)		D0* (mils)		LTE (%)	
Direction	E-EB	H-EB	E-EB	H-EB	E-EB	H-EB	E-EB	H-EB
Average	3.96	3.81	87.6	86.2	3.65	3.75	90.4	80.5
Std. Dev.	0.46	0.75	6.20	8.55	0.55	0.83	6.37	16.4
COV	11.6	19.6	7.08	9.92	15.0	22.1	7.05	20.4

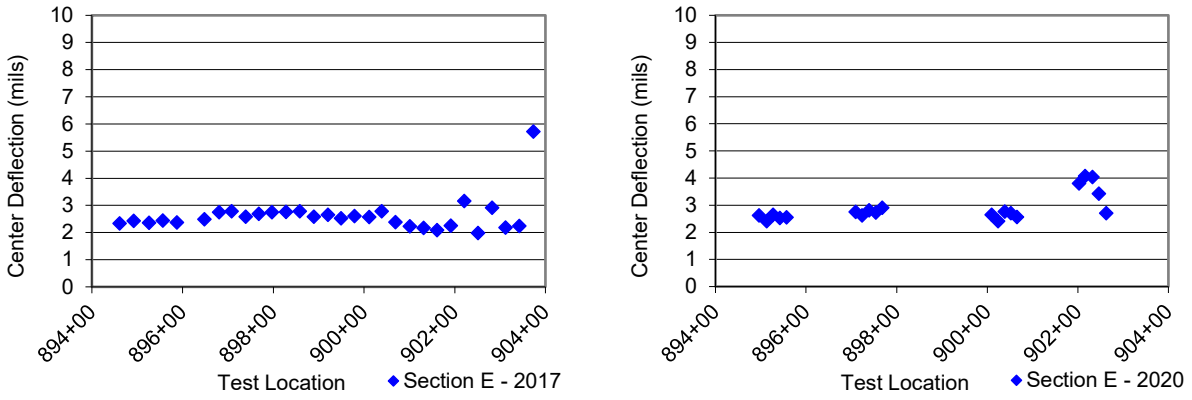

a) 10/31/2017 b) 8/20/2020

Figure 69. Graphs. Normalized 9-kip deflection, D0*, at center panel for US 20 (40455E).

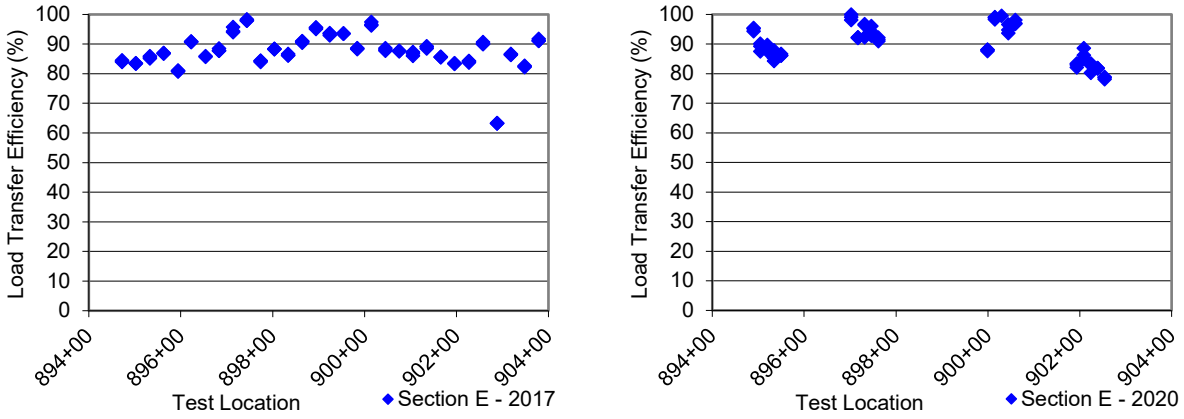

a) 10/31/2017 b) 8/20/2020

Figure 70. Graphs. Load transfer efficiency (LTE) for US 20 (40455E).

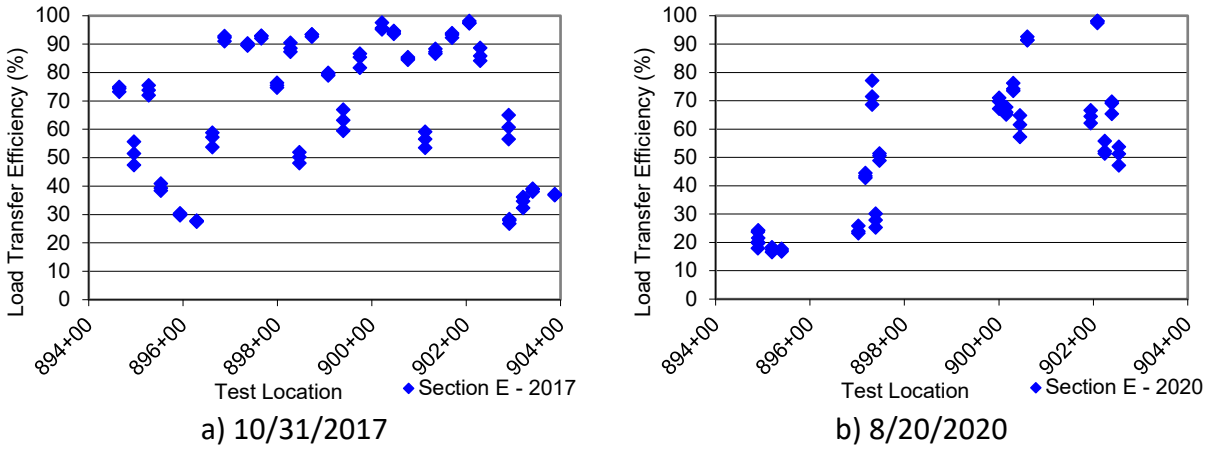

Figure 71. Graphs. Lane shoulder longitudinal joint load transfer efficiency (LTE) for US 20 (40455E).

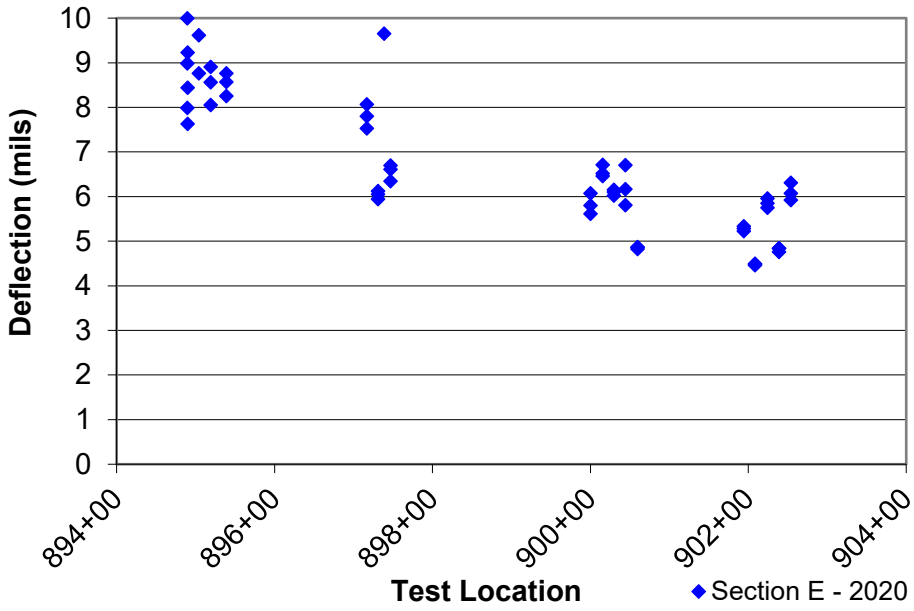

Figure 72. Graph. Normalized 9-kip deflection in the corner along the lane shoulder longitudinal joint for US 20 (40455E).

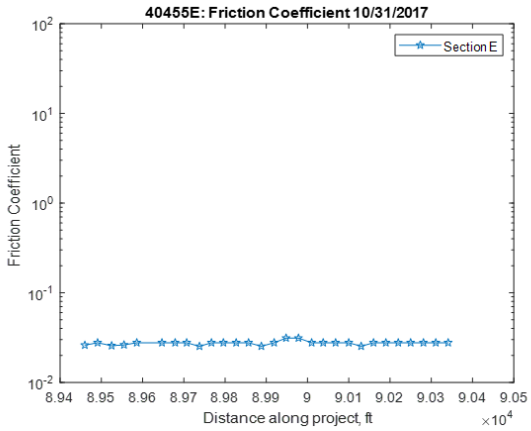

a) 10/31/2017

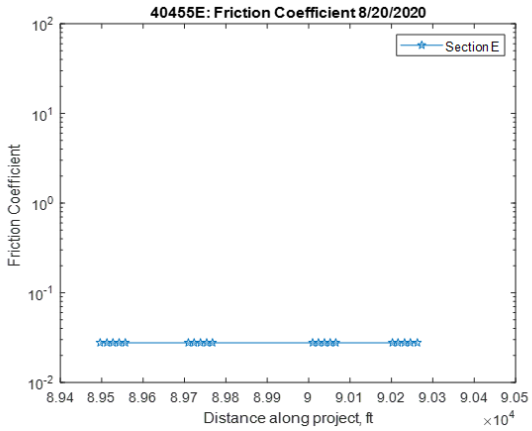

b) 8/20/2020

Figure 73. Graphs. Friction coefficient along US 20 (40455E).

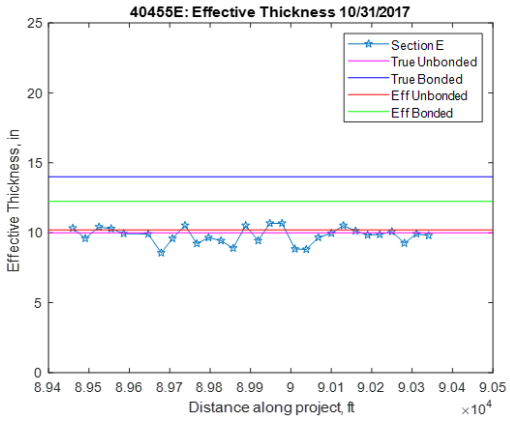

a) 10/31/2017

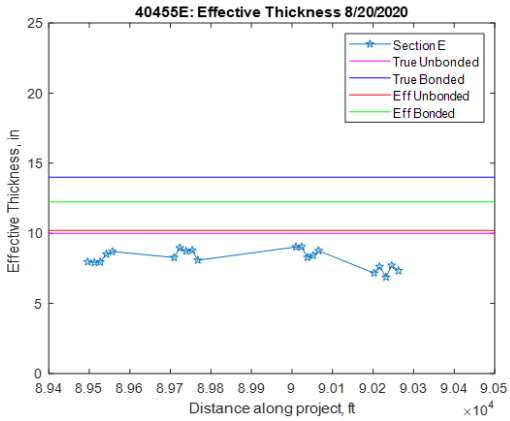

b) 8/20/2020

Figure 74. Graphs. Effective thickness along US 20 (40455E).

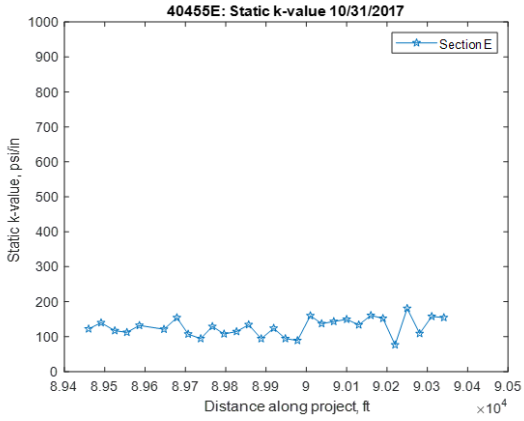

a) 10/31/2017

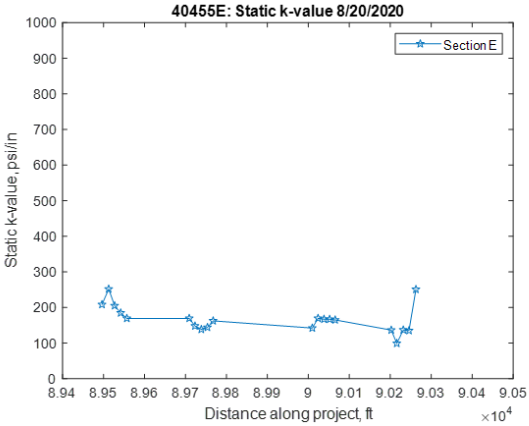

b) 8/20/2020

Figure 75. Graphs. Static k-value along US 20 (40455E).

Section H

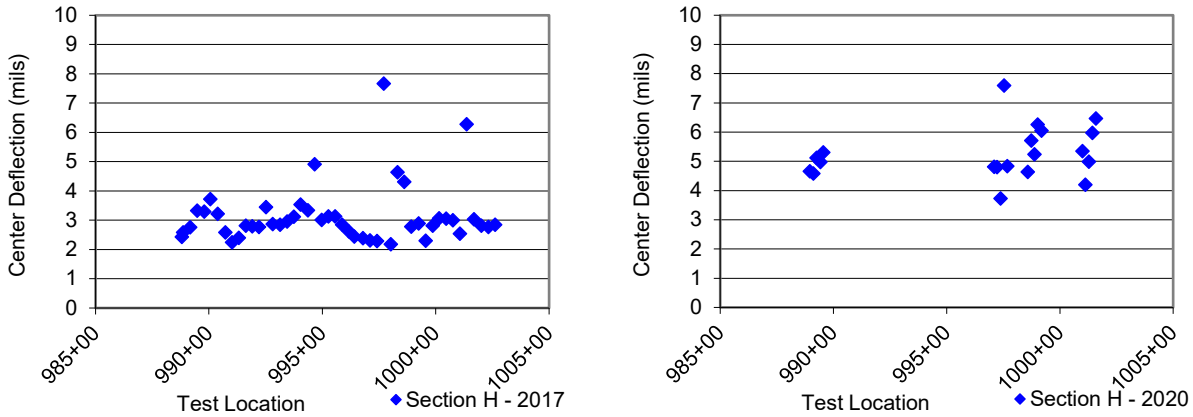

a) 10/31/2017 b) 8/20/2020

Figure 76. Graphs. Normalized 9-kip deflection, D0*, at center panel for US 20 (40455H).

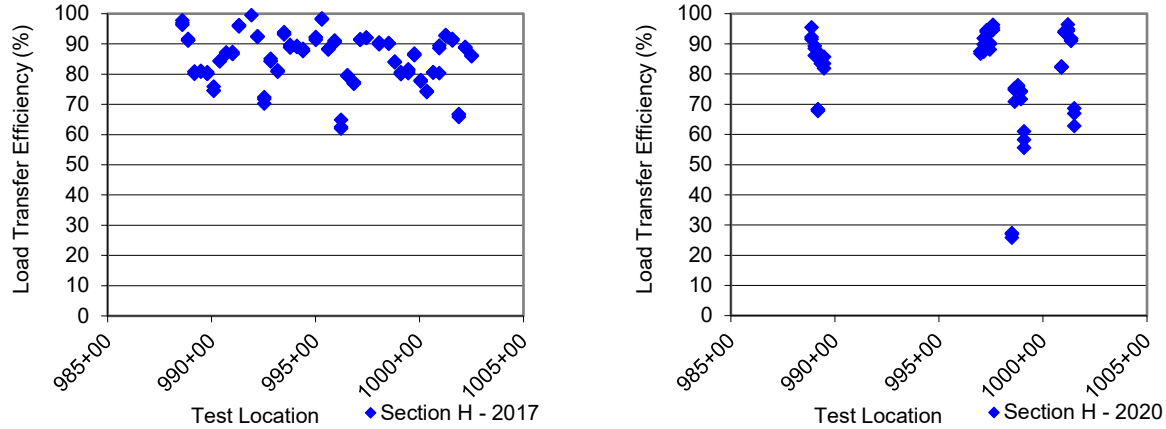

a) 10/31/2017 b) 8/20/2020

Figure 77. Graphs. Load transfer efficiency (LTE) for US 20 (40455H).

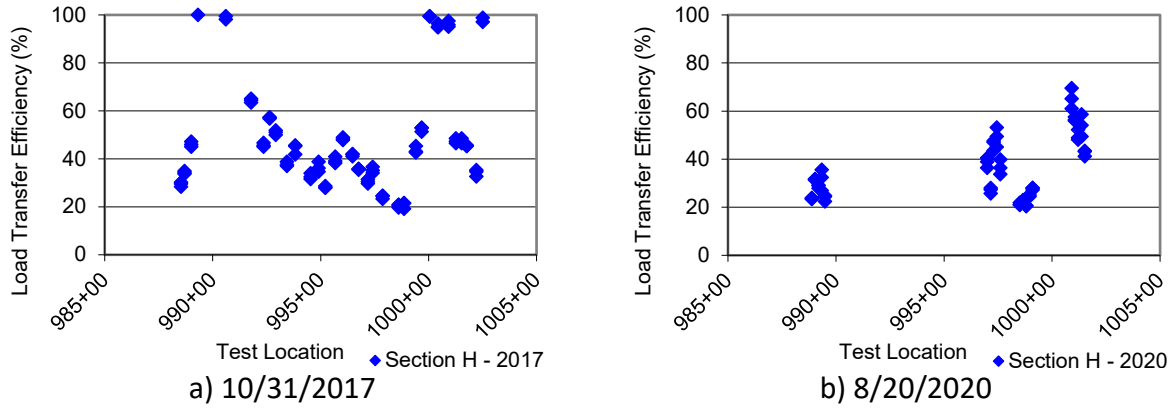

a) 10/31/2017 b) 8/20/2020

Figure 78. Graphs. Lane shoulder longitudinal joint load transfer efficiency (LTE) for US 20 (40455H).

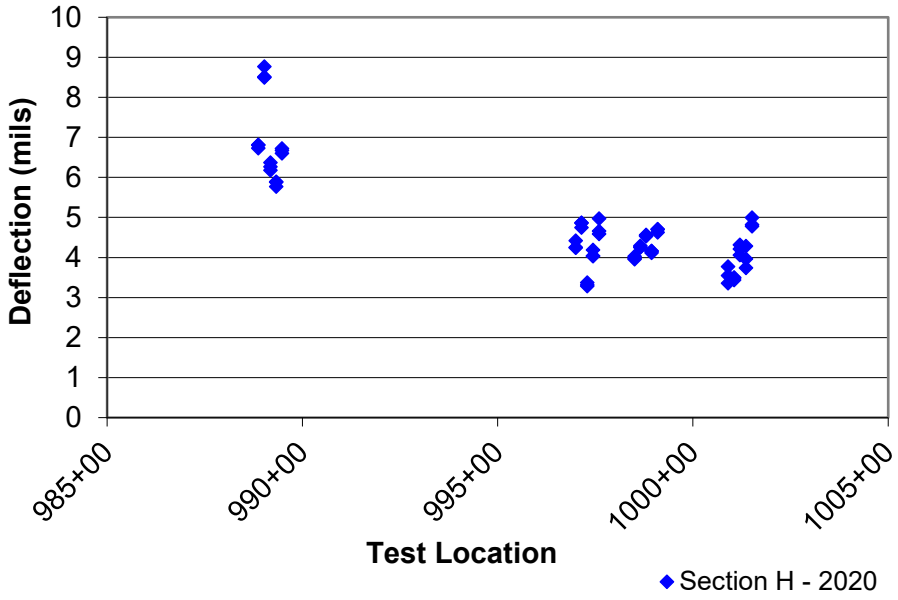

Figure 79. Graph. Normalized 9-kip deflection in the corner along the lane shoulder longitudinal joint for US 20 (40455H).

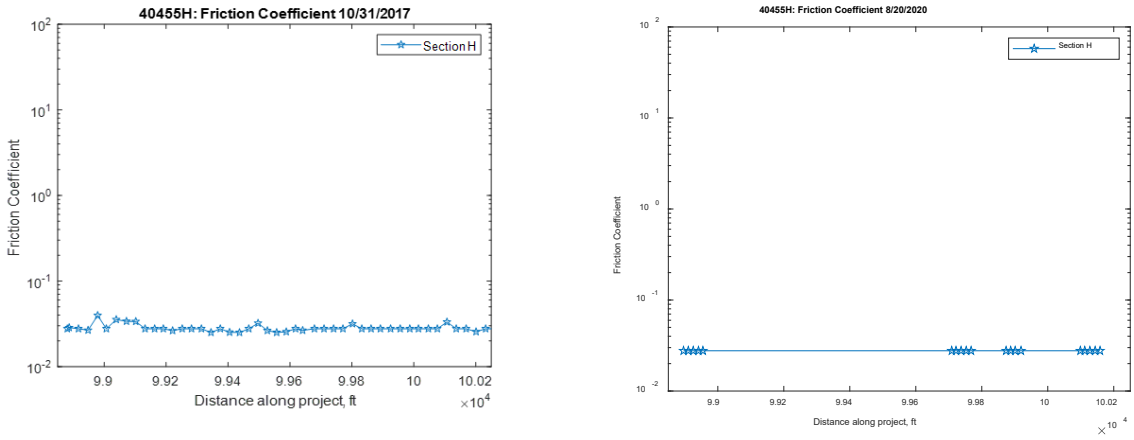

a) 10/31/2017 b) 8/20/2020

Figure 80. Graphs. Friction coefficient along US 20 (40455H).

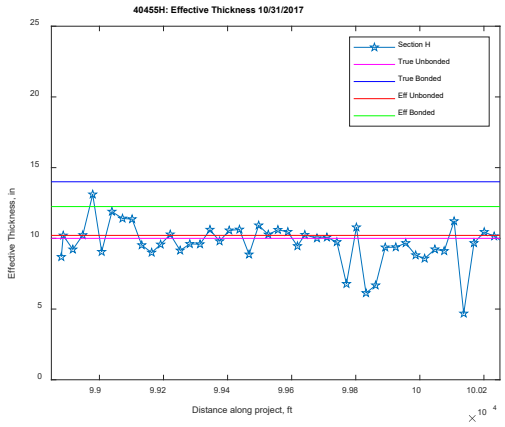

a) 10/31/2017

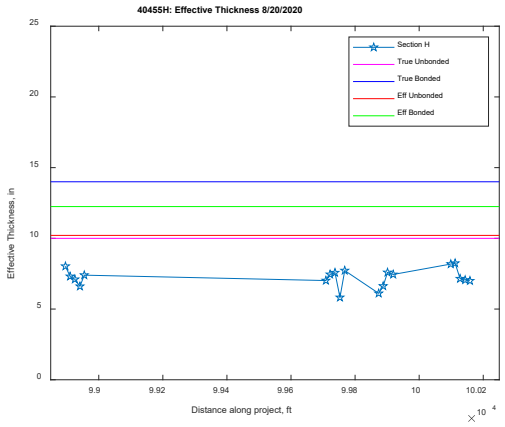

b) 8/20/2020

Figure 81. Graphs. Effective thickness along US 20 (40455H).

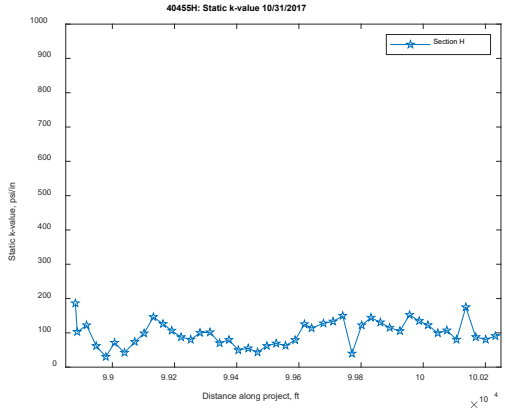

a) 10/31/2017

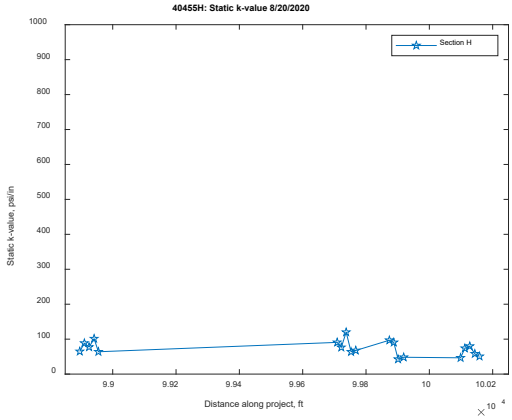

b) 8/20/2020

Figure 82. Graphs. Static k-value along US 20 (40455H).

US 30 (62277)

A summary of the FWD testing performed in 2017 and 2020 is provided. Additionally, plots are included for comparison. The HMA stiffness was assumed to be 3.0×10^6 psi during testing in 2017. The HMA stiffness was assumed to be less stiff in 2020, 0.4×10^6 psi.

Table 42. FWD Summary from Center Slab Testing for US 30 (62277)

	11/14/2017						8/13/2020					
Parameter	D0* (mils)		Area_36		Eri		D0* (mils)		Area_36		Eri	
Direction	WB	EB	WB	EB	WB	EB	WB	EB	WB	EB	WB	EB
Average	2.13	2.01	33.2	33.0	15.0	15.7	2.98	2.51	31.8	31.4	12.2	14.1
Std. Dev.	0.25	0.33	0.80	0.99	1.15	1.12	0.40	0.31	0.69	0.73	1.52	1.28
COV	11.7	16.3	2.40	3.00	7.69	7.11	13.4	12.5	2.16	2.32	12.5	9.05

Table 43. FWD Summary from Leave Joint LTE Testing for US 30 (62277)

	11/14/2017				8/13/2020			
Parameter	D0* (mils)		LTE (%)		D0* (mils)		LTE (%)	
Direction	WB	EB	WB	EB	WB	EB	WB	EB
Average	2.47	2.32	96.8	93.7	3.11	2.81	93.9	90.5
Std. Dev.	0.41	0.38	3.74	6.26	0.39	0.47	2.95	6.32
COV	16.4	16.2	3.86	6.69	12.6	16.7	3.14	6.98

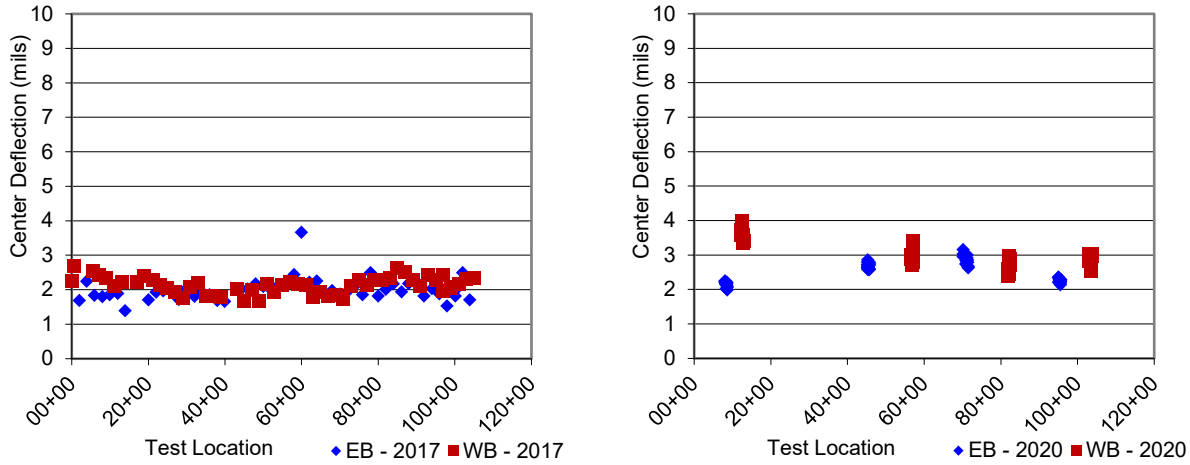

a) 11/14/2017 b) 8/13/2020

Figure 83. Graphs. Normalized 9-kip deflection, D0*, at center panel for US 30 (62277).

This section mainly consisted of curb and gutter. Instead of following the testing protocol presented in Appendix B, testing was performed in the outer wheel path (OWP) instead of the corner. Therefore, lane shoulder LTE along the longitudinal joint could not be conducted.

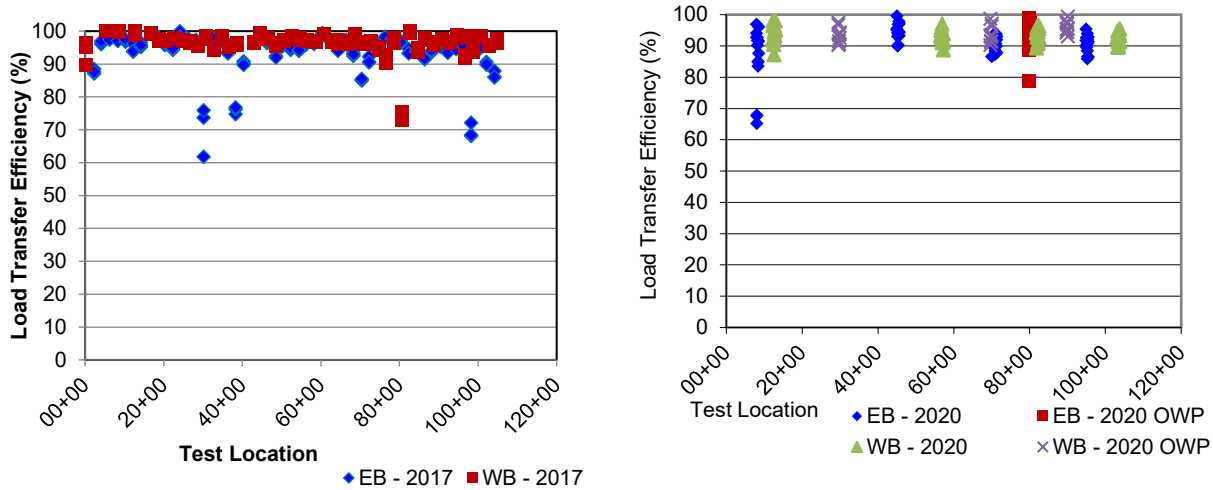

a) 11/14/2017 b) 8/13/2020

Figure 84. Graphs. Load transfer efficiency (LTE) for US 30 (62277).

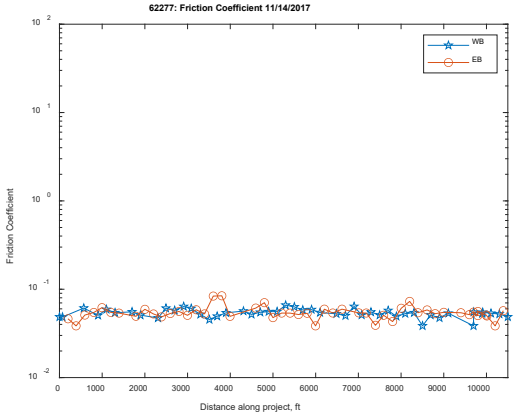

a) 11/14/2017

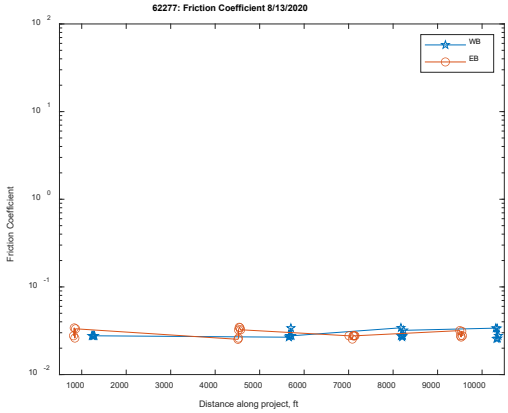

b) 8/13/2020

Figure 85. Graphs. Friction coefficient along US 30 (62277).

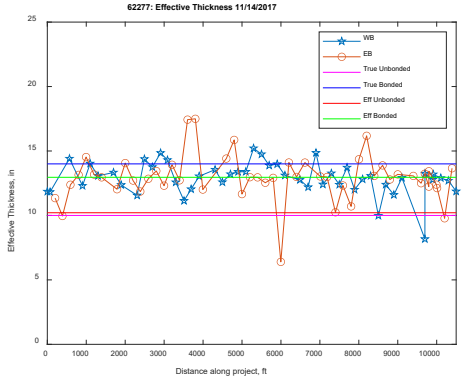

a) 11/14/2017

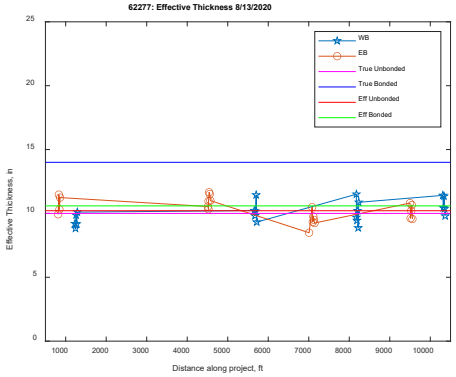

b) 8/13/2020

Figure 86. Graphs. Effective thickness along US 30 (62277).

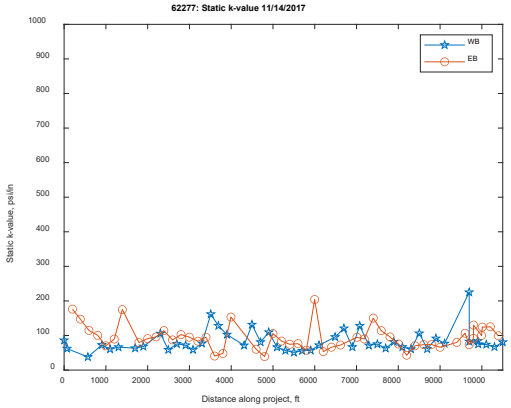

a) 11/14/2017

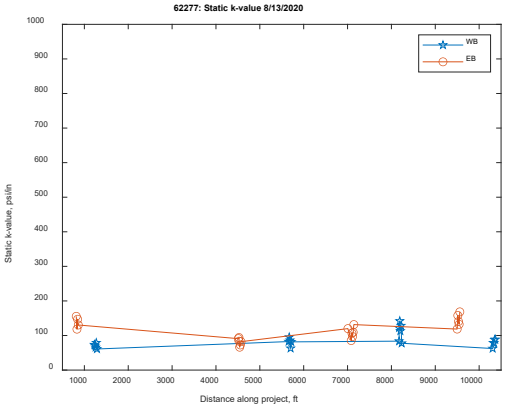

b) 8/13/2020

Figure 87. Graphs. Static k-value along US 30 (62277).

IL 64 (62410)

A summary of the FWD testing performed in 2018 and 2020 is provided. Additionally, plots are included for comparison. The HMA stiffness was assumed to be $1.0x10^6$ psi during testing in 2018. The HMA stiffness was assumed to be less stiff in 2020, $0.8x10^6$ psi.

Table 44. FWD Summary from Center Slab Testing for IL 64 (62410)

	5/15-16/2018						9/4/2020					
Parameter	D0* (mils)		Area_36		Eri		D0* (mils)		Area_36		Eri	
Direction	WB	EB	WB	EB	WB	EB	WB	EB	WB	EB	WB	EB
Average	1.69	1.70	31.8	32.0	17.7	17.6	1.51	1.79	30.1	30.5	18.8	17.5
Std. Dev.	0.27	0.47	0.65	0.97	1.23	2.39	0.16	0.28	0.93	1.13	0.76	1.45
COV	15.8	27.8	2.04	3.02	6.95	13.6	10.8	15.8	3.08	3.70	4.07	8.29

Table 45. FWD Summary from Leave Joint LTE Testing for IL 64 (62410)

	5/15-16/2018				9/4/2020			
Parameter	D0* (mils)		LTE (%)		D0* (mils)		LTE (%)	
Direction	WB	EB	WB	EB	WB	EB	WB	EB
Average	1.72	1.65	95.6	96.4	1.68	1.92	90.0	89.5
Std. Dev.	0.31	0.29	4.82	1.97	0.20	0.32	3.75	4.48
COV	17.9	17.6	5.04	2.04	12.2	16.5	4.17	5.00

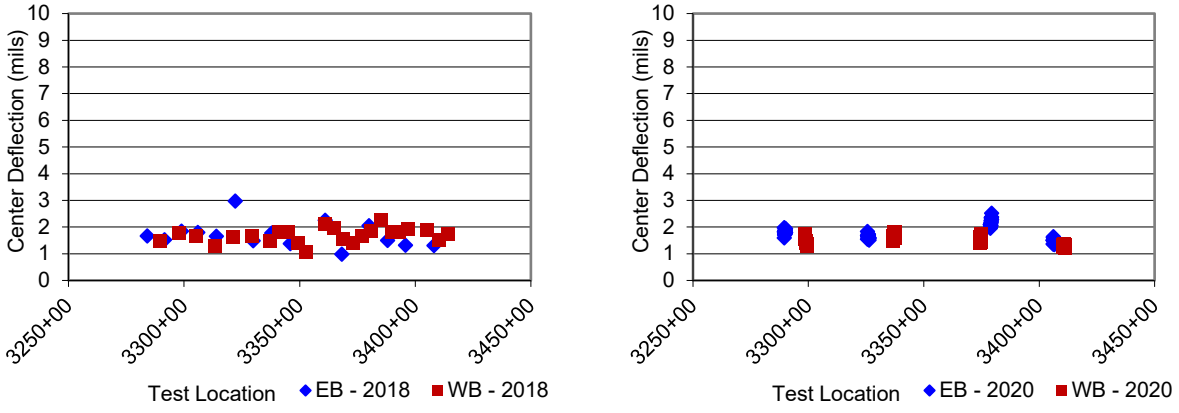

a) 5/15-16/2018 b) 9/4/2020

Figure 88. Graphs. Normalized 9-kip deflection, D0*, at center panel for IL 64 (62410).

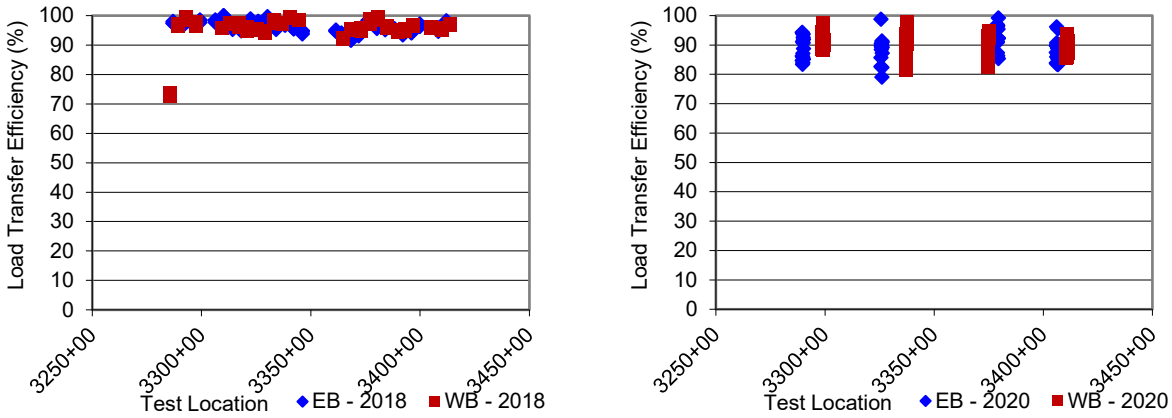

a) 5/15-16/2018 b) 9/4/2020

Figure 89. Graphs. Load transfer efficiency (LTE) for IL 64 (62410).

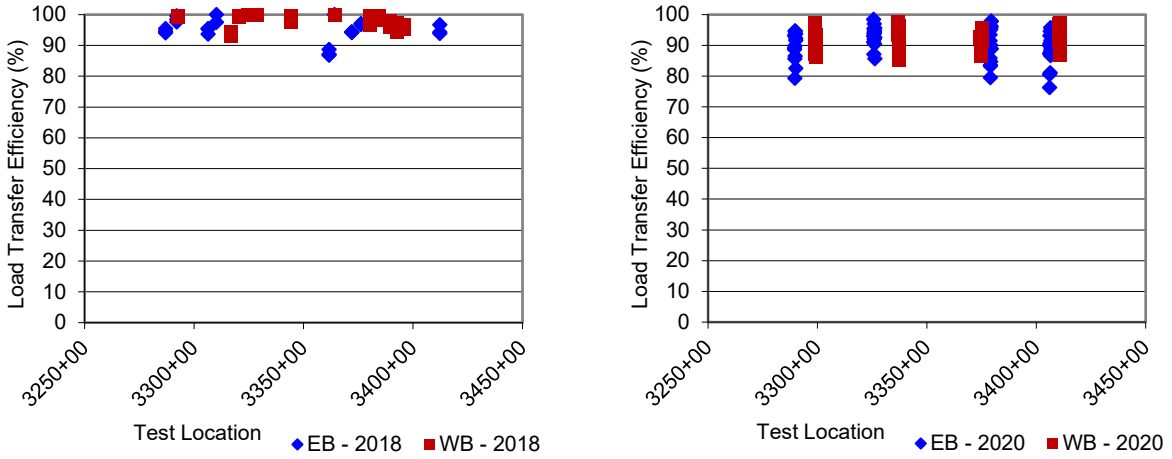

a) 5/15-16/2018 b) 9/4/2020

Figure 90. Graphs. Lane shoulder longitudinal joint load transfer efficiency (LTE) for IL 64 (62410).

Testing was not performed in the corner along the lane shoulder joint in 2018.

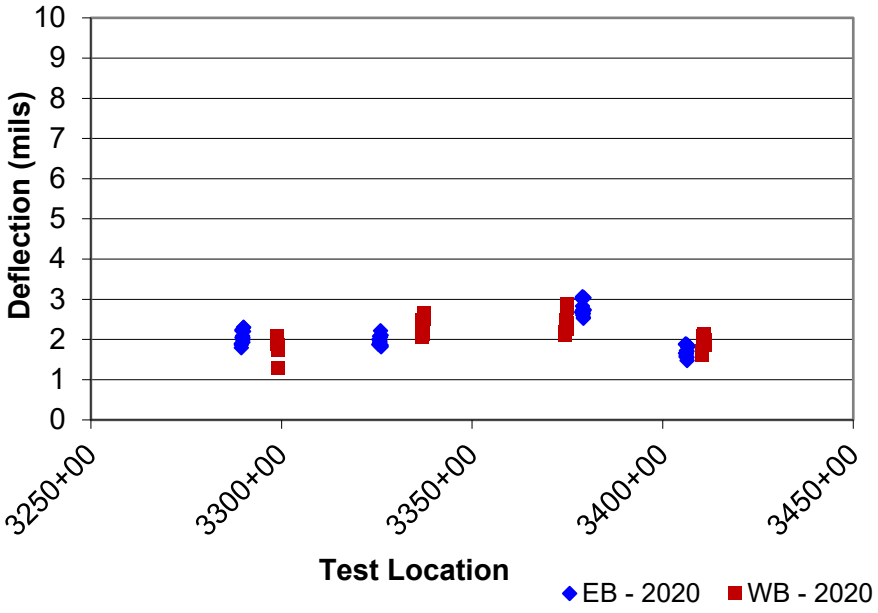

a) 9/4/2020

Figure 91. Graph. Normalized 9-kip deflection in the corner along the lane shoulder longitudinal joint for IL 64 (62410).

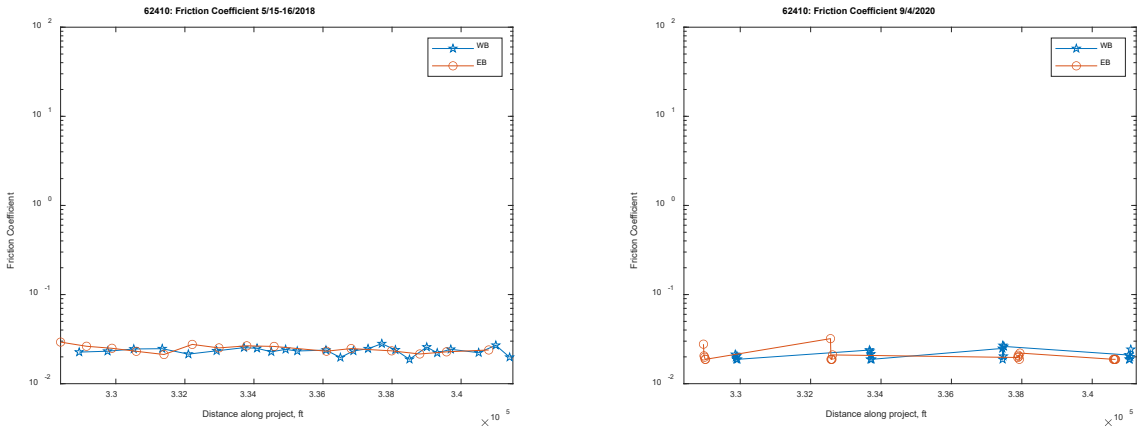

a) 5/15-16/2018 b) 9/4/2020

Figure 92. Graphs. Friction coefficient along IL 64 (62410).

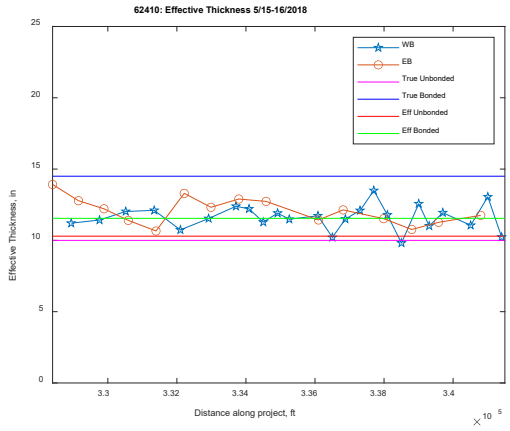

a) 5/15-16/2018

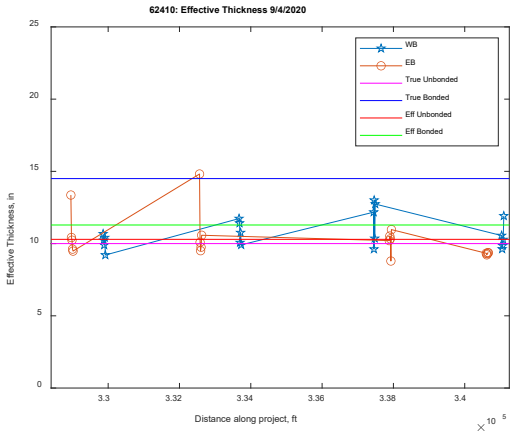

b) 9/4/2020

Figure 93. Graphs. Effective thickness along IL 64 (62410).

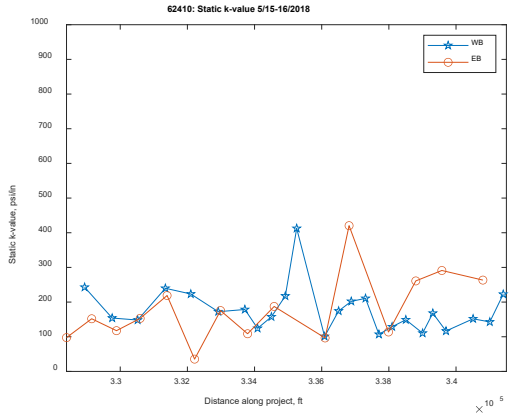

a) 5/15-16/2018

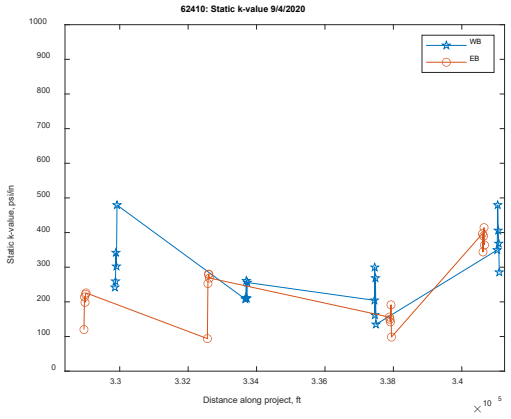

b) 9/4/2020

Figure 94. Graphs. Static k-value along IL 64 (62410).

US 12/20/45 (60927 & 60748)

60927

A summary of the FWD testing performed in 2018 and 2020 is provided. Additionally, plots are included for comparison. The HMA stiffness was assumed to be 2.0×10^6 psi during testing in 2018. The HMA stiffness was assumed to be less stiff in 2020, 0.8×10^6 psi.

Table 46. FWD Summary from Center Slab Testing for US 12/20/45 (60927)

	10/29/2018						9/3/2020					
Parameter	D0* (mils)		Area_36		Eri		D0* (mils)		Area_36		Eri	
Direction	WB	EB	WB	EB	WB	EB	WB	EB	WB	EB	WB	EB
Average	1.40	1.65	31.5	31.5	19.0	18.0	1.77	1.83	29.6	29.7	18.1	17.9
Std. Dev.	0.28	0.25	0.79	1.07	1.42	1.04	0.15	0.21	1.28	1.17	0.83	0.84
COV	20.2	15.3	2.49	3.38	7.49	5.77	8.34	11.3	4.33	3.95	4.60	4.71

Table 47. FWD Summary from Leave Joint LTE Testing for US 12/20/45 (60927)

	10/29/2018				9/3/2020			
Parameter	D0* (mils)		LTE (%)		D0* (mils)		LTE (%)	
Direction	WB	EB	WB	EB	WB	EB	WB	EB
Average	1.89	2.00	90.4	92.3	1.72	1.76	88.0	89.8
Std. Dev.	0.35	0.33	4.48	4.34	0.19	0.26	4.09	3.40
COV	18.4	16.5	4.96	4.70	11.2	14.6	4.65	3.78

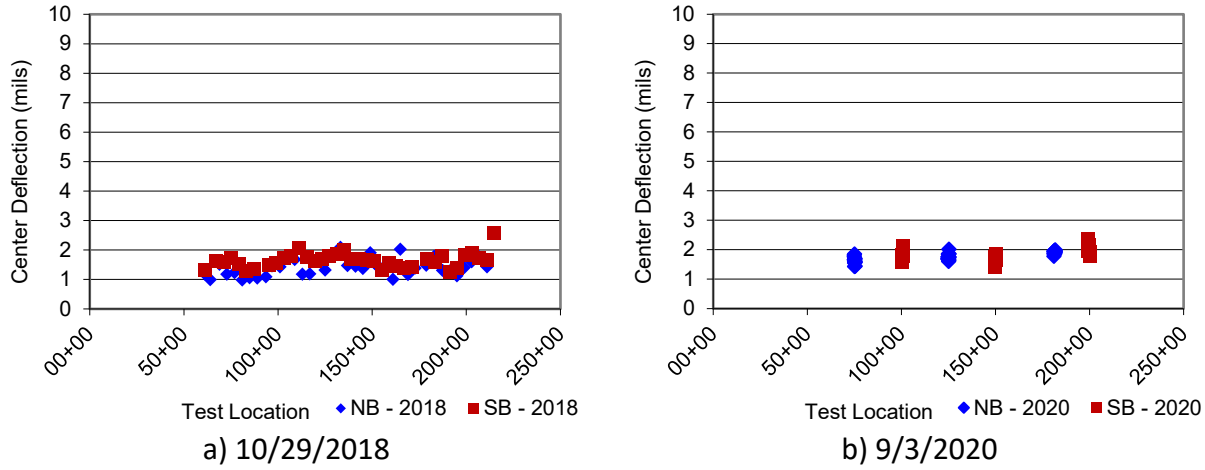

a) 10/29/2018 b) 9/3/2020

Figure 95. Graphs. Normalized 9-kip deflection, D0*, at center panel for US 12/20/45 (60927).

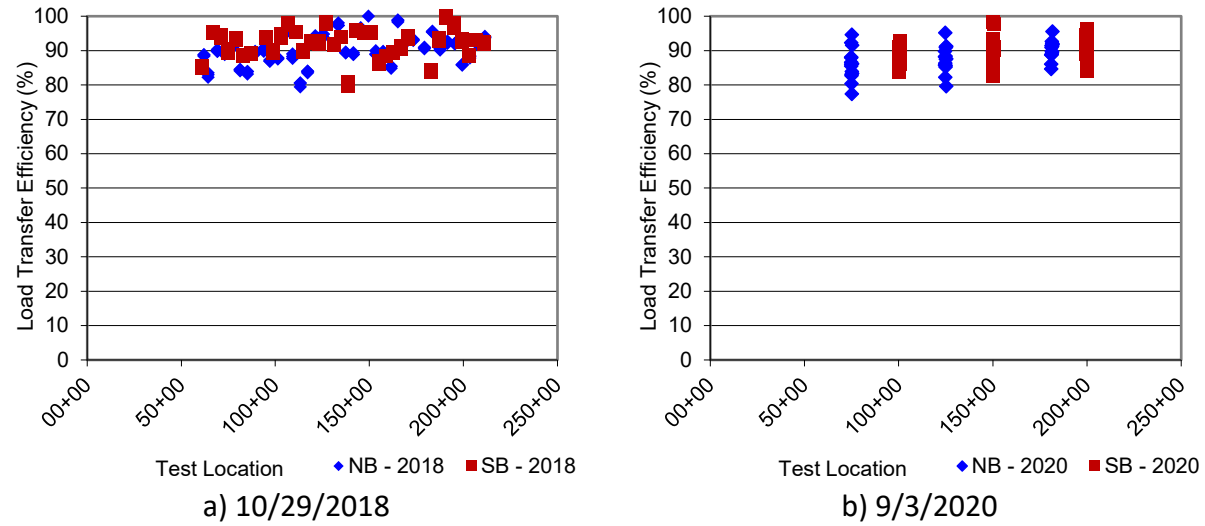

a) 10/29/2018 b) 9/3/2020

Figure 96. Graphs. Load transfer efficiency (LTE) for US 12/20/45 (60927).

Testing was not performed along the lane shoulder joint in 2018.

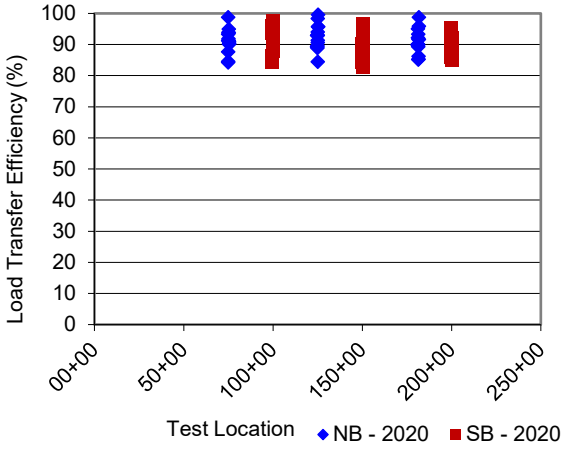

a) 9/3/2020

Figure 97. Graph. Lane shoulder longitudinal joint load transfer efficiency (LTE) for US 12/20/45 (60927).

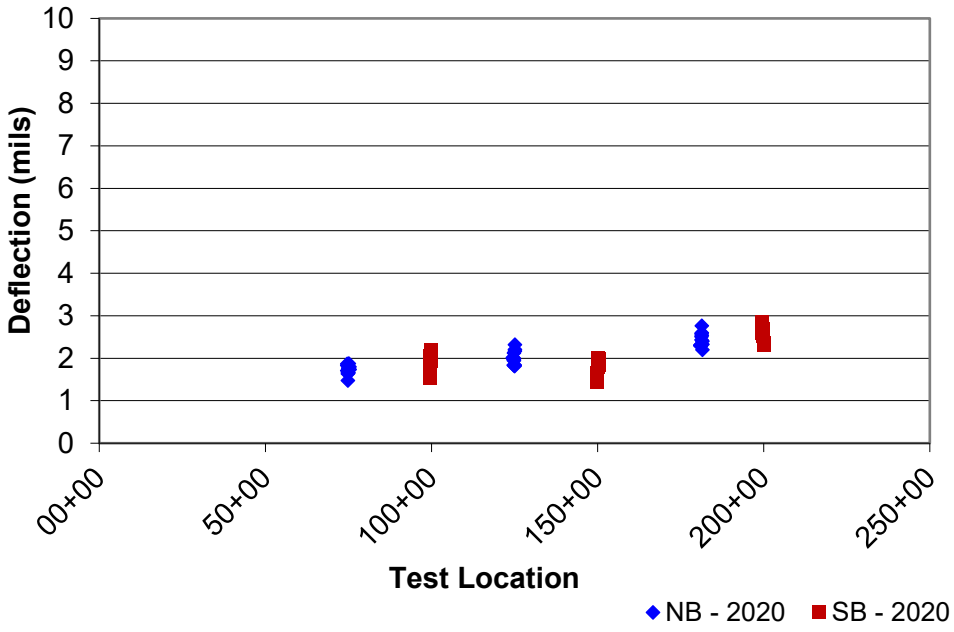

a) 9/3/2020

Figure 98. Graph. Normalized 9-kip deflection in the corner along the lane shoulder longitudinal joint for US 12/20/45 (60927).

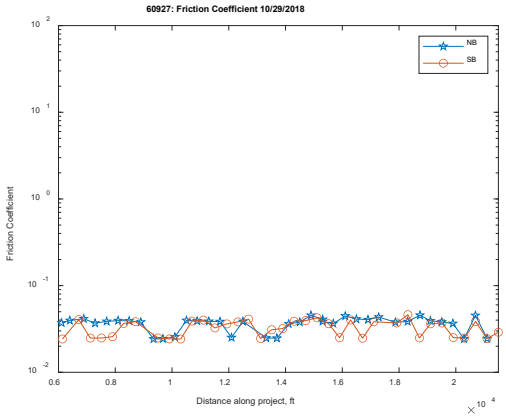

a) 10/29/2018

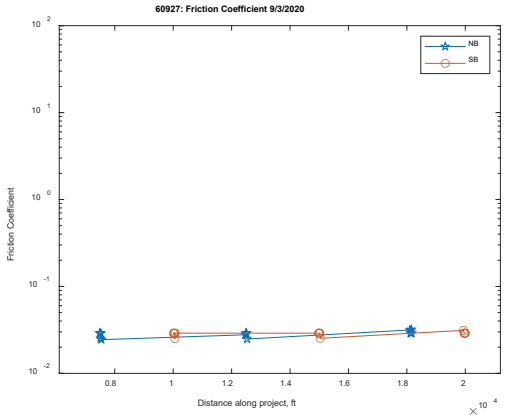

b) 9/3/2020

Figure 99. Graphs. Friction coefficient along US 12/20/45 (60927).

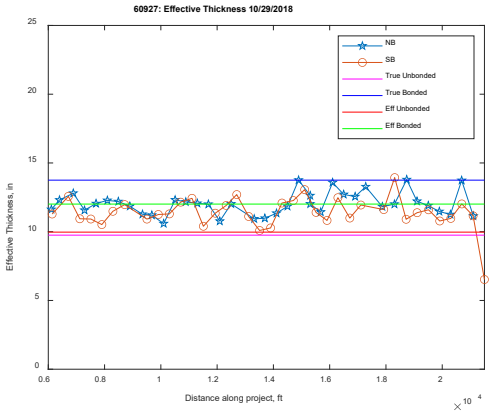

a) 10/29/2018

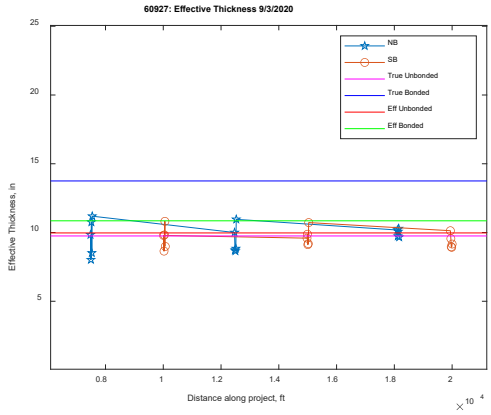

b) 9/3/2020

Figure 100. Graphs. Effective thickness along US 12/20/45 (60927).

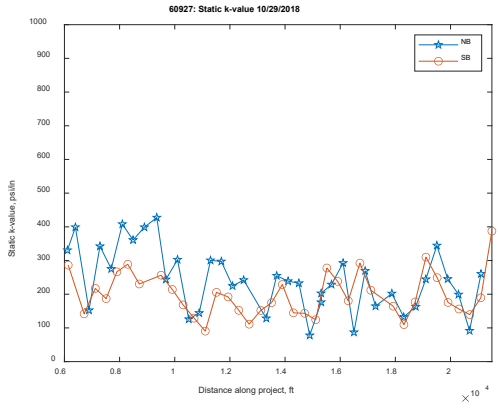

a) 10/29/2018

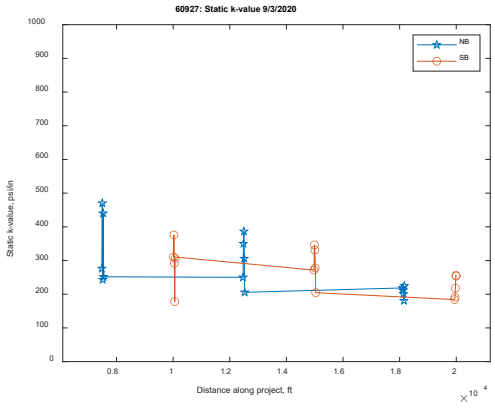

b) 9/3/2020

Figure 101. Graphs. Static k-value along US 12/20/45 (60927).

60748

A summary of the FWD testing performed in 2018 and 2020 is provided. Additionally, plots are included for comparison. Testing was only performed in the Southbound direction in 2020 due to maintenance and construction traffic control for an overpass bridge in the Northbound direction. The HMA stiffness was assumed to be $2.0x10^6$ psi during testing in 2018. The HMA stiffness was assumed to be less stiff in 2020, $0.8x10^6$ psi.

Table 48. FWD Summary from Center Slab Testing for US 12/20/45 (60748)

	10/29/2018						9/3/2020					
Parameter	D0* (mils)		Area_36		Eri		D0* (mils)		Area_36		Eri	
Direction	NB	SB	NB	SB	NB	SB	NB	SB	NB	SB	NB	SB
Average	1.72	1.35	30.1	31.1	19.2	19.5	-	1.54	-	29.1	-	19.1
Std. Dev.	1.09	0.28	3.66	0.74	0.84	1.26	-	0.56	-	1.28	-	2.35
COV	63.1	20.9	12.2	2.38	4.40	6.48	-	36.1	-	4.39	-	12.3

Table 49. FWD Summary from Leave Joint LTE Testing for US 12/20/45 (60748)

	10/29/2018				9/3/2020			
Parameter	D0* (mils)		LTE (%)		D0* (mils)		LTE (%)	
Direction	NB	SB	NB	SB	NB	SB	NB	SB
Average	1.96	1.68	90.9	90.4	-	1.68	-	86.9
Std. Dev.	0.43	0.28	8.51	4.48	-	0.60	-	5.60
COV	21.9	16.9	9.37	4.95	-	35.7	-	6.45

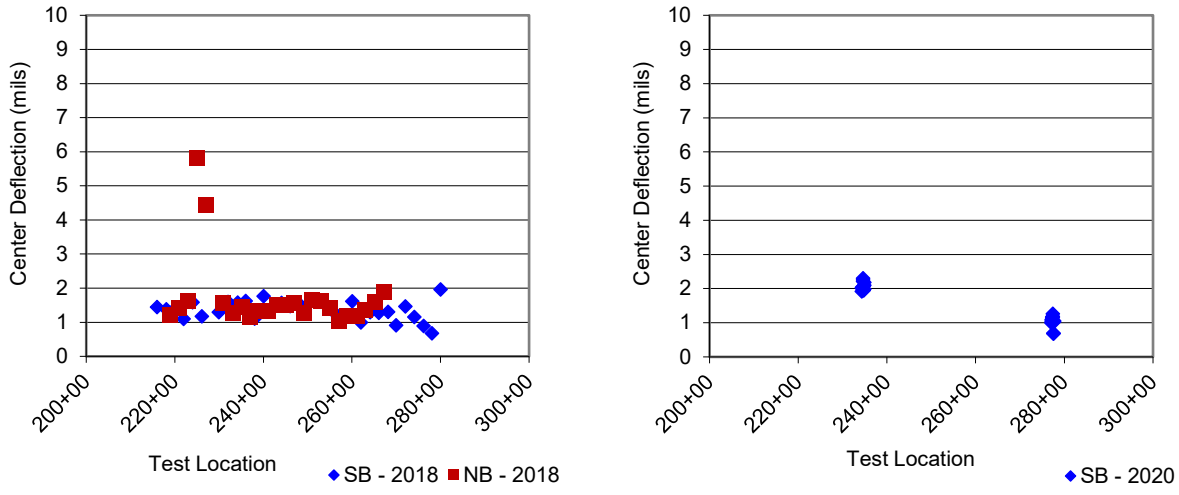

a) 10/29/2018 b) 9/3/2020

Figure 102. Graphs. Normalized 9-kip deflection, D0*, at center panel for US 12/20/45 (60748).

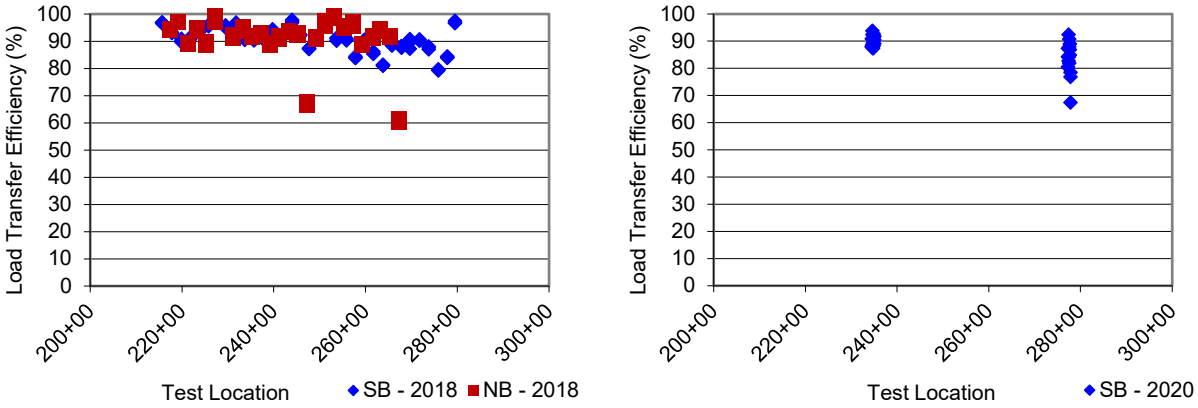

a) 10/29/2018 b) 9/3/2020

Figure 103. Graphs. Load transfer efficiency (LTE) for US 12/20/45 (60748).

Testing was not performed along the lane shoulder joint or the corner in 2018.

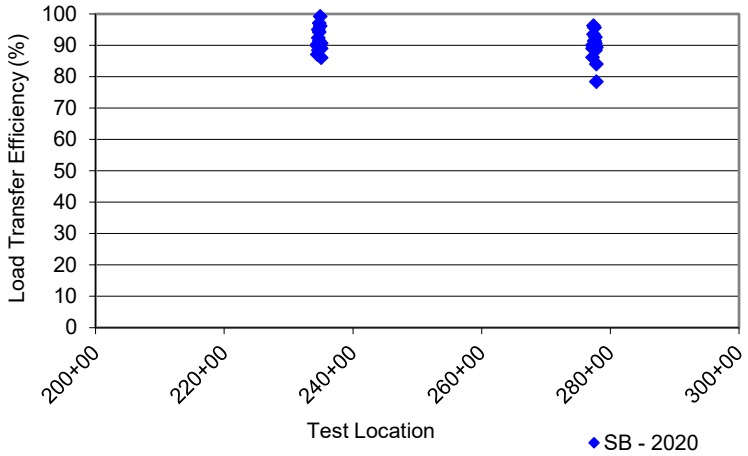

9/3/2020

Figure 104. Graphs. Lane shoulder longitudinal joint load transfer efficiency (LTE) for US 12/20/45 (60748).

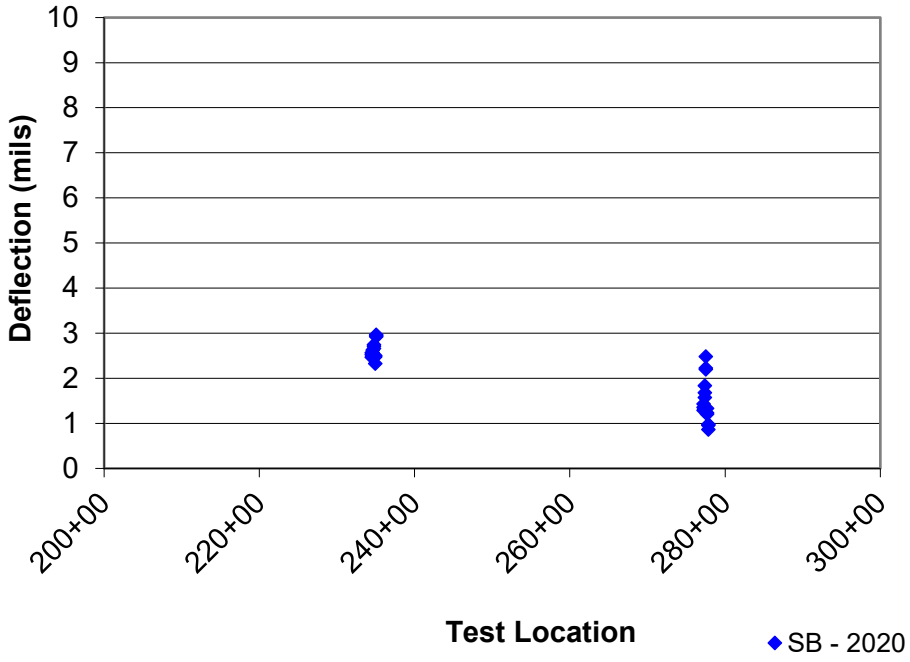

a) 9/3/2020

Figure 105. Graph. Normalized 9-kip deflection in the corner along the lane shoulder longitudinal joint for US 12/20/45 (60748).

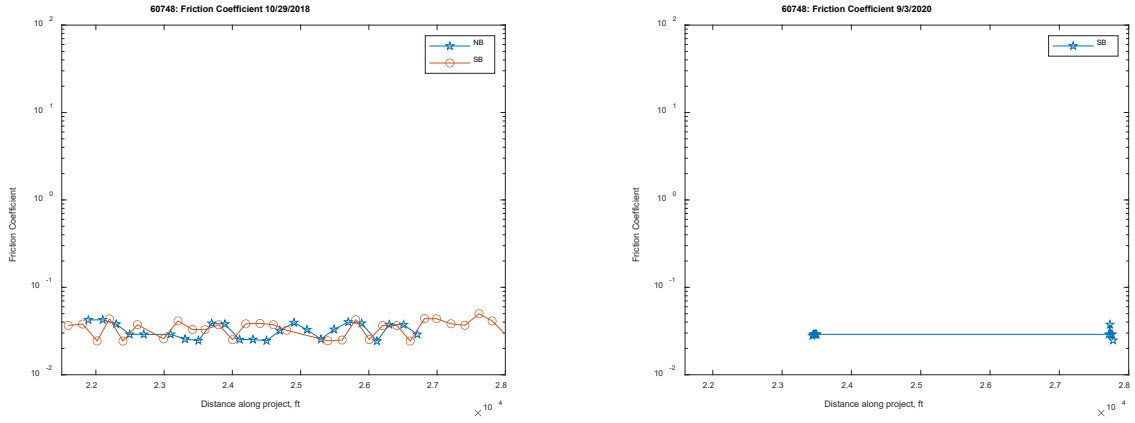

a) 10/29/2018 b) 9/3/2020

Figure 106. Graphs. Friction coefficient along US 12/20/45 (60748).

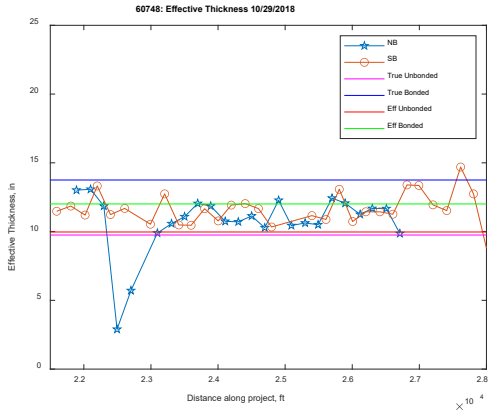

a) 10/29/2018

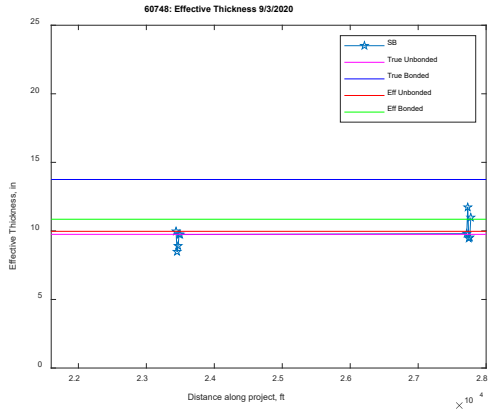

b) 9/3/2020

Figure 107. Graphs. Effective thickness along US 12/20/45 (60748).

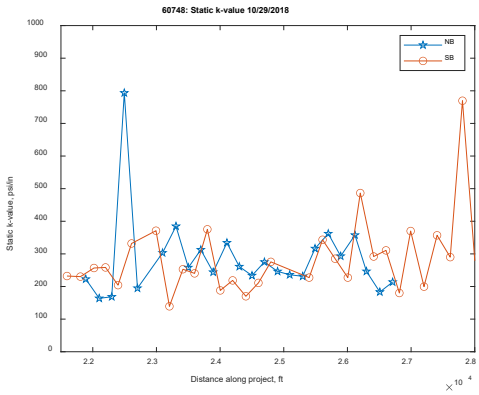

a) 10/29/2018

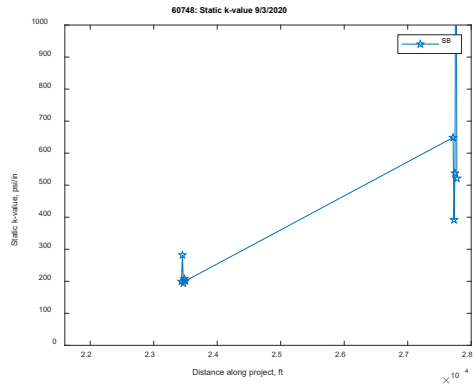

b) 9/3/2020

Figure 108. Graphs. Static k-value along US 12/20/45 (60748).

I-72 (72G92)

Eastbound – HMA Interlayer

A summary of the FWD testing performed in 2016 and 2020 is provided. Additionally, plots are included for comparison. The HMA stiffness was assumed to be 2.0×10^6 psi during testing in 2016. The HMA stiffness was assumed to be less stiff in 2020, 0.8×10^6 psi. The method for backcalculation followed King et al. (2014) using finite backcalculation methodology for smaller panels.

Table 50. FWD Summary from 10/11/2016 Testing for I-72 EB (72G92)

	10/11/2016									
	CN			LJ		Corner			TE	
	D0* (mils)	Area_36	Eri	D0* (mils)	LTE (%)	D0* (mils)	LTE (%)	TE LTE (%)	D0* (mils)	TE LTE (%)
	EB	EB	EB	EB	EB	EB	EB	EB	EB	EB
Average	2.40	32.3	13.8	2.52	90.5	3.56	90.1	94.2	3.40	93.8
Std. Dev.	0.28	1.51	1.01	0.44	5.72	0.73	6.13	6.22	0.50	8.84
COV	11.6	4.68	7.30	17.6	6.32	20.4	6.80	6.60	14.2	9.42

Tested 10/11-12/16, Avg. Air = 67, Pvmt. Surface = 68, Pvmt. Temp. @ 3" = 70

Table 51. FWD Summary from 8/5/2020 Testing for I-72 EB (72G92)

	8/5/2020									
	CN			LJ		Corner			TE	
	D0* (mils)	Area_36	Eri	D0* (mils)	LTE (%)	D0* (mils)	LTE (%)	TE LTE (%)	D0* (mils)	TE LTE (%)
	EB	EB	EB	EB	EB	EB	EB	EB	EB	EB
Average	3.54	30.2	11.4	3.54	88.2	4.57	88.6	74.9	4.49	76.4
Std. Dev.	0.58	1.36	1.10	0.62	6.35	0.53	5.01	12.9	0.49	12.1
COV	16.2	4.51	9.65	17.7	7.20	11.6	5.65	17.2	11.0	15.8

Tested 8/5-6/2020, Avg. Air = 85.2, Avg. Pvmt. Surface = 74.0, Pvmt. Temp. @ 3" = 72 (8:30 AM)

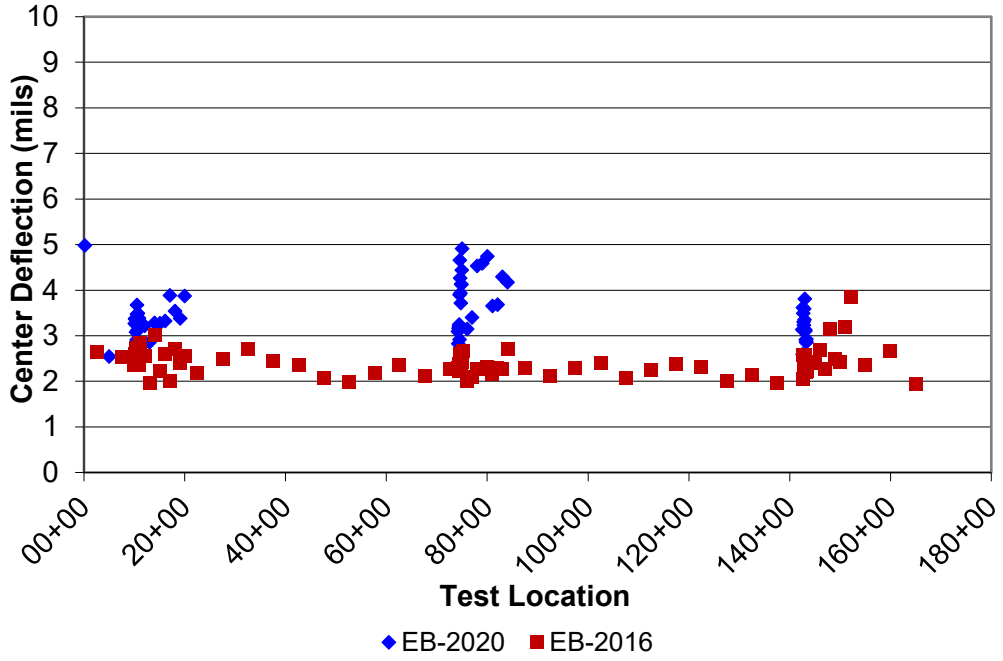

Figure 109. Graph. Normalized 9-kip deflection, D0*, at center panel for I-72 EB (72G92).

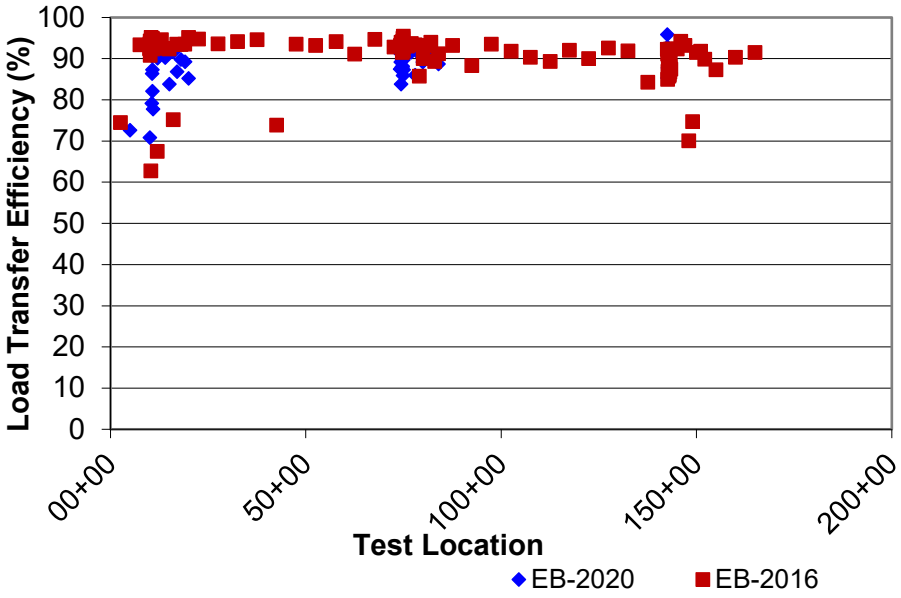

Figure 110. Graph. Load transfer efficiency (LTE) for I-72 EB (72G92).

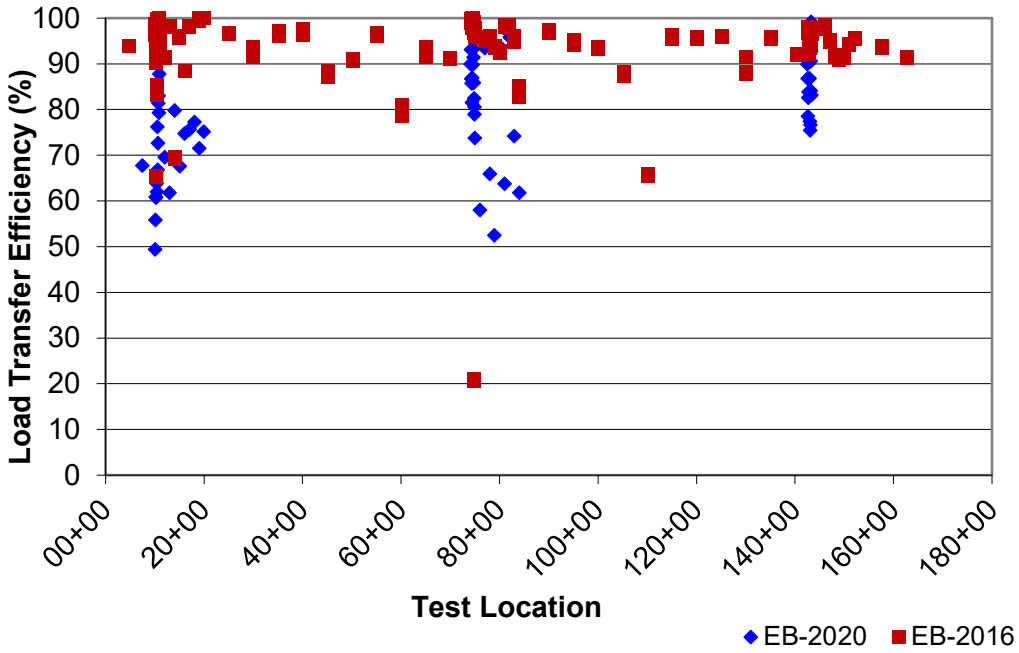

Figure 111. Graph. Lane shoulder longitudinal joint load transfer efficiency (LTE) for I-72 EB (72G92).

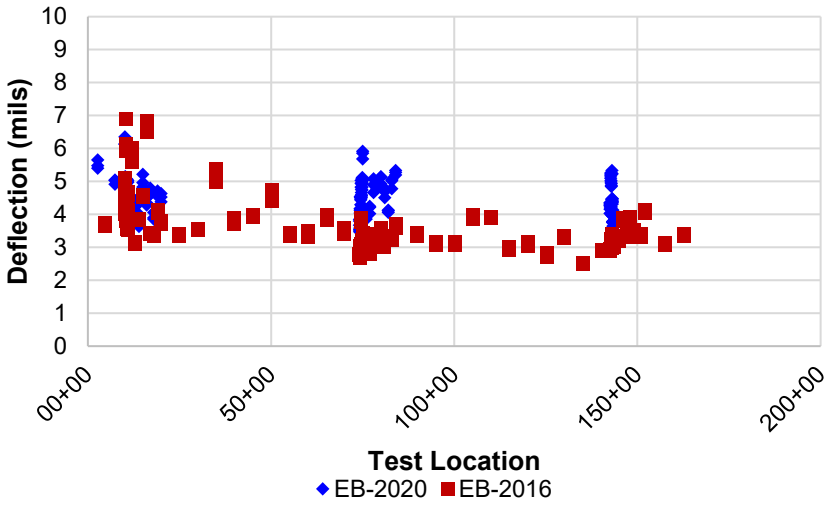

Figure 112. Graph. Normalized 9-kip deflection in the corner along the lane shoulder longitudinal joint for I-72 EB (72G92).

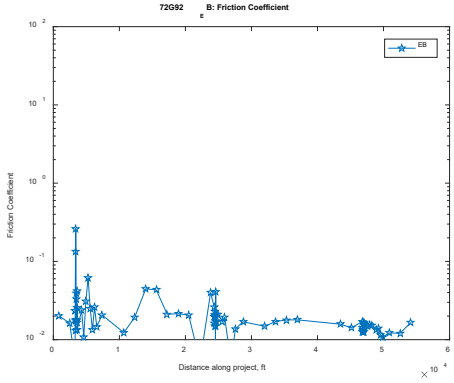

a) 10/11/2016 b) 8/5/2020*

Figure 113. Graphs. Friction coefficient along I-72 EB (72G92). *Friction coefficients for this section in 2020 were extremely low (<10^{-2}).

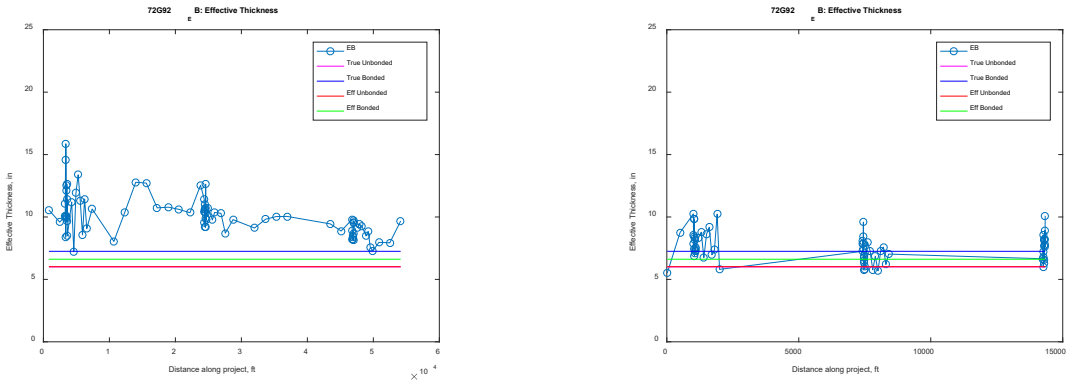

a) 10/11/2016 b) 8/5/2020

Figure 114. Graphs. Effective thickness along I-72 EB (72G92).

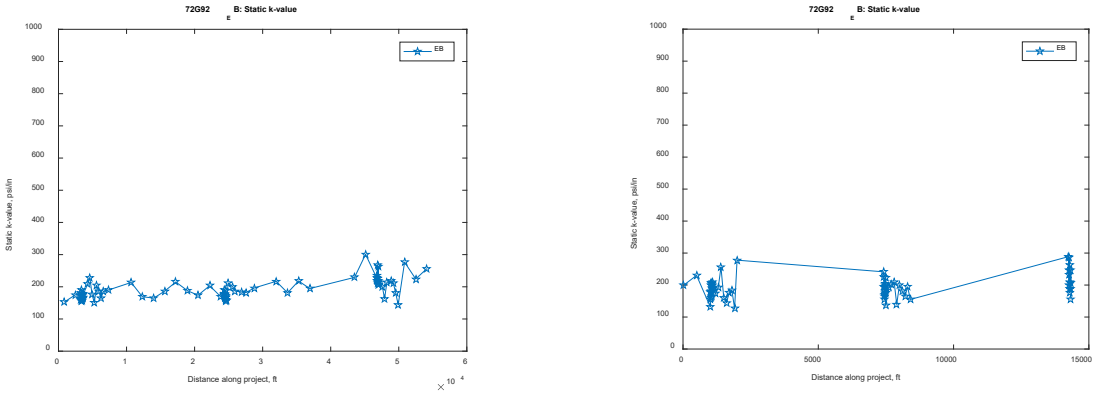

a) 10/11/2016 b) 8/5/2020

Figure 115. Graphs. Static k-value along I-72 EB (72G92).

Westbound – Fabric Interlayer

The fabric interlayer stiffness was assumed to be a constant value of 0.1×10^6 psi during testing in 2016 and 2020. The method for backcalculation followed King et al. (2014) using finite backcalculation methodology for smaller panels.

Table 52. FWD Summary from 10/12/2016 Testing for I-72 WB (72G92)

	10/12/2016									
	CN			LJ		Corner			TE	
	D0* (mils)	Area_36	Eri	D0* (mils)	LTE (%)	D0* (mils)	LTE (%)	TE LTE (%)	D0* (mils)	TE LTE (%)
	WB	WB	WB	WB	WB	WB	WB	WB	WB	WB
Average	3.93	32.5	9.20	4.88	78.2	8.63	71.5	45.6	7.20	52.0
Std. Dev.	0.48	1.76	1.76	1.27	13.9	3.02	19.3	18.8	3.90	16.5
COV	12.3	5.39	19.1	26.1	17.8	34.9	27.0	41.1	53.6	31.7

Tested 10/11-12/16, Avg. Air = 67, Pvmt. Surface = 68, Pvmt. Temp. @ 3" = 70

Table 53. FWD Summary from 8/6/2020 Testing for I-72 WB (72G92)

	8/6/2020									
	CN			LJ		Corner			TE	
	D0* (mils)	Area_36	Eri	D0* (mils)	LTE (%)	D0* (mils)	LTE (%)	TE LTE (%)	D0* (mils)	TE LTE (%)
	WB	WB	WB	WB	WB	WB	WB	WB	WB	WB
Average	4.48	31.1	7.97	5.63	74.3	9.69	63.4	44.3	7.51	53.1
Std. Dev.	0.53	1.09	1.92	1.38	14.9	2.92	16.3	24.9	1.45	23.6
COV	11.8	3.50	24.1	24.6	20.1	30.1	25.8	56.2	19.2	44.4

Tested 8/5-6/2020, Avg. Air = 85.2, Avg. Pvmt. Surface = 74.0, Pvmt. Temp. @ 3" = 72 (8:30 AM)

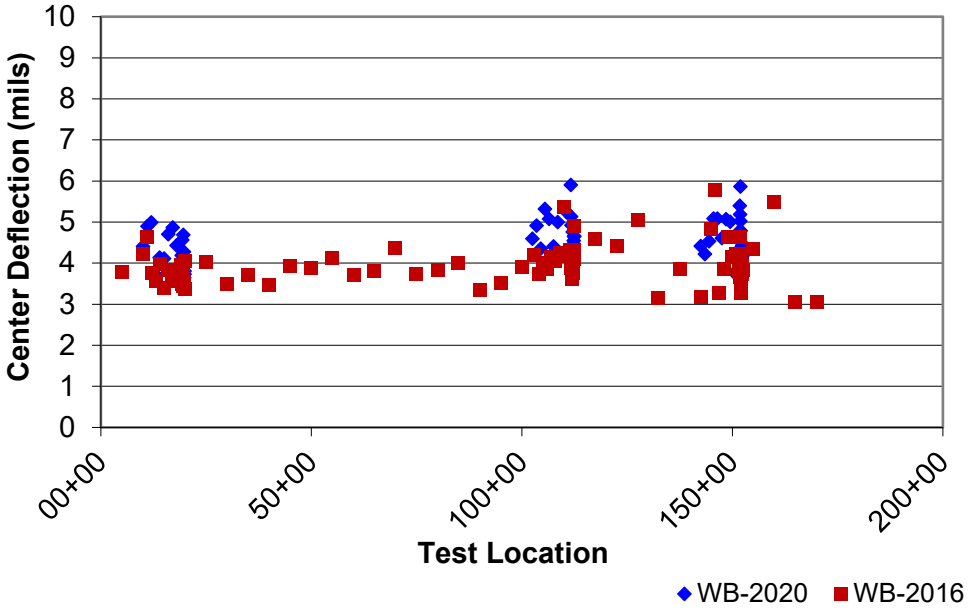

Figure 116. Graph. Normalized 9-kip deflection, D0*, at center panel for I-72 WB (72G92).

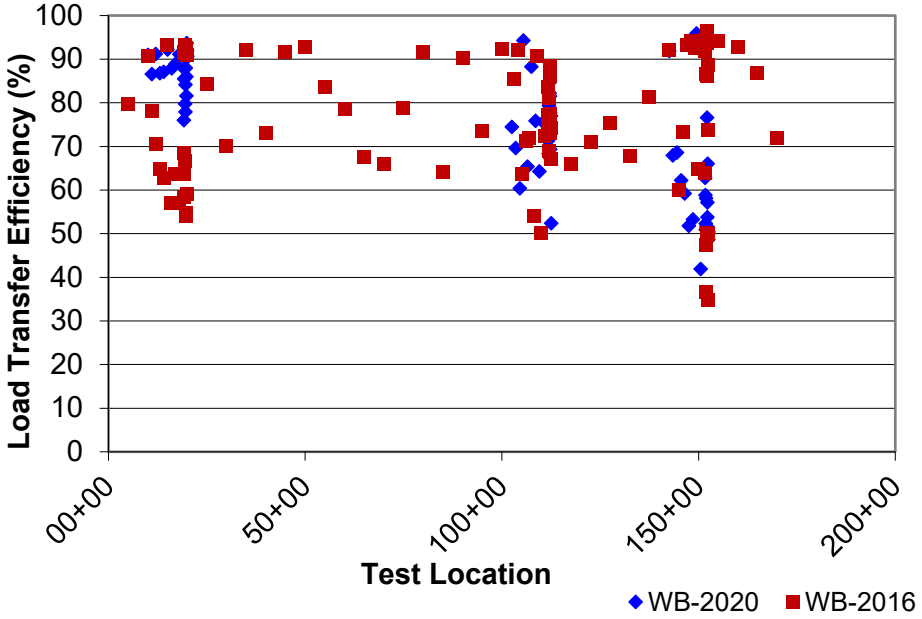

Figure 117. Graph. Load transfer efficiency (LTE) for I-72 WB (72G92).

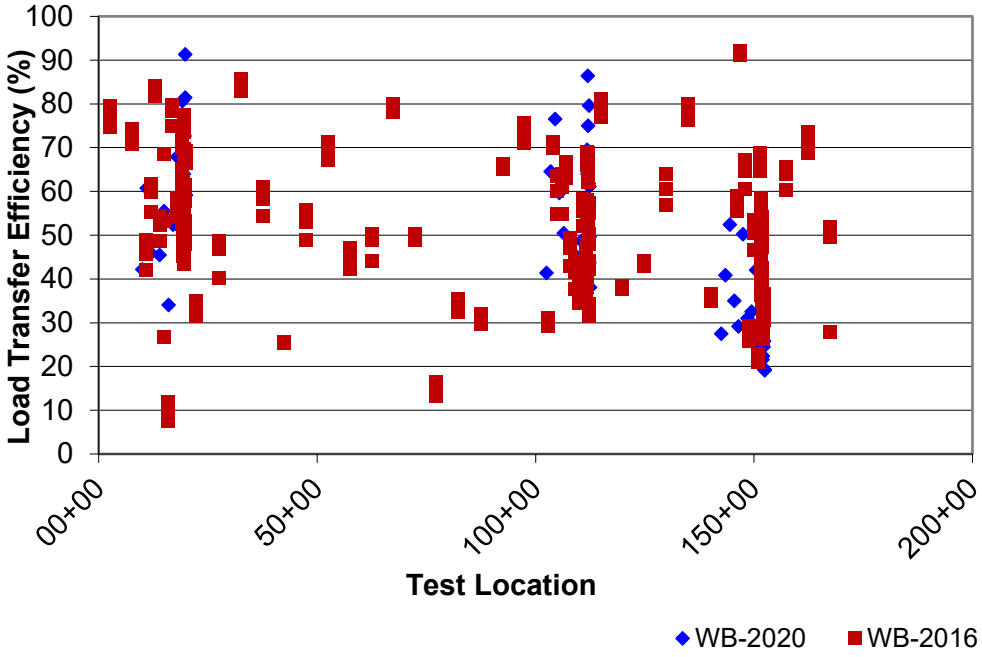

Figure 118. Graph. Lane shoulder longitudinal joint load transfer efficiency (LTE) for I-72 WB (72G92).

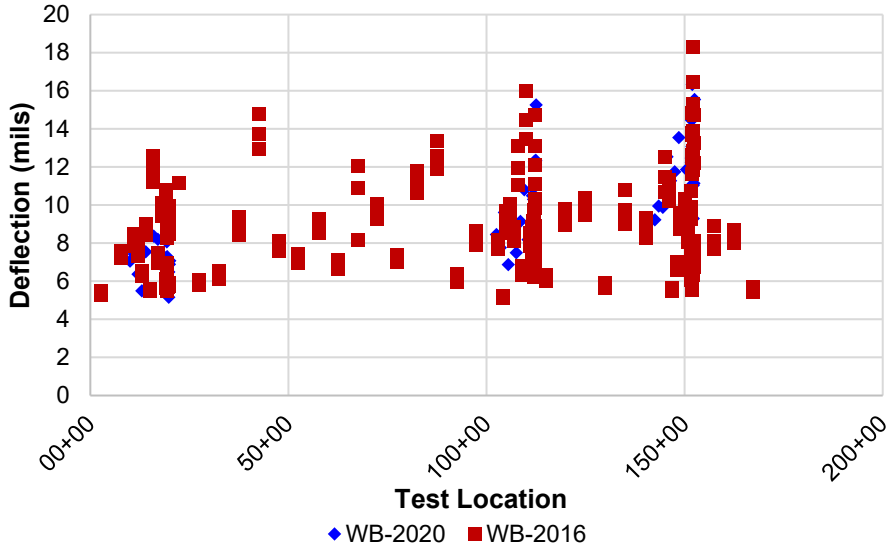

Figure 119. Graph. Normalized 9-kip deflection in the corner along the lane shoulder longitudinal joint for I-72 WB (72G92).

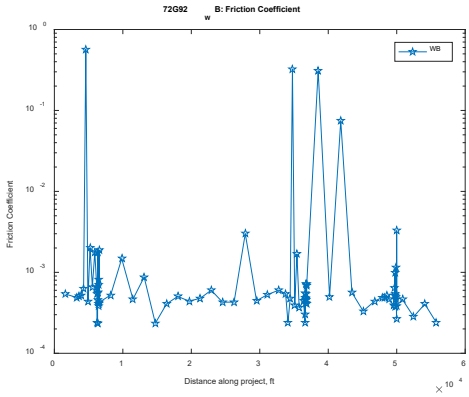

a) 10/12/2016*

b) 8/6/2020*

Figure 120. Graphs. Friction coefficient along I-72 WB (72G92). *Friction coefficients for this section were extremely low and were not able to be determined for 2020.

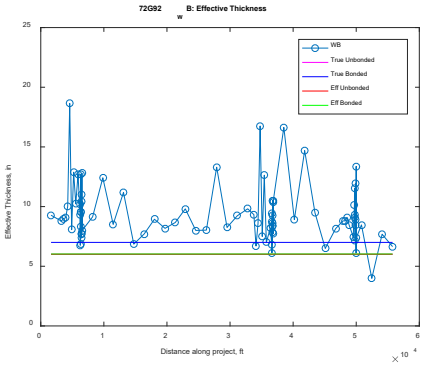

a) 10/12/2016

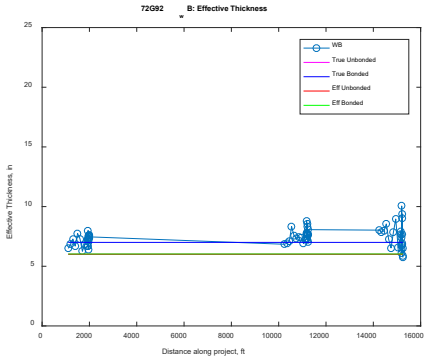

b) 8/6/2020

Figure 121. Graphs. Effective thickness along I-72 WB (72G92).

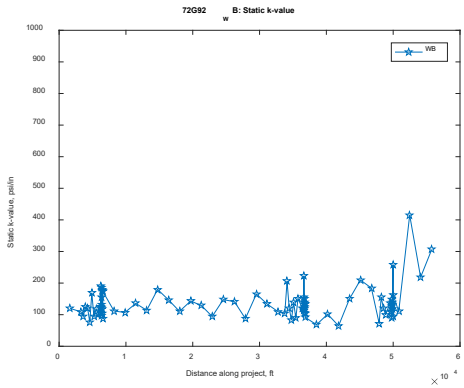

a) 10/12/2016

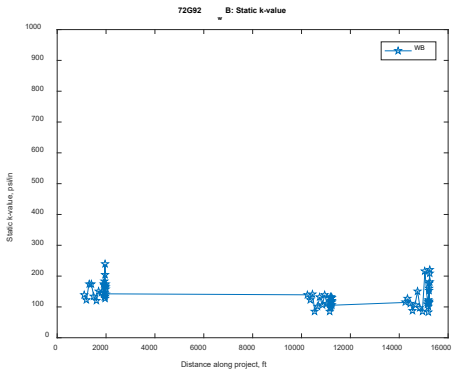

b) 8/6/2020

Figure 122. Graphs. Static k-value along I-72 WB (72G92).

I-70 (70044)

A summary of the FWD testing performed in 2020 is provided. Additionally, plots are included for comparison. No historical data was available for comparison with the 2020 testing. Two methods for backcalculation for CRCP were examined, testing performed at the center of slabs between cracks (function of different crack spacing) and testing performed along the edge between cracks (also a function of crack spacing). The average crack spacing measured was approximately 4 ft. Each figure presents FWD data conducted in 2020 using the two methods of backcalculation based on work performed by Zhang and Roesler (2018) and Zhang et al. (2020). The HMA interlayer was assumed to have a stiffness of 2.0×10^6 psi.

Table 54. FWD Summary from Center Slab Testing on 9/14/2020 for I-70 (70044)

	CN						LC			
	D0* (mils)		Area_36		Eri		D0* (mils)		LTE (%)	
	WB	EB	WB	EB	WB	EB	WB	EB	WB	EB
Average	1.23	1.07	30.5	30.5	19.9	20.5	1.22	1.07	90.9	88.9
Std. Dev.	0.20	0.21	4.10	3.98	0.94	1.10	0.21	0.18	18.4	8.26
COV	16.1	19.5	13.4	13.1	4.74	5.35	17.3	16.9	20.2	9.29

Table 55. FWD Summary from Corner Slab Testing on 9/14/2020 for I-70 (70044)

	Corner					
	D0* (mils)		LTE (%)		TE LTE (%)	
	WB	EB	WB	EB	WB	EB
Average	1.55	1.84	88.1	87.5	90.4	77.0
Std. Dev.	0.18	0.38	5.24	5.47	5.62	17.8
COV	11.4	20.5	5.95	6.25	6.22	23.2

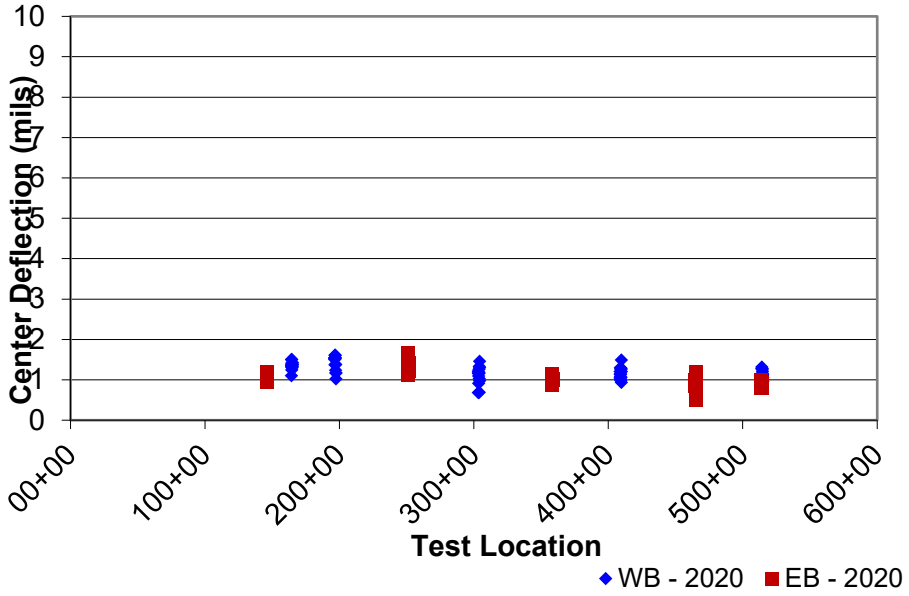

Figure 123. Graph. Normalized 9-kip deflection, D0*, at center panel for I-70 (70044).

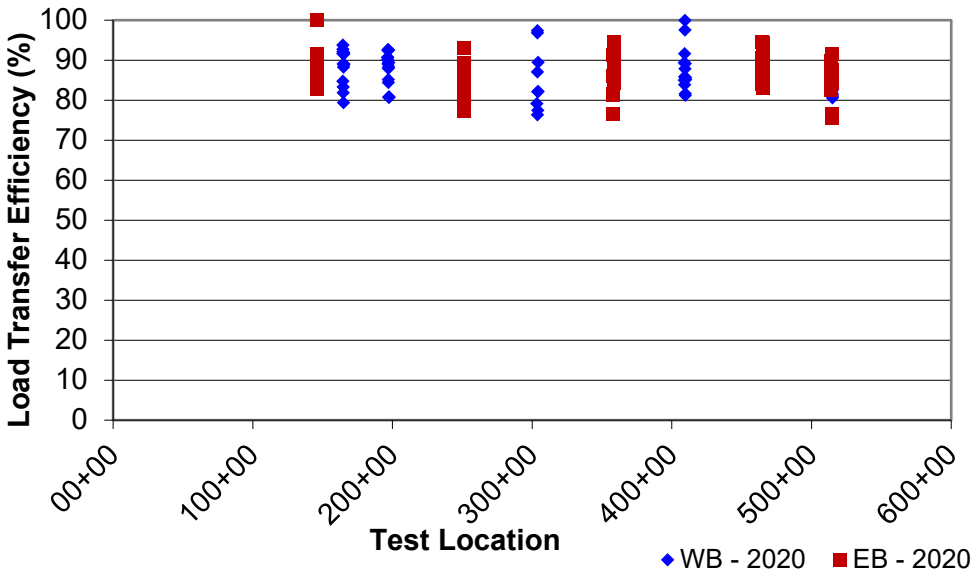

Figure 124. Graph. Crack load transfer efficiency (LTE) for I-70 (70044).

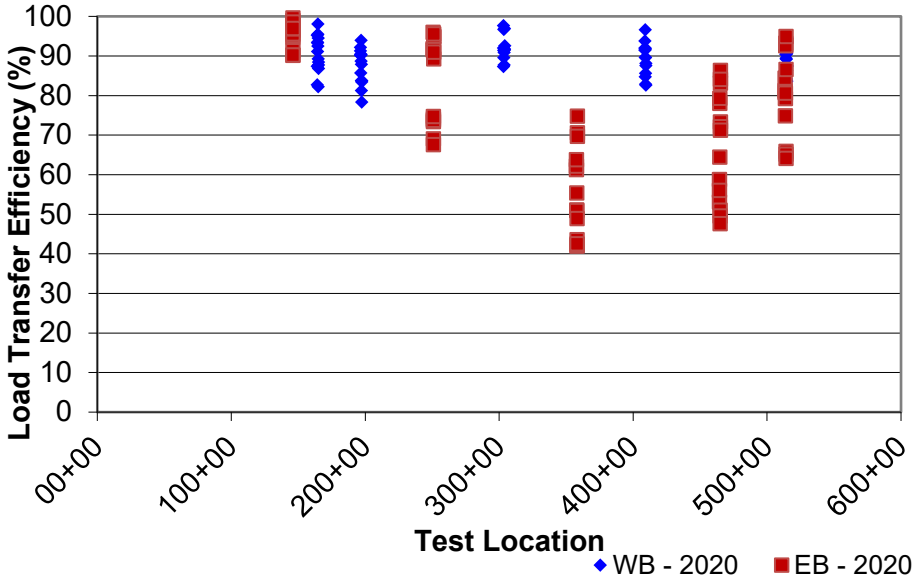

Figure 125. Graph. Lane shoulder longitudinal joint load transfer efficiency (LTE) for I-70 (70044).

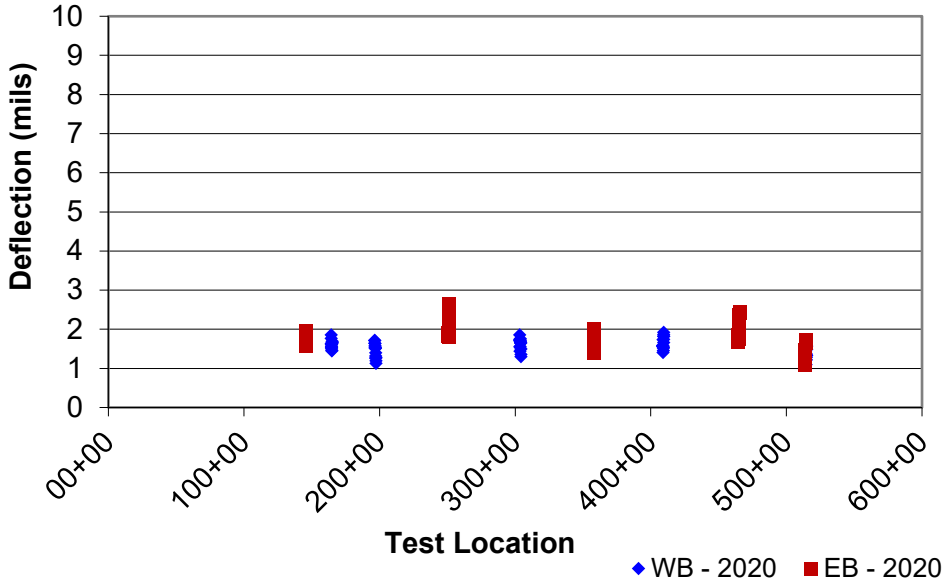

Figure 126. Graph. Normalized 9-kip deflection in the corner along the lane shoulder longitudinal joint for I-70 (70044).

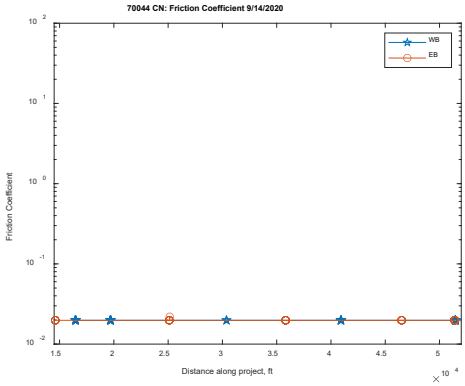

a) Center FWD location

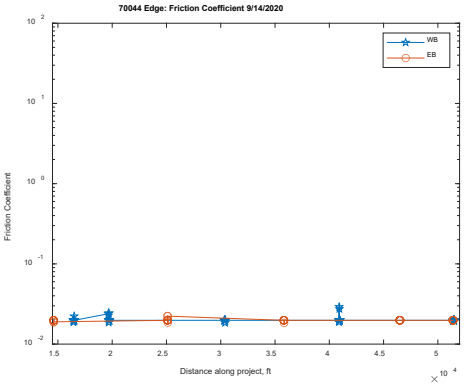

b) Edge FWD location

Figure 127. Graphs. Friction coefficient along I-70 (70044).

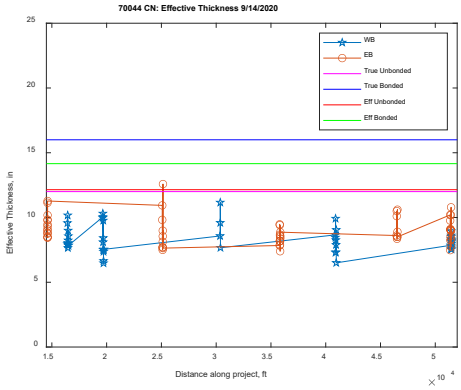

a) Center FWD location

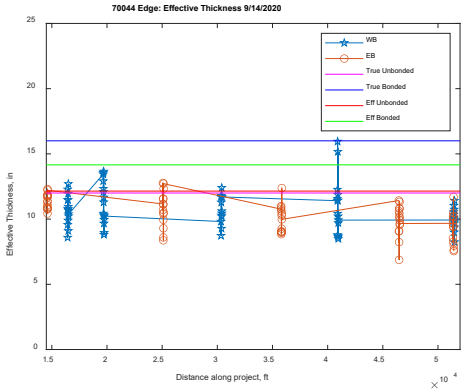

b) Edge FWD location

Figure 128. Graphs. Effective thickness along I-70 (70044).

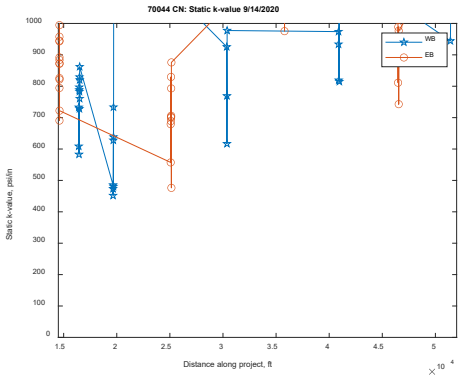

a) Center FWD location

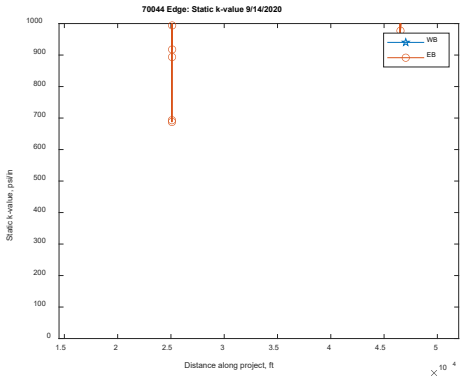

b) Edge FWD location

Figure 129. Graphs. Static k-value along I-70 (70044).

IL 53 (60N05)

A summary of the FWD testing performed in 2020 is provided. Additionally, plots are included for comparison. The method for backcalculation followed King et al. (2014) using finite backcalculation methodology for smaller panels. The HMA interlayer was assumed to have a stiffness of $2.0x10^6$ psi. Testing was only performed in the northbound direction in 2019 and southbound in 2020. The testing performed in 2019 was collected in accordance with testing performed in NCHRP 1-61 (Pierce et al. in review).

Table 56. FWD Summary from Center Slab Testing on 9/14/2020 for IL 53 SB (60N05)

	Center Panel (CN CP)				Leave Joint Center Panel (LJ CP)		Corner Center Panel (CP)		
	D0* (mils)	Area_36	Area_24	Eri	D0* (mils)	LTE	D0* (mils)	LTE (%)	TE LTE (%)
	SB	SB	SB	SB	SB	SB	SB	SB	SB
Average	6.42	26.5	19.9	8.45	6.69	79.9	6.51	78.3	80.6
Std. Dev.	1.34	1.47	0.87	2.24	1.48	6.83	1.66	7.09	5.56
COV	20.9	5.54	4.36	26.5	22.1	8.54	25.5	9.05	6.89

Table 57. FWD Summary from Right Edge Panel Testing on 9/14/2020 for IL 53 SB (60N05)

	Center Right Panel (CN RP)				Leave Joint Right Panel (LJ RP)	
	D0* (mils)	Area_36	Area_24	Eri	D0* (mils)	LTE (%)
	SB	SB	SB	SB	SB	SB
Average	7.44	27.2	20.6	7.62	8.08	76.7
Std. Dev.	2.35	1.06	0.66	3.19	4.42	13.6
COV	31.6	3.92	3.23	41.8	54.7	17.8

The major difference between the center panels and the right edge panels is potentially because the existing pavement did not extend the same width as the overlay. The right edge panels within the driving lane appear to have subsided with traffic and time, resulting in a longitudinal fault.

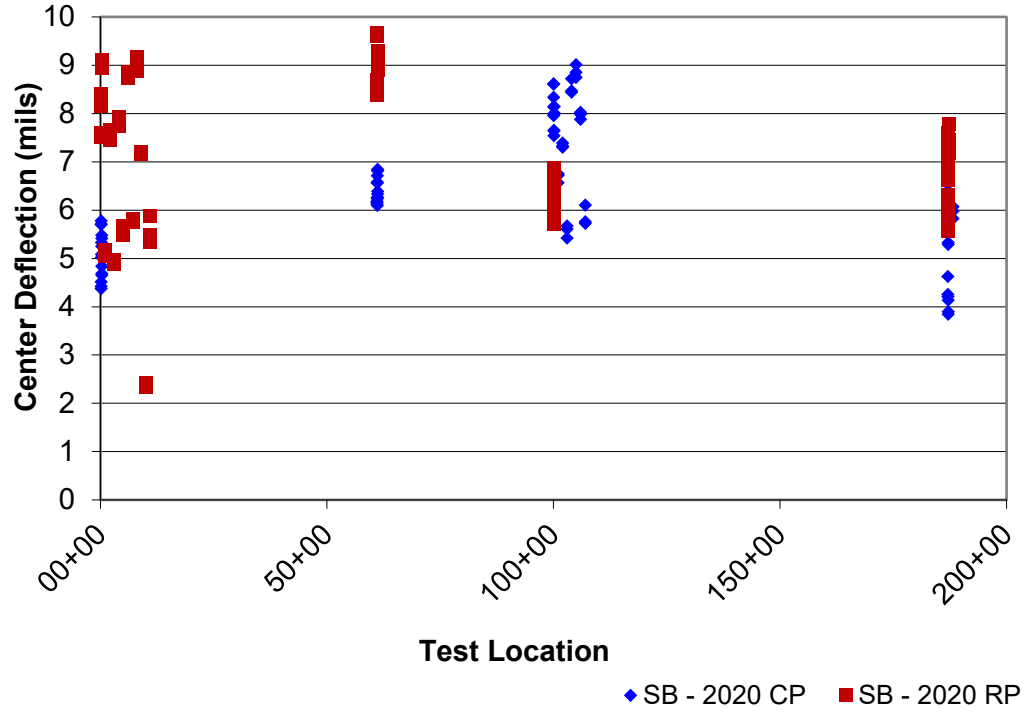

Figure 130. Graph. Normalized 9-kip deflection, D0*, at center panel for IL 53 SB (60N05).

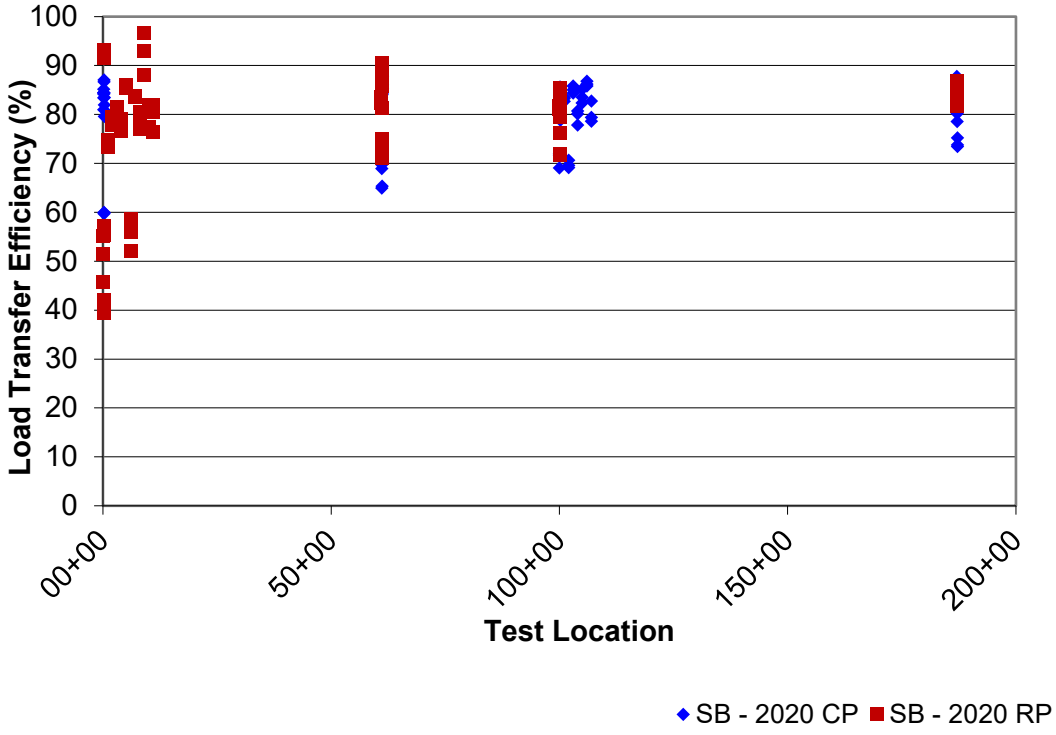

Figure 131. Graph. Load transfer efficiency (LTE) for IL 53 SB (60N05).

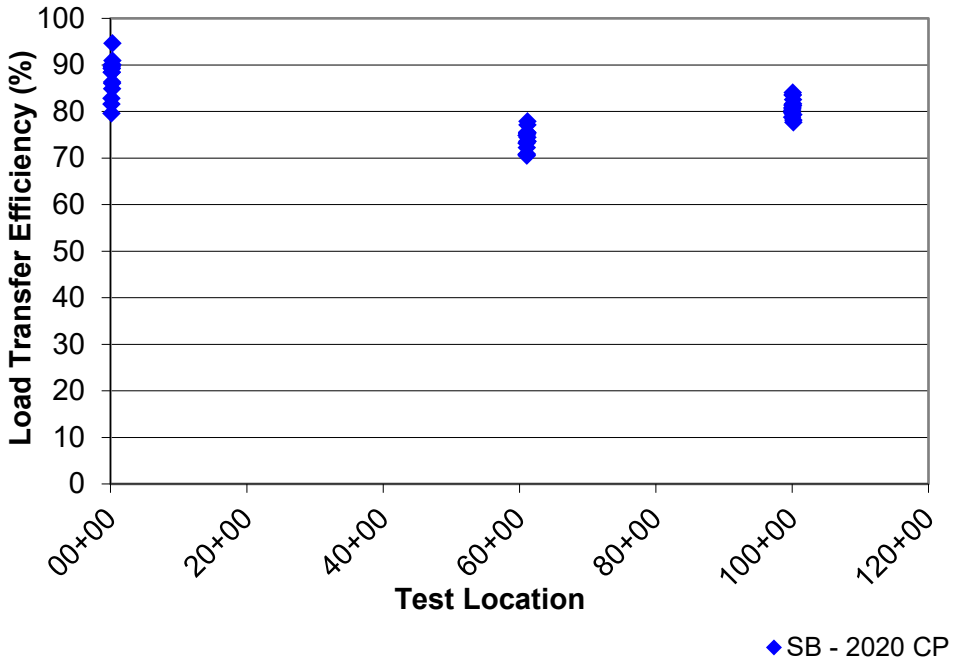

Figure 132. Graph. Center panel longitudinal joint load transfer efficiency (LTE) for IL 53 SB (60N05). No testing was performed along the longitudinal joint in the right panel.

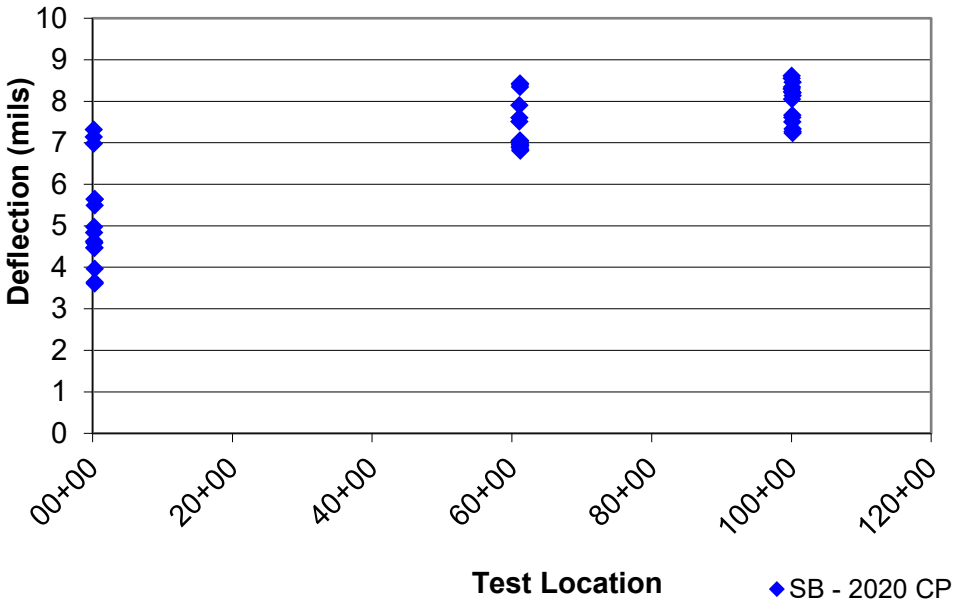

Figure 133. Graph. Normalized 9-kip deflection in the corner along the center longitudinal joint for IL 53 SB (60N05). No testing was performed along the longitudinal joint in the right panel.

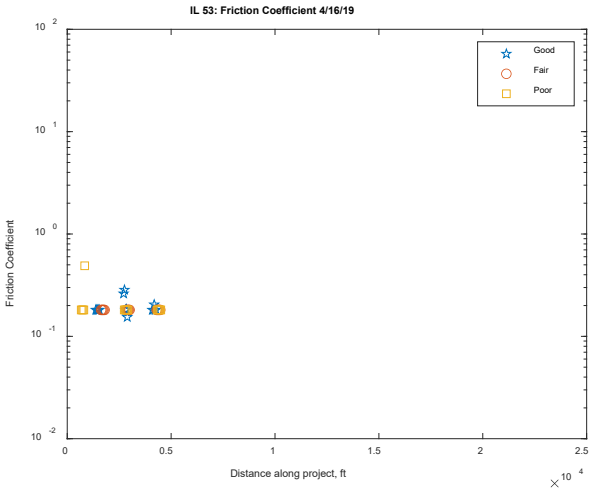

a) Center panels

Figure 134. Graph. Friction coefficient along IL 53 NB (60N05) – 4/16/2019.

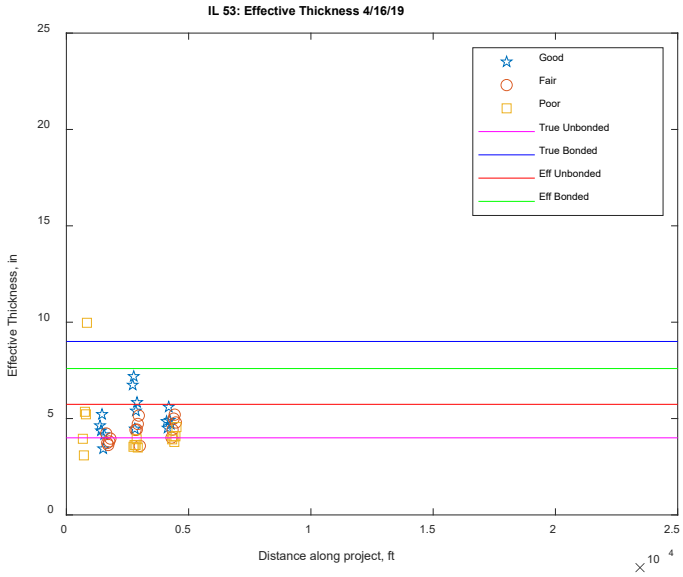

a) Center panels

Figure 135. Graph. Effective thickness along IL 53 NB (60N05) – 4/16/2019.

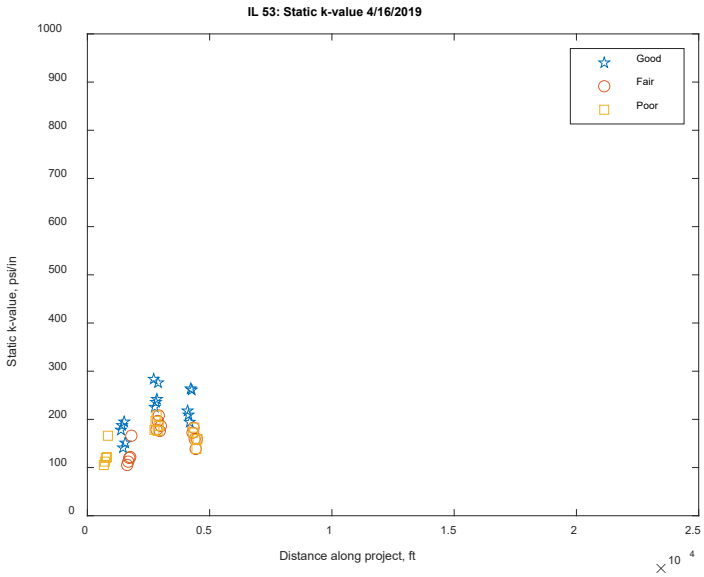

a) Center panels

Figure 136. Graph. Static k-value along IL 53 NB (60N05) – 4/16/2019.

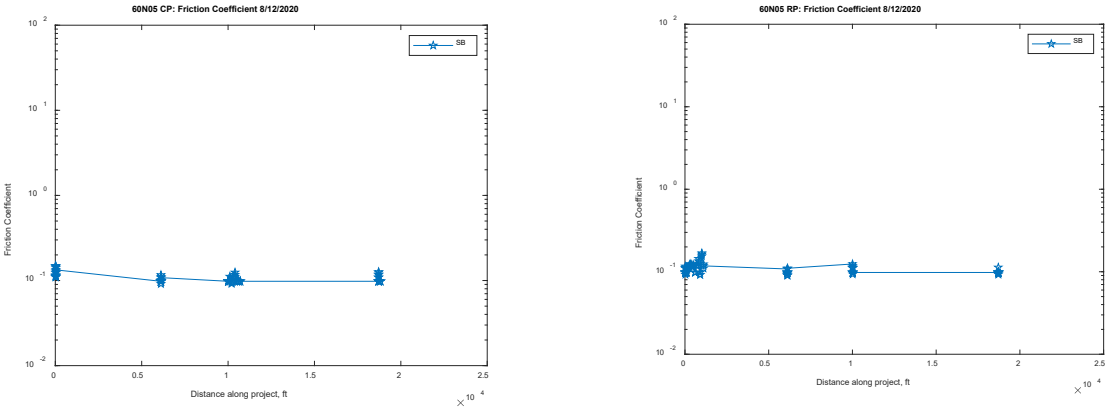

a) Center panels b) Right edge panels

Figure 137. Graphs. Friction coefficient along IL 53 SB (60N05) – 8/12/2020.

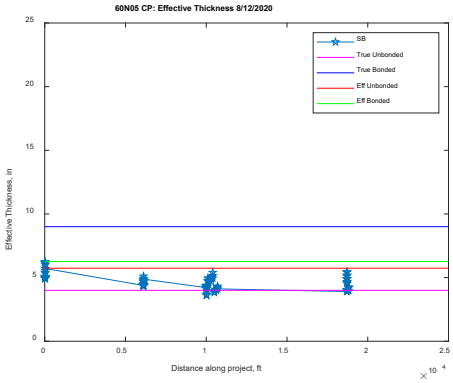

a) Center panels

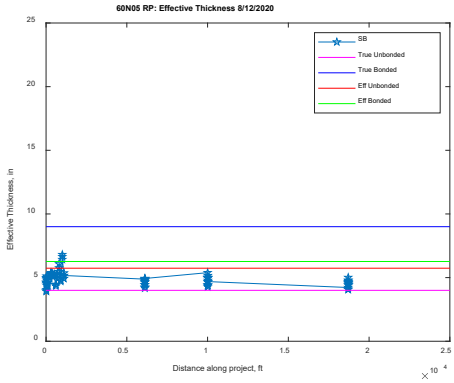

b) Right edge panels

Figure 138. Graphs. Effective thickness along IL 53 SB (60N05) – 8/12/2020.

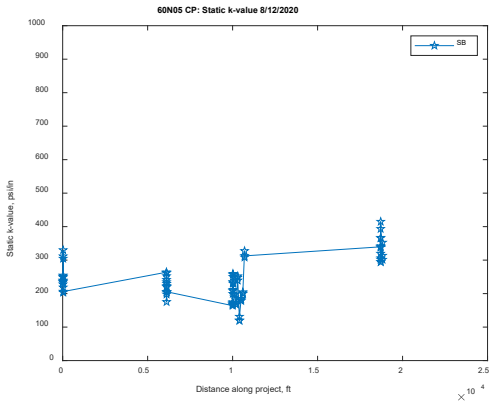

a) Center panels

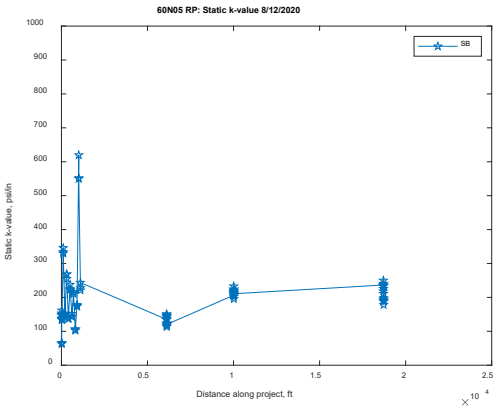

b) Right edge panels

Figure 139. Graphs. Static k-value along IL 53 SB (60N05) – 8/12/2020.

UIUC E-15 PARKING LOT

A summary of the FWD testing performed in 2021 is provided. Additionally, plots are included for comparison. Four testing locations were included for comparison. Three sections were constructed in 2006 and the fourth section was constructed in 2012. The method for backcalculation followed King et al. (2014) using finite backcalculation methodology for smaller panels. The HMA interlayer was assumed to have a stiffness of 2.0×10^6 psi.

Table 58. FWD Summary from Center Slab Testing on 5/6/2021 for UIUC E-15 Parking Lot

	Center (Center Panel - CP)															
	D0* (mils)				Area_36				Area_24				Eri			
	NW	**NE**	**E**	**SE**	***NW***	**NE**	**E**	**SE**	***NW***	**NE**	**E**	**SE**	***NW***	**NE**	**E**	**SE**
Average	13.3	13.1	10.5	11.3	18.2	18.9	18.2	20.1	15.3	16.1	15.6	16.4	10.1	11.4	14.8	9.57
Std. Dev.	0.89	1.36	1.58	0.96	0.62	1.12	1.40	0.92	0.49	1.07	1.00	0.64	0.71	1.61	1.63	0.84
COV	6.71	10.4	15.1	8.50	3.40	5.93	7.69	4.60	3.23	6.66	6.40	3.91	7.08	14.2	11.0	8.81

Table 59. FWD Summary of Transverse Joint Testing on 5/6/2021 for UIUC E-15 Parking Lot

	Transverse Joint											
	D0* (mils)				Approach LTE (%)				Leave LTE (%)			
	NW	**NE**	**E**	**SE**	***NW***	**NE**	**E**	**SE**	***NW***	**NE**	**E**	**SE**
Average	15.3	15.2	12.9	12.6	82.9	77.1	76.2	86.9	80.9	75.9	75.2	89.3
Std. Dev.	2.06	3.29	2.99	1.74	8.36	19.0	20.5	5.01	8.73	17.7	19.2	7.41
COV	13.4	21.7	23.1	13.8	10.1	24.6	26.9	5.76	10.8	23.3	25.5	8.30

Table 60. FWD Summary of Corner Testing on 5/6/2021 for UIUC E-15 Parking Lot

	Corner											
	D0 (mils)				Leave LTE (%)				TE LTE (%)			
	NW	**NE**	**E**	**SE**	***NW***	**NE**	**E**	**SE**	***NW***	**NE**	**E**	**SE**
Average	16.2	14.3	12.2	12.9	85.0	76.9	77.9	86.8	87.7	90.0	90.0	91.8
Std Dev.	1.42	3.07	2.94	1.84	3.79	18.7	18.0	5.17	3.20	2.84	2.90	3.63
COV	8.78	21.4	24.2	14.3	4.46	24.3	23.1	5.96	3.65	3.16	3.22	3.95

Table 61. FWD Summary of Lane Edge Testing on 5/6/2021 for UIUC E-15 Parking Lot

	True Edge							
	D0 (mils)				TE LTE (%)			
	NW	**NE**	**E**	**SE**	***NW***	**NE**	**E**	**SE**
Average	14.8	15.2	10.0	11.5	87.1	87.7	88.9	91.1
Std Dev.	0.92	3.29	1.67	1.05	3.90	2.64	4.10	4.48
COV	6.21	21.7	16.7	9.11	4.48	3.02	4.61	4.91

The major difference between the four locations is the Northwest (NW) section was constructed 6 years after the eastern sections within E-15.

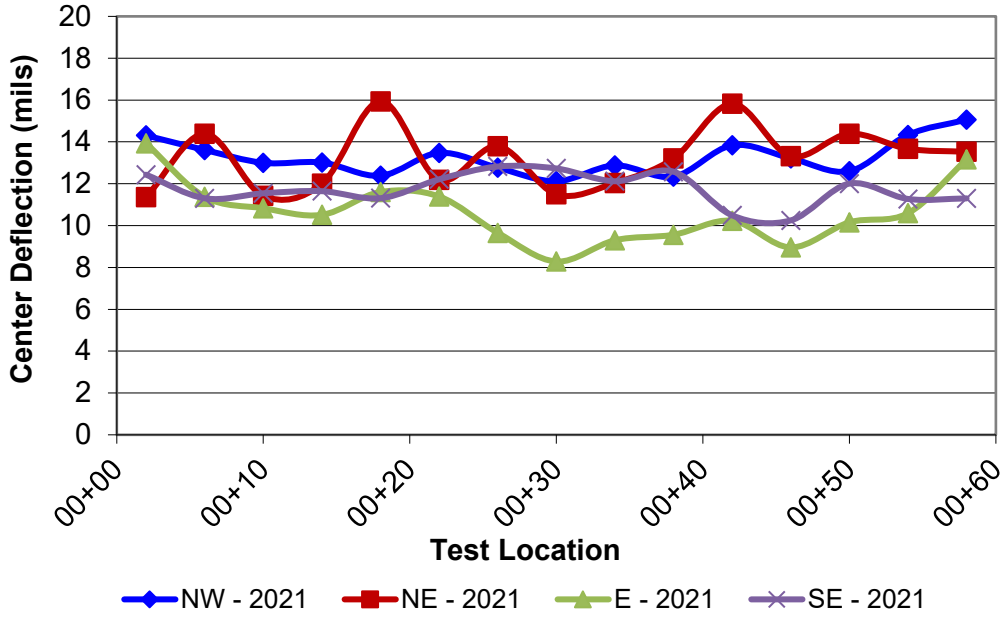

Figure 140. Graph. Normalized 9-kip deflection, D0*, at center panel for UIUC E-15 Parking Lot.

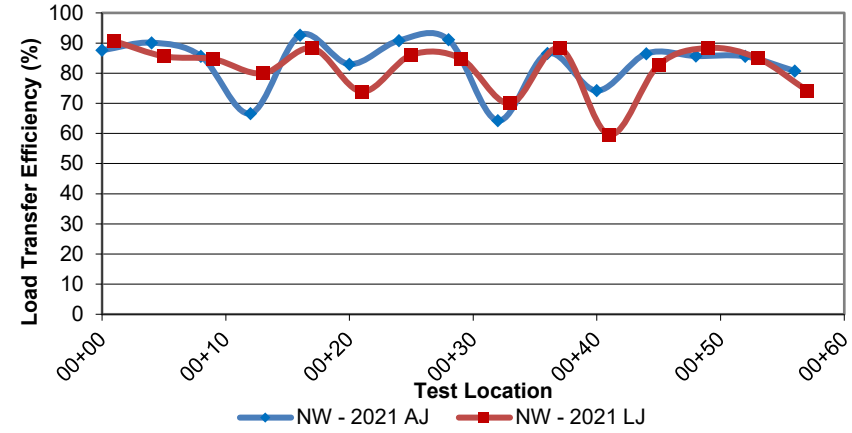

a) Northwest section

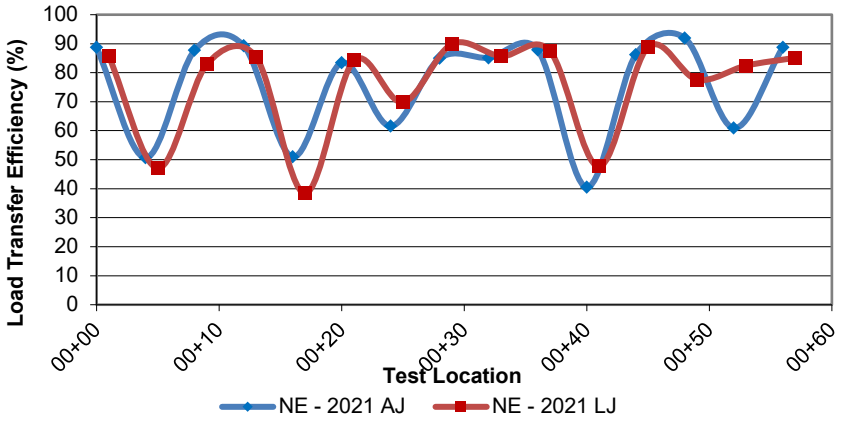

b) Northeast section

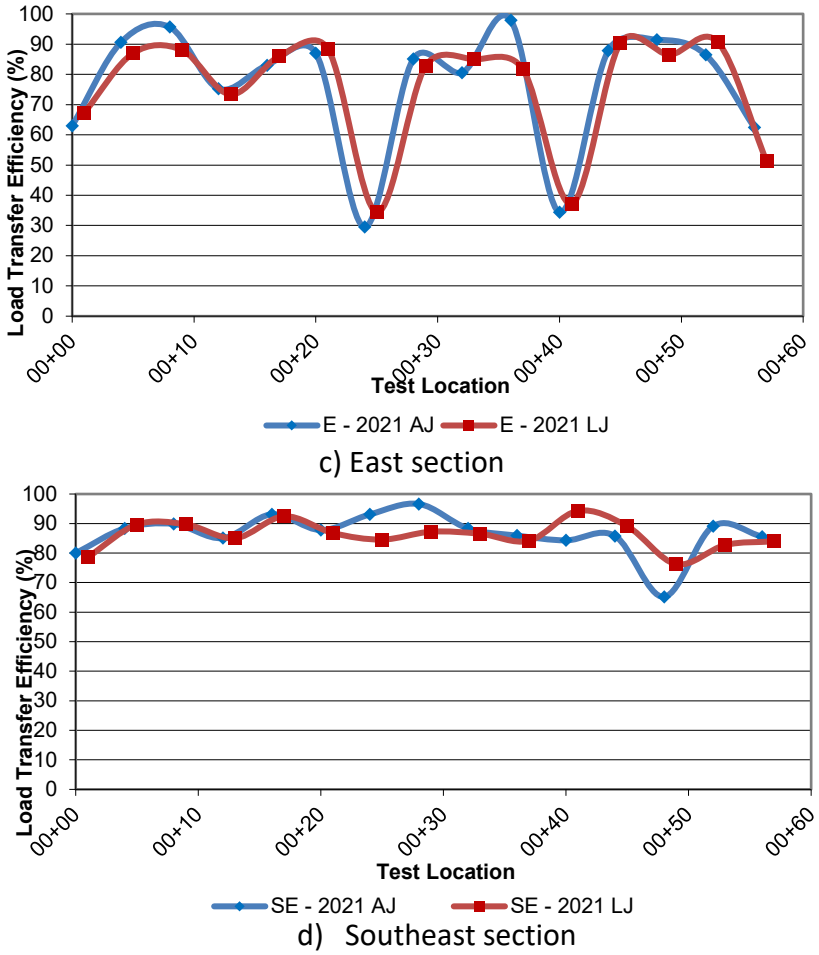

Figure 141. Graphs. Load transfer efficiency (LTE) for UIUC E-15 Parking Lot.

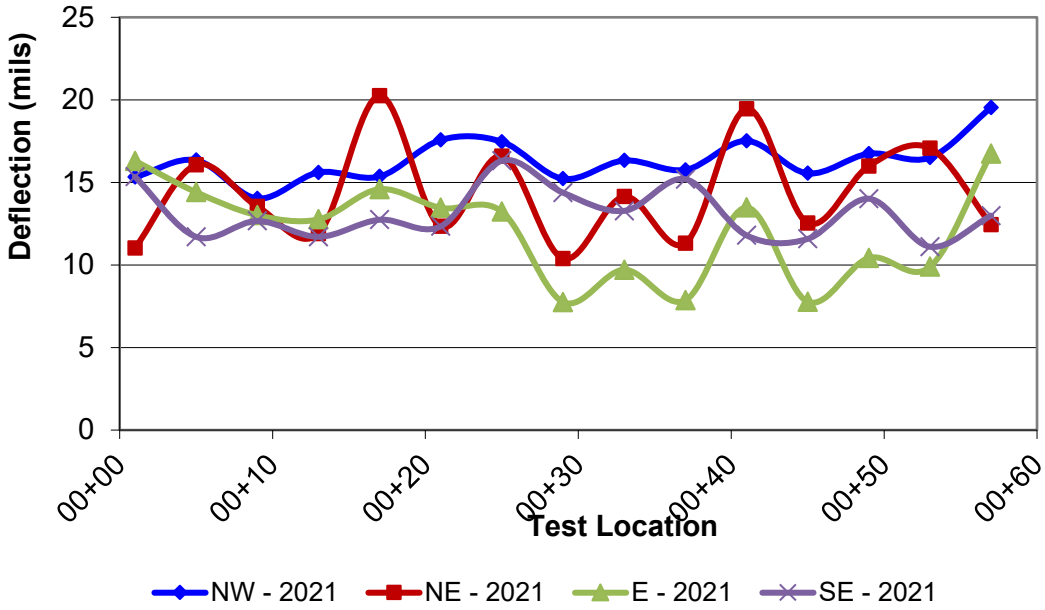

Figure 142. Graph. Center and left panel longitudinal joint corner for UIUC E-15 Parking Lot.

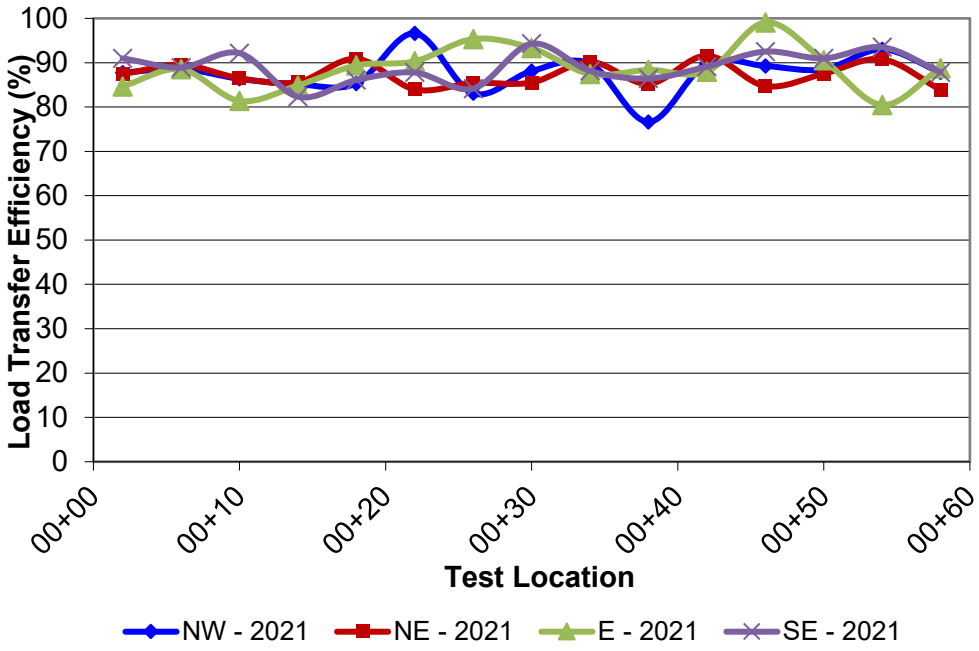

Figure 143. Graph. Normalized 9-kip deflection along the center and left panel longitudinal joint (lane edge testing) for UIUC E-15 Parking Lot.

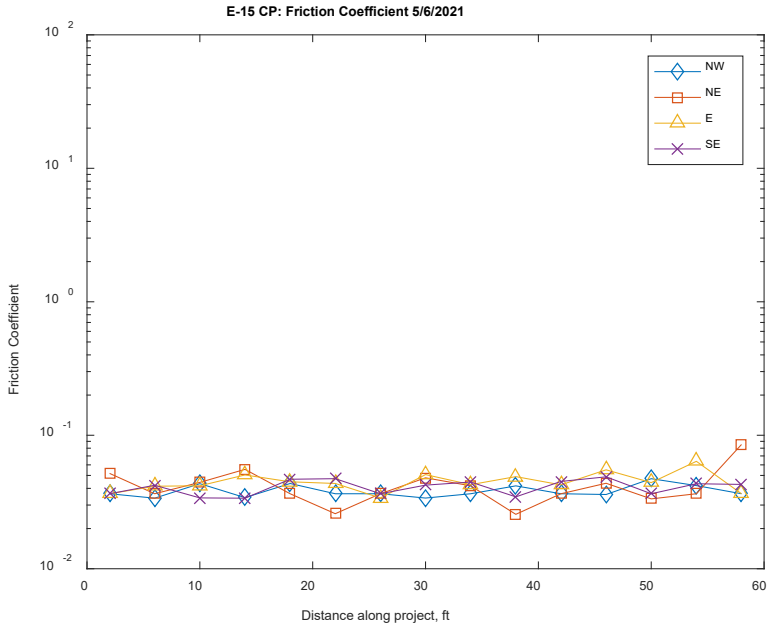

a) Center panels

Figure 144. Graph. Friction coefficient along UIUC E-15 Parking Lot.

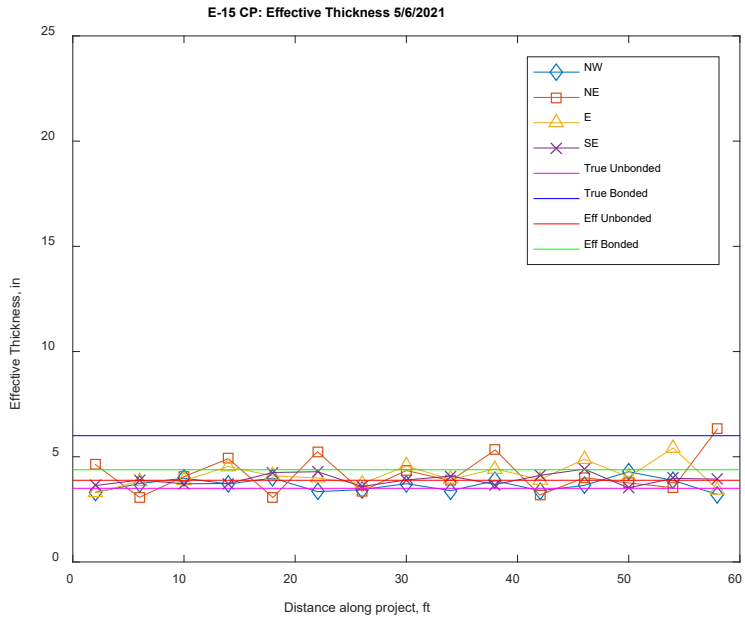

a) Center panels

Figure 145. Graph. Effective thickness along UIUC E-15 Parking Lot.

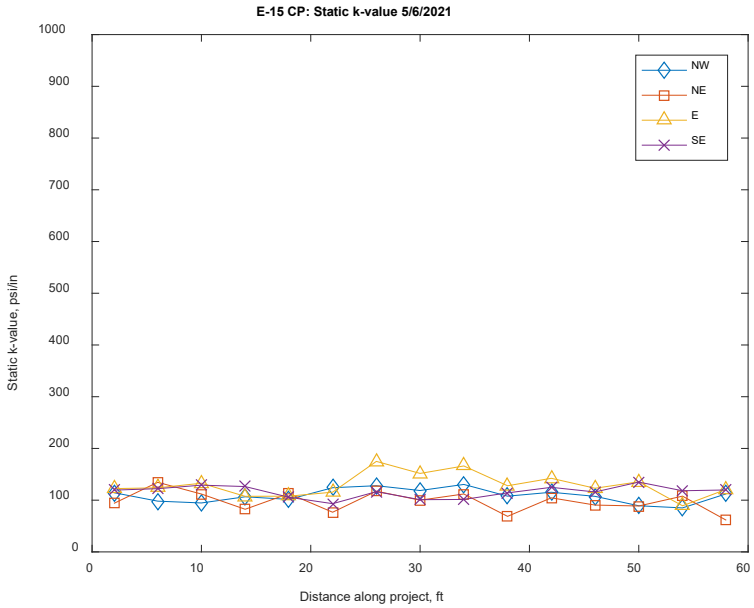

a) Center panels

Figure 146. Graphs. Static k-value along UIUC E-15 Parking Lot.

UIUC MCKINLEY HEALTH CENTER PARKING LOT

A summary of the FWD testing performed in 2021 is provided. Additionally, plots are included for comparison. Three testing locations were included for comparison. All three sections were

constructed in 2006. The method for backcalculation followed King et al. (2014) using finite backcalculation methodology for smaller panels. The HMA interlayer was assumed to have a stiffness of $0.8x10^6$ psi.

Table 62. FWD Summary from Center Slab Testing on 5/6-7/2021 for UIUC McKinley Parking Lot

	Center (Center Panel - CP)											
	D0* (mils)			Area_36			Area_24			Eri		
	NW	**NE**	**SE**	**NW**	**NE**	**SE**	**NW**	**NE**	**SE**	**NW**	**NE**	**SE**
Average	11.1	16.5	11.1	19.3	15.6	19.3	15.8	13.7	16.0	10.2	13.5	10.8
Std. Dev.	1.86	3.17	1.36	1.19	0.99	0.95	0.74	0.82	0.76	0.95	1.84	1.14
COV	16.7	19.3	12.2	6.18	6.32	4.91	4.69	5.96	4.75	9.37	13.7	10.5

Table 63. FWD Summary of Transverse Joint Testing on 5/6-7/2021 for UIUC McKinley Parking Lot

	Transverse Joint								
	D0* (mils)			Approach LTE (%)			Leave LTE (%)		
	NW	**NE**	**SE**	**NW**	**NE**	**SE**	**NW**	**NE**	**SE**
Average	12.6	20.6	12.8	78.8	73.5	87.0	75.5	73.6	81.1
Std. Dev.	5.72	4.76	2.40	18.2	15.6	6.18	16.7	14.6	7.12
COV	45.3	23.1	18.8	23.1	21.2	7.10	22.1	19.8	8.78

Table 64. FWD Summary of Corner Testing on 5/6-7/2021 for UIUC McKinley Parking Lot

	Corner								
	D0* (mils)			Leave LTE (%)			TE LTE (%)		
	NW	**NE**	**SE**	**NW**	**NE**	**SE**	**NW**	**NE**	**SE**
Average	12.4	23.1	13.7	79.8	72.7	79.9	83.1	86.6	85.5
Std. Dev.	2.33	6.31	3.02	8.59	15.9	9.59	3.08	3.23	4.13
COV	18.8	27.3	22.0	10.8	21.8	12.0	3.70	3.73	4.83

Table 65. FWD Summary of Lane Edge Testing on 5/6-7/2021 for UIUC McKinley Parking Lot

	True Edge					
	D0* (mils)			TE LTE (%)		
	NW	**NE**	**SE**	**NW**	**NE**	**SE**
Average	12.4	20.3	11.9	80.1	85.9	89.9
Std. Dev.	5.34	4.76	2.32	17.2	4.29	5.57
COV	43.0	23.4	19.5	21.4	4.99	6.20

The major difference between the three locations is the Northwest (NW) section was constructed first during high temperatures. This may have led to a large built-in temperature gradient and also affected saw-cut timing. The NW section had significant joint raveling from early entry saw-cutting. Whereas the other locations appeared to be in good condition after construction adjustments based

on the NW section. The Northeast (NE) section is the primary trafficked section and could contribute to higher deflections (potential debonding occurring in this region).

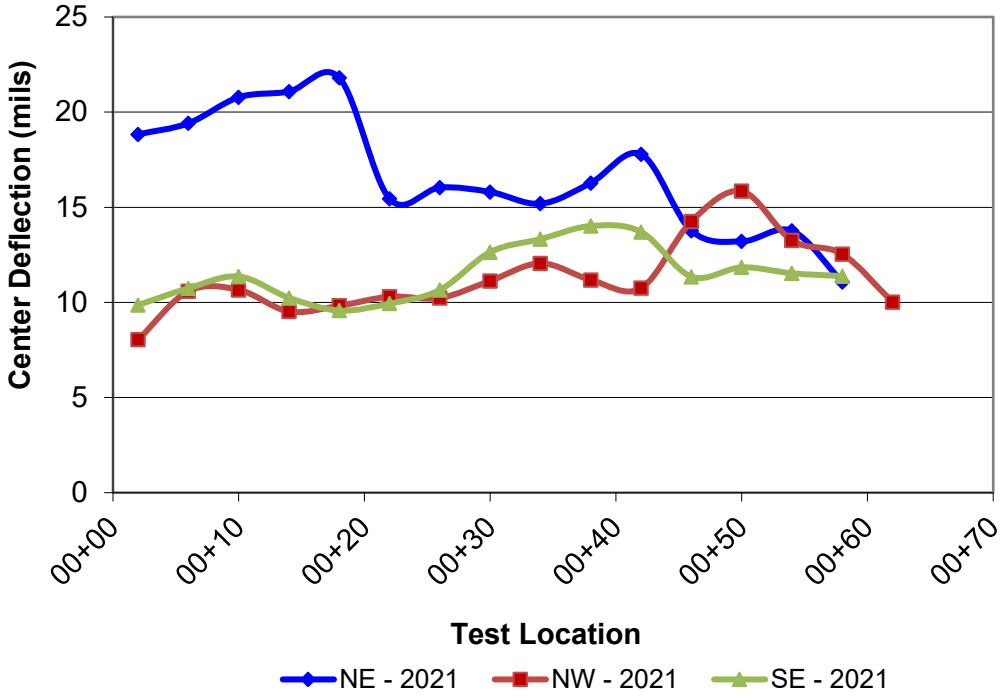

Figure 147. Graph. Normalized 9-kip deflection, D0*, at center panel for UIUC McKinley Parking Lot.

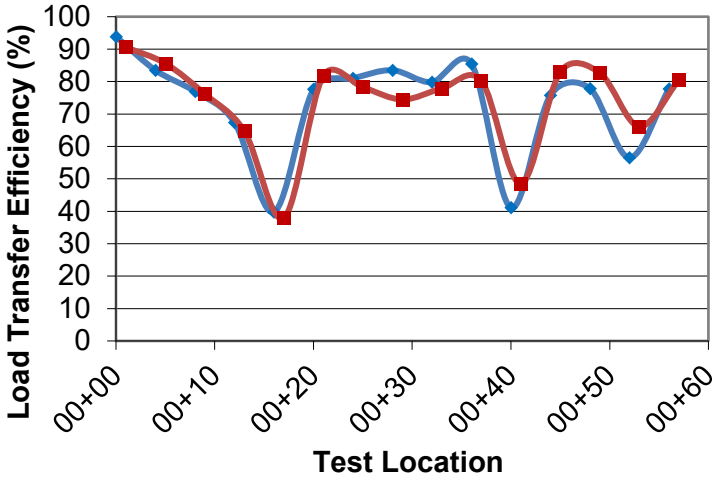

a) Northeast section

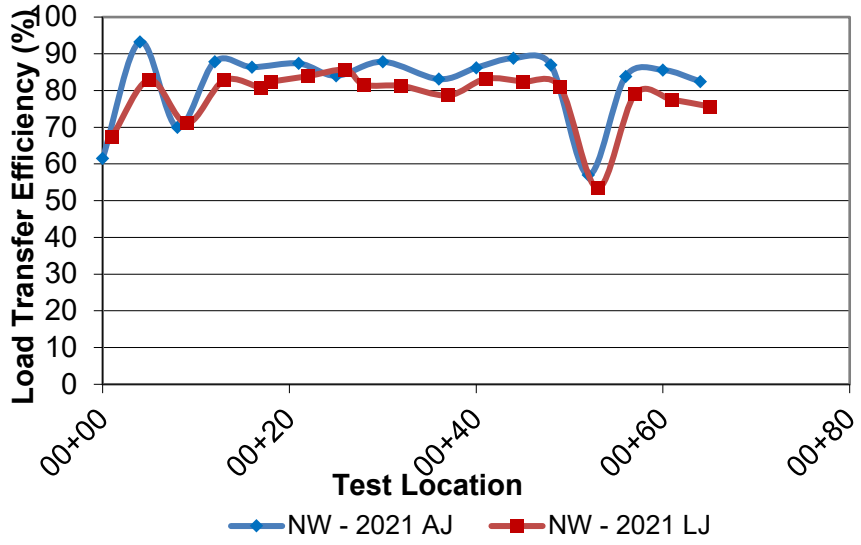

b) Northwest section

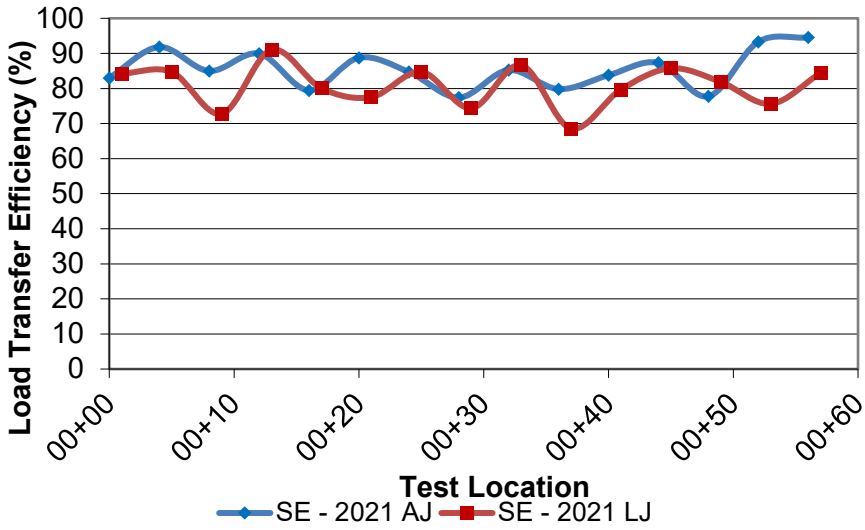

c) Southeast section

Figure 148. Graphs. Load transfer efficiency (LTE) for UIUC McKinley Parking Lot.

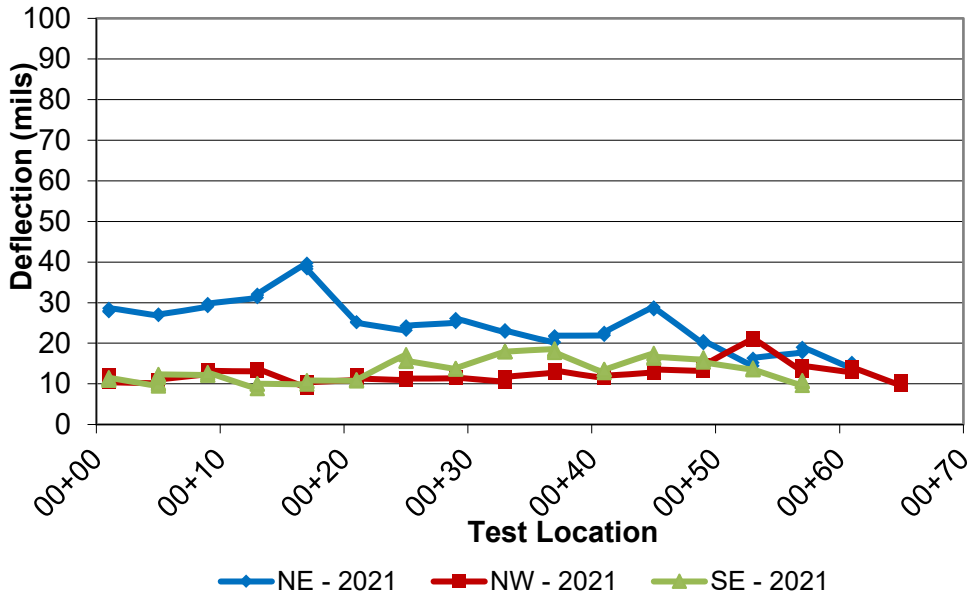

Figure 149. Graph. Center and left panel longitudinal joint corner for UIUC McKinley Parking Lot.

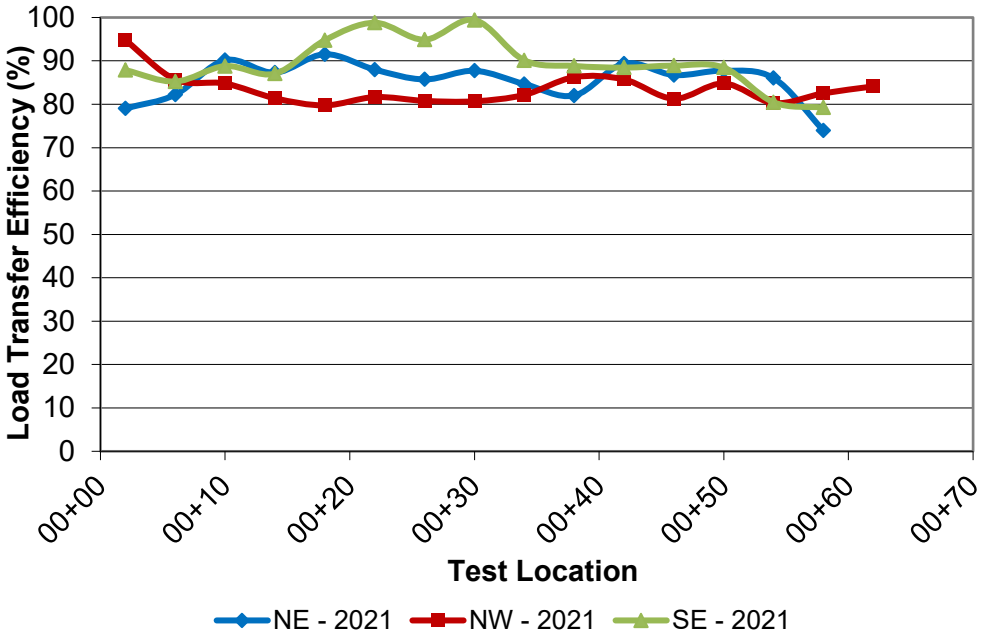

Figure 150. Graph. Normalized 9-kip deflection along the center and left panel longitudinal joint (lane edge testing) for UIUC McKinley Parking Lot.

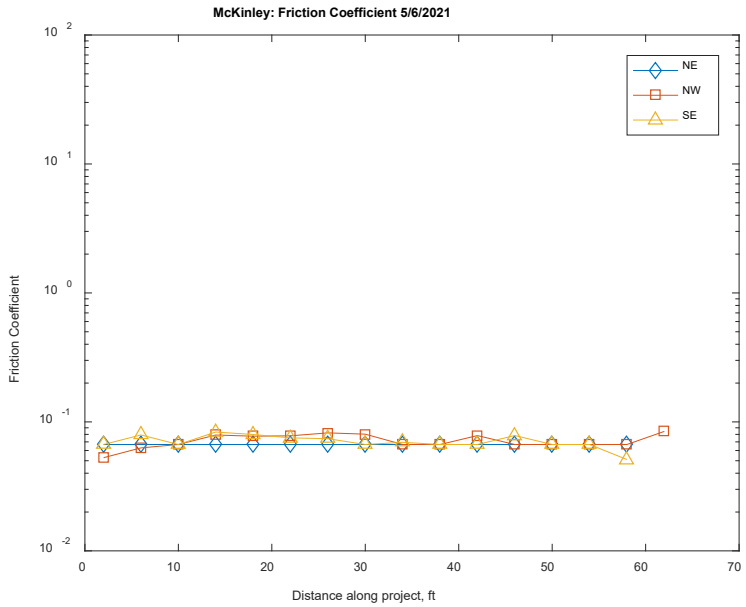

a) Center panels

Figure 151. Graph. Friction coefficient along UIUC McKinley Parking Lot.

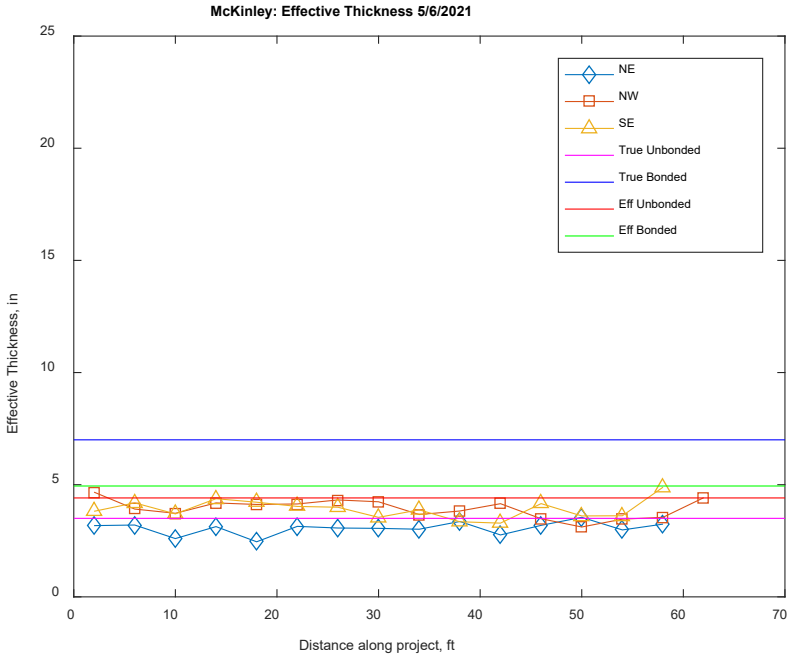

a) Center panels

Figure 152. Graph. Effective thickness along UIUC McKinley Parking Lot.

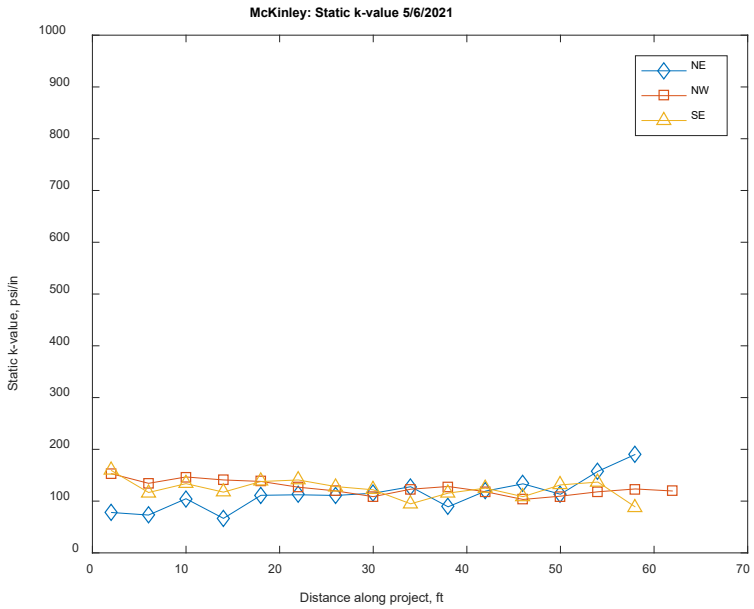

a) Center panels

Figure 153. Graph. Static k-value along UIUC McKinley Parking Lot.

In addition to the testing conducted in 2021, previous testing results presented in Roesler et al. (2008) and King and Roesler (2014) were compared with the most recent testing for the UIUC parking lots. The corresponding testing locations within a given section between dates cannot be confirmed as the exact same slabs, but the general location is the same. The backcalculated averages for joint load transfer, k-value, effective thickness, and the temperature during the different dates of testing can be seen in the following tables. The average transverse joint and longitudinal joint LTE did not appear to change drastically over the years since construction. All LTE averages are above 70%. The effective thickness has significantly decreased indicating a decrease in bond between the PCC and existing HMA. Overall, these parking lots are still in great shape in terms of limited surface distress and performance for their intended purpose and service life.

Table 66. UIUC Parking Lots FWD Backcalculation Analysis Results of Average Joint Load Transfer Efficiencies

Project/Section		Testing Date	Transverse Joint Average LTE (%)	Longitudinal Joint Average LTE (%)
McKinley Lot	Northeast	2008[1]	79.4	83.5
		2012[1]	79.7	76.6
		2021	73.5	85.9
	Northwest	2008[1]	86.9	91.6
		2012[1]	85.7	83.6
		2021	75.5	80.1
	Southeast	2008[1]	82.5	78.8
		2012[1]	74.7	82.3
		2021	81.1	89.9

Project/Section		Testing Date	Transverse Joint Average LTE (%)	Longitudinal Joint Average LTE (%)
E-15	Northeast (1)	2008[1]	78.3	88
		2012[1]	80.7	91
		2021	75.9	87.7
	East (2)	2008[1]	82.9	88.2
		2012[1]	78	90
		2021	75.2	88.9
	Southeast (3)	2008[1]	83.8	88.9
		2012[1]	81.6	90.2
		2021	86.9	91.1
	Northwest (4)	2012[1]	87.7	83.3
		2021	80.9	87.1

[1] Data presented in King and Roesler 2014.

Table 67. UIUC Parking Lots FWD Backcalculation Analysis Results of Average K-Value and Effective Thickness

Project/Section		Testing Date	Average Modulus of Subgrade Reaction, k (psi/in.)	Average Effective Slab Thickness (in.)	Thickness Standard Deviation (in.)	Design Thickness: PCC + AC (in.)
McKinley Lot	Northeast	2008	197	5.06	0.475	3.5+4 = 7.5
		2012	241	5.52	0.938	
		2021	114	3.06	0.28	
	Northwest	2008	279	6.63	0.603	
		2012	291	7.23	1.30	
		2021	126	3.94	0.415	
	Southeast	2008	421	6.89	0.583	
		2012	324	7.45	2.35	
		2021	124	3.91	0.423	
E-15	Northeast (1)	2008	182	5.71	0.603	3.5+2.5=6
		2012	152	5.81	0.963	
		2021	97.5	4.18	0.953	
	East (2)	2008	241	6.2	0.617	
		2012	202	5.8	0.81	
		2021	129	4.13	0.555	
	Southeast (3)	2008	200	6.66	2.07	
		2012	186	6.62	1.46	
		2021	116	3.913	0.273	
	Northwest (4)	2012	202	5.94	0.666	
		2021	109	3.66	0.309	

Table 68. UIUC Parking Lots FWD Testing Conditions

Project/Section		Date/Time	Average Air Temp (°F)	Average Pavement Surface Temp (°F)	Average Pavement Temp at 2-in. Depth (°F)
McKinley Lot	Northeast	10/17/2008 11:00	57	63	60
		10/19/2012 9:34	45	52	50
		5/7/2021 12:00	64	64	-
	Northwest	10/17/2008 11:00	54	63	60
		10/16/2012 11:48	69	67	67
		5/6/2021 17:30	55	64	70
	Southeast	10/17/2008 11:00	57	58	58
		10/19/2012 10:47	46	49	50
		5/6/2021 19:30	53	55	64
E-15	Northeast (1)	10/16/2008 9:36	53	68	70
		10/22/2012 9:36	63	60	65
		5/6/2021 13:00	65	69	59
	East (2)	10/16/2008 9:36	55	63	70
		10/22/2012 10:46	59	51	64
		5/6/2021 11:00	60	61	-
	Southeast (3)	10/16/2008 9:36	58	58	70
		10/24/2012 9:24	63	58	64
		5/6/2021 9:00	55	55	61
	Northwest (4)	10/24/2012 10:31	67	62	67
		5/6/2021 15:00	60	67	-

APPENDIX D: ULTRASONIC TESTING MIRA RESULTS

Ultrasonic testing was conducted on each field section in conjunction with FWD testing and distress surveying. For each section, the concrete layer thickness, estimation of base layer thickness (if possible), and the joint activation analysis is presented. The layer thicknesses were estimated using the SAFT B-scans. The subbase layer was estimated using the reflections present that were not second reflections from the PCC/subbase interface. Because different materials are present (PCC and subbase, either HMA or CAM II), there is likely a change in angle of incidence as a function of material specific acoustic impedance. Therefore, the subbase layer thicknesses are estimations with potentially large standard deviations. The joint activation analysis uses the developed algorithm by Tran and Roesler (2020).

US 67 (92774):

Layer Thickness Results

Design: 9.75-in. JPCP on 4-in. CAM II on 12-in. Lime Modified Soil

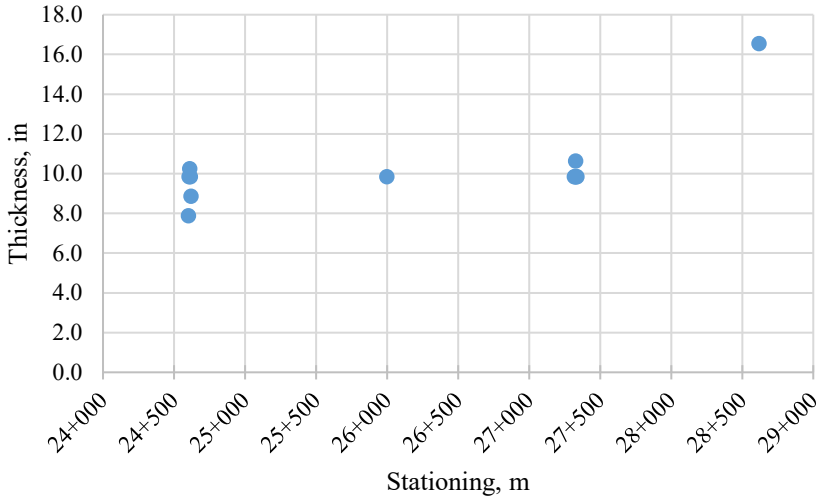

a) PCC thickness estimation along section

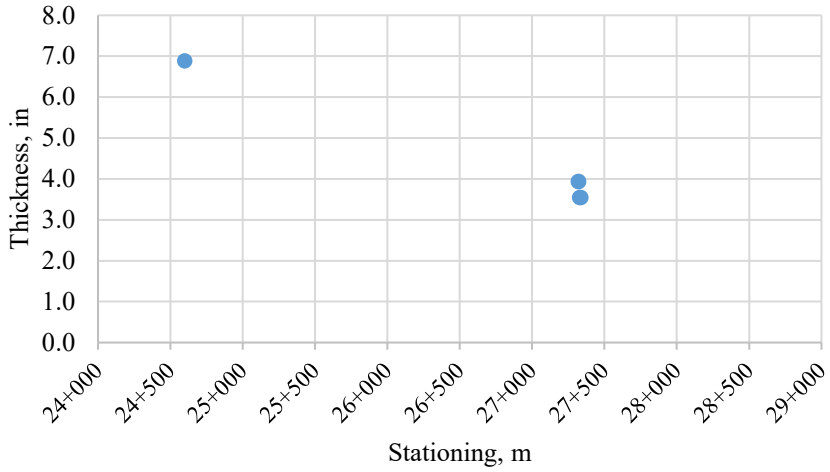

b) Subbase thickness estimation along section

Figure 154. Graphs. US 67 (92774) MIRA thickness results (Northbound).

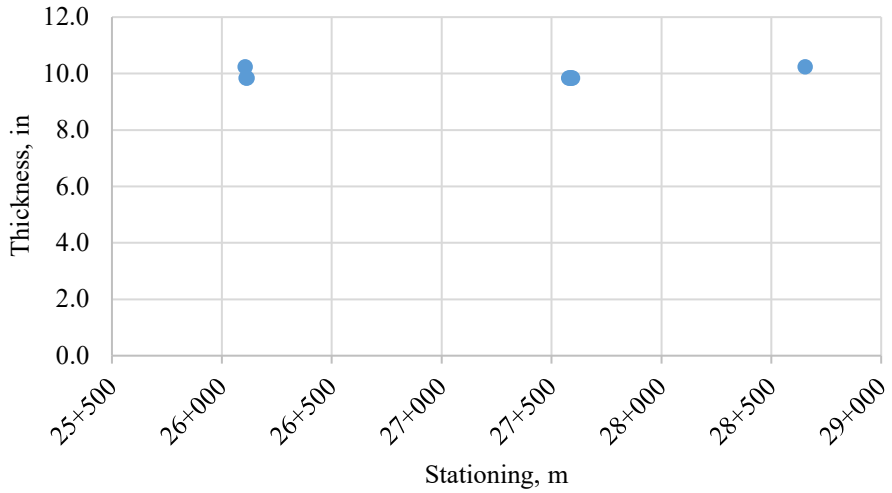

a) PCC thickness estimation along section

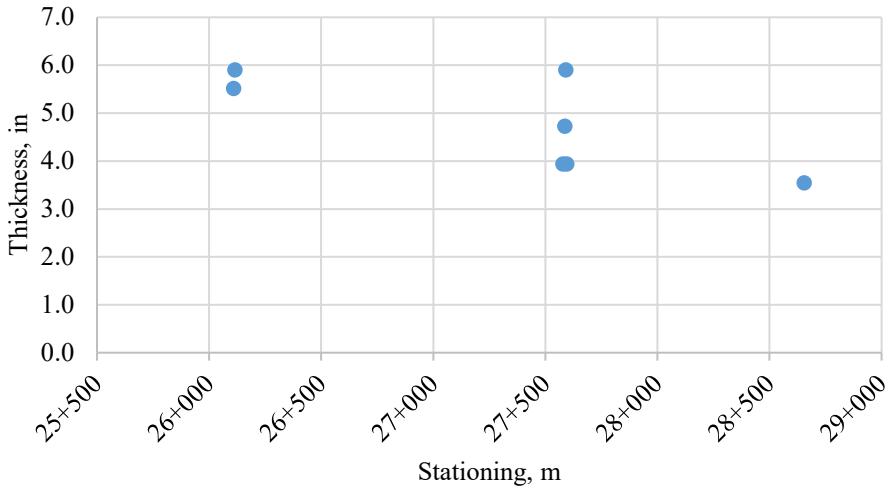

b) Subbase thickness estimation along section

Figure 155. Graphs. US 67 (92774) MIRA thickness results (Southbound).

Joint Activation Analysis

The joint activation analysis results are presented below. Four of the intensive sections were tested. From this analysis all tested joints were predicted to be fully activated.

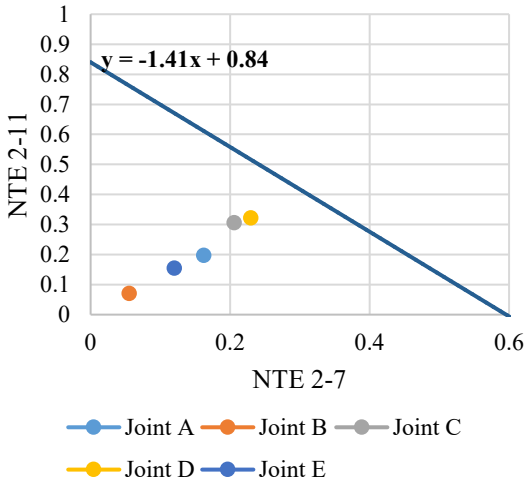

a) US 67 NB Section 1

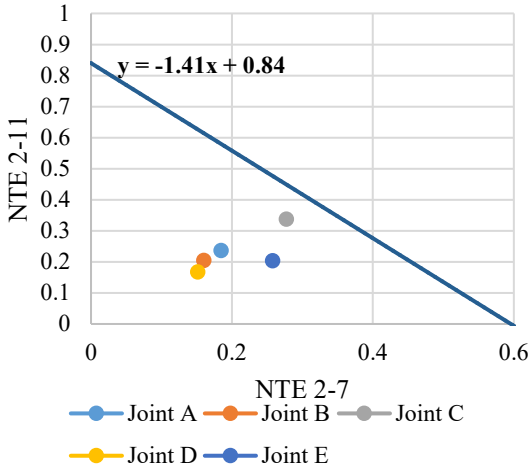

b) US 67 NB Section 3

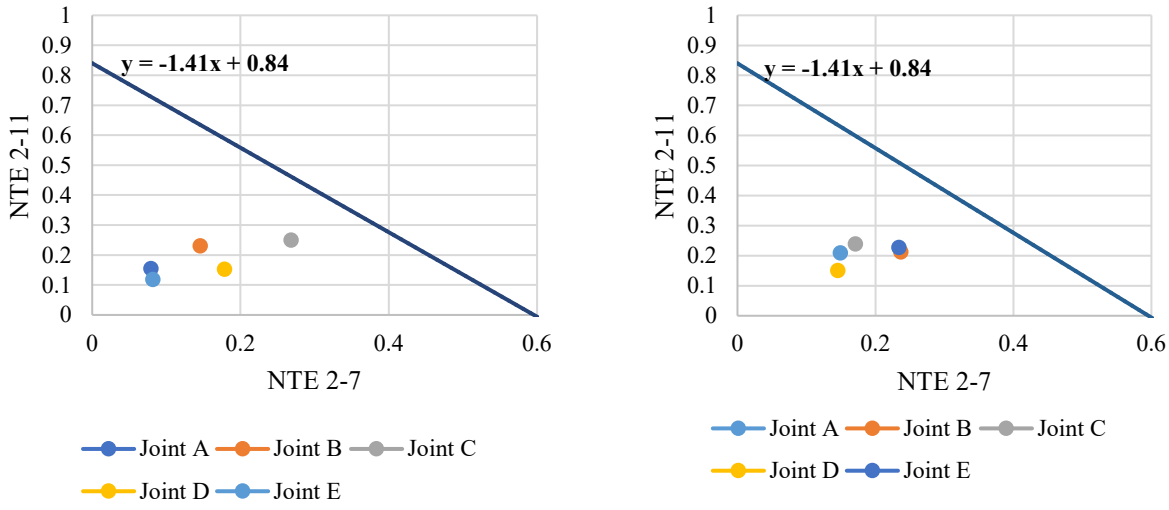

c) US 67 SB Section 2

d) US 67 SB Section 4

Figure 156. Graphs. US 67 (92774) MIRA joint activation analysis.

I-72 (92763):

Layer Thickness Results

Design: 10.0-in. JPCP on 4-in. CAM II on 12-in. Lime Modified Soil

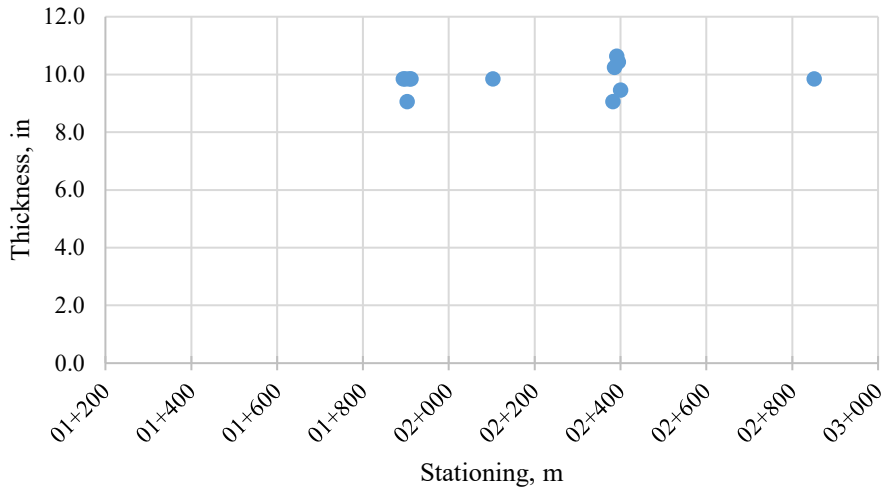

a) PCC thickness estimation along section

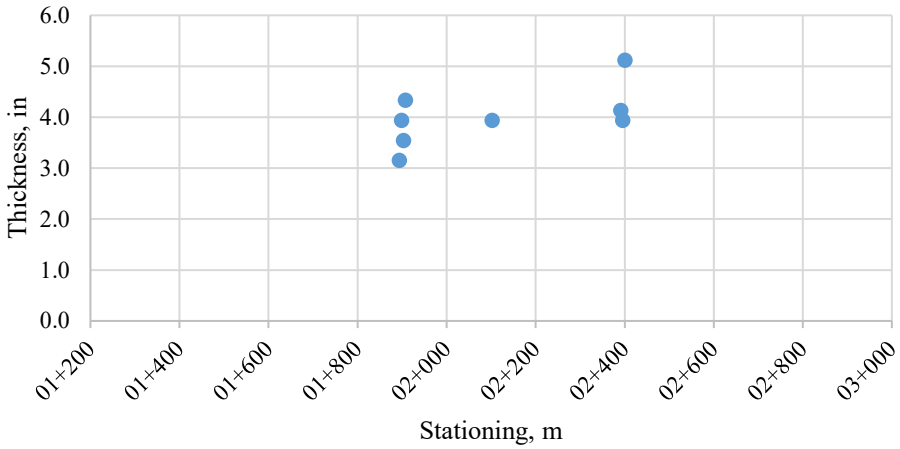

b) Subbase thickness estimation along section

Figure 157. Graphs. I-72 (92763) MIRA thickness results (Westbound).

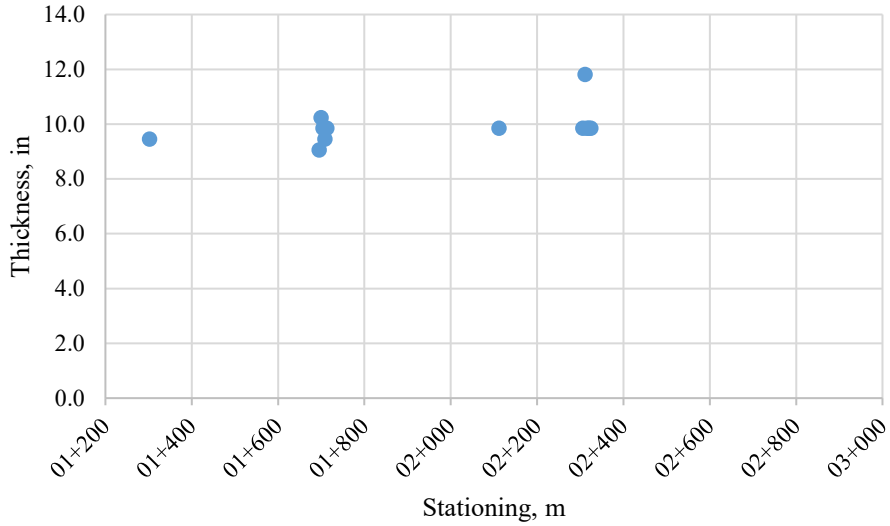

a) PCC thickness estimation along section

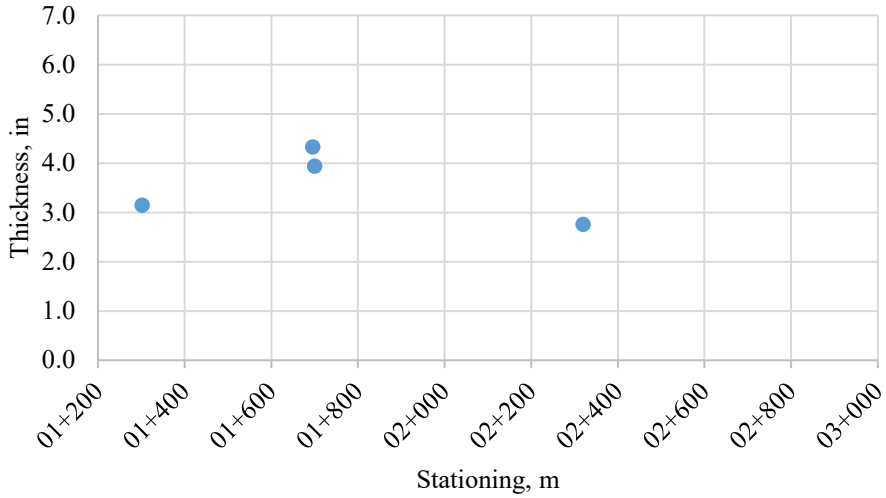

b) Subbase thickness estimation along section

Figure 158. Graphs. I-72 (92763) MIRA thickness results (Eastbound).

Joint Activation Analysis

The joint activation analysis results are presented below. Four of the intensive sections were tested. From this analysis all tested joints were predicted to be fully activated.

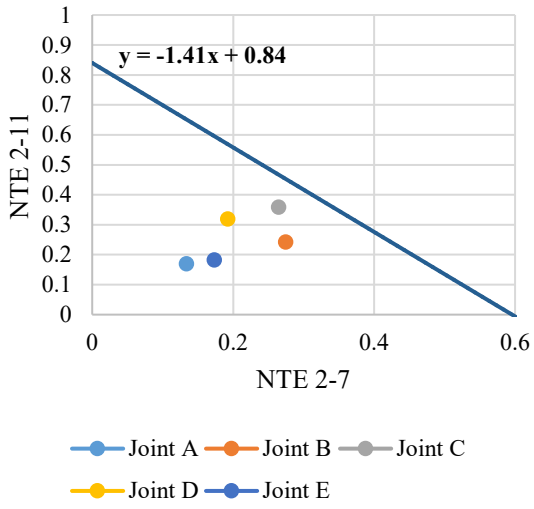

a) I-72 WB Section 2

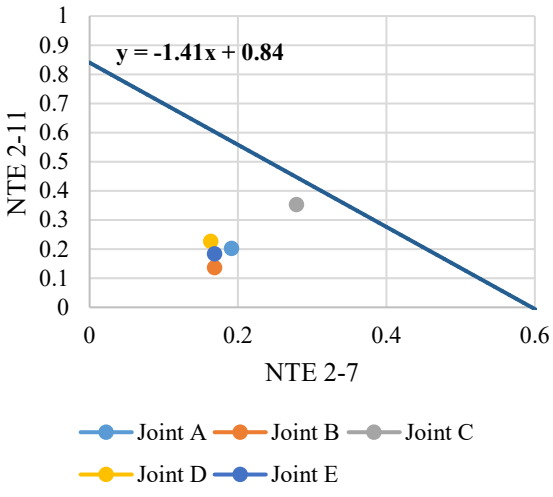

b) I-72 WB Section 4

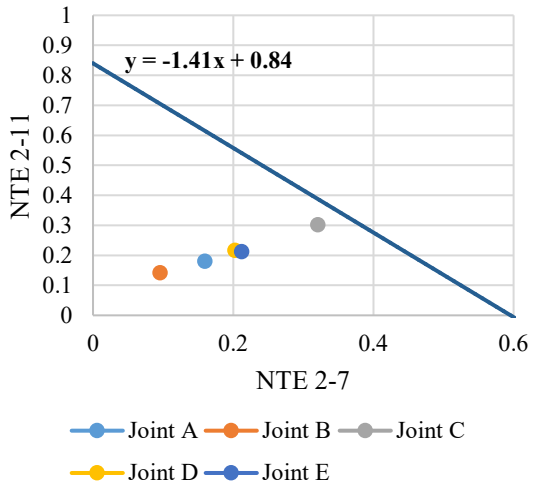

c) I-72 EB Section 2

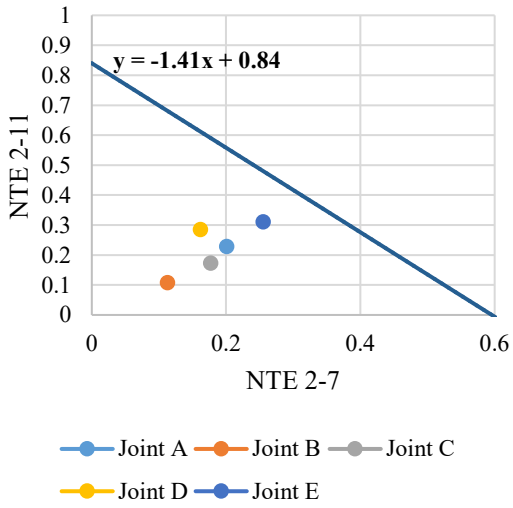

d) I-72 EB Section 4

Figure 159. Graphs. I-72 (92763) MIRA joint activation analysis.

US 20 (40455):

Layer Thickness Results

Design: 10.0-in. JPCP on 4-in. CAM II

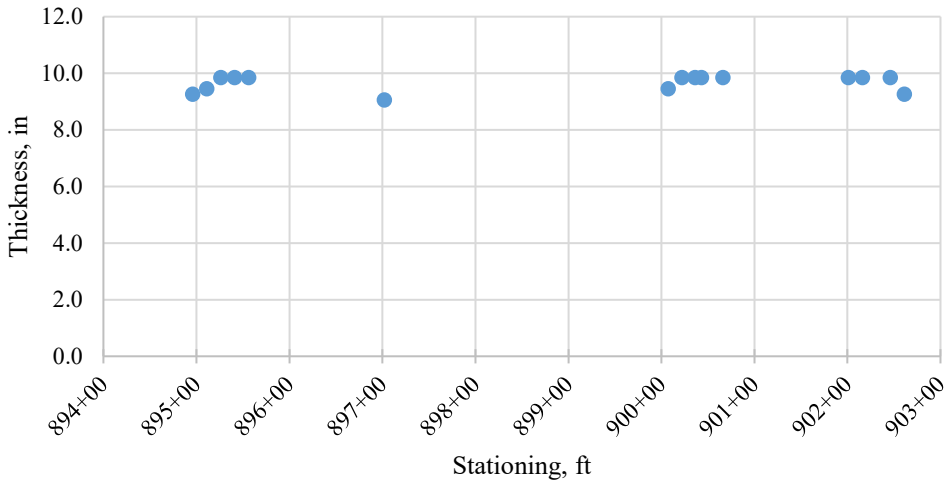

a) PCC thickness estimation along section

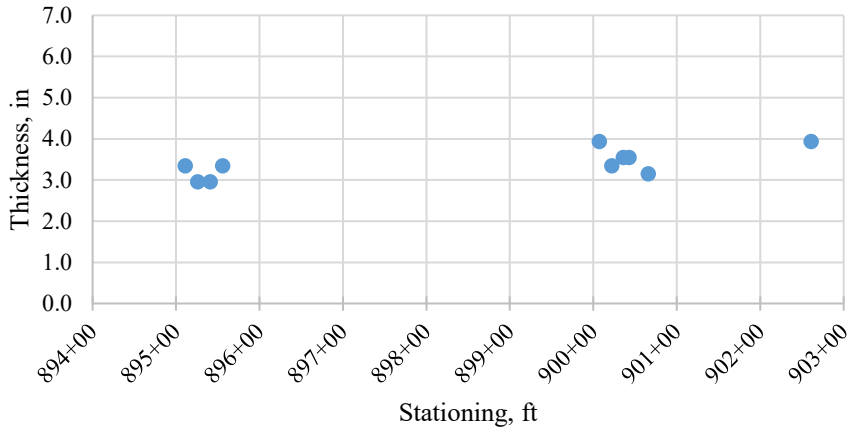

b) Subbase thickness estimation along section

Figure 160. Graphs. US 20 (40455E) MIRA thickness results (Section E).

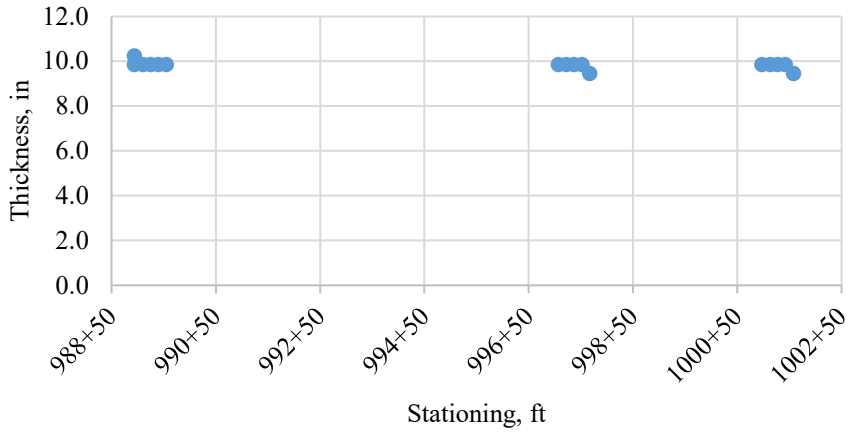

a) PCC thickness estimation along section

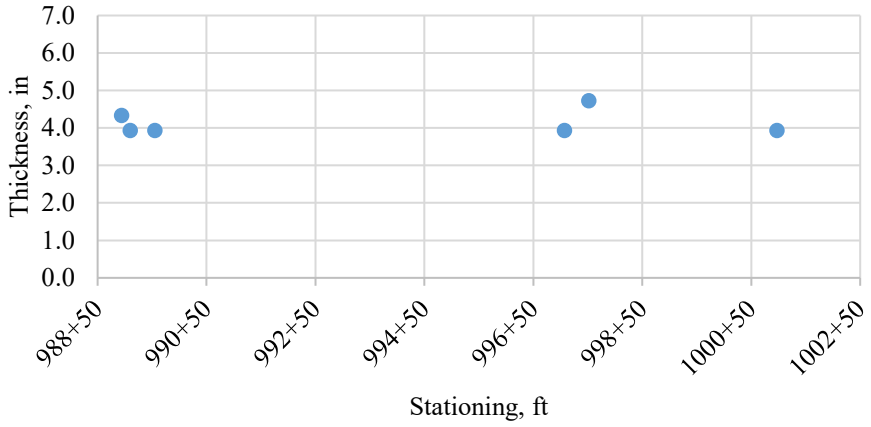

b) Subbase thickness estimation along section

Figure 161. Graphs. US 20 (40455H) MIRA thickness results (Section H).

Joint Activation Analysis

The joint activation analysis results are presented below. Three of the intensive sections were tested. From this analysis one of the tested joints appeared to be inactive out of all tested joints. There was no visible distress in this location potentially related to no joint activation. Joint widths in Section H were excessively wide and difficult for MIRA to scan across the joints. Joint widths exceeded 0.5 in.

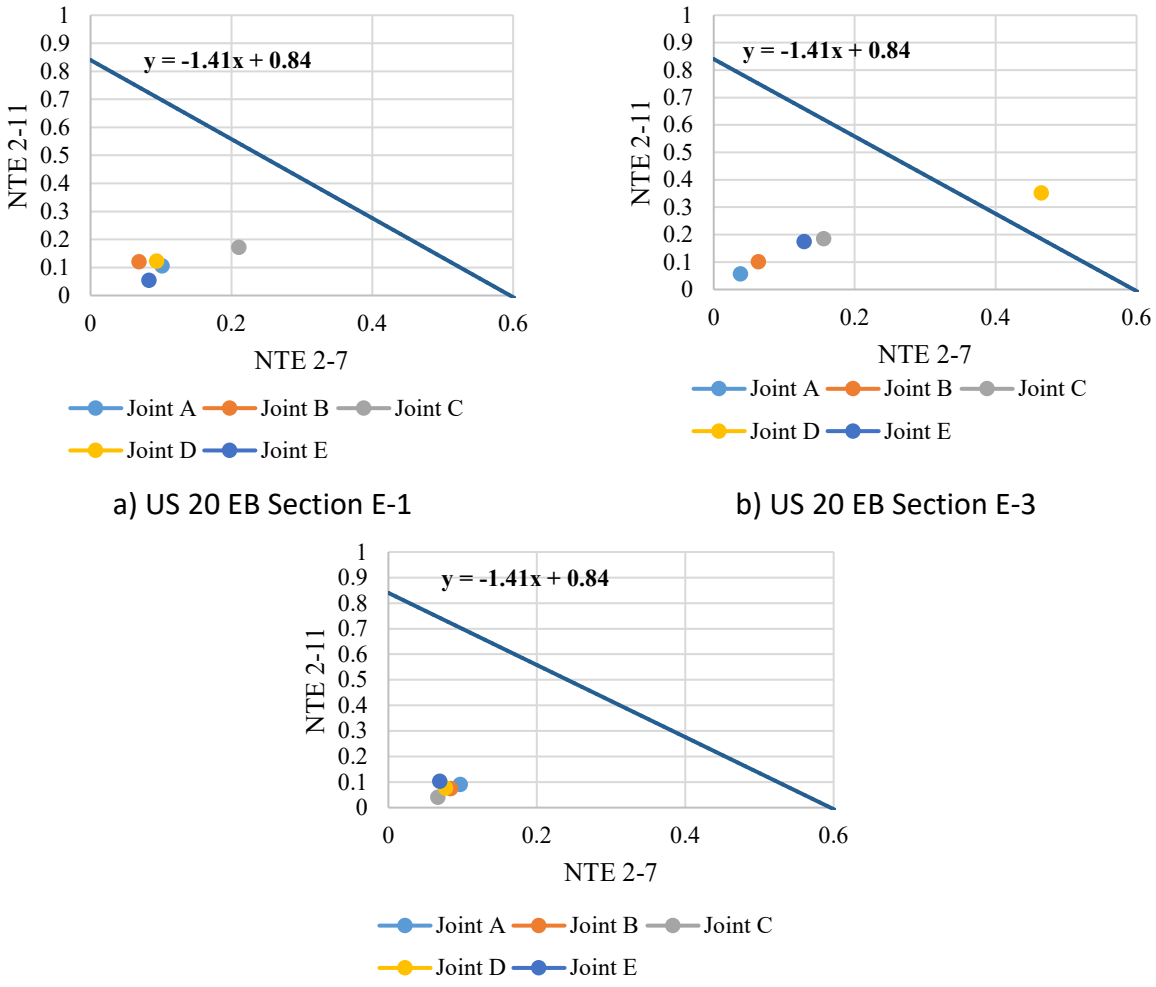

a) US 20 EB Section E-1

b) US 20 EB Section E-3

c) US 20 EB Section E-4

Figure 162. Graphs. US 20 (40455E) MIRA joint activation analysis.

US 30 (62277):

Layer Thickness Results

Design: 10.0-in. JPCP on 4-in. HMA on 12-in. Aggregate Subgrade

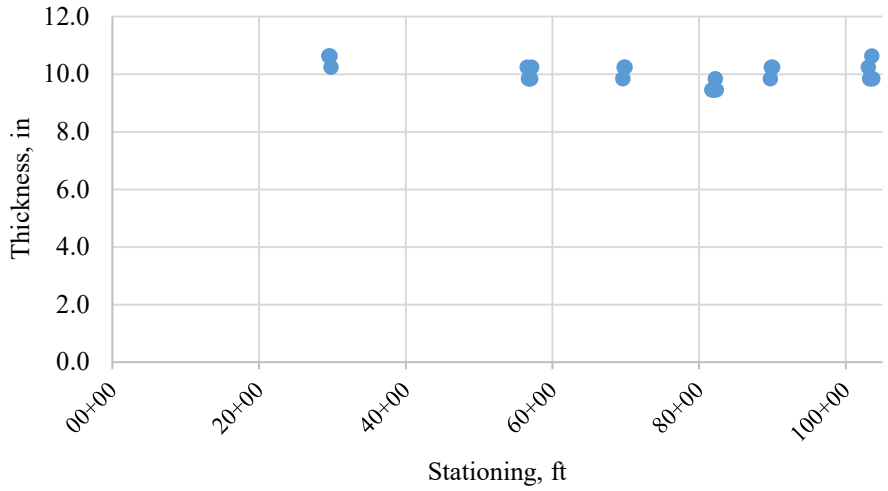

a) PCC thickness estimation along section

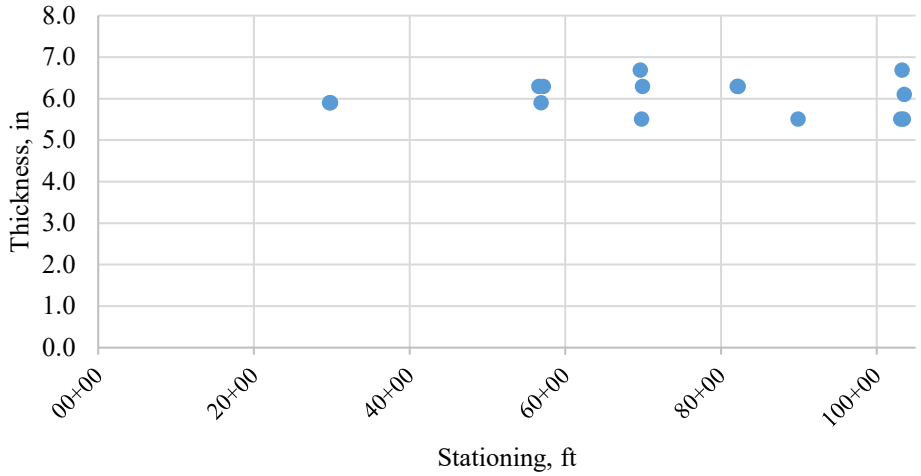

b) Subbase thickness estimation along section

Figure 163. Graphs. US 30 (62277) MIRA thickness results (Westbound).

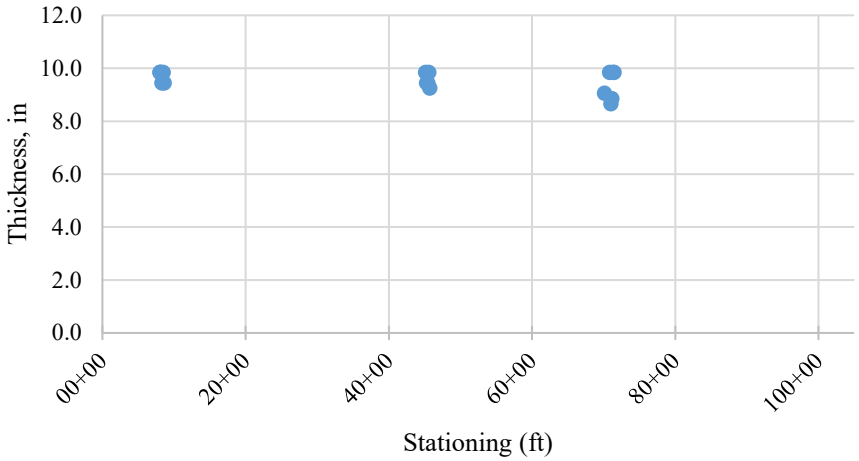

a) PCC thickness estimation along section

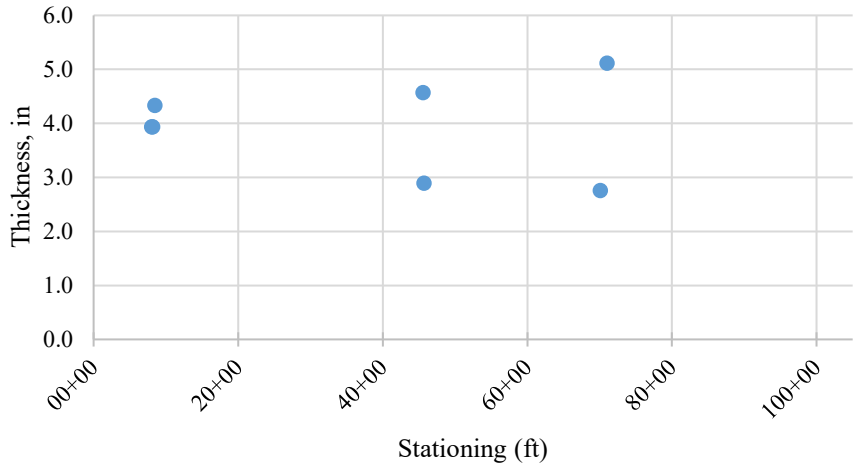

b) Subbase thickness estimation along section

Figure 164. Graphs. US 30 (62277) MIRA thickness results (Eastbound).

Joint Activation Analysis

The joint activation analysis results are presented below. Six of the intensive sections were tested (three in each direction). A few joints were predicted to not be active in both Eastbound and Westbound directions. Additionally, some joint activation predictions are close to the hyperplane and are therefore in-conclusive.

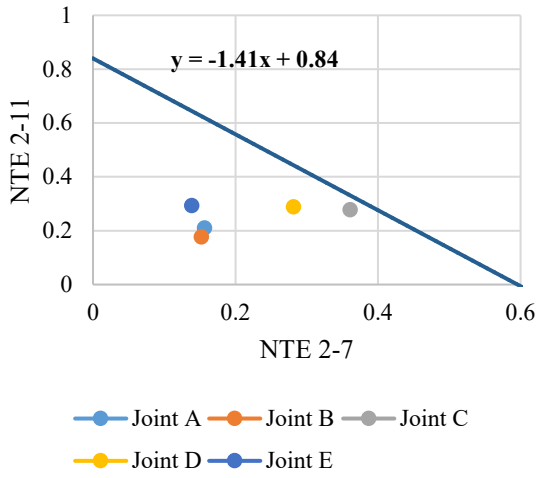

a) US 30 EB Section 1

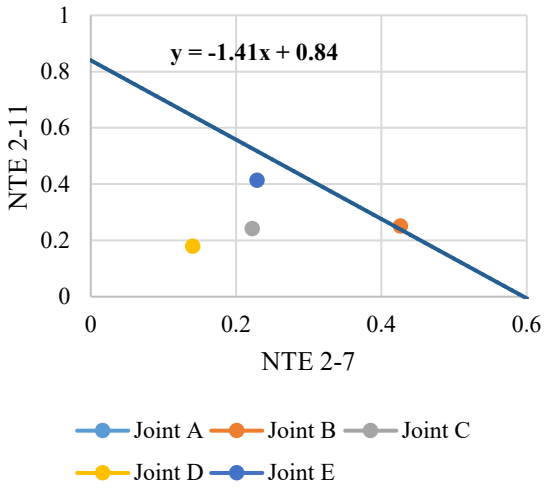

b) US 30 EB Section 2

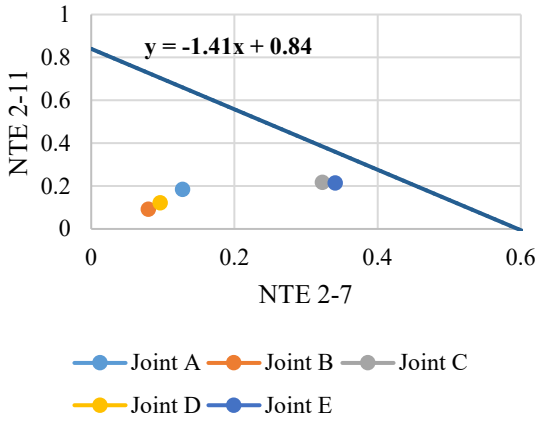

c) US 30 EB Section 3

Figure 165. Graphs. US 30 (62277) EB MIRA joint activation analysis.

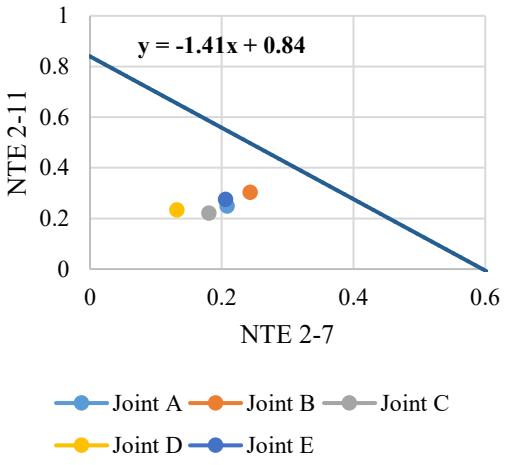

a) US 30 WB Section 1

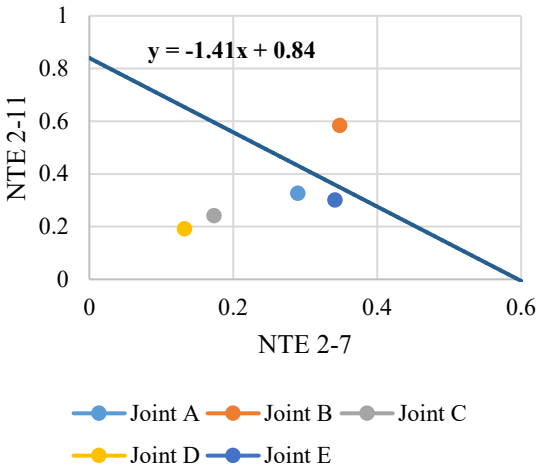

b) US 30 WB Section 3

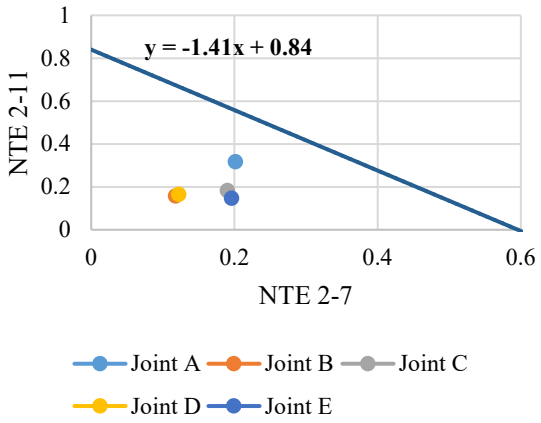

c) US 30 WB Section 5

Figure 166. Graphs. US 30 (62277) WB MIRA joint activation analysis.

IL 64 (62410):

Layer Thickness Results

Design: 10.0-in. JPCP on 4.5-in. HMA on 12-in. Aggregate Subgrade

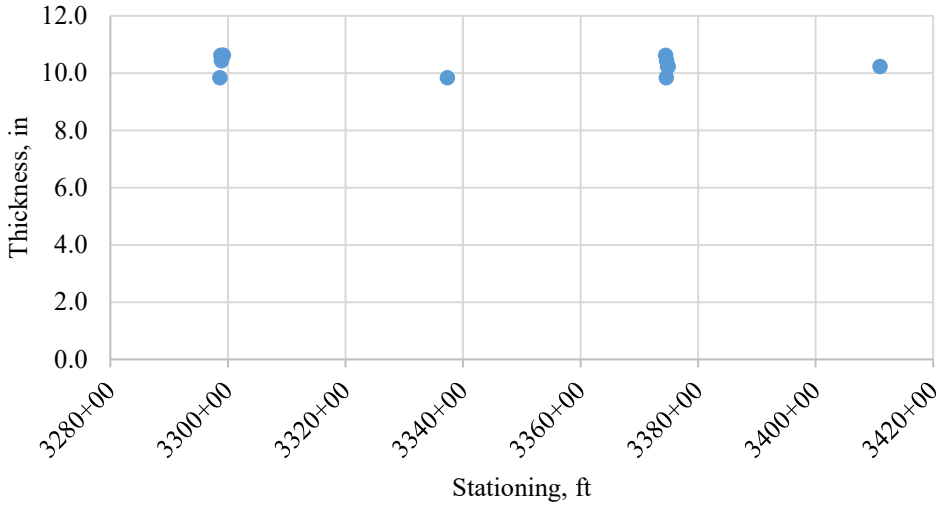

a) PCC thickness estimation along section

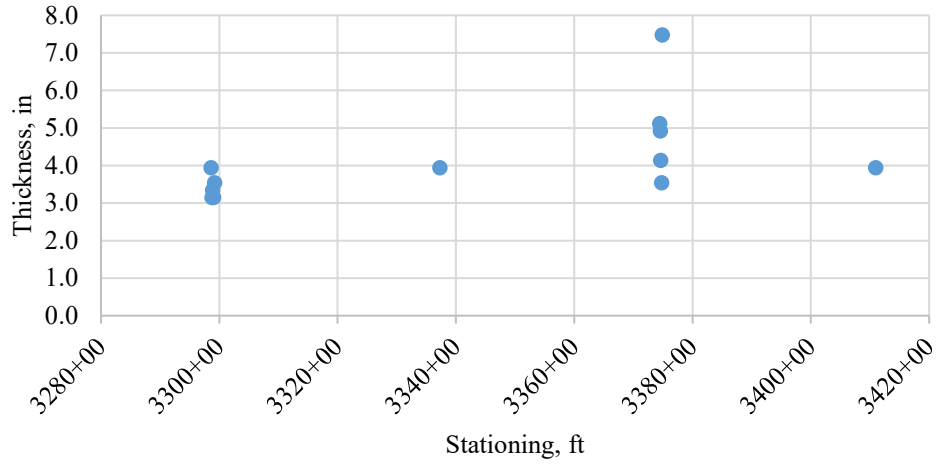

b) Subbase thickness estimation along section

Figure 167. Graphs. IL 64 (62410) MIRA thickness results (Westbound).

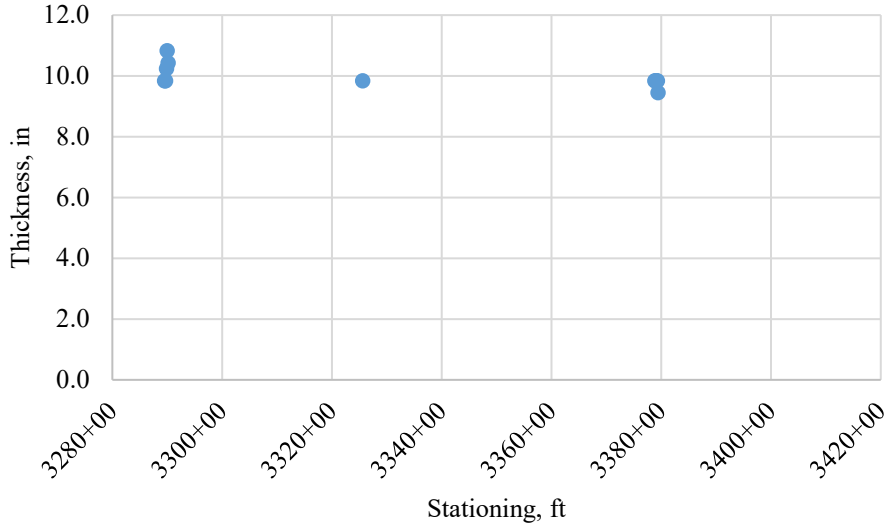

a) PCC thickness estimation along section

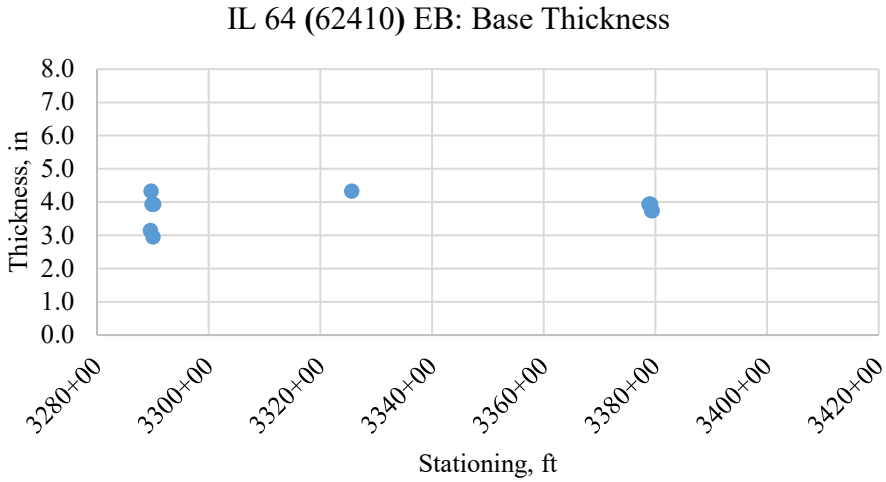

b) Subbase thickness estimation along section

Figure 168. Graphs. IL 64 (62410) MIRA thickness results (Eastbound).

Joint Activation Analysis

The joint activation analysis results are presented below. Four of the intensive sections were tested (two in each direction). Joint activation appears to be not occurring as anticipated for this pavement section. A number of joints are either not activated or have in-conclusive results (7 out of 20, 35%). These correspond with other joints being excessively wide, which have developed joint spalling, faulting, and joint damage.

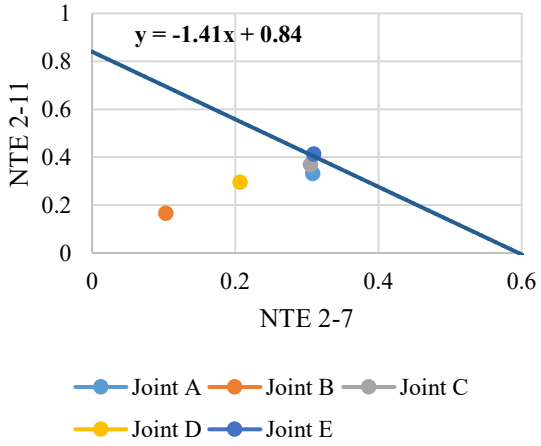

a) IL 64 WB Section 2

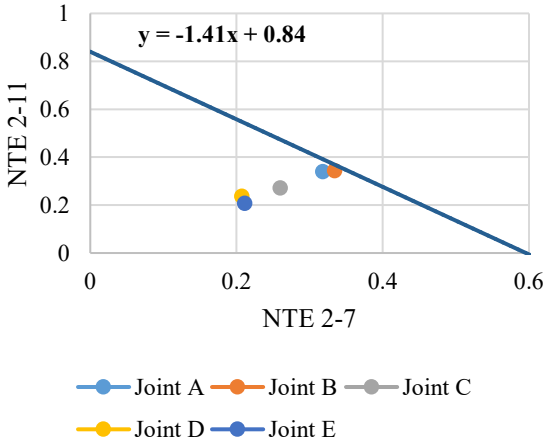

b) IL 64 WB Section 4

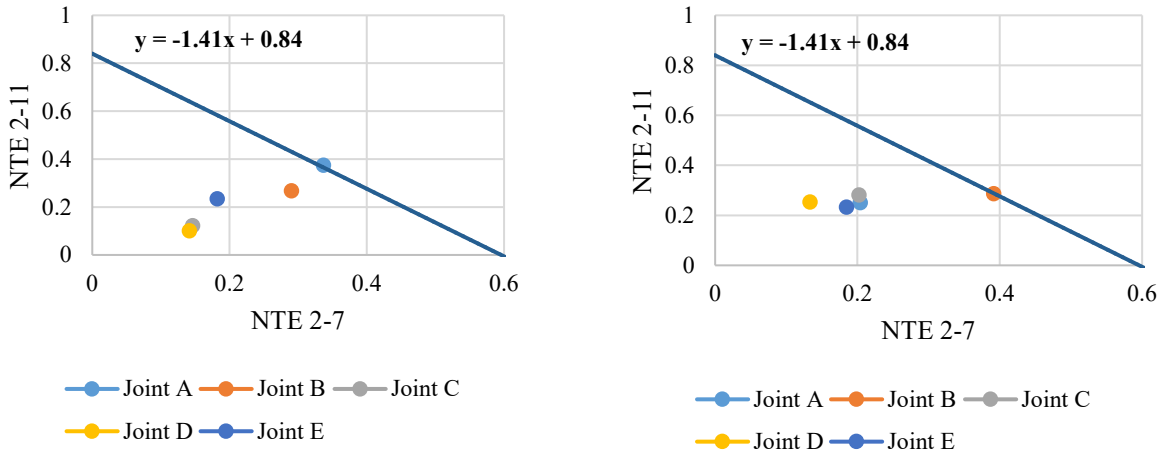

c) IL 64 EB Section 1

d) IL 64 EB Section 3

Figure 169. Graphs. IL 64 (62410) MIRA joint activation analysis.

US 12/20/45 (60927 & 60748):

Layer Thickness Results

Design: 9.75-in. JPCP on 4-in. HMA

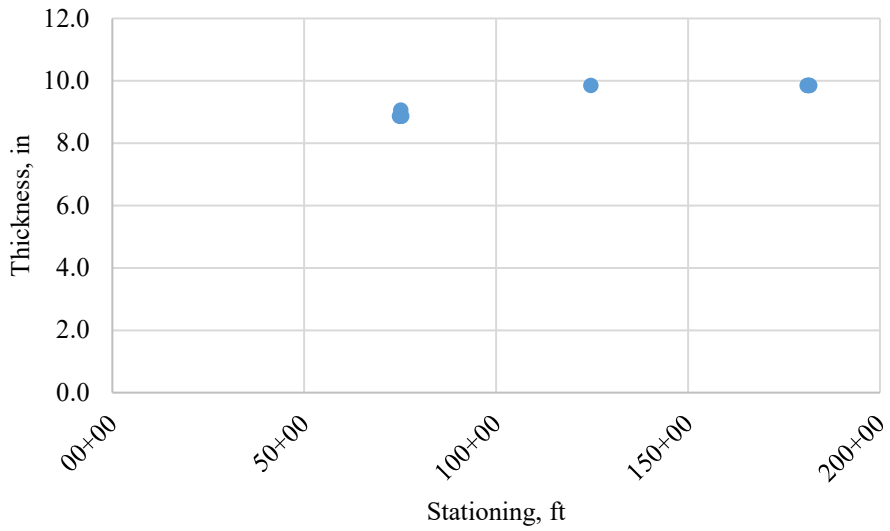

a) PCC thickness estimation along section

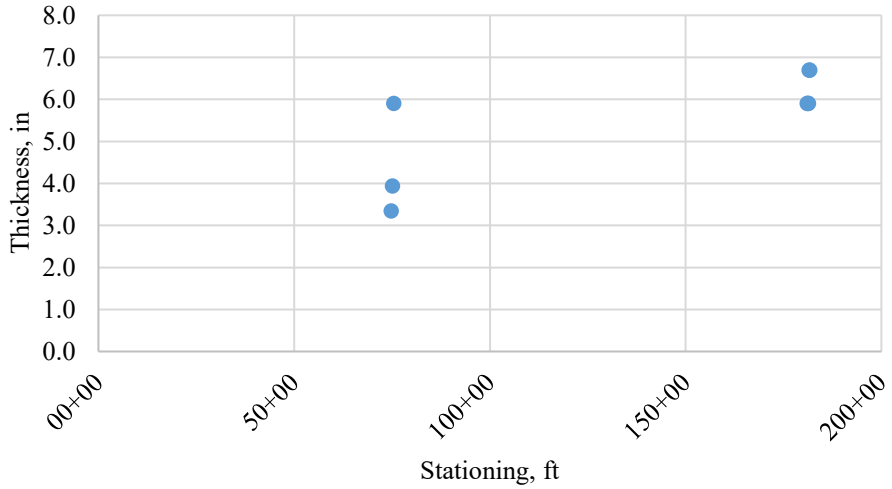

b) Subbase thickness estimation along section

Figure 170. Graphs. US 12/20/45 (60927) MIRA thickness results (Northbound).

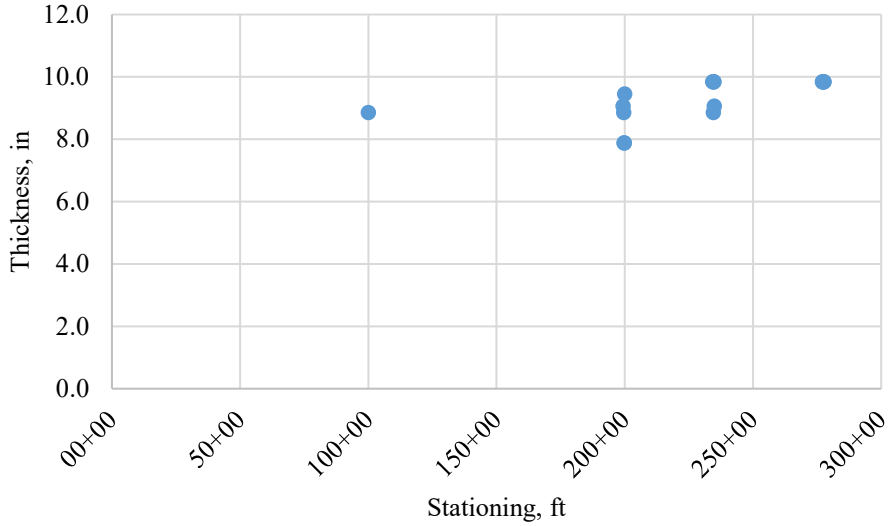

a) PCC thickness estimation along section

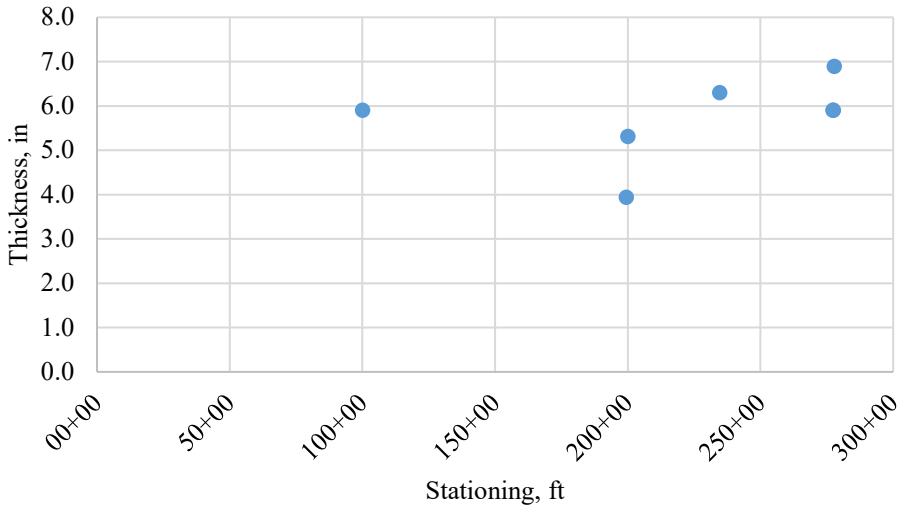

b) Subbase thickness estimation along section

Figure 171. Graphs. US 12/20/45 (60927 & 60748) MIRA thickness results (Southbound).

Joint Activation Analysis

The joint activation analysis results are presented below. Five of the intensive sections were tested (at least two in each direction). Joint activation appears to not be extremely consistent within each intensive section. These results indicate that one out of five joints is likely not activated. Some in-conclusive results were also reported.

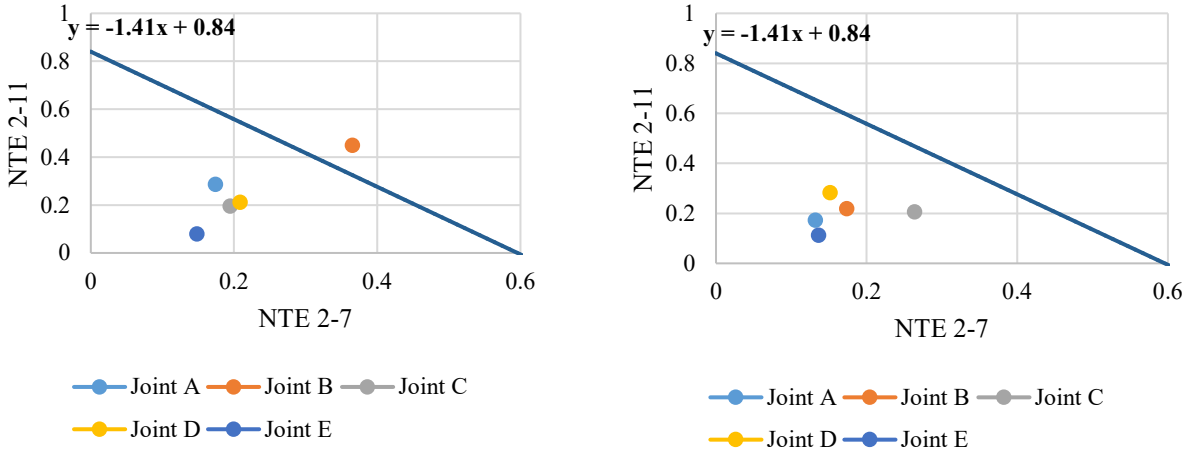

a) US 12/20/45 NB Section 1

b) US 12/20/45 NB Section 3

Figure 172. Graphs. US 12/20/45 (60927 & 60748) NB MIRA joint activation analysis.

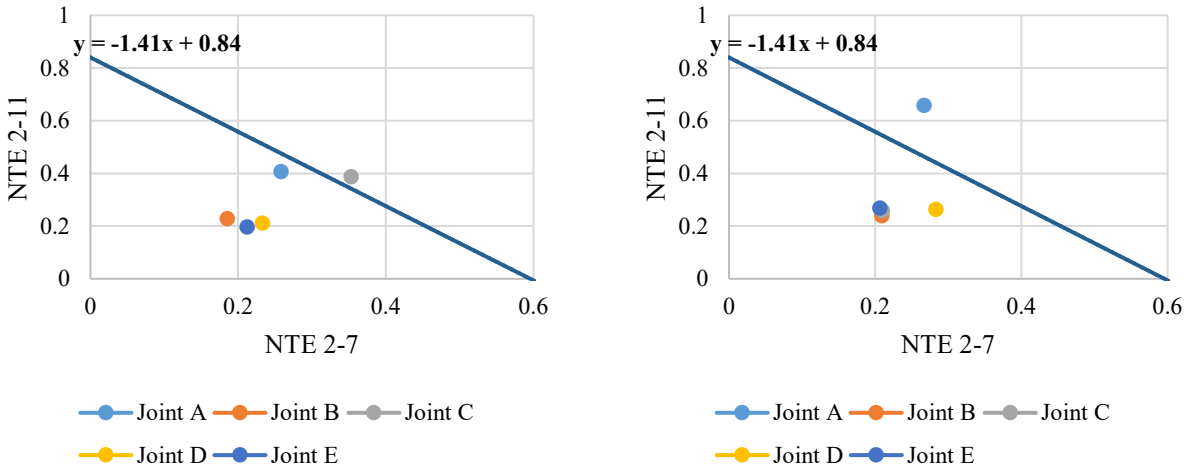

a) US 12/20/45 SB Section 1

b) US 12/20/45 SB Section 2

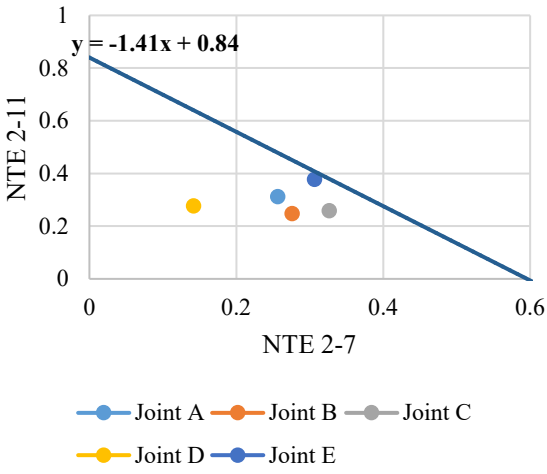

c) US 12/20/45 SB Section 3

Figure 173. Graphs. US 12/20/45 (60927 & 60748) SB MIRA joint activation analysis.

I-72 (72G92):

Layer Thickness Results

Westbound Design: 6.0-in. FRC JPCP on 0.125-in. NWGF on 8-in. CRCP.

The NWGF interlayer was difficult to record within image analysis and in interpretation of results. Therefore, this was excluded.

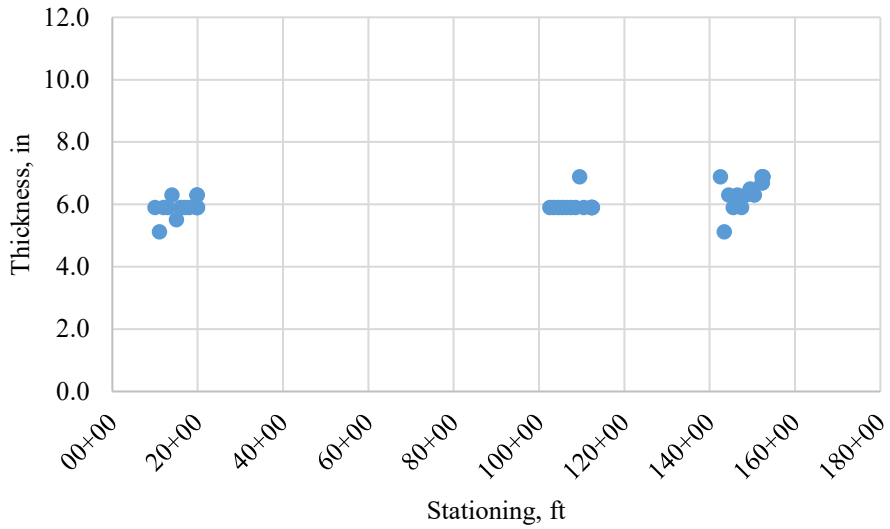

a) PCC thickness estimation along section

Figure 174. Graphs. I-72 (72G92) MIRA thickness results (Westbound).

Eastbound Design: 6.0-in. FRC JPCP on 1.25-in. HMA on 8-in. CRCP

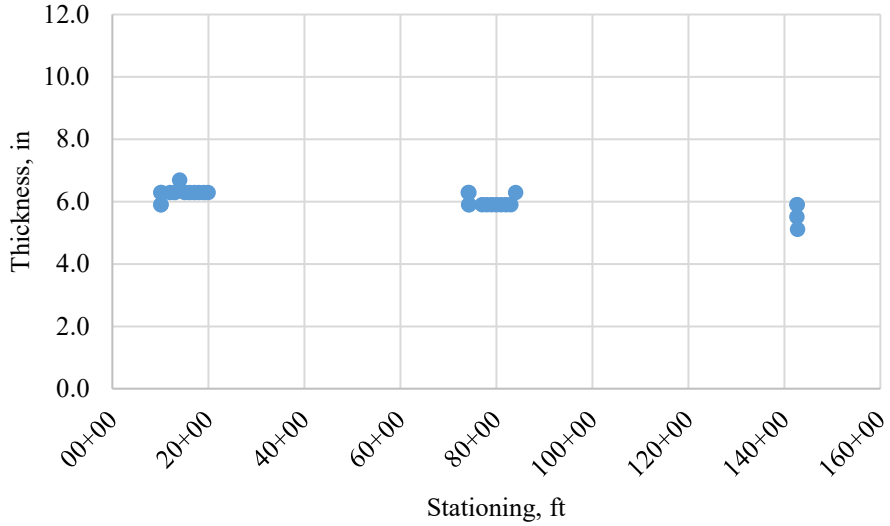

a) PCC thickness estimation along section

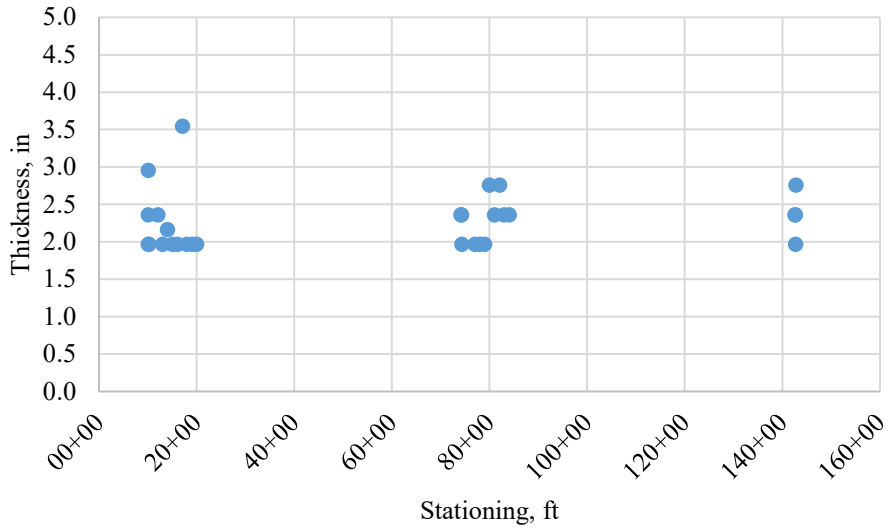

b) HMA interlayer thickness estimation along section

Figure 175. Graphs. I-72 (72G92) MIRA thickness results (Eastbound).

Joint Activation Analysis

The testing along I-72 was conducted on both Westbound (fabric interlayer) and Eastbound (HMA interlayer). Three intensive sections were tested for each direction. In addition, three stretches of 1,000 ft were examined (time constraints for Eastbound, only two interval sections). Interval testing was performed at 100-ft intervals, testing one slab and transverse joint. Although the interval testing does not indicate the likelihood of consecutive activated joints, it provides some indication if not all joints are activating.

The Westbound (NWGF interlayer) showed little concern for non-activated joints, even with a NWGF interlayer and 6-ft joint spacing. The interval testing also showed that all joints were likely activated. The Eastbound (HMA interlayer) however did not result in all predicted activated joints. Some results infer in-conclusive results or non-activated joints. It is possible the NWGF interlayer is resulting in better joint activation than the HMA interlayer. However, this analysis is only examining a small sample size and additional testing would be necessary for any true conclusion between the interlayer types.

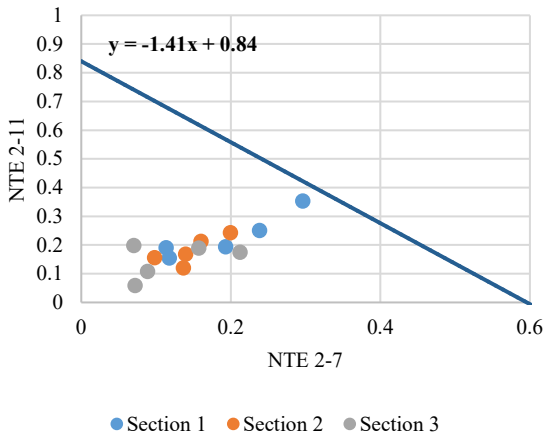

a) I-72 WB intensive sections

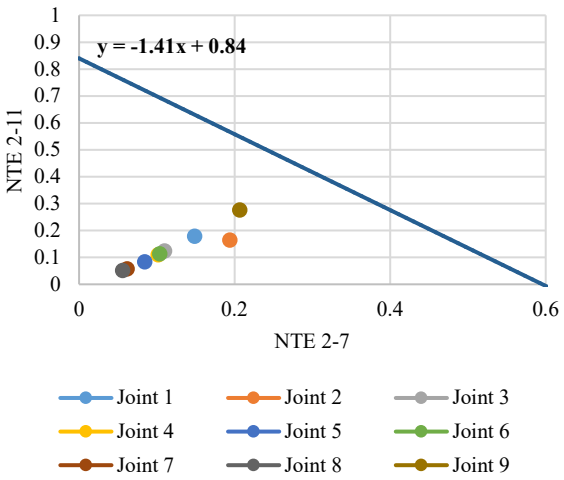

b) I-72 WB interval section 1

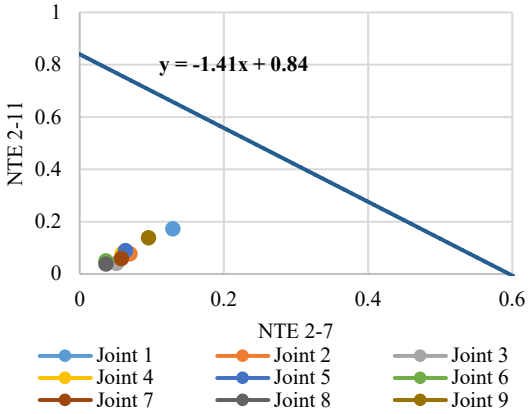

c) I-72 WB interval section 2

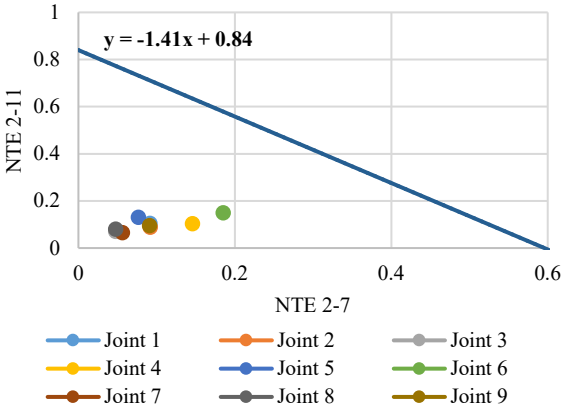

d) I-72 WB interval section 3

Figure 176. Graphs. I-72 (72G92) WB MIRA joint activation analysis.

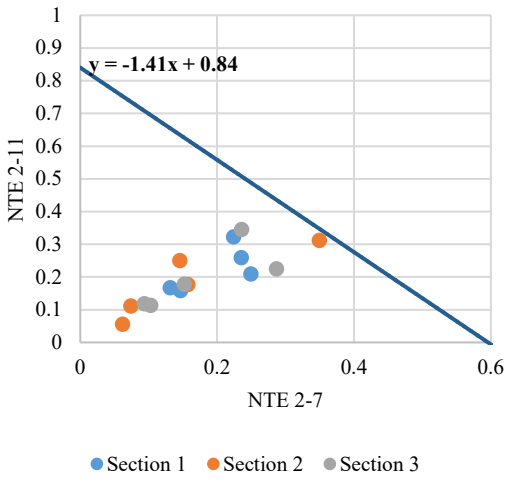

a) I-72 EB intensive sections

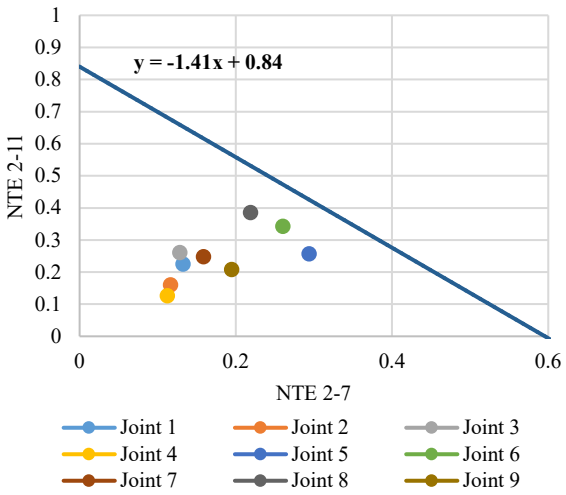

b) I-72 EB interval section 1

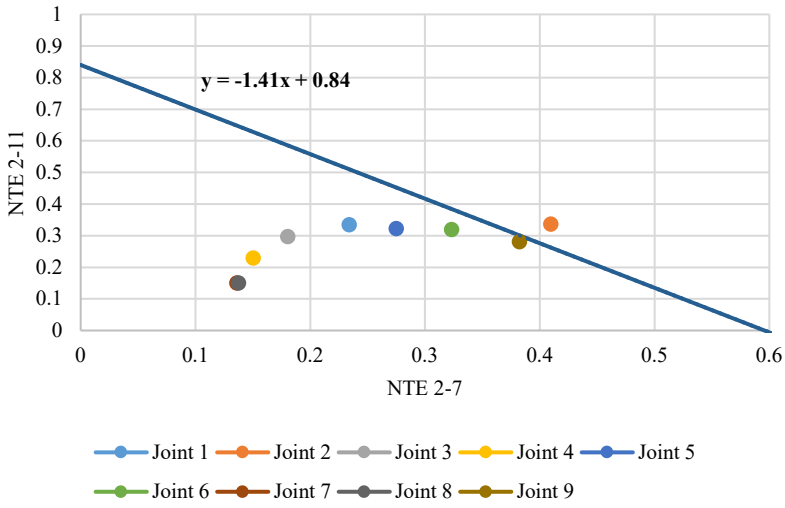

c) I-72 EB interval section 2

Figure 177. Graphs. I-72 (72G92) EB MIRA joint activation analysis.

I-70 (70044):

Layer Thickness Results

Westbound Design: 12.0-in. CRCP on 4-in. HMA on 8-in. CRCP

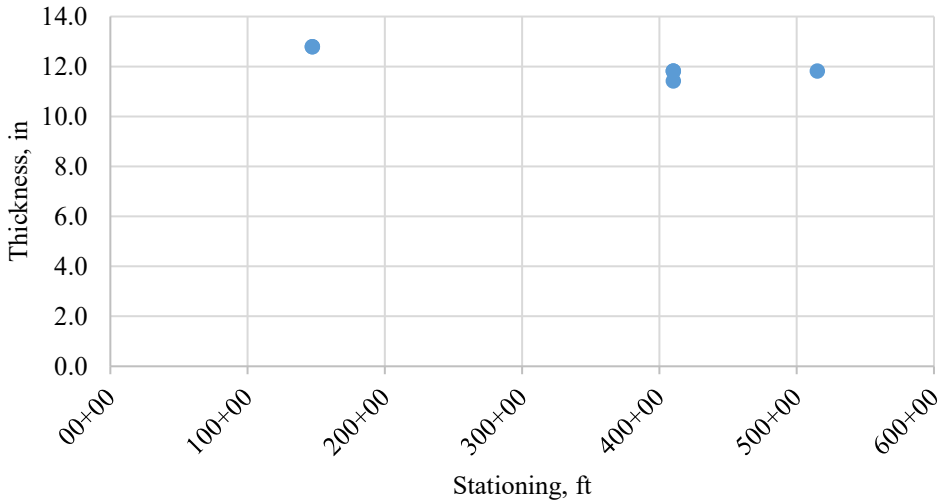

a) PCC thickness estimation along section

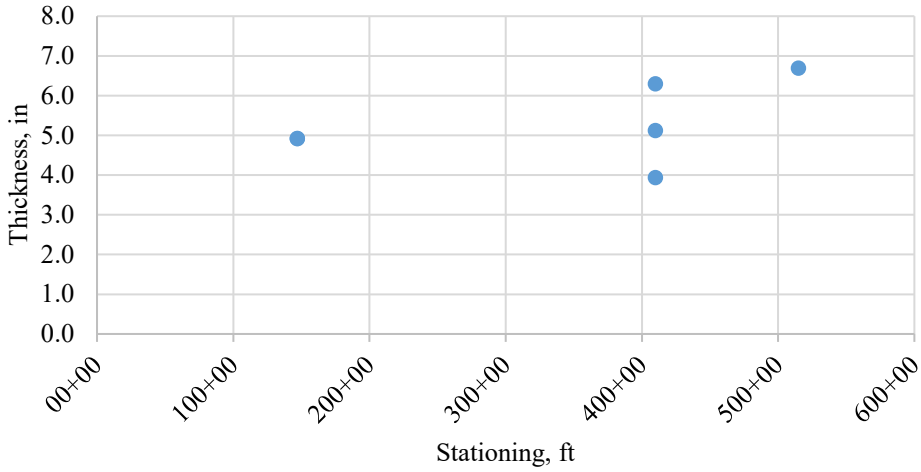

b) Interlayer thickness estimation along section

Figure 178. Graphs. I-70 (70044) MIRA thickness results (Westbound).

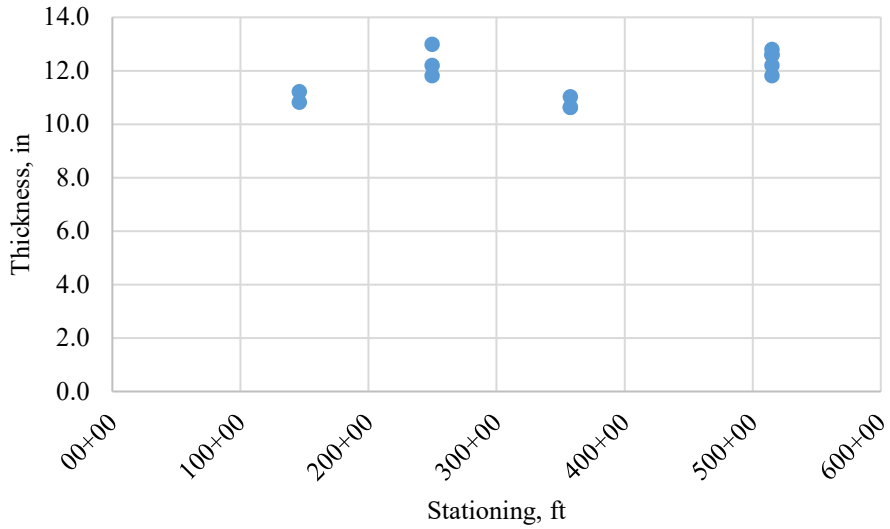

a) PCC thickness estimation along section

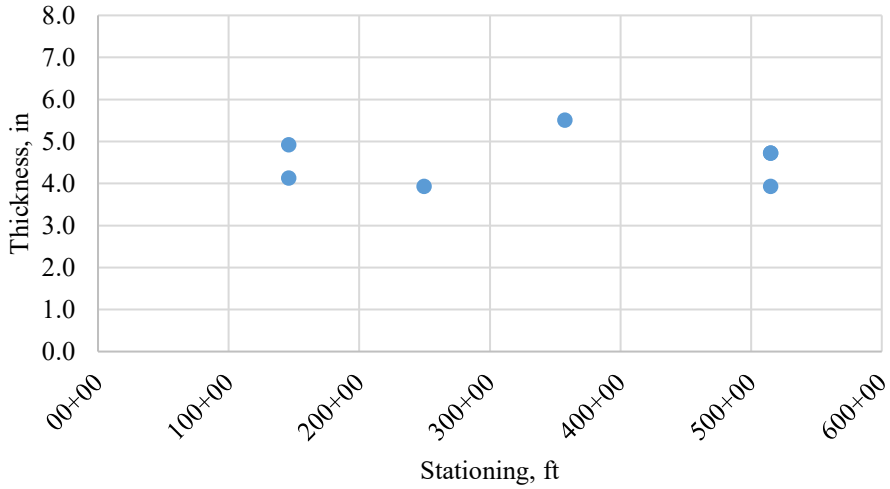

b) Interlayer thickness estimation along section

Figure 179. Graphs. I-70 (70044) MIRA thickness results (Eastbound).

Joint Activation Analysis

No joint activation analysis was performed on I-70 (70044) because this section is a CRCP UBOL pavement section. All observed cracks are fully activated.

IL 53 (60N05):

Layer Thickness Results

Westbound Design: 4.0-in. JPCP on 5-10-in. HMA on 8-in. CRCP

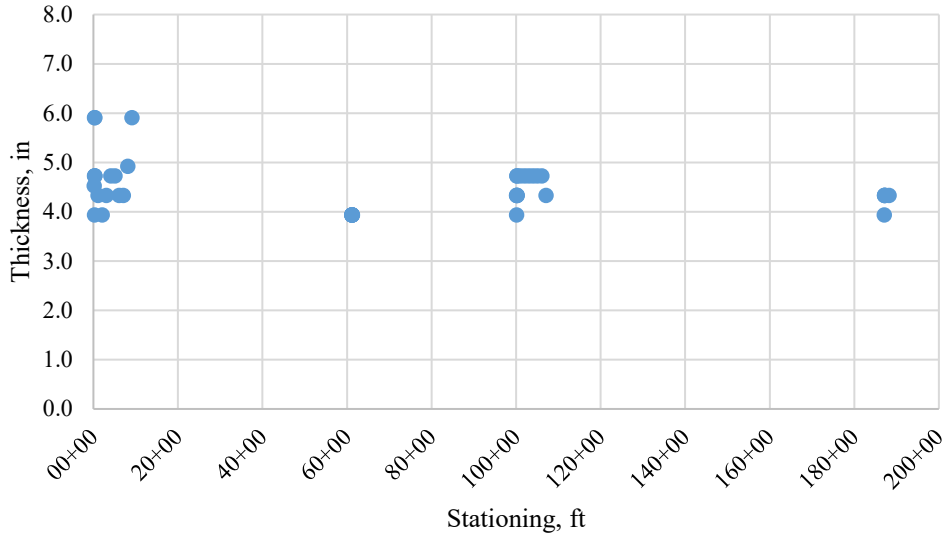

a) PCC thickness estimation along section

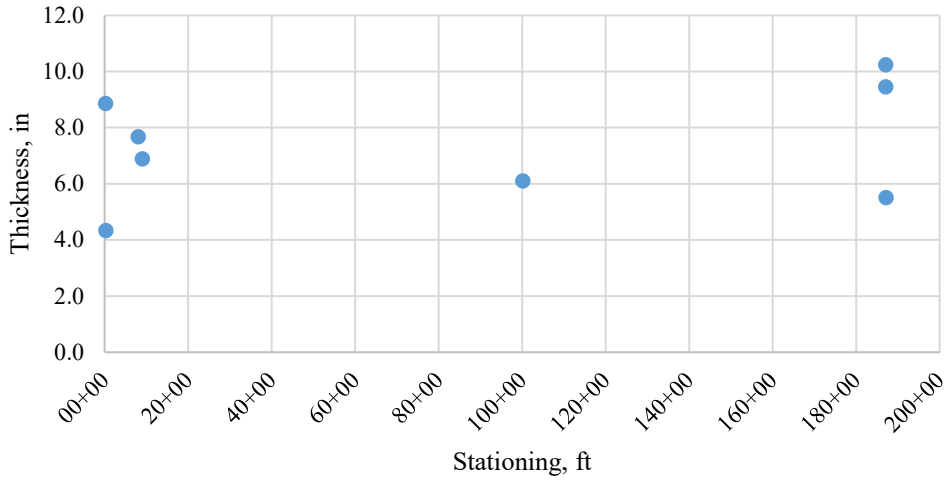

b) Existing HMA thickness estimation along section

Figure 180. Graphs. IL 53 (60N05) MIRA thickness results (Southbound).

Joint Activation Analysis

The testing along IL 53 was only conducted on the Southbound lanes. Therefore, joint activation analysis is only presented for the Southbound direction. Four intensive sections were tested. In addition, two stretches of 1,000 ft were examined. Interval testing was performed at 100 ft intervals,

testing one slab and transverse joint. Although the interval testing does not indicate the likelihood of consecutive activated joints, it provides some indication if not all joints are activating.

The intensive section testing showed consecutive joint activation for Sections 1 and 2. However, Sections 3 and 4 resulted in two out of five joints to be in-conclusive and likely not activated. The interval testing within the first section indicated all joints were activated. However, the second interval section predicted two joints were not active and a third joint to be in-conclusive.

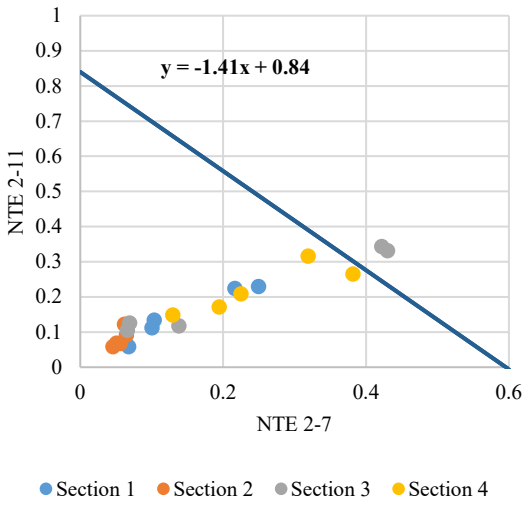

a) IL 53 SB intensive sections

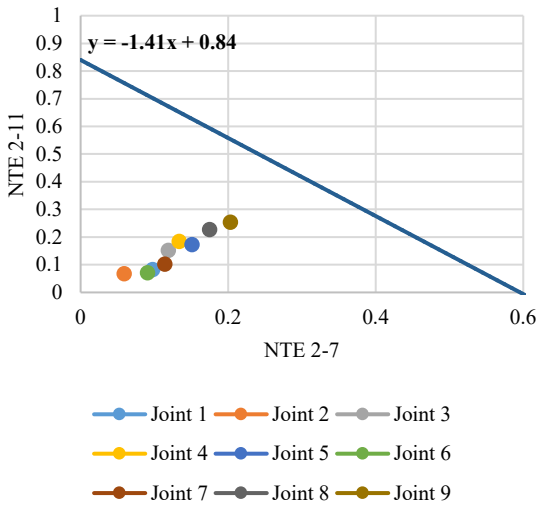

b) IL 53 SB interval section 1

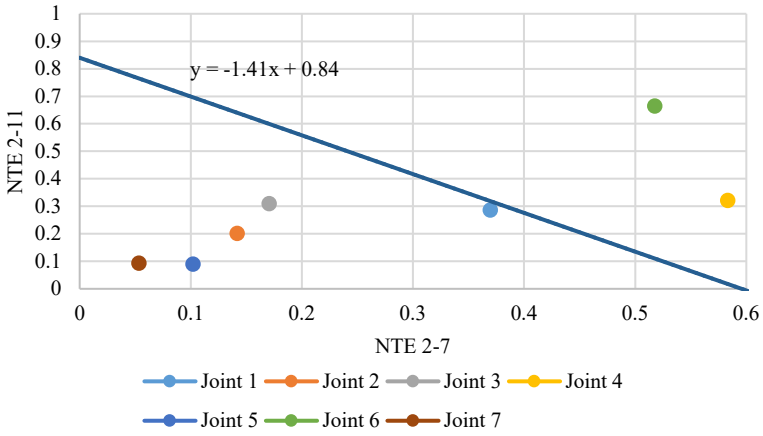

c) IL 53 SB interval section 2

Figure 181. Graphs. IL 53 (60N05) SB MIRA joint activation analysis.

UIUC E-15 PARKING LOT:

Layer Thickness Results

The ultrasonic testing in E-15 resulted in significant noise and made interpretation of results difficult. This can be attributed to scaling at the surface (poor contact interface with transducers), potential

poor consolidation of the concrete, scattering of signal from the macrofibers in the concrete, or the very thin pavement structure (depth of pavement to length of the MIRA device for signal wave reflection).

Design: 3.5-in. JPCP on 2.5-in. HMA

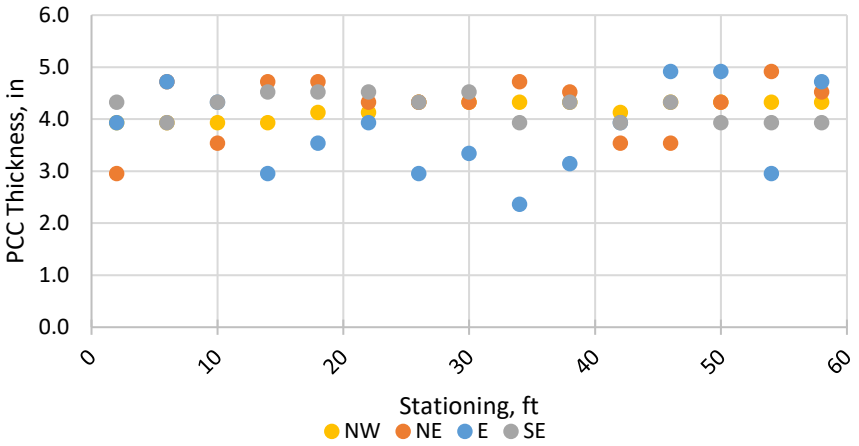

a) PCC thickness estimation along section

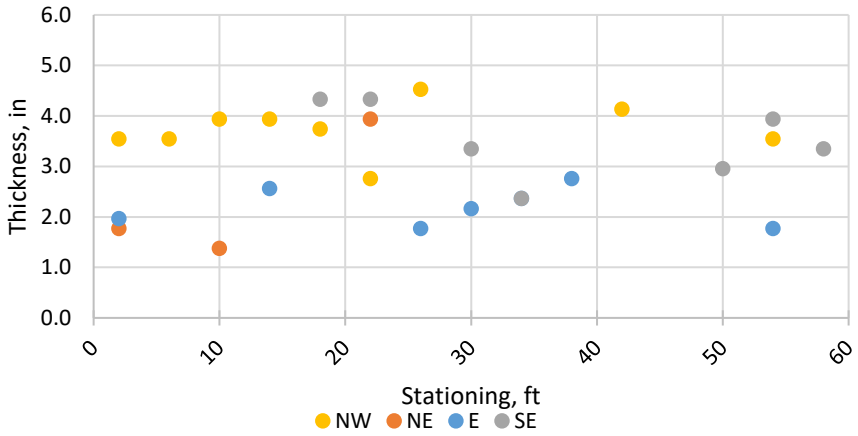

b) Existing HMA thickness estimation along section

Note: MIRA scans contained significant noise. Potential poor consolidation of concrete or reflection from fibers.

Figure 182. Graphs. UIUC E-15 Parking Lot MIRA thickness results.

Joint Activation Analysis

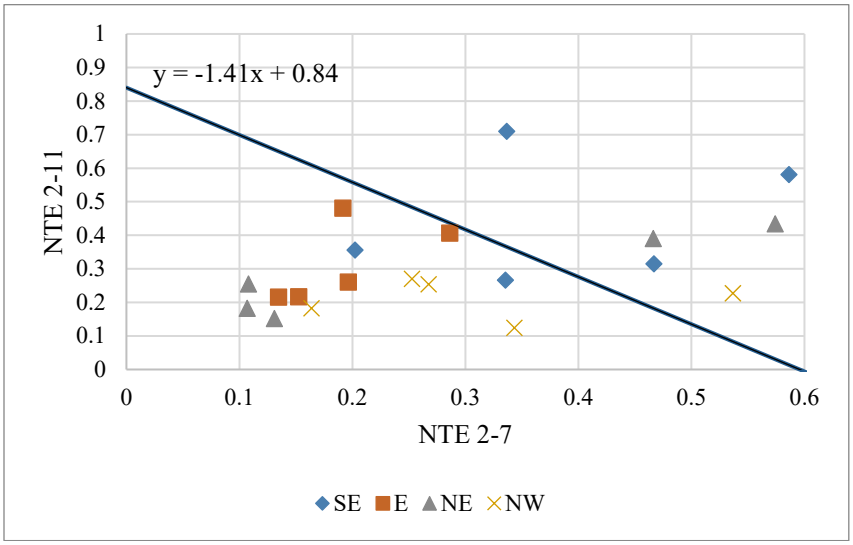

Figure 183. Graph. UIUC E-15 Parking Lot MIRA joint activation results.

UIUC MCKINLEY HEALTH CENTER PARKING LOT:

Layer Thickness Results

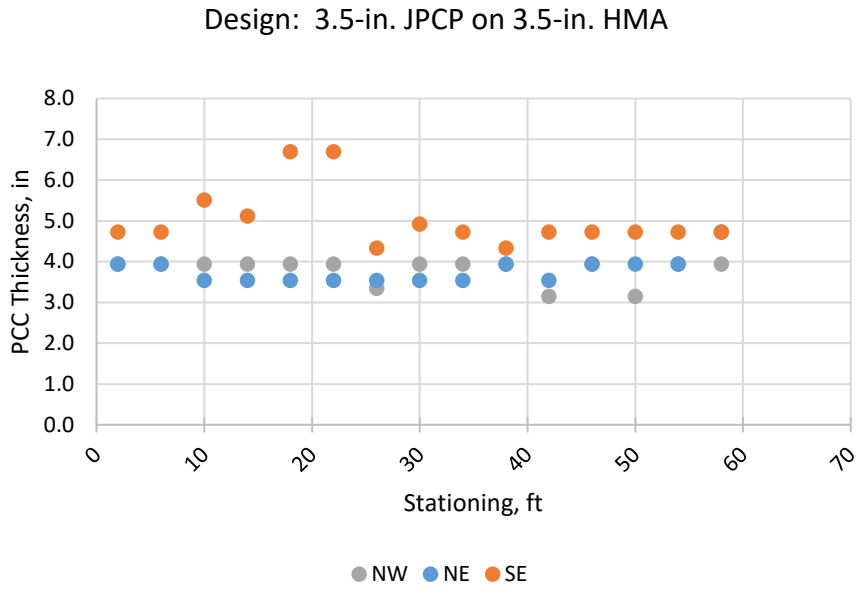

a) PCC thickness estimation along section

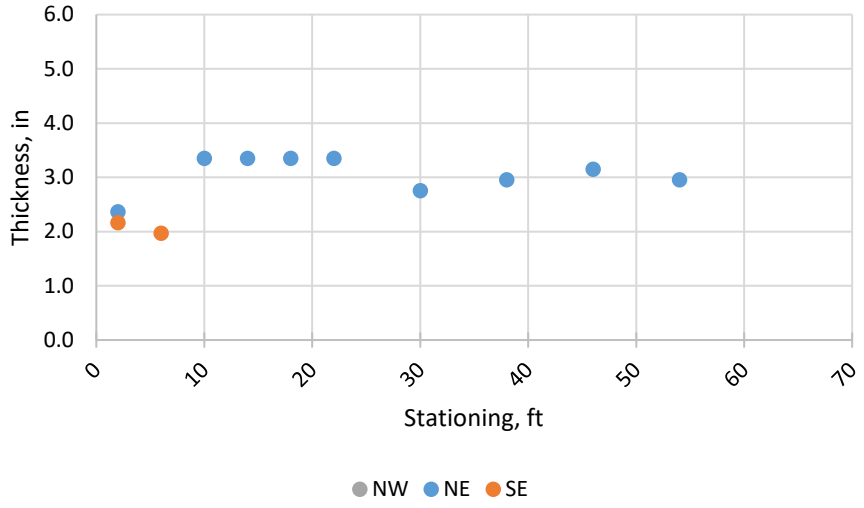

b) Existing HMA thickness estimation along section

Figure 184. Graphs. UIUC McKinley Health Center Parking Lot MIRA thickness results.

Joint Activation Analysis

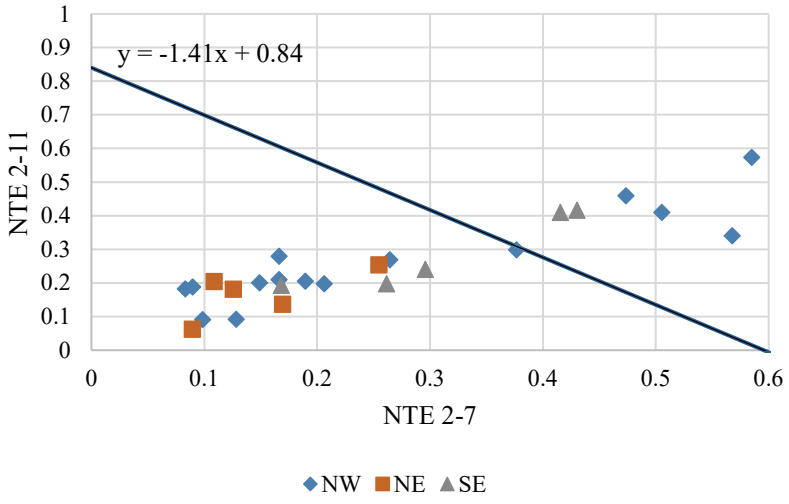

a) All testing locations

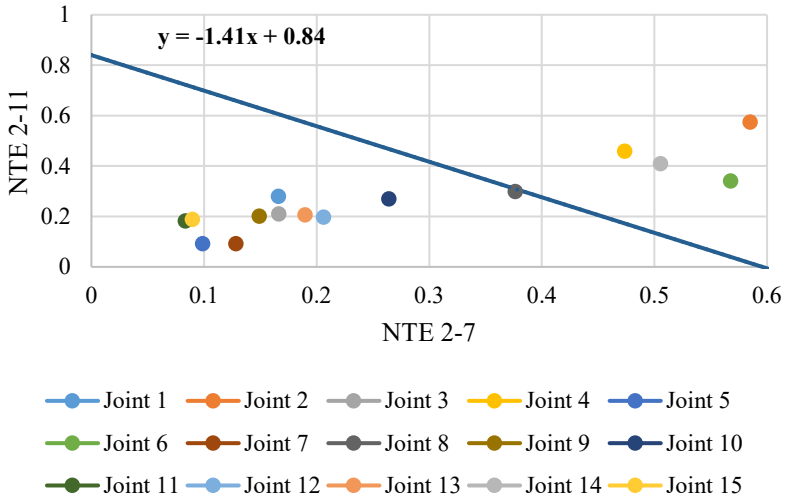

b) Northwest section (15 adjacent joints)

Figure 185. Graphs. UIUC McKinley Health Center Parking Lot MIRA joint activation results.

SLAB-SUBBASE INTERFACIAL BOND ASSESSMENT

The following techniques from previous research studies were assessed for potential use and or expansion to determine the interfacial conditions using the ultrasonic tomography MIRA device.

1. Image analysis and color intensity: Previous research conducted by Hoegh et al. (2012) assessed debonding between asphalt layers and lifts through image analysis from synthetic aperture focusing technique (SAFT) B-scans using MIRA. Layer debonding was detected by high intensity backwall reflections (red or yellow color reflections). Whereas full or partial bonds were likely to result in low-intensity reflections (blue or green color). Additionally, lower modulus materials such as asphalt can cause high-intensity reflections as a result of

unfiltered near-field reflections and surface wave arrivals. Salles et al. (2017) examined two thin bonded concrete overlays of existing asphalt pavements using this technique. He found that when the ultrasound signal had less attenuation across the interface of the two different materials, represented by a low intensity reflection, an effective bond was likely present. The opposite response was likely occurring when delamination, damage, or debonding was present at the interface.

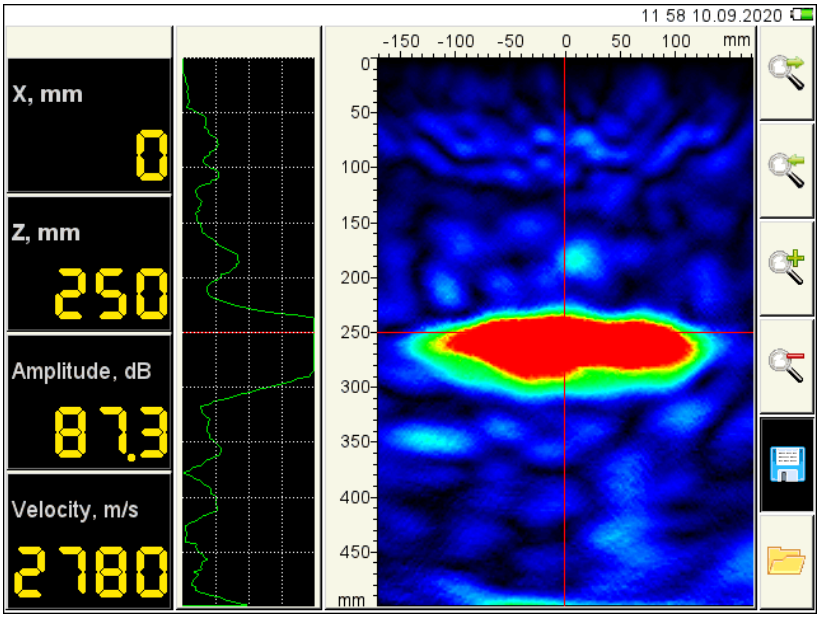

Figure 186. Image. US 67 SB MIRA B-scan with high intensity reflection (low degree of bond).

2. Normalized transmission energy (Tran and Roesler 2020): Similar to the work presented on predicting joint activation (vertical crack) through the depth of the concrete, different energy or amplitude approaches from paired sensors were examined to interrogate the interfacial bond's likely condition. A more recent study with a similar concept was established for assessing stripping potential or damage detection using non-contact ground penetrating radar (GPR) (Ma et al. 2021). If the accumulating in-layer peaks (AIP) is greater than or equal to 0.9, the asphalt pavement section is likely stripped.

$$AIP = \frac{\sum In - layer\ positive\ amplitudes}{Amplitude\ of\ peak\ surface\ reflection}$$

3. Pearson's correlation coefficient: A study performed by Schubert and Koehler (2008) evaluated grouting conditions in bridge deck tendon-ducts utilizing Pearson's correlation within an impact-echo signature analysis (IESA). Pearson's correlation coefficient (0 to 1) was used to measure the strength of the linear dependence between impact-echo intensity measurements of the intensity amplitude vectors. Schubert and Koehler (2008) showed a low coefficient (closer to 0) was indicative of damage or delamination, whereas a coefficient close

to 1.0 indicates uniformity and likely no flaws. Hoegh and Khazanovich (2012) utilized the IESA method and generalized the method into a two-dimensional ultrasonic tomography signature analysis using the reflection intensity matrices obtained from SAFT B-scans using MIRA.

$$C^{j}_{XY2D} = \frac{Cov[X_{2D}, Y^{j}_{2D}]}{\sqrt{Var[X_{2D}]Var[Y^{j}_{2D}]}} = \frac{\sum_{i=1}^{N}\sum_{k=1}^{M}(x_{ik} - x_{2Dmean})(y^{j}_{ik} - y^{j}_{2Dmean})}{\sum_{i-1}^{N}\sum_{k-1}^{M}(x_{ik} - x_{2Dmean})^{2}\sum_{i-1}^{N}\sum_{k-1}^{M}(y^{j}_{ik} - y^{j}_{2Dmean})^{2}}$$

where X_{2D} and Y^{j}_{2D} are the matrices of reflection intensity for the reference B-scan and current B-scan, respectively; x_{ik} and y^{j}_{ik} are the single intensity values of the reference signal 11 and current signal, respectively, with depth below the measurement location increasing with i and the location along the aperture of the scan increasing with k; X_{2Dmean} and Y^{j}_{2Dmean} are the mean intensities of the reference B-scan and current B-scan, respectively; N and M are the number of intensity values in the depth and device aperture direction, respectively; and C^{j}_{XY2D} is Pearson's correlation coefficient, which measures the strength of the linear dependence between X_{2D} and Y^{j}_{2D}.

Hoegh and Khazanovich (2012) concluded this algorithm was attractive for rapid subsurface damage detection in concrete structures such as pavements. However, it was also recommended more field verification is necessary and this method should be modified for identification of extended planar flaws or locations with differing structural geometries.

4. Hilbert Transform Indicator (HTI): As a potential method for determining concrete quality, Freeseman et al. (2015) developed the Hilbert Transform Indicator (HTI) to compare sound concrete with slabs experiencing freeze-thaw distress. An additional study also successfully used the HTI to show alkali-silica reaction (ASR) distresses (Dwight et al. 2016). Previous research has concluded an HTI greater than 90 indicates the presence of some damage level within the concrete likely not visible on the surface (Freeseman et al. 2015, Dwight et al. 2016, Salles et al. 2017). Salles et al. (2017) compared two thin bonded concrete overlays of asphalt and determined HTI values of 71 and 93. These values corresponded to the image analysis results of potential damage or adhesion loss between the concrete and asphalt. The first being potentially bonded (HTI = 71) and the second with potential delamination or damage (HTI = 93). However, interface bonding was not the primary focus of the study and the technique needs further examination to assess bonding condition. The HTI can be seen in the following equation.

$$HTI = \int_{0}^{500} \frac{HT(t)}{\max\left(HT(t)\right)} dt$$

Where HT(t) is the signal envelope of the Hilbert transform that is analyzed for the first 500 µs of signal time (enough time to capture the pulse of the first arrival of the direct surface wave

and for the signal to travel through the entire depth of the specimen and reflect back to the receiving transducer).

The Hilbert transform is a linear operator that takes a function, u(t) of a real variable and produces another function H(u(t)). The transform occurs from taking the actual data and imparting a phase shift of 90-degrees. This transform utilizes a discrete-time analytic signal to return a complex result of the same length of the actual data by producing two output components, real (original data) and imaginary (Hilbert transform). An example can be seen in **Figure 187**.

$$y = Hilbert(x) = real + imaginary$$

Where y is the analytic signal, “real” is the original real data, and “imaginary” is the Hilbert transform. A Hilbert transform can be defined as a 90-degree phase shift of the actual data and only affects the phase, not the amplitude.

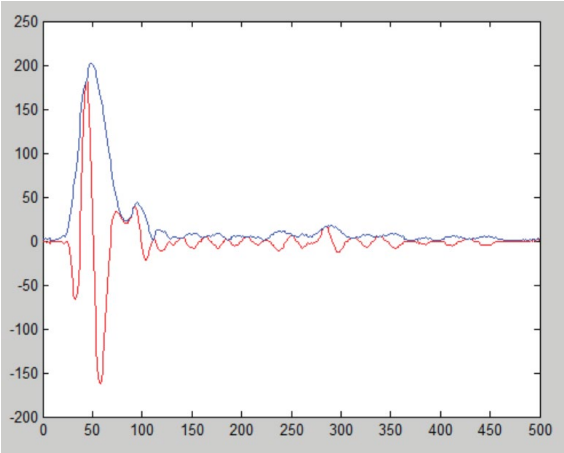

Figure 187. Graph. Hilbert transform. Blue is the instantaneous amplitude envelope as a result of the Hilbert transform. Red is the original raw signal (Freeseman et al. 2015).

5. Snell’s Law:

Snell’s Law was utilized to be able to anticipate time arrivals of transmitted waves as a function of the different layer material properties, such as wave velocity. This method allows an estimation of when the reflected wave from the PCC and stabilized layer interface and also the interface between the stabilized layer and the supporting layer directly beneath the stabilized layer are received by the signal transducers. This estimation is a function of the angle of incidence of the emitted wave and the wave velocity (function of the material the wave is passing through). **Figure 188** shows a schematic of Snell’s Law. This method then uses the recorded amplitude for the corresponding interfaces to determine the Bonding Degree Index (BDI). This index is a potential indicator for determining the degree of bond between the PCC and stabilized layer. As this value becomes closer to 0, a likely unbonded scenario is present. Whereas, as the BDI becomes closer to 1.0, a fully bonded scenario is likely present

(this value has not been fully validated but is believed to be closer to 0.75 for full bond). Further validation is required. An interpretation of the BDI can be seen in **Figure 188**.

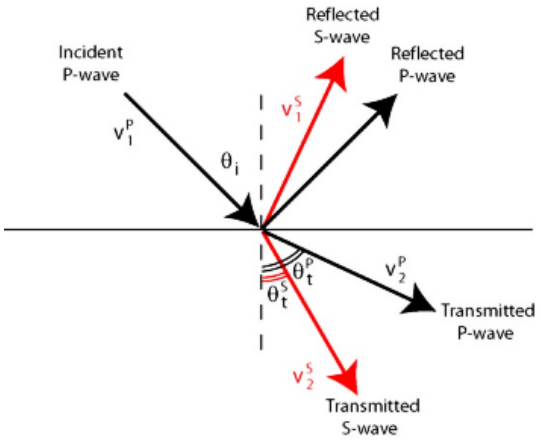

Figure 188. Image. Snell's Law.

$$\frac{Sin\ \theta_1}{Sin\ \theta_2} = \frac{v_1}{v_2}$$

Where v is the velocity of the transmissible wave through the given material (p-wave or shear wave can be used). The maximum intensity reflection for a single layer occurs at an incident angle of 45 degrees.

$$BDI = \frac{1^{st}\ reflection\ from\ bottom\ of\ base}{1^{st} reflection\ from\ bottom\ of\ PCC}$$

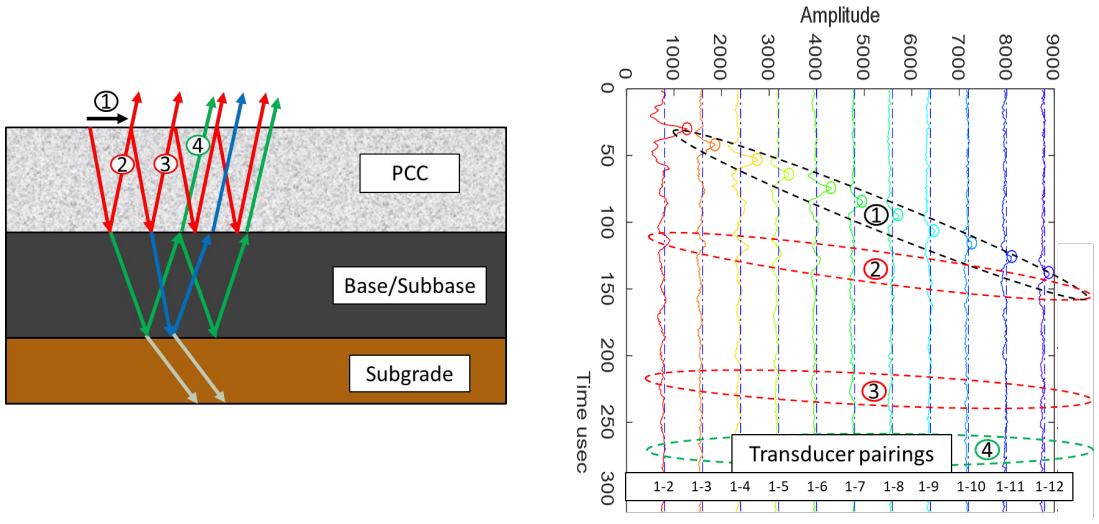

a) Wave propagation and reflection

b) Recorded amplitude for corresponding transducer pairings

Figure 189. Schematic. Bonding Degree Index (BDI) as a function of Snell's Law.

APPENDIX E: CORING RESULTS

US 67 (92774):

Coring indicated that some erosion may have been occurring beneath the concrete pavement at US 67. Cores obtained in the center of each panel from US 67 with the CAM II subbase were fully bonded with the stabilized layer for two out of three locations; the third location was not bonded and showed signs of delamination within the coring hole, but no erosion appeared to be occurring to the CAM II surface. Whereas all cores obtained in the outer wheel path were debonded and core holes showed delamination at the interface and two out of three locations were exhibiting signs of potential erosion. Although debonding and possible erosion was present, there were no visible distresses in these locations (dowels negating faulting from occurring). The corresponding thicknesses for each core location can be seen in the following table (**Table 69**). Images from the coring can be seen in the following figure.

Table 69. US 67 (92774) Coring Summary

NB/SB	Stationing		Location	PCC Thickness, in.	Subbase Thickness, in.	Additional Observations
NB	26+000	1	LJ OWP	10.25	4.25	Debonded, Delamination in core hole; some possible erosion
		2	Center	10.125	4.5	Fully bonded
NB	28+600	3	LJ OWP	10.125	4.5	Debonded with smooth interface, No observable erosion; delamination in core hole
		4	Center	10.0	3.5	Fully bonded
SB	26+600	5	LJ OWP	10.0	3.5	Debonded with significant erosion, No cracking or faulting
		6	Center	10.0	4.0	Debonded, Delamination at interface in core hole; no observable erosion

a) NB 26+000 Leave joint in outer wheel path

b) NB 26+000 Drain outlet near leave joint

c) NB 28+600 center of panel

d) NB 28+600 Leave joint in outer wheel path

e) SB 26+600 center of panel

f) SB 26+600 Leave joint in outer wheel path

Figure 190. Photos. US 67 (92774) cores.

US 30 (62277)

All cores were fully bonded between the PCC and HMA stabilized support layer. The only location that potentially had some erosion occurring was EB 8+00 in the outer wheel path. This location has pooled water along the outside shoulder edge and is most likely leading to stripping of the bottom of the HMA (See **Figure 191**). This pooling of water was present on both dates of testing, FWD (8/13/2020) and coring (11/20/2020).

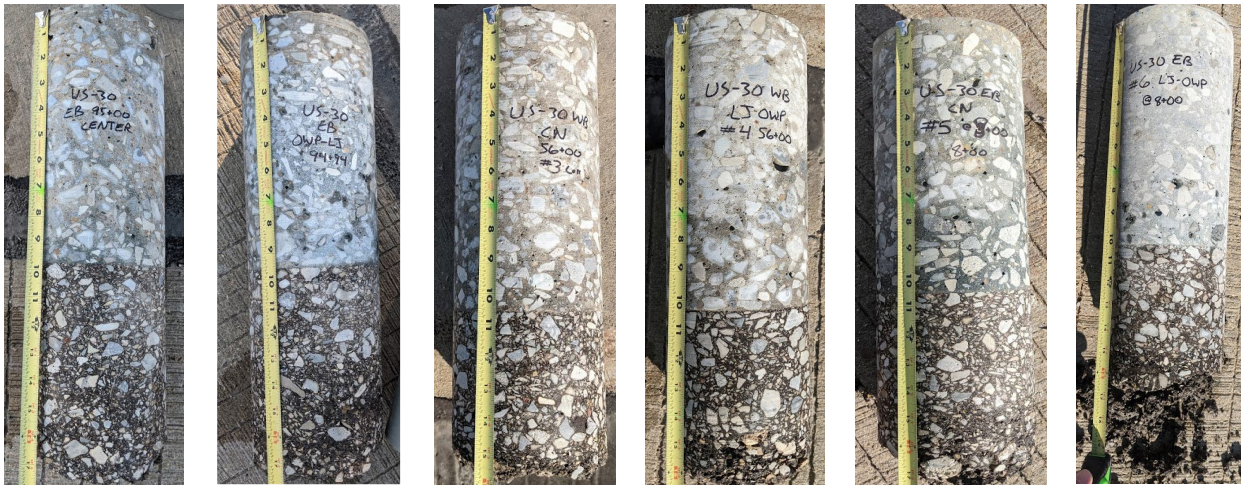

Center of panel | Leave joint in outer wheel path | Center of panel | Leave joint in outer wheel path | Center of panel | Leave joint in outer wheel path

a) 95+00 EB b) 56+00 WB c) 8+00 EB

Figure 191. Photos. US 30 (62277) cores.

Figure 192. Photo. US 30 (62277) EB 8+00 core location #3 with pooling of water along free edge.

I-72 (72G92) WB:

Coring was performed to investigate the elevation difference between the shoulder and the driving lane. This elevation difference can be seen in **Figure 193**. The coring results indicate the fabric interlayer was completely full (impregnated) with tack coat along the shoulder. The other core locations did not show as much tack coat as was seen at the cores on the shoulder. All cores showed the fabric bonded to the bottom of the PCC overlay, except for the shoulder core at 102+50 WB. This shows the cementitious bond controlled instead of the tack coat between the fabric and existing CRCP. The cores can be seen in **Figure 194** and the fabric can be seen in **Figure 195**. The resultant fabric interlayer thicknesses between the different locations shows a reduction of approximately 0.02 in. for the fabric in the outer wheel path versus the other locations (see **Table 70**).

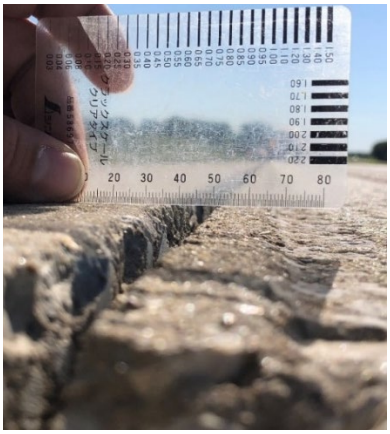

Figure 193. Photo. I-72 (72G92) WB (Fabric IL): L/S jt. elevation difference (shoulder = approx. 0.16 in. higher than driving lane).

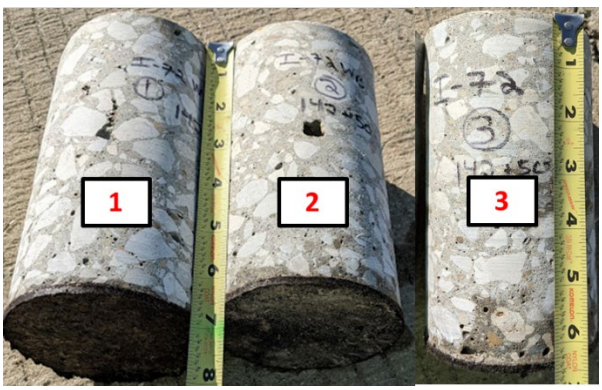

Shoulder | Outer wheel path (mid-slab) | Right edge panel (Not in wheel path)

a) 142+50 WB

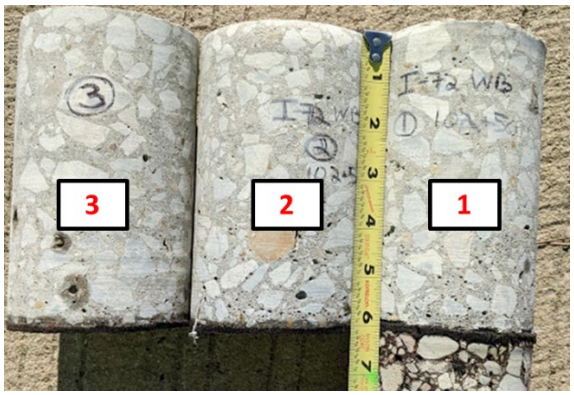

Right edge panel (Not in wheel path) | Outer wheel path (mid-slab) | Shoulder

b) 102+50 WB

Figure 194. Photos. I-72 (72G92) WB cores.

a) 142+50 WB cores: Fabric intact

b) 142+50 WB cores: Fabric removed

c) 102+50 WB: Fabric removed with existing HMA present

d) 102+50 WB: Fabric removed

Figure 195. Photos. I-72 (72G92) fabric interlayer assessment (Westbound).

Table 70. I-72 (72G92) Average Fabric Thickness Per Core Location (Westbound)

	Average fabric thickness, in.	
Core location	**142+50 WB**	**102+50 WB**
Shoulder	0.129	0.123
Outer wheel path (mid-slab)	0.105	0.107
Right edge panel (not in wheel path)	0.131	0.121

I-72 (72G92) EB:

All cores showed a bonded condition between the bottom of the PCC overlay and the HMA interlayer. There was no bond present between the bottom of the HMA interlayer and existing CRCP. The cores over the longitudinal cracks in the wheel path were held very tight due to the engaged fibers. In order for the crack to be visible, moisture needed to be present (see **Figure 196a** and **b**). Unfortunately, there was no visible permanent deformation in the wheel path versus non-wheel path. An interesting phenomenon occurring at the core locations over the longitudinal crack in the wheel path near the

transverse joint would fill back up with water after the core was extracted and drained. This did not occur for the other core locations. It is possible the asphalt is consolidating in this location, resulting in a low spot and high tensile stresses at the bottom of the PCC overlay. The results of the interlayer thicknesses are presented in **Table 71** for each coring location, respectively. Additionally, the averages and standard deviations are presented for all cores, cores only in the wheel path, and cores not in the wheel path. Cross slope adjustments were initially claimed to be performed within the HMA interlayer.

Table 71. Core Results for I-72 (72G92) EB (HMA Interlayer) from December 2020

Station (eastbound)	Core location	Core ID#	PCC overlay thickness, in.	HMA thickness, in.
15+47	AJ OWP (Crack)	1	6.75	1.50
	AJ OWP	2	6.63	1.50
		3	6.63	1.50
	Leave Non-WP	4	6.63	1.44
		5	6.63	1.38
20+00	AJ OWP (Crack)	1	6.56	1.38
	AJ OWP	2	6.63	1.38
		3	6.56	1.44
	Leave Non-WP	4	6.50	1.50
		5	6.50	1.50
80+00	AJ OWP (No Crack)	1	-	-
	AJ OWP	2	6.00	1.38
		3	6.00	1.38
	Leave Non-WP	4	6.00	1.63
		5	6.00	1.63
All cores	Average thickness, in.		6.43	1.46
	Standard deviation, in.		0.28	0.08
WP only	Average thickness, in.		6.47	1.43
	Standard deviation, in.		0.28	0.06
Non-WP	Average thickness, in.		6.38	1.51
	Standard deviation, in.		0.27	0.09

Outer wheel path (approach joint): Over longitudinal crack

Outer wheel path (approach joint): NOT over longitudinal crack

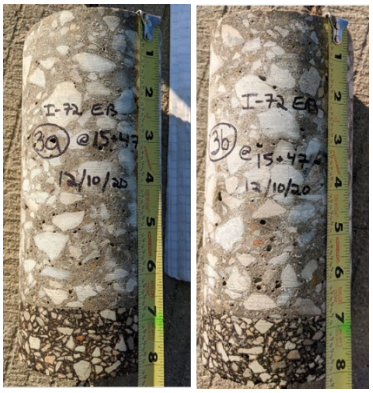

Right edge panel (Leave slab): NOT in wheel path

a) 15+47 EB

Outer wheel path (approach joint): Over longitudinal crack

Outer wheel path (approach joint): NOT over longitudinal crack

Right edge panel (Leave slab): NOT in wheel path

b) 20+00 EB

wheel path

Outer wheel path (approach joint): NOT over longitudinal crack

Right edge panel (Leave slab): NOT in wheel path

c) 80+00 EB

Figure 196. Cores from I-72 (72G92) EB taken in 2020 (no longitudinal crack in Location 3: 80+00 EB).

In order to investigate the potential mechanisms causing the longitudinal cracking in the wheel path, additional laboratory testing was conducted on the obtained cores. The additional testing of the HMA interlayer consisted of core density, conditioned split tensile (modified Lottman), and compressive strength of the concrete. This testing was performed by IDOT District 6 (Greg Heckel). The results of the density testing do not show anything unusual, and unfortunately does not appear to be any correlation between any particular test result and cracking. All specimens exceeded 60 psi conditioned tensile strength, which is the minimum acceptable for unmodified asphalt binders according to the contract provisions. All concrete compressive strengths exceeded 5,500 psi. **Table 72** presents the material testing results for the HMA interlayer.

Table 72. I-72 (72G92) EB (HMA Interlayer) HMA Material Testing Results

Station (EB)	Core location	Core ID#	Core Gmm	Core density	Conditioned Tens. Str., psi
15+47	AJ OWP	2	2.46	96.3	101
		3		96.2	137
	Leave Non-WP	4		94.4	67.0
		5		94.2	86.3
20+00	AJ OWP	2	2.47	96.3	122
		3		96.4	131
	Leave Non-WP	4		96.5	118
		5		96.6	134
80+00	AJ OWP	2	2.47	96.0	90.3
		3		96.0	112
	Leave Non-WP	4		95.8	129
		5		95.9	137
All cores	Average		2.47	95.9	114
	Standard deviation		0.003	0.75	21.9
WP only	Average		-	96.2	115
	Standard deviation		-	0.15	16.3
Non-WP	Average		-	95.6	112
	Standard deviation		-	0.94	26.3

The results from coring in June 2021 directly over the transverse joint and longitudinal crack intersection showed evidence of stripping and erosion in the HMA layer. Some of the cores showed bonding between the HMA interlayer and FRC overlay, but only on the approach side of the joint. No bond was observed for five of six cores on the leave side of the joint. This likely indicates the longitudinal cracking is initiating on the leave side of the joint. Only one core (75+30 EB #4) was fully bonded between the HMA and FRC. This location also did not have a longitudinal crack, although the HMA showed early signs of stripping. For all core locations, no bonding was observed between the HMA and existing CRCP, which is where the stripping and erosion likely initiated. The layer thicknesses for each core, as well as bond condition can be seen in table below. All cores showed

deterioration of the propagated PCC joint crack through the HMA layer. The cores remained together in the FRC overlay, as the fibers were bridging the transverse joint and working properly. Some of the cores exhibited stripping, as seen in **Figure 197**.

A. 14+02 EB OWP longitudinal crack on leave; stripping on leave only

B. 14+02 EB OWP crack deterioration in HMA at transverse joint

C. 75+30 EB IWP longitudinal crack on leave; stripping on leave only

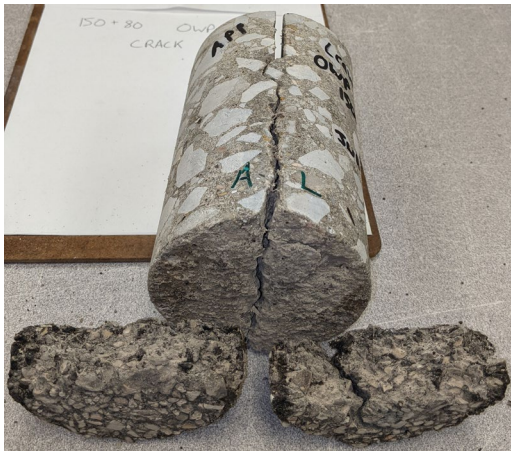

D. 150+80 EB OWP longitudinal crack on leave; stripping at bottom of HMA interlayer

Figure 197. Photos. Extracted cores from June 2021 (DeSantis and Roesler 2022).

Table 73. Coring Summary from June 2021 (DeSantis and Roesler 2022)

Station (Eastbound)	Core location	Core ID#	PCC overlay thickness, in	HMA thickness, in.	Total core thickness, in.	Bond condition[1]
14+02	OWP (Crack)	1	6.38	1.125	7.50	No bond on Leave, Bond on Approach
	IWP (Crack)	2	6.25	1.50	7.75	No bond
75+30	IWP (Crack)	3	6.25	1.44	7.69	No bond
	OWP (No Crack)	4	6.00	1.00	7.00	Good bond, Stripped HMA at bottom
150+50	IWP (No Crack)	5	6.13	1.50	7.63	Partial bond
	OWP (Crack)	6	6.00	1.31	7.31	No bond on Leave, Bond on Approach
All cored	Average thickness, in.		6.17	1.31	7.48	
	Standard deviation, in.		0.15	0.21	0.28	
OWP only	Average thickness, in.		6.13	1.15	7.27	
	Standard deviation, in.		0.22	0.16	0.25	
IWP only	Average thickness, in.		6.21	1.48	7.69	
	Standard deviation, in.		0.07	0.04	0.06	

[1]Bond condition is at the FRC-HMA interface. There was no bond at the HMA-CRCP interface when extracting the cores.

The coring results from directly over the lane-shoulder longitudinal joint also indicated stripping and erosion was occurring. The stripping and erosion at this location appears to be more severe than the transverse joint, as the HMA crumbled during coring (see **Figure 198**). Thicknesses of the HMA interlayer were not able to be determined based on the asphalt stripping and erosion. The magnitude of longitudinal lane-shoulder faulting has caused all fibers to shear, resulting in only aggregate interlock between interfaces. **Figure 198** shows the core location, inside the core hole, and the two halves of the core. It also appears as if there is some form of delamination within the HMA interlayer in the shoulder. It is difficult to determine if the shoulder is moving up a little, the driving lane moving down, or a combination of both.

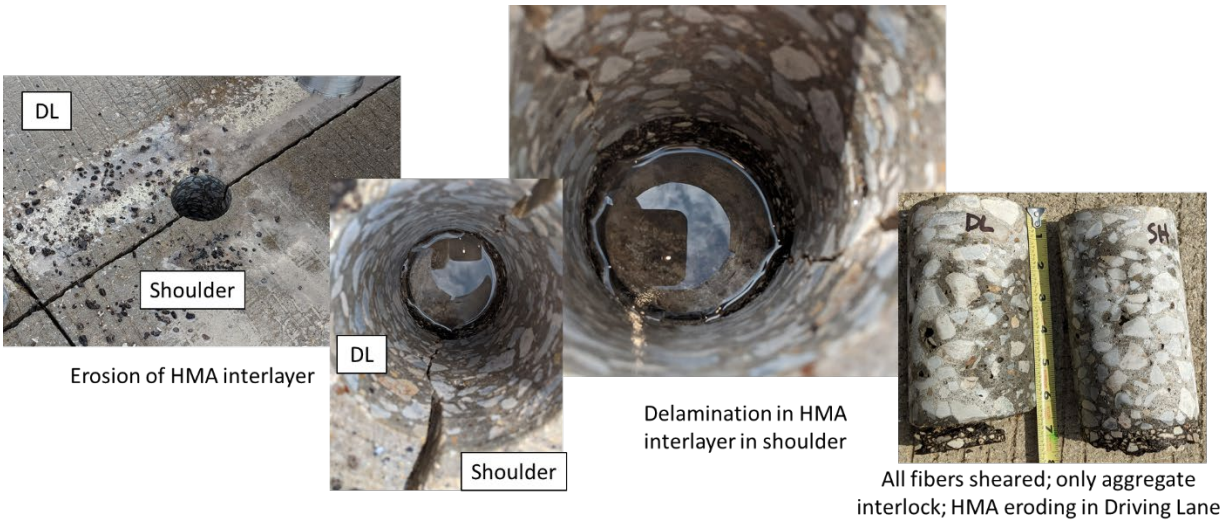

Figure 198. Photos. Core over the longitudinal lane-shoulder joint from June 2021 (DeSantis and Roesler 2022).

IL-53 (60N05):

Cores in location 1 (5+70 SB) and 2 (61+00 SB) showed full bond between the PCC and HMA. However, delamination between lifts in the HMA and loss of bond with the existing PCC layer was present. Cores in Location 3 (101+50 SB) had full bond between the PCC and HMA at the center panel (delamination near the PCC and HMA interface most likely developed from coring shear stress). However, the PCC and HMA interface at the leave joint was debonded. There was no delamination between HMA lifts in this location. The existing structure was variable throughout the project. Core Location 1, showed an existing PCC pavement. All locations showed variable existing HMA thickness, as was presented within the designs.

Center Panel: Center of panel

Center Panel: Leave joint (mid-lane)

a) 5+70 SB

Center Panel: Center of panel

Center Panel: Leave joint (mid-lane)

b) 61+00 SB

Center Panel: Center of panel

Center Panel: Leave joint (mid-lane)

c) 101+50 SB

Figure 199. Photos. IL-53 (60N05) cores.

APPENDIX F: DETAILED DISTRESS SURVEYS

IL 116 (68814):

Figure 200. Photos. IL 116 CIR process.

US 67 (92774):

Start of the project South end: Old 36 interchange (Jacksonville, IL) & US 67 NB

End of the project North end: Old 67 interchange (Jacksonville, IL) & US 67 NB

US 67 – District 6 (Sangamon Co. 92774):

- 9.75-10 in. JPCP on 4 in. CAM II Subbase on 12 in. Lime Modified Subgrade
- 15 ft x 12 ft joint spacing with hot poured joint sealant
- 2 (12 ft) lanes + inner (8 ft)/outside (10 ft) shoulders (both directions)
- 1.5-in. diameter dowels at 12 in. spacing; #6 tie bars at 24 in. spacing
- Constructed 1999
- Stationing (in meters): 28+650 to 23+700 (North to South)

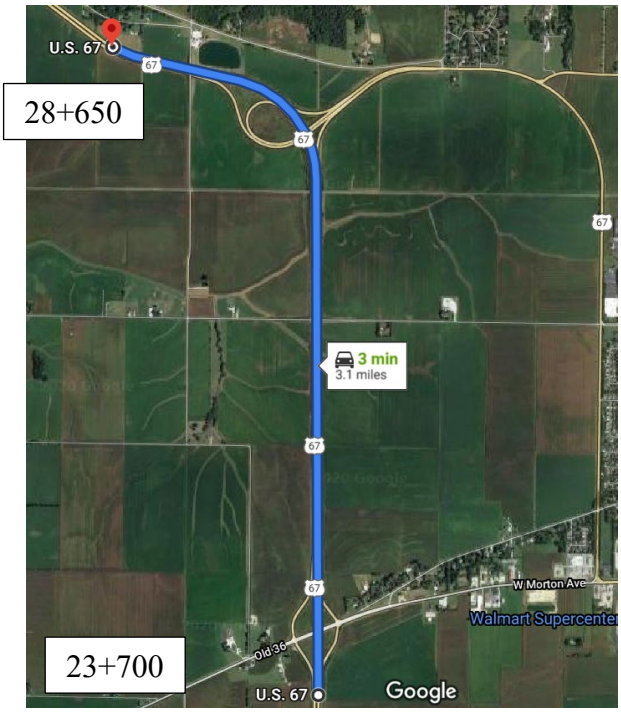

Figure 201. Photo. US 67 (92774).

US 67 (92774) Synopsis of Testing – 9/09/2020

General overview of distress observed:

A portion of US 67 southbound has been rehabilitated with an HMA overlay. This portion of US 67 southbound was not tested. A total of 10 testing locations were evaluated with five in the northbound and five in the southbound directions. A different FWD driver than the other sections was on hand and was able to complete all required testing in a timely manner. All joints were sealed very well with a hot poured sealant, both transverse and longitudinal joints. It appears this technique was applied because there is an extreme level of distress occurring along the transverse joints; it is possible the CAM II subbase is being eroded away beneath the transverse joints causing high tensile stresses near the surface and causing the transverse microcracking (cracks being held tight due to dowel bars). However, this was later confirmed to be a material-related distress (ASR).

Testing of the northbound lanes consisted of testing four locations in the morning and then testing the fifth location in the afternoon after concluding testing of the southbound lanes. The northbound lanes include full-depth repairs (FDR) of transverse joints as well as HMA patches in corners and along damaged raised pavement markers.

The southbound lanes do not appear to be performing as well as the northbound lanes and consists of a large number of FDRs (new and old repairs observed) that are tied into the existing structure with tie bars and dowel bars. A significant portion of the southbound lanes were also overlaid with an HMA recently, and therefore that portion was not tested.

Additionally, the weather was overcast with fog and a light mist throughout the morning, but cleared up in the afternoon.

Table 74. US 67 (92774) Temperature Profile (9/09/2020)

	Temperature @ corresponding depths (°F)				
Time of measurement	1.5-in. depth	5-in. depth	9-in. depth	Air	UV Index
9:00 am	69	70	72	64	0
12:15 pm	75	75	76	70	1
2:45 pm[1]	80	79	77	70	1

[1]Temperature was recorded using the same temperature holes drilled at 9:00 am.

Test sections consisted of 75 ft, with five adjacent panels and approximately 5,000 ft between testing sections. MIRA scanning was performed with 35 kHz testing frequency across transverse joints to assess joint activation. All other locations were tested with 50 kHz. Transverse joint widths were 0.25 in. and longitudinal joint widths were 0.5 in. (both were sealed well).

Table 75. US 67 (92774) Intensive Testing Sections and Stationing

Intensive test sections	**Time @ start of section**	**Stationing**	
		Beginning of test section	**End of test section**
NB-1	8:30 am	24+599	24+622
NB-2	9:00 am	25+990	26+013
NB-3	9:45 am	27+299	27+322
NB-4	10:15 am	28+587	28+610
NB-5[1]	2:15 pm	23+799	23+822
SB-1	11:45 am	28+655	28+632
SB-2	12:20 pm	27+610	27+587
SB-3	12:50 pm	26+526	26+503
SB-4	1:15 pm	26+116	26+093
SB-5	1:40 pm	25+370	25+347

[1]NB-5 was conducted in the afternoon due to the meeting location of traffic control in the morning.

Detailed distress surveying was conducted along the driving lane where FWD and MIRA testing was performed.

Table 76. US 67 (92774) Detailed Distress Survey Notes (Northbound)

Stationing	Detailed distress notes: US 67 NB (23+700 to 28+650)
Section NB-1 (24+599)	
24+600	Temperature holes drilled and recorded at 9:00 am and 2:45 pm (1.5 in., 5 in., and 9 in.)
24+594 to 24+622	Material related cracking in the shoulder (ASR); Corner failures (micro-cracking) in DL on approach and leave slab along longitudinal joint between PL and DL (Raised pavement markers in PL near corners potentially relieve stress and not causing corner cracking to occur in PL); Concrete pop-outs also occurring throughout section
24+622	End of Section NB-1 intensive FWD testing and MIRA
Section NB-2 (25+990)	
25+995	Corner failures (micro-cracking) in DL on approach and leave slab along longitudinal joint between PL and DL (Raised pavement markers in PL near corners potentially relieve stress and not causing corner cracking to occur in PL)
26+016	Durability cracking in the DL near approach joint; construction flaws in section with pop-outs
26+013	End of Section NB-2 intensive FWD testing (No MIRA)
Section NB-3 (27+299)	
27+299 to 27+322	Full-depth repairs of transverse joints near intensive testing section (6 ft lengths with full-lane widths); Corner failures (micro-cracking) in DL on approach and leave slab along longitudinal joint between PL and DL (Raised pavement markers in PL near corners potentially relieve stress and not causing corner cracking to occur in PL); Concrete pop-outs also occurring
27+309	Severe corner failure resulted in loss of material
27+329	Slab NB-3F has a larger joint width than others in test Section NB-3 (~0.5 in.), joint is activated, resulting in some spalling
27+322	End of Section NB-3 intensive FWD testing and MIRA
Section NB-4 (28+587)	
28+587 to 28+610	Corner failures (micro-cracking) in DL on approach and leave slab along longitudinal joint between PL and DL (Raised pavement markers in PL near corners potentially relieve stress and not causing corner cracking to occur in PL); Some HMA patching of severe corner failures
28+587	Good bond recording with MIRA; Coring location NB-4A
28+645	Concrete pop-outs occurring
28+610	End of Section NB-4 intensive FWD testing (No MIRA)
Section NB-5 (23+799)	
23+799 to 23+822	Concrete popouts occurring; Full-depth repairs of transverse joints near intensive testing section (6 ft lengths with full-lane widths); Damage mostly occurring in DL; ASR in majority of DL panels near transverse joints
23+814	Corner failures with HMA patching; ASR in DL in approach and leave slab
23+839	Severe ASR causing a depression near the joint, approach and leave slab feel unsupported near the joint
23+822	End of Section NB-5 intensive FWD testing (No MIRA)

a) Durability cracking in the Outer Shoulder (24+594 NB)

b) Corner distress or durability cracking in DL (24+609 NB)

c) Clear drain outlet (26+000 NB)

d) Durability cracking in the DL and PL with pop-out (26+016 NB)

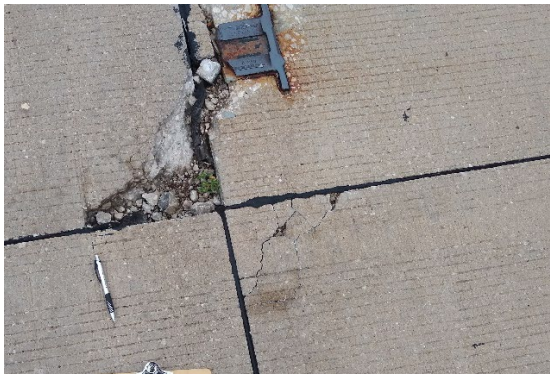

e) Corner distress in the DL and PL (27+309 NB)

f) Severe ASR (23+839)

Figure 202. Photos. Distress photos within US 67 (92774) NB.

Table 77. US 67 (92774) Detailed Distress Survey Notes (Southbound)

Stationing	Detailed distress notes: US 67 (28+650 to 21+537)[1]
Section SB-1 (28+655)	
28+660	New full-depth repair (FDR) performing well (6 ft length 12 ft wide; DL only); should have extended into PL due to corner failures
28+655	Temperature holes drilled and recorded at 12:15 pm (1.5 in., 5 in., and 9 in.)
28+655 to 28+632	Corner failures throughout section similar to NB (DL approach and leave along the DL/PL longitudinal joint); severe failures include AC patches
28+646	Reflector in PL has HMA patch over reflector
28+615	Old FDR joints are excessively wide and spalling (7.5 ft length spanning DL and PL); some HMA patching has been done along the joints
28+632	End of Section SB-1 intensive FWD testing (No MIRA testing performed)
Section SB-2 (27+610)	
27+610 to 27+587	Corner failures throughout section (DL and PL approach and leave) with majority in PL; severe failures include HMA patches in corners and over damaged raised pavement markers
27+587	End of Section SB-2 intensive FWD testing and MIRA
Section SB-3 (26+526)	
26+526	Corner failures in DL along DL/PL longitudinal joint
26+498	Severe transverse crack spanning entire pavement width and shoulder; spalling and faulting occurring along crack (~3 mm); MIRA was conducted across both adjacent transverse joints and tested along the leave crack in three locations similar to MIRA testing protocol
26+503	End of Section SB-3 intensive FWD testing (No MIRA testing performed)
Section SB-4 (26+116)	
26+116 to 26+093	MIRA scans at center of slabs reporting first reflection at 16 in. (400 mm) for some locations and others resulting in 10 in. (250 mm); Suggested coring location to assess bonding conditions
26+056	Longitudinal joint spalling; micro-cracking occurring parallel to transverse joint in approach and leave slabs
26+026	New FDR 6 ft x 12 ft in DL; PL also has transverse microcracking along the transverse joint
26+093	End of Section SB-4 intensive FWD testing and MIRA
Section SB-5 (25+370)	
25+370 to 25+347	Corner failures in DL along DL/PL longitudinal joint; severe locations include HMA patches in corners and over damaged raised pavement markers
25+340	Corner failures in DL on approach and leave along DL/PL longitudinal joint
25+330	Spalling along transverse joint
25+347	End of Section SB-5 intensive FWD testing (No MIRA testing performed)

[1]US-67 SB was rehabilitated with an HMA overlay from ~25+000 to ~21+537.

a) New FDR performing well in DL; corner failure in PL (28+660 SB)

b) Old FDR with excessively wide joints and HMA or spray injection patches (28+615 SB)

c) Corner distress in DL and PL (27+590 SB)

d) Transverse crack with spalling and faulting (26+498 SB)

e) Longitudinal joint spalling and transverse micro-cracking along joint (26+056 SB)

f) Corner distress in DL (25+340 SB)

Figure 203. Photos. Distress photos within US 67 (92774) SB.

I-72 (92763):

Start of the project West end: IL 106 interchange (Hull, IL) & I-72 WB

End of the project East end: IL 106 interchange (Hull, IL) & I-72 WB

I-72 – District 6 (Pike Co. 92763):

- 10-in. JPCP on 4-in. CAM II Subbase on 12-in. Lime Modified Subgrade
- 15-ft x 12-ft joint spacing with joint sealant (transverse and longitudinal)
- Two (12 ft) lanes + inner (8 ft)/outside (10 ft) shoulders (both directions)
- 1.5 in. diameter dowels at 12-in. spacing; #6 tie bars at 24-in. spacing
- Constructed in 1999 and 2000
- Stationing (in meters): 1+200 to 2+850 (West to East)

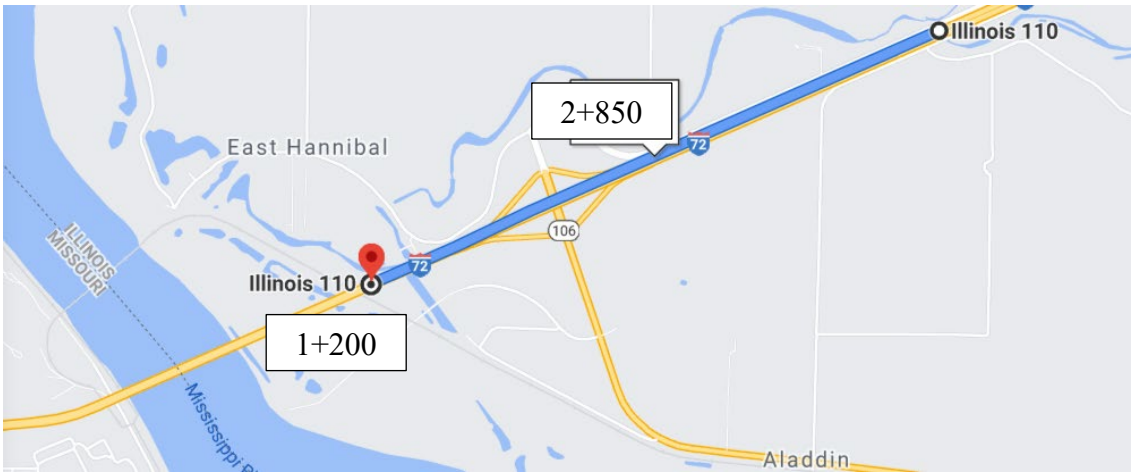

Figure 204. I-72 (92763).

I-72 (92763) Synopsis of Testing – 9/10/2020

General overview of distress observed:

A total of 10 testing locations were evaluated with five in the Westbound and five in the Eastbound directions. A different FWD driver than the initial sections was on hand and was able to complete all required testing in a timely manner. All joints appear to be sealed with a hot poured sealant and were sealed very well, both transverse and longitudinal joints. Transverse tining is very exaggerated and led to diamond grinding to increase rideability near project start in westbound direction and project end in eastbound direction.

Westbound was performing well for a 20-year-old pavement but has signs of distress. A major failure was observed in the driving lane close to the overpass prior to test Section WB-2 that is likely due to poor drainage and possibly some erosion. The longitudinal joint between the driving and passing lane was excessively wide in locations with joint faulting also occurring with the passing lane greater than the driving lane. Additionally, there were locations that did not include dowel bars in the driving lane (identified using ultrasonic testing – MIRA). This is likely from missing the dowels when saw cutting, because adjacent joints were observed to include dowels. In some locations in which dowel bars were identified, longitudinal cracking was observed to develop initiating at the transverse joint over top of the dowel bars in the wheel paths in the driving lane.

Similar to westbound, eastbound was also performing well. However, a major failure was observed in the driving lane close to the overpass prior to test Section EB-4, which involved a longitudinal crack that spanned multiple slabs with diagonal cracking. The large failure is likely due to poor drainage and erosion because it is in the exact same location as the major failure in the westbound direction. It appeared no missed dowels were occurring in eastbound direction. Additionally, in some locations longitudinal cracking was observed to develop initiating at the transverse joint over top of the dowel bars in the wheel paths in the driving lane (similar to westbound).

Additionally, the weather was overcast with fog and a light mist throughout the day. There was light rain in the afternoon.

Table 78. I-72 (92763) Temperature Profile (9/10/2020)

	Temperature @ corresponding depths (°F)				
Time of measurement	1.5-in. depth	5-in. depth	9-in. depth	Air	UV Index
8:40 am	70	73	76	59	0
12:15 pm	72	73	73	69	1
2:00 pm[1]	-	-	-	70	1

[1]Temperature holes were not drilled, ran out of time based on traffic control. Weather was consistent.

Test sections consisted of 75 ft, with five adjacent panels and approximately 1,500 ft between testing sections. MIRA scanning was performed with 35 kHz testing frequency across transverse joints to assess joint activation. All other locations performed with 50 kHz. Transverse joint widths are 0.375 in. and longitudinal joint widths are 0.5 in. (both are sealed well).

Table 79. I-72 (92763) Intensive Testing Sections and Stationing

Intensive test sections	Time @ start of section	Stationing	
		Beginning of test section	End of test section
WB-1	8:30 am	2+850 WB	2+800 WB
WB-2	8:50 am	2+396 WB	2+350 WB
WB-3	9:30 am	2+100 WB	2+050 WB
WB-4	9:55 am	1+912 WB	1+862 WB
WB-5	10:30 am	1+311 WB	1+261 WB
EB-1	12:00 pm	1+315 EB	1+365 EB
EB-2	12:30 pm	1+705 EB	1+755 EB
EB-3	12:50 pm	2+120 EB	2+170 EB
EB-4	1:15 pm	2+315 EB	2+365 EB
EB-5	1:40 pm	2+690 EB	2+740 EB

[1]NB-5 was conducted in the afternoon due to the meeting location of traffic control in the morning.

Detailed distress surveying was conducted along the Driving Lane where FWD and MIRA testing was performed.

Table 80. I-72 (92763) Detailed Distress Survey Notes (Westbound)

Stationing	Detailed distress notes: I-72 WB (2+850 to 1+200)
Section WB-1 (2+850)	
2+850	Temperature holes drilled and recorded at 8:40 am (1.5 in., 5 in., and 9 in.); Rebound hammer index ranged between 5.8-7.2 ksi (40-50 MPa)
2+800	Deep transverse tining led to diamond grinding in patches and exposing aggregate; reflector pop-out with HMA patch and replaced using epoxy material
2+800	End of Section WB-1 intensive FWD testing (No MIRA testing performed)
Section WB-2 (2+396)	
2+396 to 2+350	Dowel bar misplacement – saw cutting missed dowels between A-B, C-D, and D-E, Dowels were identified correctly between B-C; Longitudinal faulting between PL and DL (~6.5 mm PL>DL); Longitudinal faulting along construction joint between DL and shoulder (~2.0 mm), possibly due to construction; corner failures occurring with microcracking in DL along DL/PL longitudinal joint
2+350	Longitudinal cracking initiating at transverse joint (+/- 12 in. in length) over top of dowel bars; Occurring in five separate locations in this section all in or near the wheel paths (outer and inner)
2+250	Severe edge failure in DL due to lack of support spanning multiple slabs (See Photo); possible erosion of subbase in this area
2+350	End of Section WB-2 intensive FWD testing and MIRA
Section WB-3 (2+100) – under the overpass	
2+090	Corner crack with HMA Patch in DL approach along DL/PL longitudinal joint
2+070	Corner crack and pop-out in DL approach along DL/PL longitudinal joint
2+030	Full-depth repair with HMA patch in DL approach joint; longitudinal joint faulting between PL and DL (~10 mm PL>DL)
2+050	End of Section WB-3 intensive FWD testing (No MIRA testing performed)
Section WB-4 (1+912)	
1+912 to 1+862	Section is performing well with no observed distress
1+862	End of Section WB-4 intensive FWD testing and MIRA
Section WB-5 (1+311)	
1+311 to 1+261	Testing location was near bridge approach and likely on fill material beneath pavement structure; Section performing well
1+280	Corner crack in DL leave slab along PL/DL longitudinal joint (~8 in. radius)
1+275	Corner crack in PL approach slab along PL/DL longitudinal joint (~5 in. radius)
1+261	End of Section WB-5 intensive FWD testing (No MIRA testing performed)

a) Test Section WB-1 (2+850 WB)

b) Surface diamond ground (2+800 WB)

c) Longitudinal joint faulting (Section WB-2)

d) Edge failure due to lack of support (2+250 WB)

e) Longitudinal crack over dowel bar and longitudinal faulting (2+350 WB)

f) Corner failures (Section WB-2)

Figure 205. Photos. Distress photos within I-72 (92763) WB.

g) Corner failure with pop-out in DL between PL/DL (2+070 WB)

h) FDR with HMA patch and Longitudinal faulting (2+030 WB)

i) Test Section WB-5 (1+311 WB)

Figure 205 (contd.). Photos. Distress photos within I-72 (92763) WB.

Table 81. I-72 (92763) Detailed Distress Survey Notes (Eastbound)

Stationing	Detailed distress notes: I-72 EB (1+200 to 2+850)
Section EB-1 (1+315)	
1+315 to 1+365	Longitudinal joint between PL/DL excessively wide (~1 in.) and faulting with PL>DL; Longitudinal joint is sealed but due to width, sealant may not be able to prevent infiltration; Rebound Index in DL and Shoulder between 6-8 ksi (45-55 MPa)
1+315	Temperature holes drilled and recorded at 12:15 pm (1.5 in., 5 in., and 9 in.); Corner failures in PL leave slab along PL/DL longitudinal joint
1+330	Corner failure with pop-out (~5 in. radius) in DL approach along PL/DL longitudinal joint; Reflector damaged and replaced, new reflector has cracking
1+365	End of Section EB-1 intensive FWD testing (No MIRA testing performed)
Section EB-2 (1+705)	
1+705 to 1+755	Minor corner failures in DL approach along DL/Shoulder longitudinal joint, occurring in multiple panels
1+715	Corner failure in PL approach slab along PL/DL longitudinal joint; Reflector damage; Wide longitudinal joint between PL/DL
1+720	Minor transverse joint spalling
1+755	End of Section EB-2 intensive FWD testing and MIRA
Section EB-3 (2+120)	
2+135	Longitudinal crack initiated at the transverse joint directly over dowel in OWP (between testing slabs C and D)
2+140	Longitudinal crack initiated at the transverse joint directly over dowel in OWP (between testing slabs D and E)
2+170	End of Section EB-3 intensive FWD testing (No MIRA testing performed)
Section EB-4 (2+315)	
2+290	Severe edge failure in DL due to lack of support spanning multiple slabs (See Photo); possible erosion of subbase in this area, also possible longitudinal cracking initiated first over dowel bars in the OWP of consecutive panels; Same region as large failure in WB
2+315 to 2+365	Longitudinal crack initiated at the transverse joint directly over dowel in OWP recurring frequently
2+330 to 2+345	Corner failures in PL along PL/DL longitudinal joint in three consecutive corners (Leave, approach, and approach slabs) – approximately 12 in. radius
2+365	End of Section EB-4 intensive FWD testing and MIRA
Section EB-5 (2+690)	
2+690 to 2+740	Section is diamond ground in areas in DL near on ramp; No distresses observed
2+740	End of Section EB-5 intensive FWD testing (No MIRA testing performed)

a) Wide longitudinal joint between PL/DL (Section EB-1)

b) Corner distress in DL and Reflector damage (1+330 EB)

c) Corner failure in PL approach and reflector damage (1+715 EB)

d) Longitudinal crack over dowel in OWP (2+140 EB)

e) Edge failure due to lack of support (2+290 EB)

f) Corner distress in PL (Section EB-4)

Figure 206. Photos. Distress photos within I-72 (92763) EB.

US 20 EB (40455 E & H):

US 20 near Pecatonica River Bridge east of Freeport. Test eastbound only.

- E: 894+60 to 904+27
- H: 988+50 to 1002+75

US 20 EB – District 2 (Stephenson Co. 40455 E & H):

- 10 in. JPCP on 4 in. CAM II Subbase
- 15 ft x 12 ft joint spacing with joint sealant (transverse and longitudinal)
- Two (12 ft) lanes + inner (8 ft)/outside (10 ft) tied PCC shoulders (both directions)
- 1.5-in. diameter dowels at 12 in. spacing; #6 tie bars at 36 in. spacing
- Constructed in 1996

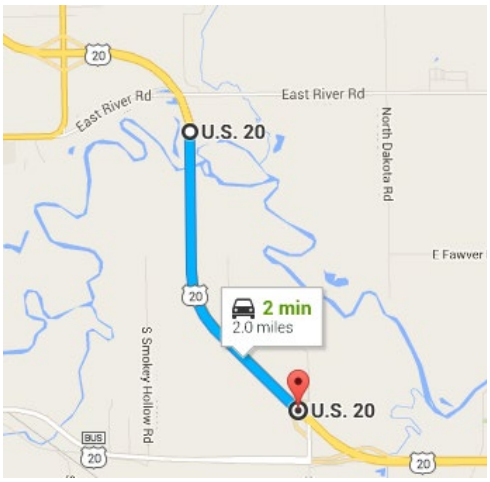

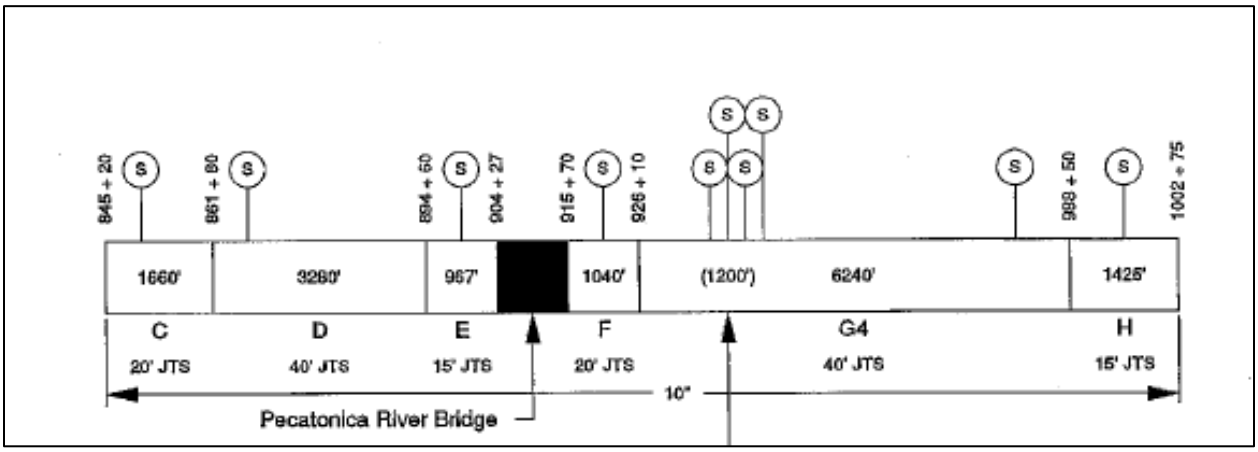

Figure 207. Photos. US 20 (40455).

US 20 (40455 E & H) Synopsis of Testing – 8/20/2020

General overview of distress observed:

In general, the main failures observed include wide transverse joints with joint sealant damage and low severity spalling along transverse and longitudinal joints. Some maintenance has been performed, including hot poured joint sealant in Section E and HMA patching along spalled joints. Another common failure observed in Section E is corner spalling or cracking in the shoulder along the L/S longitudinal joint (approach and leave slab). This appears to be related to the construction joint (some locations very tight and other locations it is wide with vegetation). The shoulder appears to be much older than the DL concrete. Rehabilitation has been performed near the end of Section E (~902+00 to 904+00) to repair the corner failures in the shoulder with a 4-ft wide and 2-in. thick HMA patch. These failures were not common in Section H.

Section H also exhibited wide transverse joints with joint sealant damage. Transverse joints are full of incompressible materials (fine material and debris). Some maintenance has been performed, including HMA patching along spalled joints. Potentially some erosion is occurring within the subbase layer and causing cracking in the concrete layer. In addition to this potential erosion, there appears to be some drainage issues near Section H-3 in the DL (near the exit ramp) that led to shattered slabs for adjacent panels in the DL. Another instance of possible erosion is at the end of Section H-4, severe cracking has developed near the transverse joint causing a punchout and exposing a dowel bar.

Table 82. US 20 (40455) Temperature Profile (8/20/2020)

	Temperature @ corresponding depths (°F)		
Time of measurement	2-in. depth	5-in. depth	9-in. depth
8:30 am	70	72	73
11:00 am	90	87	83
1:30 pm	101	95	89

MIRA scanning was performed with 35 kHz testing frequency across transverse joints to assess joint activation. All other locations performed with 50 kHz. During field surveying, majority of joints were wide (sawcut). This made it very difficult to be able to run the MIRA scan across the joint (sensors were not able to rest on both sides of the joint) and therefore many joints were unable to be tested. Joint conditions were wide and most joints were initially sealed but exhibiting joint sealant failure with incompressible fines in the joints.

Table 83. US 20 (40455) Intensive Testing Sections and Stationing

Intensive test sections	Time @ start of section	Stationing	
		Beginning of test section	End of test section
E-1	7:45 am	895+00	895+75
E-2	9:00 am	898+00	898+75
E-3	9:30 am	900+00	900+75
E-4	10:00 am	902+00	902+75
H-1	11:00 am	989+00	989+75
H-2	12:00 pm	998+50	999+25
H-3	12:30 pm	997+00	997+75
H-4	1:00 pm	1001+00	1001+75

Test sections consisted of 75 ft, with five adjacent panels and approximately 200 ft between testing sections. Test Section H has an off ramp in the middle of the section and due to safety testing near the ramp was avoided. This resulted in approximately 900 ft between Section H-1 and H-2. Section H-3 was tested after H-2 to try and test near the ramp exit, but with safety precautions.

Detailed distress surveying was conducted along the Driving Lane where FWD and MIRA testing was performed.

Table 84. US 20 (40455) Detailed Distress Survey Notes (Section E)

Stationing	Detailed distress notes: Section E (895+00 to 904+00)
Section E-1 (895+00)	
895+00 to 904+00	Trans. jts. all are ~0.75-in. wide; joint spalling common along section; appears all trans. jts. sealed with hot poured jt. sealant and HMA patches along large spalled jts.; common corner cracking along shoulder leave jt. L/S long. jt. (~8 in. radius)
894+00	Long. cracking across two adjacent panels in DL (~1.5 mm width)
895+60	Corner break leave slab along L/S long. jt. (~9-in. radius)
896+00	L/S long. jt. inconsistent height between lanes and wide with spalling; unclear if long. faulting is occurring or if construction elevation differences between L/S
896+20	Trans. jt. spalling with HMA patch, vegetation growing out of jt.
895+75	End of Section E-1 intensive FWD and MIRA testing
Section E-2 (898+00)	
897+60	Trans. crack DL; jt. sealant damage and jt. full of incompressible fines
898+00	Corner crack along shoulder (L/S long. jt.) – leave slab, fines slurry appears to have pumped under crack (~2 in. depth from surface of concrete)-see photo
898+15	HMA patch of corner spall along L/S long. jt. – both approach and leave slab
898+75	End of Section E-2 intensive FWD testing (No MIRA testing performed)
Section E-3 (900+00)	
899+85	Corner crack in PL along leave jt. (~14 in. radius)
901+00	DL/PL long. jt. damage; corner cracking; HMA patch present but distress deteriorating
900+75	End of Section E-3 intensive FWD and MIRA testing
Section E-4 (902+00)	
901+65 to 904+00	HMA partial depth repair along L/S long. jt., repair is 4-ft wide and 2-in thick
902+00	Corner crack along L/S long. jt. (approach and leave) – DL and Shoulder (~8-in. radius)
902+30	Long. cracking in shoulder (mid-panel); HMA patch present but crack length extends on both ends of patch to adjacent trans. jts.
903+00	Corner failure in approach slab of DL and PL with HMA partial depth repair. See photo
902+75	End of Section E-4 intensive FWD and MIRA testing

a) Lane-shoulder long. jt. (896+00)

b) Trans. cracking and vegetation growth in long. jt. (897+60)

c) Corner crack and popout with fines slurry along lane-shoulder long. jt – leave slab in shoulder (898+00)

d) Long. jt. deterioration with HMA patch (901+00)

e) HMA partial depth repair along shoulder (901+65 to 904+00)

f) Corner break spanning DL and PL with HMA partial depth repair (903+00)

Figure 208. Photos. Distress photos within US 20 (40455) Section E.

Table 85. US 20 (40455) Detailed Distress Survey Notes (Section H)

Stationing	Detailed distress notes: Section E (895+00 to 904+00)
Section H-1 (989+00)	
989+00 to 1002+50	Trans. jts. all are >0.75-in. (~1-in.) wide; joint sealant damage common if any sealant is remaining; HMA patches along large spalled jts.; common corner cracking along DL/PL long. jt
989+00	Trans. jts. = 1 in., no faulting (dowels are working)
989+50	Corner crack with HMA patch in DL approach slab along DL/PL long. jt. (~8-in. radius); 3-in. diam. core not filled
989+75	End of Section H-1 intensive FWD and MIRA testing
Section H-2 (998+50)	
998+50	Mid-lane long. cracking in DL (two consecutive panels); HMA patching along trans. jt., jt. sealant damage (large jt. widths)
999+25	End of Section H-2 intensive FWD testing (No MIRA testing performed)
Section H-3 (997+00)	
996+70	Shattered slabs in DL (two adjacent slabs) with some HMA patching
997+00	Trans. jt. sealant damage
997+50	Trans. crack mid-panel spanning width of pavement, no faulting; HMA patching along L/S longitudinal jt.
997+75	End of Section H-3 intensive FWD and MIRA testing
Section H-4 (1001+00)	
1001+15	Trans. crack mid-panel spanning width of pavement, no faulting; HMA patching along L/S longitudinal jt.
1001+80	Diagonal cracking with punchout and dowel bar exposure (OWP); excessively wide joint (~1 in.) with minimal HMA patching
1001+75	End of Section H-4 intensive FWD and MIRA testing

a) Joint deterioration (989+50)

b) Mid-lane long. cracking in DL (998+50)

c) Shattered slabs in DL with some HMA patching (996+70)

d) Mid-panel trans. cracking (997+50)

e) Mid-panel trans. cracking and jt. sealant damage (1001+15

f) Diagonal cracking with slab punch down and dowel exposure (10001+80)

Figure 209. Photos. Distress photos within US 20 (40455) Section H.

US 30 (62277):

Start of the project West end: IL 394 interchange (Ford Heights, IL) & US 30 EB

End of the project East: IL 83 interchange (Lynwood, IL) & US 30 EB

US 30:

a) JPCP with 15 x 12 ft panels constructed in September 2003
b) 10 in. PCC constructed on 4 in. HMA stabilized subbase
c) First 1,000 ft (eastbound) – 6-ft tied PCC shoulder; remainder of section (eastbound & westbound) curb and gutter
d) Dowels spaced at 12 in.
e) Tie bars spaced at 24 in.
f) Speed limit = 55 mph
g) 2-mile segment (IL 394 (West) to IL 83 (East))
h) 4-lanes with a center turning lane (two eastbound and two westbound)

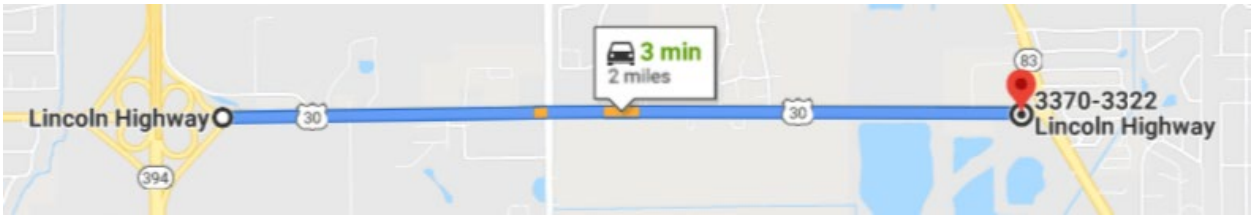

Figure 210. Photo. US 30 (62277).

US 30 (62277) Synopsis of Testing – 8/13/2020

General overview of distress observed:

FWD testing crew (APTech) was a new crew, only 3rd day of testing. Truck issues and setting up took an hour (issues when lining up the sensors and truck with appropriate testing locations); started testing first section at 8:00am (supposed to start testing at 7am). Three temperature holes were drilled at 1.5-in., 5-in., and ~8-in. depths into the pavement. Temperatures were recorded three times (8:30am, 12:00pm, and 2:30pm) at different locations. Air temperature was between 70 – 85 ^{o}F, with an increasing UV index throughout the day (~8 when finished testing).

Eastbound was tested first in the morning and westbound was tested in the afternoon. The first five slabs were able to follow the original testing protocol with testing performed in the corner on the leave joint. However, the remainder of testing (both eastbound and westbound) had a curb and gutter along the shoulder and restricted testing in the corner. Therefore, testing was performed in the outer wheel path on the leave joint. Testing in the outer wheel path was conducted periodically and not conducted on the five adjacent slabs, rather testing was performed in-between intensive

testing locations. This allows for a better representation of testing along the entire pavement section and also made things easier on the FWD testing crew when aligning the sensor layout.

Five segments were tested on the eastbound and seven segments were tested on the westbound. Four out of the 5 segments in the eastbound direction consisted of the intensive testing of five adjacent slabs with FWD drop locations mid-lane on the leave joint and center of the panel. The remaining tested segment (#4), consisted of testing the leave joint in the outer wheel path for three adjacent slabs. Four out of the seven segments tested in the westbound direction consisted of the intensive testing of five adjacent slabs with FWD drop locations mid-lane on the leave joint and center of the panel (Segments 1, 3, 5, and 7). The remaining tested segments (2, 4, and 6), consisted of testing the leave joint in the outer wheel path for a minimum of three adjacent slabs.

Table 86. US 30 (62277) Temperature Profile

	Temperature @ corresponding depths (°F)		
Time of measurement	1.5-in. depth	5-in. depth	8-in. depth
8:30 am	77	77	79
12:00 pm	100	97	89
2:30 pm[1]	110	-	-

[1]Battery died for drill, only first hole was able to be drilled; Air Temp. = 83°F, Surf. Temp. = 115°F

MIRA scanning was performed with 35 kHz testing frequency across transverse joints to assess joint activation. All other locations performed with 50 kHz.

Eastbound Sections 2, 3, and 4 appear to have poor consolidation in the concrete. MIRA images show potential delamination/ poor consolidation between the top 50-100 mm (2-4 in.). Removed concrete where full-depth repairs performed show large air voids in the concrete confirming MIRA scanning. Potentially able to see the reflection of the bottom of the HMA subbase layer within Section 3A.

Large truck distribution center along the eastbound lane near start of project (~10+00 EB). Additionally, a number of commercial businesses along westbound (failures observed at entrances to these businesses along the driving lane and shoulder).

Westbound Section 3 was around storm drains. The slab prior to Section 3 panel A has a storm drain and also in Section 3 panel E. Section 2, 4, and 6 consisted of FWD testing in the outer wheel path only; MIRA testing was performed in the outer wheel path and the center of the slab.

The predominant distress observed was longitudinal cracking mid-lane and is likely due to drainage or possibly some erosion issues within the subbase layer. There have already been a number of slabs that have been rehabilitated with full-depth repairs. Additionally, longitudinal cracking occurred throughout the eastbound direction between the driving lane and passing lane. It appears these cracks were from late sawing of the longitudinal joint. Fortunately, there are tie bars between lanes to be able to keep this crack tight. However, it appears in Section 3 that severe spalling has occurred along these cracks.

Table 87. US 30 (62277) Intensive Testing Sections and Stationing

Intensive test sections	Time @ start of section	Stationing[1]	
		Beginning of test section	End of test section
1 EB	8:00 am	08+00	8+75
2 EB	9:00 am	45+00	45+75
3 EB	9:45 am	70+00	70+75
4 EB (OWP only)	10:00 am	79+75	80+20
5 EB	10:30 am	94+90	95+65
1 WB	11:45 am	103+75	103+00
2 WB (OWP only)	12:15 pm	90+10	89+65
3 WB	12:30 pm	82+42	81+70
4 WB (OWP only)	1:00 pm	70+00	69+55
5 WB	1:20 pm	57+25	56+50
6 WB (OWP only)	1:50 pm	29+90	29+45
7 WB	2:15 pm	13+00	12+25

[1]Stationing started at western most point of the project (near IL-394).

Figure 211. Photo. US 30 (62277) Testing performed in the outer wheel path of driving lane (~18 in. from lane-shoulder joint).

Detailed distress surveying was conducted along the driving lane where FWD and MIRA testing was performed.

Table 88. US 30 (62277) Detailed Distress Survey Notes (Eastbound)

Stationing	Detailed distress notes
Section 1 (8+00 EB)	
8+22 EB	Minimal to negligible long. faulting along L/S jt. (~0.14 in. [3.5 mm] along Section 1)
8+35 EB	Trans. jt. faulting (~0.4 in. [10 mm])
8+75 EB	End of intensive testing (Section 1)
~10+00 EB	Full panel replacement (Full-depth repair) performed
~20+00 EB	Full panel replacement (Full-depth repair) performed
Section 2 (45+00 EB)	
45+00 EB	Long. cracking between DL and PL (late sawing); tie bars holding crack tight
45+75 EB	End of intensive testing (Section 2)
46+50 to 47+00 EB	Full panel replacement (Full-depth repair) performed
~50+00 EB	Long. cracking in OWP of DL; spanning two panels
~55+00 EB	Full-depth repair performed over jt.
~64+00 EB	Long. cracking in OWP of DL
Section 3 (70+00 EB)	
70+30 EB	Full-depth repair performed (6 ft length and full-lane width)
70+75 EB	Long. cracking between DL and PL (late sawing), tie bars holding crack tight leading to spalling of crack; End of intensive testing (Section 3)
72+00 EB	Long. and transverse cracking; shallow culvert below (cause of cracking)
Section 4 (79+75 EB)	
80+20 EB	No noticeable distress in this section; end of intensive testing (Section 4)
Section 5 (94+90 EB)	
95+65 EB	No noticeable distress in this section; end of intensive testing (Section 5)

Table 89. US 30 (62277) Detailed Distress Survey Notes (Westbound)

Stationing	Detailed distress notes
Section 1 (103+75 WB)	
103+60 WB	Corner distress in PL on LJ along DL/PL long. jt.; transverse jt. is wide ~0.63 in. (16 mm)
103+00 WB	End of intensive testing (Section 1)
Section 2 (90+10 WB)	
89+60 WB	No noticeable distress in this section; End of intensive testing (Section 2)
Section 3 (82+45 WB)	
82+45 WB	Drain opening at beginning of section; Slab A likely constructed over a transverse drain
82+30 WB	Corner distress in PL on AJ (~8 in. radius) along DL/PL long. jt.
81+70 WB	End of intensive testing (Section 3)
Section 4 (70+00 WB)	
69+55 WB	No noticeable distress in this section; end of intensive testing (Section 4)
Section 5 (57+25 WB)	
57+25 WB	Long. cracking (high severity) mid-lane in DL, spanning two panels; faulting (~0.12 in. [3 mm]); Long. jt. wide between DL and PL, Long. faulting (PL>DL)
56+50 WB	End of intensive testing (Section 5)
Section 6 (29+90 WB)	
29+45 WB	Corner distress in PL on AJ (~8 in. radius) along DL/PL long. jt., spanning two panels; end of intensive testing (Section 6)
Section 7 (13+00 WB)	
12+25 WB	Full-depth repair performed at transverse jt.; end of intensive testing (Section 7)

a) Free edge has pooling of water (8+00 EB)

b) Severe long. cracking along long. jt between DL & PL (70+75 EB)

c) Full-depth repair (70+30 EB)

d) Long. cracking mid-slab spanning two panels (72+00 EB)

e) Concrete shows entrapped air

f) Culvert causing cracking in PCC (72+00 EB)

Figure 212. Photos. Distresses observed in US 30 (62277) EB.

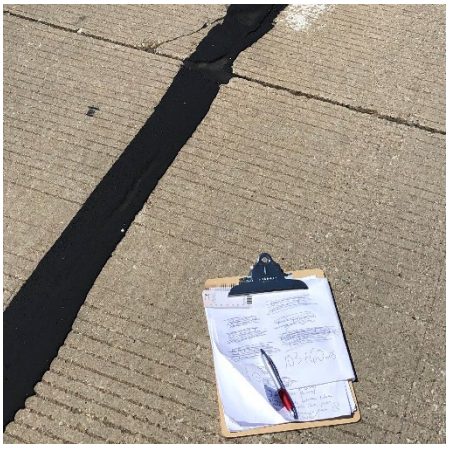

a) Small corner distress w/ wide trans. jt. (103+60 WB)

b) Avoided testing over drain locations

c) Corner distress in PL (82+30 WB)

d) Long. cracking spanning two panels (57+25 WB)

e) Full-depth repairs (12+25 WB)

f) Corner distress in PL (13+15 WB)

Figure 213. Photos. Distresses observed in US 30 (62277) WB.

IL 64 (62410):

Start of the project West end: Smith Rd/Kautz Rd interchange & IL 64 EB

End of the project East: IL 59 interchange (West Chicago, IL) & IL 64 EB

IL 64 – District 1 (DuPage Co.):

- 10-in. JPCP on 4-in. HMA Subbase on 12-in. Aggregate Subgrade
- 15-ft x 12-ft joint spacing with joint sealant
- 3 lanes + inner/outside shoulders (both directions)
- 1.5-in. diameter dowels at 12-in. spacing; #6 tie bars at 24-in. spacing
- Constructed 2012 & 2013

Stationing: 3284+00 to 3412+00 (West to East)

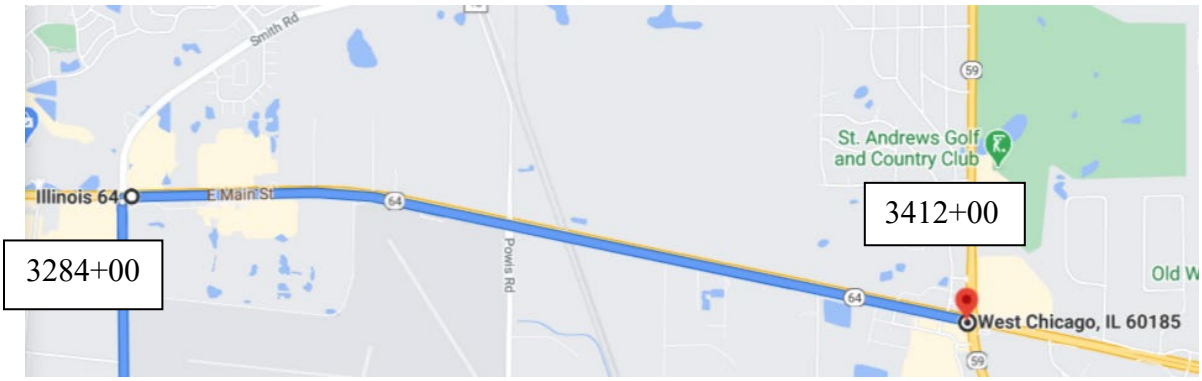

Figure 214. Photo. IL 64 (62410).

IL 64 (62410) Synopsis of Testing – 9/04/2020

General overview of distress observed:

A total of eight testing locations were evaluated with four in the westbound and four in the eastbound directions. Westbound appears to be in very good condition after 8 years of being in-service. There is very minimal cracking throughout the section. However, in general the transverse joint spacing is not consistent and varies from location to location. For instance, six adjacent panels near Test Section WB-4 were 15 ft, 18 ft, 16 ft, 15 ft, 11 ft, and 15 ft. It is not clear why this was conducted but appears to follow designs because dowel bars were located at these joints. The inside shoulder and two passing lanes appear to have been paved together and the driving lane and outside shoulder were paved together at a separate time.

Eastbound also appears to be performing well. Minimal distress was observed. However, signs of low severity cracks are beginning to develop in the eastbound direction. These cracks could potentially be directly over the dowel bars (perpendicular to transverse joints). Diamond grinding was performed and exposed defects in the concrete consolidation near the surface of the pavement. Similar to

westbound, transverse joint spacing varies from location to location and is not a consistent 15 ft joint spacing.

Table 90. IL 64 (62410) Temperature Profile (9/04/2020)

	Temperature @ corresponding depths (ºF)				
Time of measurement	1.5-in. depth	5-in. depth	9-in. depth	Air	UV Index
9:00 am	69	70	71	63	2
11:45 am	84	80	78	73	7
1:30 pm[1]	-	-	-	75	7

[1]Not enough time to be able to take temperature measurements when finishing testing.

MIRA scanning was performed with 35 kHz testing frequency across transverse joints to assess joint activation. All other locations performed with 50 kHz.

Table 91. IL 64 (62410) Intensive Testing Sections and Stationing

Intensive test sections	**Time @ start of section**	**Stationing**	
		Beginning of test section	**End of test section**
WB-1	8:45 am	3411+04	3340+29
WB-2	9:15 am	3375+12	3374+37
WB-3	9:50 am	3337+40	3336+65
WB-4	10:15 am	3299+30	3298+55
EB-1	11:40 am	3289+45	3290+20
EB-2	12:10 pm	3325+56	3326+31
EB-3	1:00 pm[1]	3378+76	3379+51
EB-4	1:30 pm	3405+96	3406+71

[1]Shoulder was covered with loose gravel, obstructing stations along project and took additional time locating testing station.

Test sections consisted of 75 ft, with five adjacent panels and approximately 2,500 ft between testing sections. Detailed distress surveying was conducted along the driving lane where FWD and MIRA testing was performed.

Table 92. IL 64 (62410) Detailed Distress Survey Notes (Westbound)

Stationing	Detailed distress notes: IL 64 (3284+00 to 3412+25)
Section WB-1 (3411+04)	
3411+04	Minor spalling along transverse joints
3411+00	Corner cracking (partial depth pop-out) Leave slab adjacent to L/S longitudinal joint; potential void under leave slab causing cracking
3340+29	End of Section WB-1 intensive FWD testing (No MIRA testing performed)
Section WB-2 (3375+12)	
3375+12 to 3374+37	Slab lengths appear to range between 15 ft +/- 8 in.; causing joint widths to be larger than others within subsection WB-2
3375+27	Transverse joint between slabs A and B is 0.4 in. with mild joint spalling; all other joints in section are 0.25 in. (no spalling)
3374+37	End of Section WB-2 intensive FWD testing and MIRA
Section WB-3 (3337+40)	
3337+40 to 3336+65	Mild joint spalling along the joints
3337+40	Slab A MIRA scan at center (WB-3A-4 (CN)) clearly shows PCC=10 in. and Subbase = 4 in.
3336+65	End of Section WB-3 intensive FWD testing (No MIRA testing performed)
Section WB-4 (3299+30)	
3301+00	Transverse crack over drain; avoided testing over drain
3299+99	Corner distress, joint spalling, and faulting
3299+84	Joint spalling
3299+68	Severe joint damage, very tight joint and potential location of blow-up to develop (late sawcutting – led to crack to develop along trans joint in shoulder)
3298+55	End of Section WB-4 intensive FWD testing and MIRA

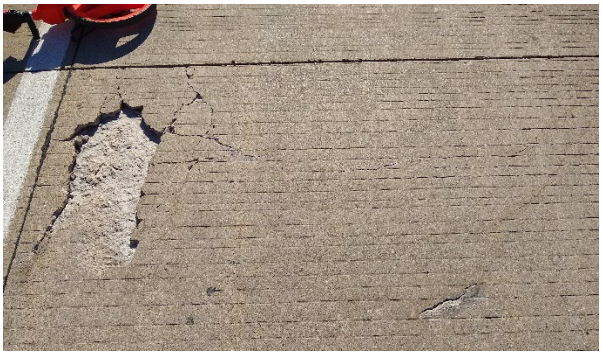

a) Corner distress (partial depth pop-out) (3411+04 WB)

b) Corner failure, joint spalling and faulting in DL and Shoulder – Leave (3299+99 WB)

c) Severe joint damage in DL and Shoulder - Approach (3299+68 WB)

d) Severe joint damage in DL and Shoulder - Approach (3299+68 WB)

Figure 215. Photos. Distress photos within IL 64 (62410) WB.

Table 93. IL 64 (62410) Detailed Distress Survey Notes (Eastbound)

Stationing	Detailed distress notes: IL 64 (3284+00 to 3412+25)
Section EB-1 (3289+45)	
3289+45	Temperature holes drilled and recorded at 11:40 am (1.5 in., 5 in., and 9 in.)
3290+75	Longitudinal impression in OWP of DL from tining machine (see **Figure 216a**)
3290+20	End of Section EB-1 intensive FWD testing and MIRA
Section EB-2 (3325+56)	
3326+31 to 3327+66	Random joint spacing observed (15 ft, 15 ft, 14 ft, 13 ft, 17 ft, 15 ft, 16 ft, and 14.5 ft)
3325+56 to 3326+31	No visible distress observed
3326+31	End of Section EB-2 intensive FWD testing (No MIRA testing performed)
Section EB-3 (3378+76)	
3380+26	Longitudinal cracking in DL on Leave slab near transverse joint; cracking potentially directly over top of dowel bars.
3379+51	End of Section EB-3 intensive FWD testing and MIRA
Section EB-4 (3405+96)	
3405+96 to 3406+71	Diamond grinding performed in the DL; exposing voids in the concrete near the surface (extends longer than intensive Section EB-4)
3405+51	Joint spalling with corner spalling along Approach joint in DL between PL and DL; joint does not have joint sealant (all others do within same section)
3405+96	Poor consolidation in concrete surface – large voids
3407+46	Surface cracking near transverse joint
3406+71 to 3407+31	Random joint spacing observed (15 ft, 11 ft, 16 ft, and 18 ft)
3406+71	End of Section EB-4 intensive FWD testing (No MIRA testing performed)

a) Longitudinal impression in OWP of DL from tining machine (random locations in EB)

b) Longitudinal Cracking in DL on Leave slab near transverse joint (3380+26)

c) Joint spalling with corner spalling along Approach joint in DL (3405+51)

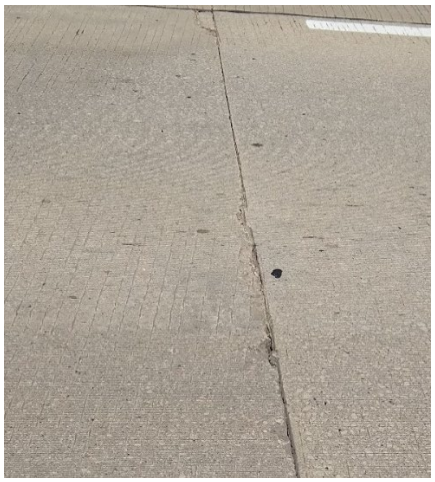

d) Joint spalling with corner spalling along Approach joint in DL (3405+51)

e) Poor consolidation in concrete surface – large voids (3405+96)

f) Surface cracking diamond ground (3407+46)

Figure 216. Photos. Distress photos within IL 64 (62410) EB.

US 12/20/45 (60748 & 60927):

Contract 60748: (1.2 miles = 6,400 ft)
Start of the project South end: 87th street interchange (Justice, IL) & US 12/20/45 NB
End of the project North end: I-294 interchange (Willow Springs, IL) & US 12/20/45 NB

Contract 60927: (2.9 miles = 15,500 ft)
Start of the project South end: 111th street interchange (Justice, IL) & US 12/20/45 NB
End of the project North end: 87th street interchange (Justice, IL) & US 12/20/45 NB

US 12/20/45 (2004) – District 1 (Cook Co.):

- 9.75-in. JPCP on 4-in. HMA subbase
- 15-ft x 12-ft panels (two lanes with 10-ft outside shoulder and 6-ft inside shoulder)
- Good drainage system and design
- Transverse joints:
    - 1.5-in. diameter dowels at 12-in. spacing
    - #6 tie bars at 24 in. spacing
    - 0.25 in. saw cuts with no joint sealant
- Longitudinal joints:
    - 0.5 in. joint widths with hot poured joint sealant (good shape)
- Stationing: 216+00 to 280+00 (South to North) – 60748
- Stationing: 60+00 to 212+00 (South to North) – 60927

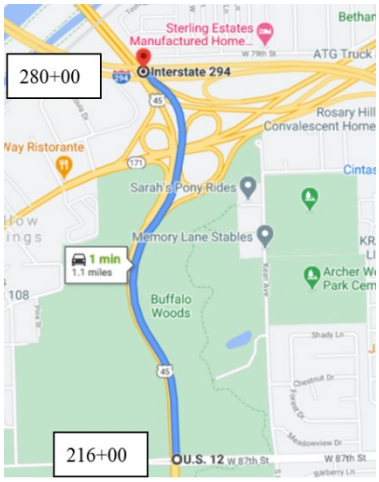

Figure 217. US 12/20/45 (60748 & 60927).

US 12/20/45 (60748 & 60927) Synopsis of Testing – 09/03/2020

General overview of distress observed:

A total of eight testing locations were evaluated with five in the southbound direction and three in the northbound direction. Northbound was down to a single lane near the start of the project and restricted testing to be conducted along with time constraints. Southbound is performing very well with minimal distress. Northbound is also performing very well and minimal distress was observed.

Figure 218. Photo. US 12/20/45 (60748 & 60927) FWD testing operations.

Table 94. US 12/20/45 (60748 & 60927) Temperature Profile (9/3/2020)

	Temperature @ corresponding depths (°F)				
Time of measurement	1.5-in. depth	5-in. depth	9-in. depth	Air	UV Index
8:30 am	72	72	72	69	1
1:00 pm	98	93	91	86	7
2:30 pm[1]	-	-	-	88	7

[1]Not enough time to be able to take temperature measurements when finishing testing.

MIRA scanning was performed with 35 kHz testing frequency across transverse joints to assess joint activation. All other locations performed with 50 kHz. Transverse joint widths were 0.25 in. with approximate depths of 2.5 in. (information used in ultrasonic joint activation algorithm).

Table 95. US 12/20/45 (60748 & 60927) Testing Sections and Stationing

Intensive test sections	**Time @ start of section**	**Stationing**	
		Beginning of test section	**End of test section**
SB-1	7:45 am	277+82	276+00
SB-2	9:30 am	235+04	234+00
SB-3	10:00 am	200+08	199+00
SB-4	10:30 am	150+45	149+00
SB-5	11:00 am	100+00	99+00
NB-1	11:00 am	74+73	76+00
NB-2	12:00 pm	124+56	126+00
NB-3	12:30 pm	181+00	182+00

Test sections consisted of approximately 75 ft, with five adjacent panels. Detailed distress surveying was conducted along the Driving Lane where FWD and MIRA testing was performed.

Table 96. US 12/20/45 (60748 & 60927) Detailed Distress Survey Notes (Southbound)

Stationing	Detailed distress notes: Section US 12/20/45 SB (280+00 to 60+00)
Section SB-1 (277+82)	
277+82 to 276+00	Transverse joints not sealed, longitudinal joints sealed and in good condition; Longitudinal joint faulting between shoulder and DL (0.2 in.: Shoulder > DL) for all panels within Section SB-1 likely construction related; Rebound Index in DL between 6-7.2 ksi
277+82	Temperature holes drilled at 1.5 in., 5 in., and 9 in. depths
276+00	End of Section SB-1 intensive FWD and MIRA testing
Section SB-2 (235+04)	
235+04	Minor spalling on longitudinal construction joint between DL and shoulder
234+47	Grinding performed on pavement surface; corner spalling (6-in. radius) in PL along PL/DL longitudinal joint on approach and leave joints
234+59	Joint 2D-5 is wider than the other joints in SB-2 (~0.43 in.)
234+00	End of Section SB-2 intensive FWD testing and MIRA testing
Section SB-3 (200+08)	
200+08 to 199+00	Minor longitudinal faulting between shoulder and DL (+/- 0.2 in.: Shoulder > DL) – likely construction related
199+50	Minor transverse joint spalling in DL; no faulting
199+00	End of Section SB-3 intensive FWD and MIRA testing
Section SB-4 (150+45)	
150+45 to 149+00	Minor corner failures (< 1-in. radius) throughout Section SB-4 between PL and DL longitudinal joint
125+00	Longitudinal crack (mid-panel) in DL spanning three consecutive panels outside of intensive testing section near 125+00
149+00	End of Section SB-4 intensive FWD (No MIRA testing performed)
Section SB-5 (100+00)	
100+00 to 99+00	No observed distress in Section SB-5; Rebound Index in DL between 6-7.2 ksi
99+65	Maintenance hole in shoulder and possible drain under Panel C
99+00	End of Section SB-5 intensive FWD (No MIRA testing performed)

a) Long. joint faulting: Shoulder > DL (0.2 in.) – (277+82 to 276+00 SB)

b) Transverse and Longitudinal joints performing well (276+20)

c) Corner distress and diamond grinding (234+47 SB)

d) Transverse joint spalling (199+50 SB)

e) Minor corner spalling (150+45 to 149+00 SB)

f) Maintenance hole along shoulder (99+65 SB)

Figure 219. Photos. Distress photos within Section US 12/20/45 (60748 & 60927) SB.

Table 97. US 12/20/45 (60927) Detailed Distress Survey Notes (Northbound)

Stationing	Detailed distress notes: Section US 12/20/45 NB (60+00 to 280+00)
Section NB-1 (74+73)	
74+73	Temperature holes drilled at 1.5-in., 5-in., and 9-in. depths; Rebound Index in Shoulder was between 4.5-6 ksi
76+00	End of Section NB-1 intensive FWD and MIRA testing
Section NB-2 (124+56)	
124+56 to 126+00	No visual distress observed – section performing well
126+00	End of Section NB-2 intensive FWD testing (No MIRA testing performed)
Section NB-3 (181+00)	
181+00 to 182+00	Distress rooting from embedded raised pavement markers (multiple locations)
180+45	Corner failure along approach joint in DL between DL and shoulder
180+90	Raveling on concrete surface in DL (~3 ft^2)
181+55	Severe corner break with HMA patch in PL on Approach and Leave
182+00	End of Section NB-3 intensive FWD and MIRA testing

a) Testing Section NB-1 (74+73 NB)

b) Testing Section NB-2 (124+56 NB)

c) Corner distress along approach joint in DL (180+45 NB)

d) Ravelling on concrete surface in DL (180+90 NB)

e) Corner break with HMA patch in PL on Approach and Leave (181+55 NB)

f) Distress from embedded raised pavement markers (multiple locations)

Figure 220. Photos. Distress photos within US 12/20/45 (60927) NB.

I-72 (CONTRACT 72G92):

I-72, east of Springfield (from 0.48 miles east of Overpass Rd to 0.15 miles east of Dawson Road overpass) (STA 0+00 to 171+09)

I-72 EB – District 6 (Sangamon Co.):

- 6.0-in. JPCP on 1.25-in. HMA interlayer on 8-in. CRCP

I-72 WB – District 6 (Sangamon Co.):

- 6.0 in. JPCP on 0.125 in. non-woven geotextile fabric interlayer on 8-in. CRCP

- 6-ft x 6-ft panels (two lanes with 10-ft outside shoulder and 6-ft inside shoulder)
- Transverse joints:
    - Undoweled
    - 0.125-0.250 in. wide saw cuts to 1.50 in. depth with no joint sealant
    - #4 x 24 in. tie bars at 15 in. spacing at construction joints only (end of a day's paving)
- Longitudinal joints:
    - 0.125-0.250 in. wide saw cuts to 1.50 in. depth with no joint sealant
    - #4 x 24 in. tie bars at 36 in. spacing at construction joints only (centerline) with hot poured joint sealer
- Constructed 2015

Test sections - EB:

- 10+00 to 20+00, 74+15 to 84+15, 142+50 to 152+50

Test sections - WB:

- 10+00 to 20+00, 102+50 to 112+50, 142+50 to 152+50

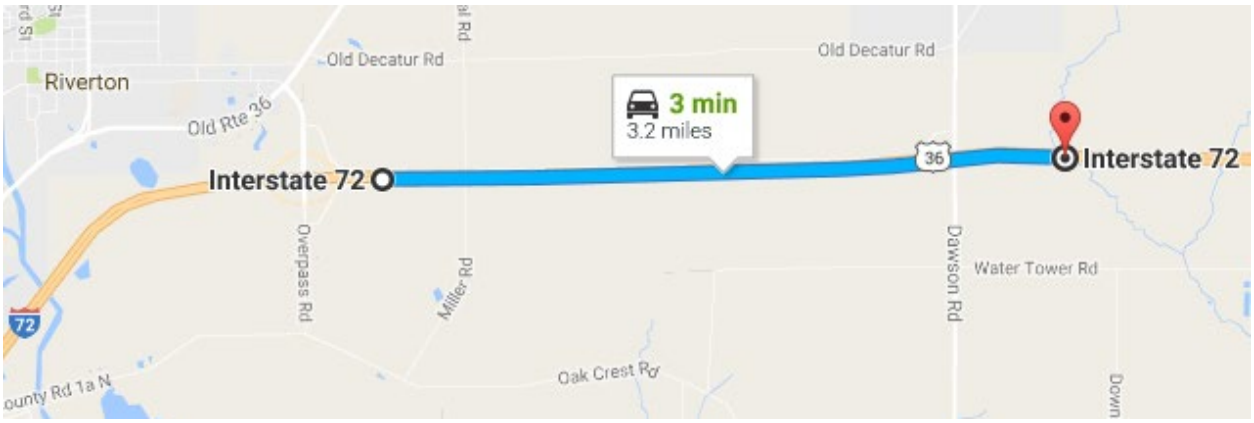

Figure 221. I-72 (72G92).

I-72 (72G92) Synopsis of Testing – 08/05-06/2020

*Synopsis of distress in **Eastbound** (HMA interlayer):*

- The prominent distress in the eastbound direction was longitudinal cracks in the wheel paths of the driving lane (each panel). On average, cracks appear to be 2 ft in length on each panel and a total of 4 ft across transverse joints. Longitudinal cracking spanning a full slab or greater was not observed. Approximately 30 locations had longitudinal cracking occurring across the transverse joint (tested two sections of 1,000 ft and 3rd section of 100 ft). This distress has been commonly seen in UBOL with HMA interlayers (Alland et al. 2016 and Souder et al. 2020). One possible mechanism for this distress is permanent deformation in the HMA layer (densification or shear flow) resulting in a void, gap, or settlement beneath the PCC in the wheel path. As traffic accumulates the deformation or gap increases, resulting in an increase in the tensile stress at the bottom of the PCC and eventually leads to a bottom-up crack to develop if the flexural stiffness and strength of concrete is not sufficiently high (See **Figure 222c** below). With the lower vertical pressure reaching the HMA interlayer, this mechanism is less likely. The vertical pressure on the interlayer is likely less than 25 psi if the joint is ignored.

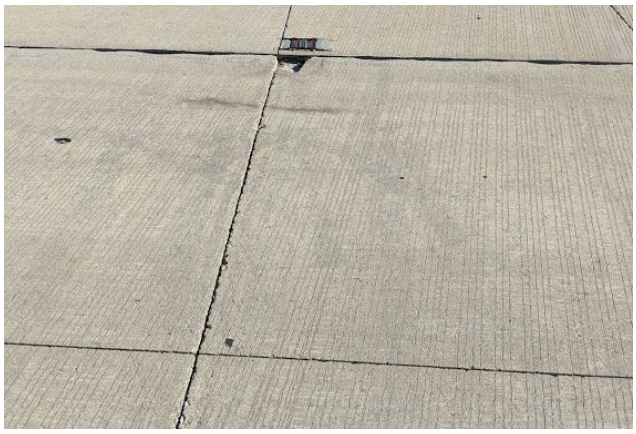

a) Long. cracking in the inner wheel path

b) Long. cracking in both wheel path (inner and outer)

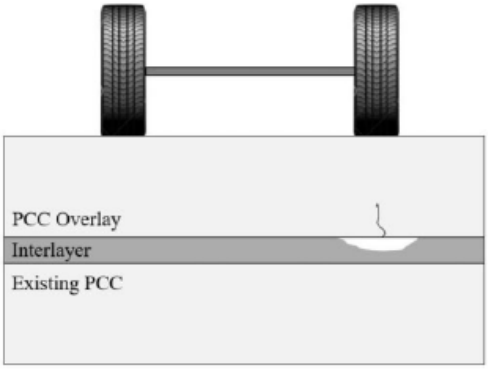

c) Hypothetic mechanism of permanent deformation in HMA resulting in 1D densification or shearing that enables tensile crack to initiate at bottom of PCC overlay

Figure 222. Unbonded short jointed concrete overlay on HMA interlayer.

a) Length of long. crack (approx. 4 ft across the trans. jt.)

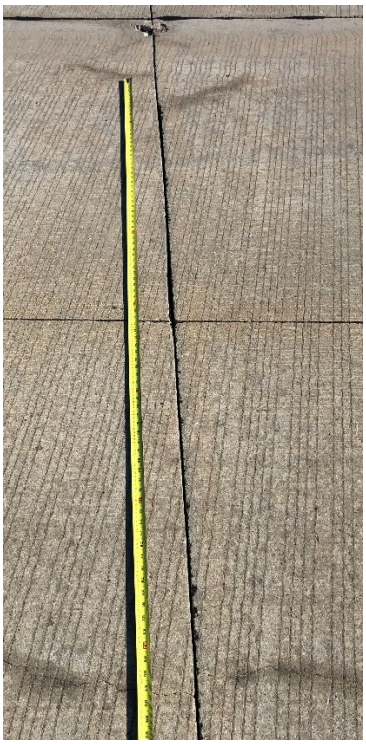

b) Distance between long. cracks at the trans. jt. (approx. 7.5-8 ft)

Figure 223. Photos. Distress photos of longitudinal cracking in I-72 (72G92) EB.

- Proper compaction of the HMA interlayer is still very important, even though it is not the surface layer. This mixture was tested under the HWTD to check rutting and stripping potential prior to construction. The HMA interlayer passed the required 7,500 load cycles without exhibiting deformation levels greater than 0.5 in. However, coring performed in 2021 showed evidence of stripping and erosion.

- There are several proposed ways to mitigate this potential distress mechanism, which are not verified yet. Increasing the thickness of the concrete overlay will decrease the stress on the interlayer, and therefore decrease the risk of degradation and/or consolidation. Reducing differential deflections and minimize any potential water pressure by using load transfer devices may be helpful. Finally, using an interlayer system which is not prone to consolidation or stripping, will help minimize this distress as well (Alland et al. 2016).

- To assess and confirm this is occurring, the design information and mixture designs can be used into the newly developed permanent deformation of HMA interlayers model for UBOL (Souder et al. 2020). In addition, cores can be taken from the HMA interlayer to assess the density of the HMA in the wheel path versus mid-lane where the HMA is less trafficked. However, coring performed in 2021 showed evidence of stripping and erosion.

- At the project start on the westbound, the left panel in the driving lane is shattered. This is likely from the construction process when starting the UBOL versus the existing HMA surface layer. This panel needs to be replaced with a full-depth repair.

Figure 224. Photo. Distress photos of shattered slab in I-72 (72G92) EB.

- Clumping of the fibers were observed once. It appears the mixing was done very well and fibers were distributed evenly throughout concrete material production and construction.

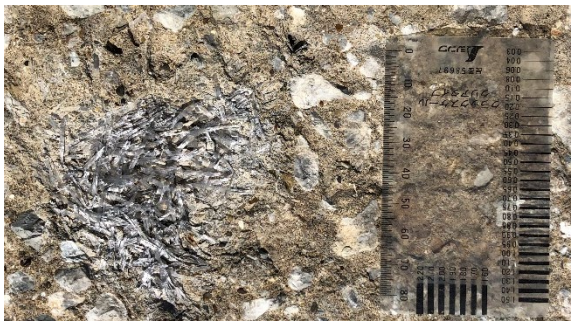

Figure 225. Photos. Clumping of fibers in I-72 (72G92) EB.

*Synopsis of distress in **Westbound** (Non-woven Geotextile Fabric interlayer):*

- No longitudinal cracking is observed like was seen in eastbound driving lane. The main observation made from the westbound lane was a difference in elevation across the lane/shoulder joint in the outer wheel path. This difference in elevation was consistent along the test section, with an average difference of 0.16 in. (4 mm). There are two possible hypotheses behind this observation.
    1. The fabric interlayer in the driving lane has been vertically compressed from the truck traffic in addition to slab's self-weight, whereas no traffic is occurring on the shoulder and the fabric is only compressed due to slab's self-weight
    2. There is a cross-slope change between the driving lane and outside shoulder, and it is possible that the shoulders have separated from the mainline since there are no tie bars at that joint. This joint was observed to be wider than the initial 0.25 in. (6.4 mm) longitudinal saw cut. It seems that it is also possible that it is a combination of these two potential reasons, such that the heavy truck traffic

compresses the fabric in the driving lane and not in the shoulder (assumes fabric is continuous across the lane/shoulder joint). The compressed driving lane fabric settles slightly relatively to the shoulder. There may be some upheaval in the shoulder as well but only coring may determine this.

- Without incompressible fines getting in the joint or under the shoulder slab, this difference in elevation should not increase because there is a maximum compression thickness of the fabric interlayer. In addition, the macrofibers in the concrete are engaged and should be contributing to keeping the joint together. However, if differential movement is too high then joint width across the lane/shoulder joint increases and macrofibers are less effective.
- If this joint had a steel tie bar, the separation and differential elevation may have been limited and potentially negated or if displacement large enough this could lead to cracking and spalling. It is likely that separation would have occurred along the longitudinal joint within the driving lane (6 ft offset from shoulder). There is a construction joint between the passing and driving lane with steel tie bars. This joint was still remaining tight.

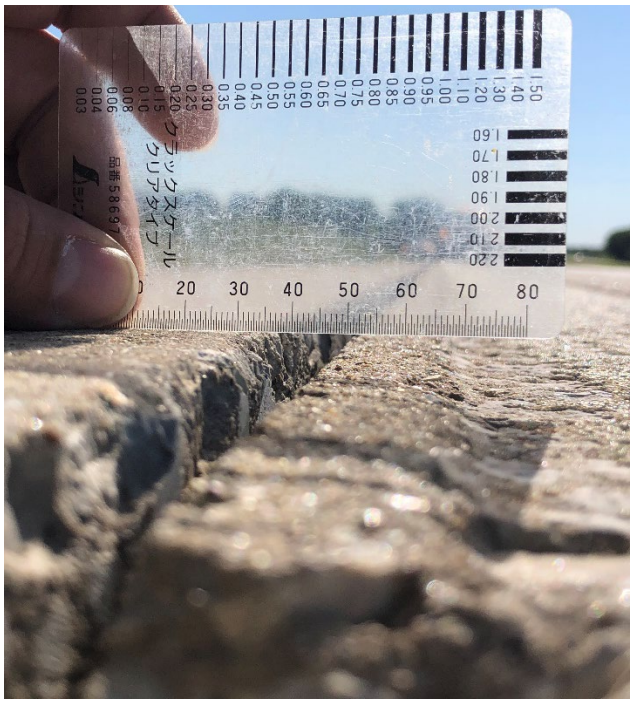

a) Lane/shoulder jt. elevation difference (shoulder = approx. 0.16 in [4 mm] higher than driving lane)

b) Potential distress occurring from elevation difference

Figure 226. Photos. Distress photos of longitudinal faulting in I-72 (72G92) WB.

- Corner distress is also occurring on the leave joint in the driving lane along the driving lane and passing lane longitudinal joint. It appears to be a form of chipping or spalling with a radius of 4 in. This is really the only distress being observed; approximately seven corner spalls observed over the three 1,000 ft test sections.

a) Corner distress on leave joint left panel in driving lane

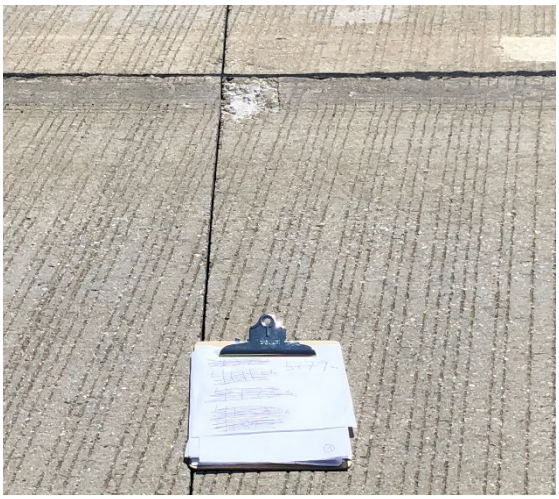

b) Corner distress on leave joint left panel in driving lane

Figure 227. Photos. Distress photos of corner spalling in I-72 (72G92) WB.

Both directions:

- All approach slabs have the distress shown in the figure below. It appears the milling head grinding performed for the rumble strips near the lane/shoulder joint, where the lane marking was painted, resulted in taking a chunk out of the approach slab. This can result in small corner spalls to eventually occur.

a) Milling of rumble strips effect on approach joint spalling

b) Milling of rumble strips effect on approach joint causing corner distress

c) Milling of rumble strips effect on leave joint corner distress

Figure 228. Photos. Distress photos of improper milling on I-72 (72G92) EB and WB.

Table 98. I-72 (72G92) Temperature Profile for Eastbound (8/5/2020)

	Temperature @ corresponding depths (°F)		
Time of measurement	1.5-in. depth	3-in. depth	5.5-in. depth
8:45 am	72	73	78
1:00 pm	93	90	82
2:45 pm[1]	96	95	95

[1]Temperature readings are possibly erroneous due to operating errors.

Table 99. I-72 (72G92) Temperature Profile for Westbound (8/6/2020)

	Temperature @ corresponding depths (°F)		
Time of measurement	1.5-in. depth	3-in. depth	5.5-in. depth
8:30 am	67	68	70
1:00 pm	88	86	81
2:45 pm[1]	98	95	95

[1]Temperature readings are possibly erroneous due to operating errors.

MIRA scanning was performed with 50 kHz testing frequency across transverse joints to assess joint activation (Optimal testing frequency is 35 kHz). All other locations performed with 50 kHz. During field surveying, majority of joints appeared activated and working. Joint conditions were clear to be able to determine if the joint activated/cracked or not by looking into the joint (both westbound and eastbound). This was not expected for the westbound with the fabric IL because of the low level of friction it provides. However, this is a good result.

Table 100. I-72 (72G92) Testing Sections and Stationing

Intensive test sections	**Time @ start of section**	**Stationing**	
		Beginning of test section	**End of test section**
1 EB	8:45 am	10+00	20+00
2 EB	10:15 am	74+15	84+15
3 EB	12:45 pm	142+50	152+50
1 WB	8:30 am	152+50	142+50
2 WB	10:00 am	112+50	102+50
3 WB	1:00 pm	20+00	10+00

Test sections consisted of 1000 ft, with the first 90 ft consisting of 15 adjacent panels and then every 100 ft was tested. Test Sections 1 and 2 on eastbound were tested in full, however time only permitted Section 3 to include the 15 consecutive panels to be tested and not the additional nine locations spaced at 100 ft within the 1,000 ft section. All three sections in the westbound direction were tested in full.

Detailed distress surveying was conducted along the driving lane where FWD and MIRA testing was performed.

Table 101. I-72 (72G92) Detailed Distress Survey Notes (Eastbound)

Stationing	Detailed distress notes
Section 1 (10+00 EB)	
9+38	Long. crack DL outer wheel path (OWP) across trans. jt.; corner spall approach jt. along long. jt. between DL/PL
11+08	Long. crack DL OWP and inside wheel path (IWP) across trans. jt.
11+43	Long. crack DL OWP and IWP across trans. jt. (~0.02 in. [0.45 mm] width)
11+80	Long. crack DL OWP across trans. jt.
11+97	Long. crack DL OWP and IWP across trans. jt. (~0.016 in. [0.40 mm] width)
12+46	Long. crack DL OWP across trans. jt.
12+58	Long. crack DL OWP across trans. jt.
12+94	Long. crack DL OWP across trans. jt.; corner spall approach jt. along long. jt. between DL/PL
13+54	Long. crack DL OWP and IWP across trans. jt. (~0.014 in. [0.35 mm] width)
14+02	Long. crack DL OWP and IWP across trans. jt.; corner spall approach jt. along long. jt. between DL/PL
14+32	Long. crack DL OWP across trans. jt.
14+68	Long. crack DL OWP across trans. jt.
15+04	Long. crack DL OWP across trans. jt.
15+35	Long. crack DL OWP and IWP across trans. jt. (~0.012 in. [0.30 mm] width)
15+47	Long. crack DL OWP across trans. jt.
15+95	Long. crack DL OWP across trans. jt.
16+30	Long. crack DL OWP across trans. jt.
16+49	Trans. jt. spalling
16+54	Long. crack DL OWP across trans. jt.
16+84	Long. crack DL OWP across trans. jt.
17+32	Long. crack DL OWP and IWP across trans. jt.
18+04	Long. crack DL OWP and IWP across trans. jt. (~0.016 in. [0.40 mm] width)
18+35	Long. crack DL OWP across trans. jt.
18+47	Long. crack DL OWP across trans. jt.
18+59	Long. crack DL OWP across trans. jt.
18+72	Long. crack DL OWP across trans. jt.; corner spalling L/S long. jt.
18+84	Long. crack DL OWP and IWP across trans. jt.
19+08	Long. crack DL OWP across trans. jt.
19+44	Long. crack DL OWP and IWP across trans. jt.
19+99	Long. crack DL OWP across trans. jt.; end of Section 1 (20+00)
Section 2 (74+15 EB)	
74+63	Long. crack DL IWP across trans. jt.
75+18	Long. crack DL IWP across trans. jt.
75+36	Long. crack DL IWP across trans. jt.
78+85	Long. crack DL IWP across trans. jt.
80+60	Spalling/ raveling along trans. jt.
84+15	End of EB Section 2

Stationing	Detailed distress notes
Section 3 (142+50 EB) – 5/13/2021	
142+50-150+00	Longitudinal faulting: Shoulder elevation > driving lane; spanning entire section; ~0.5 in. difference in elevation
143+10	Long. crack DL IWP across trans. jt. (observed in 2020 survey)
143+47	Long. crack DL IWP across trans. jt.
143+50	End of FWD testing for EB Section 3
143+89	Excessive joint width from saw cut
144+24	Long. crack DL IWP across trans. jt. (observed in 2020 survey)
144+60	Long. crack DL IWP across trans. jt. (observed in 2020 survey)
145+72	Drain outlet location along shoulder edge; standing water pooling
145+86	Long. crack DL IWP at trans. jt. (observed in 2020 survey); Leave slab only
146+00	2020 distress survey ends due to time constraints
146+26	Long. crack DL IWP across trans. jt.
146+99	Long. crack DL IWP across trans. jt.
147+44	Long. crack DL IWP across trans. jt.
147+60	Long. crack DL IWP across trans. jt.
148+15	Long. crack DL IWP across trans. jt.
149+23	Long. crack DL IWP across trans. jt.; not connected across joint
149+71	Long. crack DL IWP across trans. jt.
150+25	Long. crack DL IWP across trans. jt.; not connected across joint
150+80	Long. crack DL OWP at trans. jt.; Leave slab only (~6 in.)
151+33	Long. crack DL OWP at trans. jt.; Leave slab only (~6 in.)
152+06	Long. crack DL IWP across trans. jt.
152+24	Long. crack DL IWP across trans. jt.; not connected across joint
152+43	Long. crack DL IWP across trans. jt.; not connected across joint

Table 102. I-72 (72G92) Detailed Distress Survey Notes (Westbound)

Stationing	Detailed distress notes
Section 1 (152+50 WB)	
151+29	Corner distress leave slab along long. jt. between DL/PL (~4-in. radius)
149+85	Corner distress leave slab along long. jt. between DL/PL (~4-in. radius)
148+34	Corner distress leave slab along long. jt. between DL/PL (~4-in. radius)
142+50	End of WB Section 1
Section 2 (112+50 WB)	
109+68	Corner distress leave slab along long. jt. between DL/PL (~4-in. radius)
108+05	Corner distress leave slab along long. jt. between DL/PL (~3-in. radius)
106+71	Corner distress leave slab along long. jt. between DL/PL (~1.5-in. radius)
102+80	Corner distress leave slab along long. jt. between DL/PL (~4-in. radius)
102+50	End of WB Section 2
Section 3 (20+00 WB)	
19+69	Corner distress leave slab along long. jt. between DL/PL (~4-in. radius)
16+61	Poor finishing of concrete surface across DL right edge panels
15+89	Corner distress and chip leave slab along long. jt. between DL/PL (~5-in. radius)
15+77	Corner distress and chip leave slab along L/S long. jt.
15+47	Corner distress and chip leave slab along long. jt. between DL/PL (~8-in. radius)
15+11	Corner distress and chip leave slab along long. jt. between DL/PL (~6-in. radius)
14+21	Corner distress and chip leave slab along long. jt. between DL/PL
13+01	Corner distress and chip leave slab along long. jt. between DL/PL
12+58	Corner distress and chip leave slab along long. jt. between DL/PL (~6-in. radius)
10+00	End of WB Section 3

I-70 (70044):

Start of the project West end: West of Township Road 107 & I-70

End of the project East: IL/IN state line & I-70

I-70 – District 7 (Clark Co. 70044):

- 12-in. CRCP on nominal 5 in. HMA on 8-in. existing CRCP (Unbonded concrete overlay)
    - HMA was existing overlays (7-8 in.) and milled prior to placing CRCP overlay
- Joint sealant in longitudinal joints
- Two (12 ft) lanes + inner (8 ft)/outside (12 ft) shoulders (both directions)
    - Shoulders consisted of 12 in. non-reinforced concrete with 20-ft joint spacing
- Longitudinal steel: #7 epoxy-coated bars, 25 bars at 6.25 in. centers, 0.8% steel
- Transverse steel: #4 epoxy-coated bars at 2-ft intervals, placed below longitudinal steel
- Nominal top cover of 4 in.
- Constructed in 2002
- Stationing: 17.92 to 27.38 (West to East)
    - 1592+50 to 1620+00, 147+50 to 556+00 (all continuous and same project)

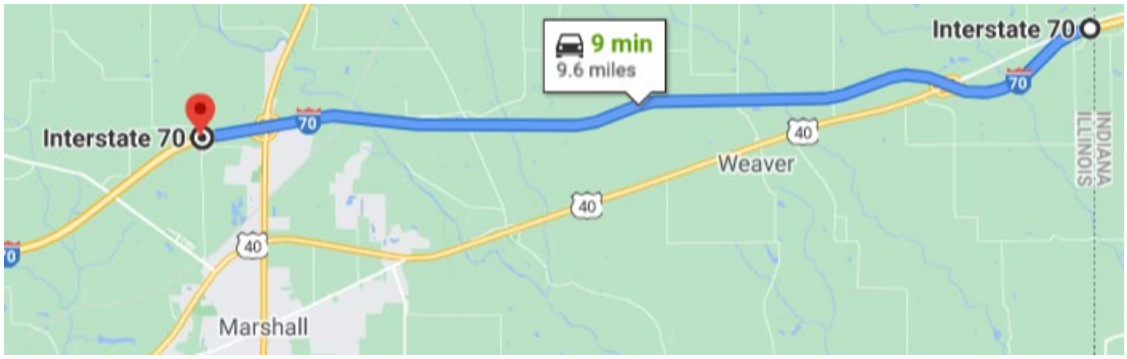

Figure 229. I-70 (70044).

I-70 (70044) Synopsis of Testing – 09/14/2020

General overview of distress observed:

A total of 10 testing locations were evaluated with five in the westbound and five in the eastbound directions. A different FWD driver than the initial sections was on hand and was able to complete all required testing in a timely manner. This section is a continuously reinforced concrete pavement (CRCP) which altered the testing procedure. The stationing was confusing and testing was performed based on mile postings (MP). The shoulders consisted of 20x12 ft tied concrete shoulders with sawed transverse joints. Transverse cracks in the driving lane tend to run parallel to the transverse joints in the shoulder. In general, the majority of cracks are developing over the tie bars between the shoulder and driving lane longitudinal joint. Additionally, if the transverse cracks do not run parallel to the transverse joints in the shoulder, they run parallel or along the transverse tining. The weather was clear throughout the day.

The eastbound direction was tested and surveyed first. The different test sections contained y-cracking, divided cracks, cluster cracking (tightly spaced transverse cracks), and punchouts (some with HMA patches and others that need to be repaired). There has been a lot of diamond grinding performed throughout the eastbound direction with the majority being in the wheel paths of the driving and passing lanes. Some of the test sections were performing better than others regarding the number of y-cracks and divided cracks that could potentially result in punchouts; but in general, everything was performing the same.

The westbound direction was tested in the afternoon with five testing sections. Similar to the eastbound direction, the different westbound sections contained y-cracking, divided cracks, cluster cracking (tightly spaced transverse cracks), and punchouts (some with HMA patches and others that need to be repaired). The westbound seemed to have fewer punchouts than the eastbound direction. Test sections WB-4 and WB-5 were performing better than the other test sections in terms of less Y-cracking and divided cracks that could potentially result in punchouts.

Table 103. I-70 (70044) Temperature Profile (9/14/2020)

	Temperature @ corresponding depths (°F)				
Time of measurement	1.5-in. depth	6-in. depth	11-in. depth	Air	UV Index
8:40 am	68	69	73	68	2
12:30 pm	87	81	79	79	7
2:00 pm[1]	-	-	-	81	7

[1]Temperature holes were not drilled, ran out of time based on traffic control. Weather was consistent in afternoon.

Test sections consisted of approximately 100 ft and approximately 11,000 ft between testing sections. MIRA scanning was performed to determine layer thickness and steel reinforcement details (depth and spacing).

Table 104. I-70 (70044) Testing Sections and Stationing

Intensive test sections	Time @ start of section	Stationing	
		Beginning of test section	End of test section
EB-1	8:30 am	146+00 (MP 148)	147+00 (MP 148)
EB-2	9:00 am	249+75 (MP 150)	250+75 (MP 150)
EB-3	9:40 am	357+50 (MP 152)	358+50 (MP 152)
EB-4	10:15 am	464+00 (MP 154)	465+00 (MP 154)
EB-5	10:45 am	514+00 (MP 155)	515+00 (MP 155)
WB-1	12:00 pm	515+00 (MP 155)	514+00 (MP 155)
WB-2	12:30 pm	410+00 (MP 153)	409+00 (MP 153)
WB-3	1:00 pm	304+00 (MP 151)	303+00 (MP 151)
WB-4	1:30 pm	197+50 (MP 149)	196+50 (MP 149)
WB-5	2:00 pm	1652+50 (MP 147)	1651+50 (MP 147)

[1]NB-5 was conducted in the afternoon due to the meeting location of traffic control in the morning.

Detailed distress surveying was conducted along the driving lane where FWD and MIRA testing was performed.

Table 105. I-70 (70044) Detailed Distress Survey Notes (Eastbound)

Stationing	Detailed distress notes: I-70 EB (MP 146 to MP 155)
Section EB-1 (146+00: MP 148)	
146+00	Temperature holes drilled and recorded at 8:30 am (1.5 in., 6 in., and 11 in.);
146+65	Spalling along transverse crack
146+86	Y-crack
147+00	Y-crack; End of Section EB-1 intensive FWD testing (No MIRA testing performed)
147+46	Y-crack
147+84	Y-crack across shoulder
148+04	Cluster cracking
148+26	Y-crack
149+45	Y-crack
150+07	Y-crack across DL into PL
165+00	Two punchouts near 165+00
Section EB-2 (249+75: MP 150)	
247+08	Divided crack
247+15	Complex Y-cracking and cluster cracking
247+35	Punchout along DL/Shoulder longitudinal joint
247+54	Complex Y-cracking
247+88	Y-crack
247+94	Y-crack; potential punchout location
247+95	Y-crack; potential punchout location
248+12	Y-crack
248+34	Y-crack

Stationing	Detailed distress notes: I-70 EB (MP 146 to MP 155)
248+40	Y-cracking cluster
248+44	Y-crack
248+51	Y-cracking cluster
248+57	Y-crack
248+93	Y-crack
249+15	Y-cracks
249+56	Y-crack and Divided crack; potential punchout location
249+72	Divided crack
259+75	End of Section EB-2 intensive FWD testing (No MIRA testing performed)
Section EB-3 (357+50: MP 152)	
355+00	Y-crack
355+39	Y-crack and close cluster cracking
355+46	Y-crack
355+80	Y-crack and cluster cracking
356+04	Y-crack
356+61	Y-crack and close cluster cracking
356+79	Y-crack
356+84	Y-crack in PL
356+99	Y-crack
357+03	Y-crack
357+22	Y-crack
357+26	Y-crack
357+44	Y-crack
358+50	End of Section EB-3 intensive FWD testing (No MIRA testing performed)
Section EB-4 (467+50: MP 154)	
463+73	Y-crack
463+92	Y-crack
464+59	Y-crack
464+73	Y-crack
464+80	Y-crack and cluster Y-cracking
464+88	HMA Patch over punch-out; HMA patch has deformed
465+54	Y-crack
465+88	Y-crack
466+76	Y-crack
466+87	Complex Y-crack
468+50	End of Section EB-4 intensive FWD testing (No MIRA testing performed)
Section EB-5 (515+00: MP 155)	
512+50	Start of distress survey
513+34	Y-crack
513+37	Y-crack and cluster Y-cracking
513+57	Y-crack
513+70	Construction flaw between DL and shoulder
514+56	Complex Y-crack and cluster cracking
514+98	Y-crack
516+00	End of Section EB-5 intensive FWD testing (No MIRA testing performed)

a) Y-crack (147+46 EB)

b) Punchout filled with HMA patch (247+35 EB)

c) Y-cracking and cluster cracking (248+40 EB)

d) Y + Divided cracking (249+56 EB)

e) HMA Patch over punch-out (464+88 EB)

f) Construction flaw between DL and shoulder (513+70 EB)

Figure 230. Photos. Distress photos within I-70 (70044) EB.

Table 106. I-70 (70044) Detailed Distress Survey Notes (Westbound)

Stationing	Detailed distress notes: I-70 WB (MP 155 to MP 146)
Section WB-1 (515+00: MP 155)	
517+50	Start of distress survey
517+33	Complex Y-crack
517+02	Y-crack
516+97	Y-crack
516+93	Y-crack
516+80	Y-crack
516+60	Y-crack
516+38	Y-crack
516+30	Divided crack
516+19	Complex Y-crack
516+79	Y-crack
516+62	Complex Y-crack
516+35	Y-crack
516+07	Y-crack
515+00	Temperature holes drilled and recorded at 12:15 pm (1.5 in., 6 in., and 11 in.); Y-crack
514+00	End of Section WB-1 intensive FWD testing (No MIRA testing performed)
Section WB-2 (410+00: MP 153)	
412+50	Start of distress survey; A combination of Y-cracking and Divided cracking with cracking initiating over tie bars between the DL and shoulder longitudinal joint
412+48	Y-crack
412+40	Y-crack
412+25	Y-crack
412+21	Y-crack
411+90	Y-crack and Divided crack
411+73	Y-crack and Divided crack
411+55	Complex Y-crack
411+49	Complex Y-crack; potential punchout location
411+45	Complex Y-crack
411+28	Complex Y-crack; potential punchout location
411+08	Y-crack
410+88	Complex Y-crack
410+31	Complex Y-crack
410+27	Complex Y-crack
410+10	Y-crack and Divided crack
410+00	End of distress survey
409+98	Small punchout from Divided crack with HMA patch
409+96	Y-crack developing over tie bars between shoulder and DL; potential punchout location
409+80	Reflector damage and Divided cracking
409+00	End of Section WB-2 intensive FWD testing and MIRA

Section WB-3 (304+00: MP 151)	
307+15 to 303+00	Distress survey performed on end of paving section instead of across different days of construction and to avoid the construction joint; FWD testing also avoided this construction joint and tested the CRCP cast on 9/4/2002; This section contained a lot of Y-cracking and Divided cracks with cracks developing over top of the tie bars between the DL and shoulder longitudinal joint; transverse cracking in shoulder is likely due to poor joint activation of adjacent joint (very tight and does not appear to be a working joint).
307+15	Start of distress survey
307+11	Y-crack
306+89	Y-crack
306+77	Y-crack
306+53	Y-crack
306+33	Y-crack
306+13	Y-crack
306+07	Complex Y-cracking
305+95	Y-crack and Divided cracking
305+90	Y-crack
305+70	Y-crack
305+53	Y-crack
305+30	Y-crack
305+15	Y-crack
305+12	Y-crack
304+94	Y-crack
304+72	Cluster cracking
304+67	Complex Y-cracking
304+55	Y-crack
304+50	Y-crack
304+46	Y-crack
304+36	Y-crack
304+32	Y-crack
304+30	Y-crack
304+00	Construction joint; End of distress survey
303+50	Y-cracking and complex Y-cracking
303+00	End of Section WB-3 intensive FWD testing (No MIRA testing performed)
Section WB-4 (197+50: MP 149)	
200+00 to 196+50	Appears to not have nearly as many Y-cracks or Divided cracks as Section WB-2 and WB-3; Testing section was on an upward slope with good drainage system
200+00	Start of distress survey
199+78	Y-crack
199+61	Y-crack
199+26	Y-crack
198+92	Y-crack
198+76	Y-crack

198+72	Y-crack
198+43	Y-crack
198+39	Y-crack
198+09	Y-crack
198+06	Y-crack
198+04	Y-crack
197+50	End of distress survey
196+50	End of Section WB-4 intensive FWD testing and MIRA
Section WB-5 (1652+50: MP 147)	
1655+00 to 1651+50	Appears to have larger crack spacing than other sections with more cluster cracking
1655+00	Start of distress survey
1654+90	Y-crack
1654+79	Y-crack
1654+61	Y-crack
1654+29	Y-crack
1653+69	Y-crack
1653+12	Cluster cracking
1652+50	End of distress survey
1651+50	End of Section WB-5 intensive FWD testing (No MIRA testing performed)

a) Complex Y-cracking (411+28 WB)

b) Complex Y-cracking (411+49 WB)

c) Small punchout (409+98 WB)

d) Y-cracking (409+96 WB)

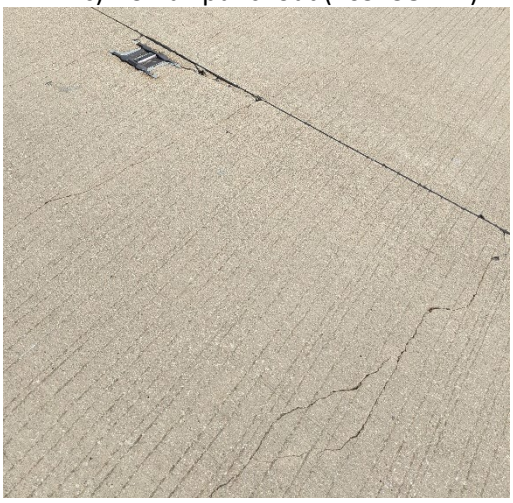

e) Reflector damage and Divided cracking (Test Section WB-2)

f) Y-cracking and complex Y-cracking (304+00 WB)

Figure 231. Photos. Distress photos within I-70 (70044) WB.

IL 53 (60N05):

IL 53 (Old 66) BCOA - Will County – constructed 2012:

a) 4-ft x 4-ft with 4-in. overlay (4-in. inlay, 4 in. of existing HMA milled)
b) 4-lane divided highway (two northbound and two southbound)
c) 4-mile segment (Arsenal Road (south) to Hoff Road (north))
d) ADT=7,750 and 55 mph speed limit
e) Acts more like an UBOL: 4-in. PCC overlay, 7- to 10-in. HMA, 8- to 10-in. existing PCC
f) Cores already sent to UIUC for previous testing (All discarded/ different mechanism tested)
g) No dowels, no joint sealant, structural fibers with 4lbs/yd^3
h) Historical performance data: IL-53 has been tested on multiple occasions throughout the BCOA service life.

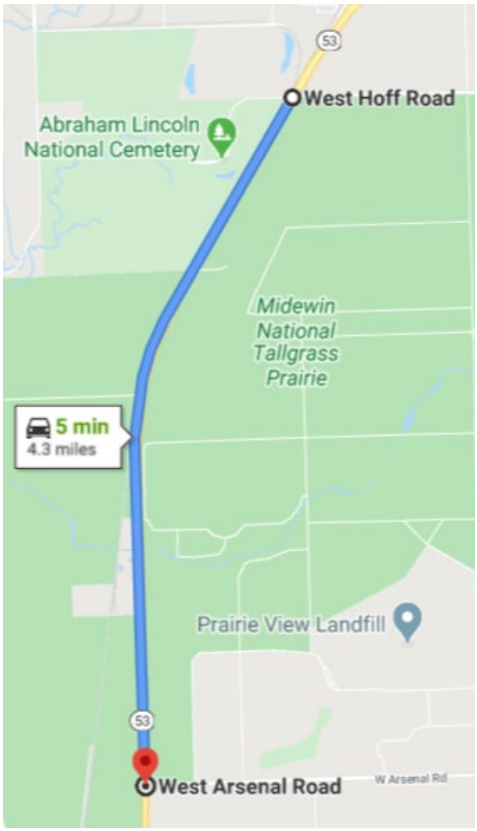

Figure 232. IL 53 (60N05).

IL 53 (60N05) Synopsis of Testing – 8/12/2020

General overview of distress observed:

FWD testing crew (APTech) was a new crew, only 2nd day of testing. Truck issues and setting up took well over an hour (4x4 ft panel sizes gave additional issues when lining up the sensors throughout the day); started testing first section at 8:45am (supposed to start testing at 7am). Three temperature holes were drilled at 1-in., 2-in., and ~7-in. depths into the pavement. Temperatures were recorded three times (8:45am, 11:30am, and 2:30pm) at the same location of the initial drilled holes. Air temperature was between 70 – 80°F, with an increasing UV index throughout the day (~7 when finished testing).

Four test sections were tested. Test Sections 1 and 3 included the intensive testing with the five adjacent slabs and testing the center panel (leave joint at mid-panel and center of slab) every 100 ft (total section is 1,000 ft). Whereas test Sections 2 and 4 only included the intensive testing with the five adjacent slabs.

Table 107. IL 53 (60N05) Temperature Profile (8/12/2020)

	Temperature @ corresponding depths (°F)		
Time of measurement	1-in. depth	2-in. depth	7-in. depth
8:45 am	75	74	75
11:30 am	98	96	81
2:30 pm	122	122	104

MIRA scanning was performed with 35 kHz testing frequency across transverse joints to assess joint activation. All other locations performed with 50 kHz.

Table 108. IL 53 (60N05) Testing Sections and Stationing

Intensive test sections	Time @ start of section	Stationing[1]	
		Beginning of test section	End of test section
1	8:45 am	00+00	10+00
2	10:00 am	61+00	61+20
3	11:45 am	100+00	110+00
4	1:30 pm	187+00	187+20

[1]No stationing was provided, assumed 00+00 was the northern most point of the project near Hoff Rd. Increased stationing as traveling south.

Figure 233. Photo. Start of IL 53 (60N05) SB (assigned stationing of 00+00).

Notes regarding joint activation:

- The longitudinal joint in the inner wheel path of the driving lane was excessively wide (Sections 3 and 4) and was clearly activated. This was beneficial to be able to see joint activation of transverse cracks. However, because all joints are not sealed this will allow incompressible fine material and water to enter the system more easily and lead to more failures.

a) Long. jt in driving lane

b) Long. jt in driving lane ~0.5 in.

Figure 234. Photos. Distress photo of wide longitudinal joint in IL 53 (60N05) SB.

Test Section 3:

a. Intensive testing (5 adjacent slabs)
    i. 3A-5: activated joint and experiencing faulting
    ii. 3B-5: unlikely joint active
    iii. 3C-5: active with faulting (~0.22 in. [5.7 mm])
    iv. 3D-5: unlikely joint active
    v. 3E-5: likely joint activation
b. 100 ft interval testing
    i. 3-C/J-2: active joint and experiencing faulting
    ii. 3-C/J-(3-7): unlikely active joint

Test Section 4: (Longitudinal joint in the IWP not as wide as Section 3 but clearly active)

c. 4A-5: active joint with faulting
d. 4B-5: unknown
e. 4C-5: likely active
f. 4D-5: unknown
g. 4E-5: unknown

Detailed distress surveying was conducted along the driving lane where FWD and MIRA testing was performed.

Table 109. IL 53 (60N05) Detailed Distress Survey Notes (Southbound)

Stationing	Detailed distress notes
Section 1 (0+00 SB)	
0+00 SB	Long. faulting between OWP (DL) longitudinal jt ~0.37 in. [9.3 mm]; panel rocking
0+24 SB	Wide trans. jt. (0.63 in. [16 mm]); small corner spall with trans. faulting (~0.18 in. [4.5 mm])
0+40 SB	Lane/Shoulder jt. full of debris and vegetation, in okay condition
0+50 SB	Trans. jt. spalling
0+79 SB	Long. faulting between OWP (DL) longitudinal jt ~0.53 in. (13.5 mm); panel rocking
0+99 SB	Trans. jt. ravelling
1+11 SB	Corner break and Long. faulting; panel rocking
1+15 SB	Shattered slab (fully cracked panel) with HMA patching; panel rocking
1+19 SB	Shattered slab (fully cracked panel) with HMA patching; panel rocking
1+27 to 1+39 SB	Corner breaks along DL OWP long. jt.; panel rocking
1+64 SB	Shattered slabs (three consecutive slabs) with HMA patching; panel rocking
1+98 SB	Shattered slab with HMA patching; panel rocking
2+07 SB	Trans. cracking and corner break
2+13 SB	Corner break on approach and leave slabs
2+27 SB	Shattered slabs (three consecutive slabs) with HMA patching; panel rocking
2+36 SB	Trans. cracking (two consecutive slabs)
2+56 SB	Trans. cracking (two consecutive slabs) with HMA patching; panel rocking
2+64 SB	Shattered slab (Corner breaks with long. crack across three consecutive slabs)
2+84 SB	Shattered slabs with HMA patching
3+52 SB	Shattered slabs in passing lane with HMA patching
3+72 SB	Corner breaks (eight consecutive slabs) with some HMA patching; panel rocking
4+24 SB	Long. faulting of 12 consecutive panels with HMA patching; panel rocking
4+61 SB	Corner break on approach slab
5+08 SB	Long. and corner cracking (eight consecutive slabs) with HMA patching; shoulder condition is poor in this location
5+40 SB	Long. faulting (five consecutive slabs); panel rocking
5+64 SB	Severe Long. cracking (eight consecutive slabs) with spalling along crack
6+28 SB	Shattered slab in Passing lane
8+24 SB	Long. faulting (~0.35 in. [9 mm]); panel rocking
8+84 SB	Shattered slabs (four consecutive slabs) with HMA patching; panel rocking
8+96 SB	Long. faulting (1.8 in. [46 mm]) with corner break
9+48 SB	Shattered slabs (seven consecutive slabs) with HMA patching
11+12 SB	Scaling on surface of PCC (four consecutive panels)
Section 2 (61+00 SB)	
61+02 SB	Corner break (27-in. radius)
61+28 SB	Corner break with cracking and joint spalling (two consecutive slabs)

Stationing	Detailed distress notes
62+50 SB	End of section (potential coring location – Slab B of right panel edge)
Section 3 (100+00 SB)	
100+07 SB	Corner break with (32-in. radius); longitudinal joint in DL inner wheel path is excessively wide; trans. jt. faulting (~0.22 in. [5.7 mm])
100+31 SB	Corner break (Leave slab – 31-in. radius)
101+27 SB	Long. and corner cracking; some pop-outs observed along PCC surface
102+81 SB	Corner break (8-in. radius)
103+22 SB	Corner break (Leave slab - 22-in. radius)
103+42 SB	Corner break (Approach and Leave slabs - 10-in. radius) with Long. jt faulting (panel rocking)
103+74 SB	Corner break (Leave slab – 31-in. radius)
Section 4 (187+00 SB)	
187+00 SB	Trans. crack mid-panel
187+66 SB	Corner breaks (Leave slabs – 23-in. radius)
187+81 to 188+17 SB	Extra trans. jt and additional long. jts in L/S jt. of Passing Lane; Cause of a lot of cracking and almost acting like a punchout in CRCP
188+10 SB	Trans. cracking and jt. spalling
188+94 SB	Corner break (Leave slab – 38-in. radius)
189+02 SB	Additional trans. jt. causing severe damage and slab cracking
189+17 SB	Additional trans. jt. causing severe damage and slab cracking

General notes about the condition of IL 53 and distresses occurring:

This pavement was performing as expected, with a lot of corner breaks along the longitudinal joints in the wheel paths; the quantity of corner breaks in the outer wheel path are greater than the number of corner breaks in the inner wheel path, but are definitely still occurring. Some panel rocking is also occurring instead of corner breaks, resulting in high magnitudes of longitudinal joint faulting along the longitudinal joint in the outer wheel path of the driving lane. Since construction in 2012, there have been a few major truck distribution centers built along the route to serve the large intermodal facility. This large increase in truck traffic is definitely decreasing the lifespan. Transverse joint faulting is also occurring, but when driving on the section it does not seem to have a big impact (still rides pretty nice). Overall, the majority of the southbound pavement is performing well. The northbound pavement is in worse condition based on previous surveys but was not tested for this project.

a) Severe long. faulting along OWP DL long. jt.

b) Lane/shoulder long. jt. degradation

c) Trans. jt. ravelling

d) Corner breaks and distress

e) Long. faulting along OWP DL long. jt. (8+96 SB): ~1.8 in. (46 mm)

f) Additional Long. jt. causing cracking and punchout (similar to CRCP)

Figure 235. Photos. Distress photos of severe distress in IL 53 (60N05) SB.

a) Shattered slabs with HMA patching (2+27 SB)

b) Trans. cracking (2+36 SB)

c) Slab cracking across three panels (L/S jt. edge)

d) Shattered slab (2+64 SB)

e) Shattered slabs in passing lane

f) Typical observed failures in DL OWP

g) Corner breaks in IWP of DL

h) Severe long. cracking & corner breaks in OWP

Figure 236. Photos. Distress photos of severe cracking in IL 53 (60N05) SB.

UNIVERSITY OF ILLINOIS E-15 PARKING LOT

E-15 is located on the southeast corner of Pennsylvania and 4th Street in Champaign. This parking lot consisted of distressed and aged HMA roughly 2.5-in. thick. The eastern portion of the parking lot was overlaid in 2006 and the western portion in 2012. The concrete overlay contained 3 lb/yd^3 of straight synthetic fibers and 24 percent fly ash replacement of the cement. The overlay was 3.5 in. with 4- by 4- ft panels. The existing asphalt surface was untreated prior to the concrete overlay. The overlay details for the 2012 section are unknown, but likely similar to the 2006 construction (Roesler et al. 2008 and King and Roesler 2014).

Figure 237. E-15 Parking Lot and corresponding testing locations.

The overall condition of E-15 is excellent and not much has changed since the previous surveying and testing performed in 2012. The major distress present consisted of fiber clumping near the surface, causing small pop-outs. Some scaling is also apparent in the traveling lanes in the eastern section. Previous reports indicated areas of debonding were found mainly near the construction joints (King and Roesler 2014), however no indication of debonding was visually apparent during the current surveying. Additional cracking present was documented during the previous survey and included low severity cracks (corner breaks and diagonal cracks) near islands or propagated from drains.

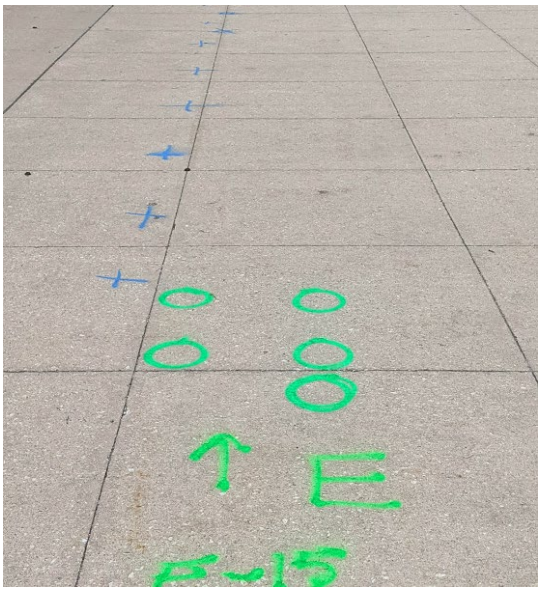

a) Surface scaling

b) Fiber clumping

Figure 238. Photos. E-15 distress survey.

UNIVERSITY OF ILLINOIS MCKINLEY HEALTH CENTER PARKING LOT

The McKinley parking lot is located behind the McKinley Health Center along Lincoln Avenue in Urbana. This parking lot consisted of distressed and aged HMA roughly 3.5 to 4.5-in. thick. The concrete overlay was placed in 2006 and contained 3 lb/yd^3 of straight synthetic fibers and 24 percent fly ash replacement of the cement. The overlay was 3.5 in. with 4- by 4- ft panels (Roesler et al. 2008).

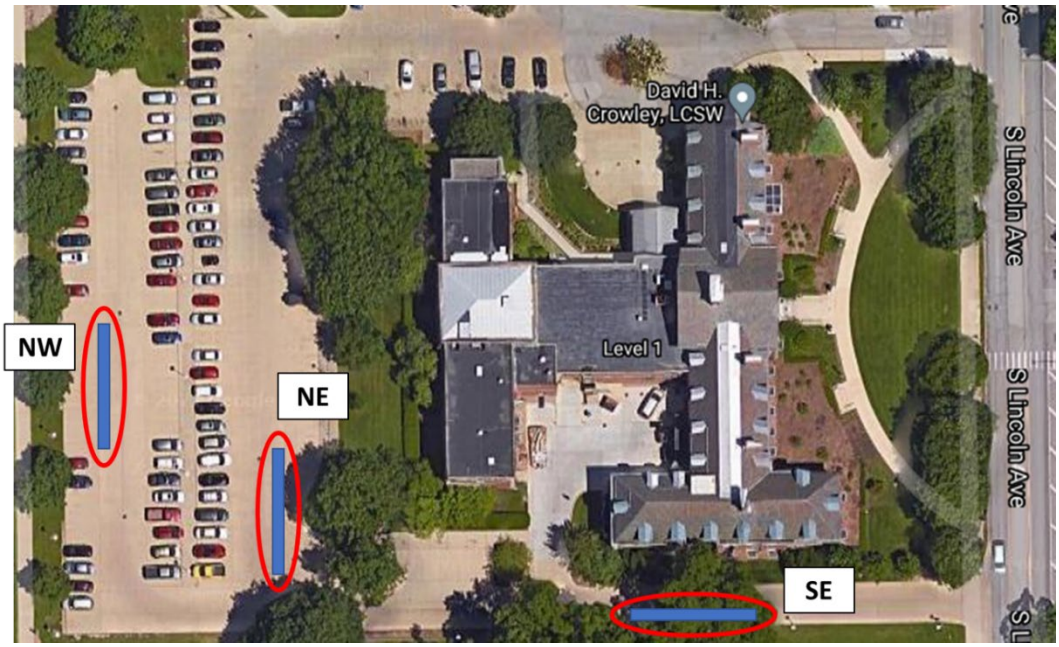

Figure 239. McKinley Health Center Parking Lot and corresponding testing locations.

The most common distress in the McKinley parking lot consisted of joint raveling. Previous reports indicate the combination of high temperatures during summer-time placement, wind conditions, and the hydrating concrete resulted in premature cracking 4 hours after casting (Roesler et al. 2008). This is visible in the northwest bay with severe joint raveling and deterioration. The contractor eliminated these issues by increasing the application of curing compound and grooving joints every 24 ft to relieve surface stresses generated by the environmental conditions prior to saw-cutting practices (Roesler et al. 2008).

In addition, scaling and plastic shrinkage cracking was apparent in the northwest bay and likely related to paving conditions. A previous study indicated areas of debonding were observed near construction joints and in low spots where water is directed for drainage purposes (King and Roesler 2014), however no indication of debonding was visually apparent during the current surveying.

a) Corner break in southeast bay

b) Fiber clumping and surface scaling in southeast bay

c) Diagonal cracking in northeast bay

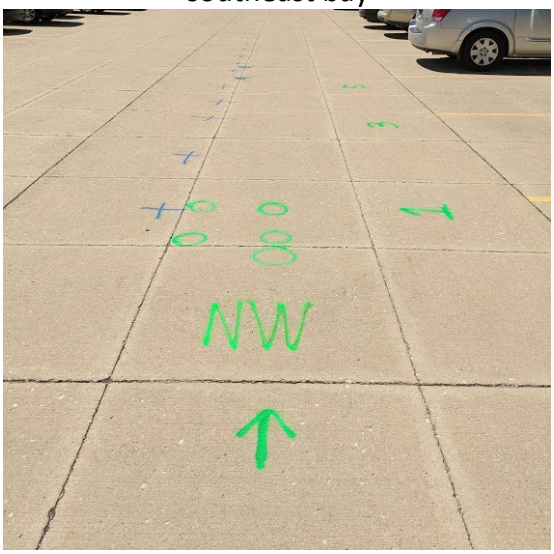

d) Joint raveling in northwest bay

Figure 240. Photos. McKinley parking lot distress survey.

APPENDIX G: PROPOSED EROSION RESISTANCE PERFORMANCE TEST PROCEDURE USING HAMBURG WHEEL-TRACKING DEVICE

1.0 SCOPE

This test method provides an erosion resistance performance indication for different stabilized subbase layers. This method can be used to evaluate the erosion susceptibility of stabilized subbase layers due to mechanical and hydraulic shear under an applied moving wheel load. The testing protocol follows AASHTO T 324-17 in accordance with the Illinois Modified test procedure for "Hamburg Wheel-Tracking Device Testing of Compacted Hot Mix Asphalt (HMA)." This test method measures the erosion depth versus number of passes and the amount of material loss as a function of erosion.

2.0 APPARATUS

The wheel-tracking apparatus defined in AASHTO T 324-17 should be utilized. This standard equipment is currently used in accordance with the Illinois Modified test procedure for "Hamburg Wheel-Tracking Device Testing of Compacted Hot Mix Asphalt (HMA)." This device needs to have the following attributes for successful completion of the developed procedure:

1. Wheel load of 158 ± 5 lb.
2. Wheel loading rate of 52 passes per minute (maximum speed of the wheel is reached at the midpoint between specimens).
3. Temperature control system to reach and maintain required water testing temperatures (122 ± 1.8°F).
4. Capability of water circulation throughout water bath.
5. Linear variable differential transducers (LVDTs) and fully automated data acquisition system to measure the erosion depth induced by the steel wheel.
6. Erosion depth measurements at least every 100 passes of the wheel.
7. Stainless steel trays that can be mounted rigidly to HWTD testing frame in the water bath.

3.0 MATERIALS

The following materials are required for successful completion of this testing procedure:

1. Two high-density polyethylene (HDPE) molds, standard dimensions in accordance with AASHTO T 324-17, for each wheel to secure the cylindrical test specimens. A total of four HDPE molds are required to conduct testing using two wheels (test four cylindrical specimens).

2. Two vibration absorbing neoprene pads, 0.25 to 0.375-in. thick with dimensions of 12 by 11 in. to fit within the mounting tray. These pads are to simulate the subgrade layers that support and prevent additional compressive stresses and deterioration at the bottom of the specimens.

4.0 SPECIMENS

1. Laboratory constructed specimens:

    a. Prepare specimens to appropriate dimensions, 5.91-in. diameter by 2.4±0.1-in. thick in accordance with AASHTO R 39 and AASHTO T 23. For PCC specimens: Only one lift is required utilizing 25 blows (number of rods) with tapping the exterior of the mold with a rubber mallet 10-15 times. Specimens can also be compacted using a gyratory compactor to achieve proper density and dimensions, and later sawed to the appropriate thickness.

    b. Specimens are to be cured for 28 days (PCC) in a moist-cure setting. Testing can be performed within a shorter period, such as 14 days. However, erosion susceptibility is likely to increase with less curing time and an adjustment factor would need to be established.

    c. Density of test specimens should be consistent and are recommended to be within 95 ±0.5% (Jung et al. 2012, TxDOT 2021). Increased density results in an increase in strength and resistance to erosion.

    d. Use the bottom of the cured specimen as the top of the specimen when placed in the HWTD. The finished surface will be placed directly on the absorbing neoprene pad.

    e. HMA specimens should be constructed in accordance with IDOT Modified AASHTO T 324-17 (2018).

2. Field-cored specimens:

    a. Specimens need to be the appropriate dimensions, 5.91-in. diameter by 2.4±0.1-in. thick.

    b. Specimens need to be cut to appropriate dimensions.

    c. When no bond is present from coring, the surface of the core should be tested. When a bond is present, use the smooth cut surface at this interface as the top of the specimen for testing.

5.0 PROCEDURE

1. Prepare specimens to appropriate dimensions, 5.91-in. diameter by 2.4±0.1-in. thick. Specimens can either be cores obtained from the field or prepared within the laboratory by molding or compacting.

2. Splice two specimens together. Cut a vertical face on each specimen to be fitted together in accordance with AASHTO T 324-17.

3. Measure and record the sample weight prior to placement into the mounting tray.

4. Place a thin layer of neoprene rubber into the mounting tray, then the high-density polyethylene molds, and finally the specimens into the mounting tray molds.

5. Ensure the cut interface is flush with each specimen. Any difference in elevation between specimens can cause differential deflections and increase the force exhibited on the specimens.

6. Shim the molds in the mounting tray as necessary. Secure the molds into the mounting tray by hand-tightening the bolts of the edge plate.

7. Fasten the mounting trays into the empty water bath.

8. Start the HWTD device software and enter the required information into the computer (52 passes per minute and 10,000 load repetitions).

9. Fill the water bath until the specimens are fully submerged and the water temperature is at the desired test temperature (testing temperature should be 122 ± 1.8°F [50 ± 1.0°C].

10. Enter a start delay of 30 min to precondition the test specimens once the desired water temperature is reached.

11. Lower the wheels (158 ± 5 lb) onto the specimens after the test specimens have preconditioned at the selected test temperature for 30 min.

12. Start the test after the specimens have been fully submerged for the 30 minutes at the desired water temperature. Measurements should be recorded at 11 different locations in the wheel path on the specimens at least every 100 passes of the wheel using a fixed LVDT in accordance with AASHTO T 324-17. The testing device automatically stops the test when the maximum allowable erosion depth, 0.5 in. (13 mm) is reached or the total number of desired passes, 10,000 is reached.

13. Once testing is completed, save the data and remove the specimens from the mounting tray. Clean the device extensively to avoid excessive material build up. Follow the manufacturer's recommendations for lubrication and cleaning.

14. Record the weight of the specimens after 24 hours in oven dried conditions at 230 ± 41°F (110 ± 5°C) according to ASTM C 642 (2013).

6.0 REPORT

1. For each test, report the following items:

    a. The erosion depth versus number of passes at all 11 sensing locations. Measurements should be made at least every 100 passes of the wheel.

    b. The average erosion depth versus number of passes for each specimen. Measurements should be made at least every 100 passes of the wheel.

    c. The average erosion depth versus number of passes for all 11 sensing locations. Measurements should be made at least every 100 passes of the wheel.

    d. Maximum erosion depth at 10,000 passes.

    e. The weight of each specimen prior to submersion and testing.

    f. The weight of each tested specimen after 24 hours in oven dried conditions.

7.0 FAILURE CRITERIA

The failure criteria for PCC stabilized (CAM II) specimens is a function of the mixture design and material properties of a given mixture. The CAM II mix first needs to pass the Illinois Modified AASHTO T 161-08 "Standard Method of Test for Resistance of CAM II Mixes to Rapid Freezing and Thawing, Procedure B." The CAM II mixture shall meet the test requirements in Article 312.26 of IDOT's *Standard Specifications for Road and Bridge Construction* for relative durability (freeze/thaw resistance), air-entrainment, and slump. The mix design with the lowest cement content or cement and fly ash contents that meets the requirements will be reported to the IDOT District. HWTD testing shall be performed to assess if the amount of cement stabilization is sufficient enough to provide erosion resistance. Higher volumes of traffic and traffic speeds likely need a higher level of stabilization as a function of pore water pressure build-up.

The failure criteria for CAM II mixtures should result in average erosion depths less than or equal to 0.08 in. (2 mm) after 10,000 load cycles. The failure criteria for new HMA stabilized subbases should follow the current criteria outlined in Article 1030.05(d) of IDOT's *Standard Specifications for Road and Bridge Construction* for HWTD Test and presented in **Table 110**. This testing should be performed on new mixtures to be used prior to placement of a new concrete pavement. Additionally, this testing should be conducted on existing asphalt pavements that are to be overlaid (bonded concrete overlay or unbonded concrete overlay). This test can be a good indicator of the suitability and candidacy of the existing HMA for a concrete overlay.

Table 110. IDOT HMA HWTD Failure Criteria

Binder grade	Minimum number of passes at 0.5-in. rut depth
PG 58 or lower	5,000
PG 64	7,500
PG 70	15,000
PG 76 or higher	20,000

It may be useful to run every test for 20,000 wheel passes to collect additional data on moisture sensitivity.


Illinois Department
of Transportation


ILLINOIS